

AD-787 549

PROCEEDINGS OF THE FLUIDIC STATE-OF-THE-ART
SYMPOSIUM HELD AT NAVAL ORDNANCE LABORATORY,
WHITE OAK, MARYLAND ON 30 SEPTEMBER -
3 OCTOBER, 1974
VOLUME IV

HARRY DIAMOND LABORATORIES

1974

DISTRIBUTED BY:

NTIS

National Technical Information Service
U. S. DEPARTMENT OF COMMERCE

REPORT DOCUMENTATION PAGE		READ INSTRUCTIONS BEFORE COMPLETING FORM
1. REPORT NUMBER	2. GOVT ACCESSION NO.	3. RECIPIENT'S CATALOG NUMBER
4. TITLE (and Subtitle) Proceedings of the Fluidic State-of-the-Art Symposium, 30 Sep - 3 Oct 74, Vol. IV		5. TYPE OF REPORT & PERIOD COVERED
		6. PERFORMING ORG. REPORT NUMBER
7. AUTHOR(s) Various		8. CONTRACT OR GRANT NUMBER(s) HDL Proj. No. 302531
9. PERFORMING ORGANIZATION NAME AND ADDRESS		10. PROGRAM ELEMENT, PROJECT, TASK AREA & WORK UNIT NUMBERS
11. CONTROLLING OFFICE NAME AND ADDRESS		12. REPORT DATE
		13. NUMBER OF PAGES 391
14. MONITORING AGENCY NAME & ADDRESS (if different from Controlling Office)		15. SECURITY CLASS. (of this report) Unclassified
		15a. DECLASSIFICATION/DOWNGRADING SCHEDULE
16. DISTRIBUTION STATEMENT (of this Report) Unlimited		
<div style="border: 1px solid black; padding: 5px; width: fit-content; margin: 0 auto;"> <p>DISTRIBUTION STATEMENT A</p> <p>Approved for public release; Distribution Unlimited</p> </div>		
17. DISTRIBUTION STATEMENT (of the abstract entered in Block 20, if different from Report)		
18. SUPPLEMENTARY NOTES → contents		
19. KEY WORDS (Continue on reverse side if necessary and identify by block number) Computer aided fluidic circuit design, fluidic compensation networks, fluidic multiplier, fluidic impedance measurement, fluidic interconnections, pneumatic transmission lines, Sixth Cranfield Fluidics Conference, fluidics stabilization contamination effects on fluidic devices. ←		
20. ABSTRACT (Continue on reverse side if necessary and identify by block number) This volume contains twelve papers for a total of 391 pages. end		

AD 787549

FLUIDIC
STATE-OF-THE-ART

SUMMARY

30 SEPTEMBER - OCTOBER

DDC
RECEIVED
OCT 23 1974
RECEIVED
D

VOLUME IV

Reproduced by
NATIONAL TECHNICAL
INFORMATION SERVICE
U S Department of Commerce
Springfield VA 22151

U.S. Army Materiel Command
Harry Diamond Laboratories
Washington, D.C.



DISTRIBUTION STATEMENT A
Approved for public release;
Distribution Unlimited

Volume IV

Computer-Aided Circuit Analysis and Design
J. Iseman, Harry Diamond Labs, Washington, D.C. 1

*A Circuit Analysis Approach to the Solution of Passive
Pneumatic Fluidic Compensation Networks*
J. Iseman, Harry Diamond Labs, Washington, D.C. 77

*A Laminar Fluidic Multiplier and a Review of the
State-of-the-Art*
R. Woods, Harry Diamond Labs, Washington, D.C. 179

Fluidic Impedance Measurement With a Half Bridge Circuit
K. Toda and S. Katz, Harry Diamond Labs, Washington, D.C. 201

Engineering Approximations for Fluidic Interconnections
H. L. Moses, Virginia Polytechnic Institute and State
University, Blacksburg, Virginia
R. A. Comparin, Newark College of Engineering 233

*Comparison of the Linear Response of Circular, Rectangular
and Annular Pneumatic Transmission Lines*
M. E. Franke and E. I. Moore, Air Force Institute of Technology . . 255

The Effect of Through Flow on Signal Propagation Fluid Lines
N. Eisenberg, A. Hausner, and S. Katz, Harry Diamond Labs,
Washington, D.C. 269

Report on the Sixth Cranfield Fluidics Conference
J. K. Royle, University of Sheffield, United Kingdom 299

Fluidic Standardization Efforts
P. Trask, Harry Diamond Labs, Washington, D.C. 317

Fluidics Standards and Practices
H. Ott, Naval Air Engineering Center 333

Contamination Effects in a Laminar Proportional Amplifier
R. A. Comparin, Newark College of Engineering, Newark, New Jersey
H. L. Moses, Virginia Polytechnic Institute and State University,
Blacksburg, Virginia
E. F. Rowell III, Dow Badische Co., Williamsburg, Virginia 347

Effects of Contamination on Fluoric System Reliability
Wm. J. Westerman, Jr., McDonnell-Douglas Astronautics Co.,
Titusville, Florida 361

1d

**COMPUTER-AIDED FLUIDIC CIRCUIT
ANALYSIS AND DESIGN**

by

JOSEPH M. ISEMAN

**HARRY DIAMOND LABORATORIES
WASHINGTON, D.C. 20438**

ABSTRACT

Electronic circuit analysis programs and simulation programs exist that have provided a quick easy method of determining the response of electronic circuits. These programs have now been restructured as indicated in this paper to provide an easy means of performing analysis, design, and sensitivity studies on many fluidic circuits. Specifically three computer programs have been examined: DSL/90, SLIC, and NET-2. These programs can be applied without modification to simulate the most basic fluidic equivalent circuit models. However, new computer codes or subroutines have been written and incorporated into existing programs to handle sophisticated fluidic models. For many components in the ranges of interest, both nonlinear (amplitude dependent) and frequency dependent equivalent circuit models have been developed. Of these the more sophisticated fluidic models were designed into NET-2 because of its basic versatility.

Several programs for simple fluidic summing and distribution junctions, lead networks, lag networks, lead-lag networks are implemented in this paper using DSL/90, SLIC, and NET-2. For fluidic problems SLIC is best suited for simple, small-signal, linear or nonlinear, dc or ac problems. DSL/90 is good for simple, nonlinear transient analyses, problems that do not fit into any existing circuit analysis programs. NET-2 seems to be the best program for complex nonlinear problems within the framework of circuit analysis, and consequently a major portion of this paper is a catalog of non-linear fluidic NET-2 models of passive components and a computerized description of the laminar proportional amplifier.

ACKNOWLEDGEMENTS

The author expresses his gratitude to the following individuals: Howard Bloom and Arthur Hausner, for guiding the nonlinear approaches in DSL/90.

Brian Biehl, for introducing the author to SLIC and setting up the first nonlinear fluidic resistor in SLIC.

Allan Malmberg (Braddock, Dunn and McDonald) and Robert Puttcamp, for modifying and designing basic NET-2 software, for suggesting possible new approaches in NET-2, and for debugging and helping to debug NET-2 programs.

LIST OF FIGURES

PAGE

1. Schematic Illustrating Circuit Terminology
2. Lead Network with Diaphragm
3. Equivalent Circuit for Lead Network with Diaphragm
4. Lag-Lead Network
5. Equivalent Circuit for Lag-Lead Network
6. Lead-Lag Network
7. Lead-Lag Network Prepared for SLIC Program
8. Nonlinear Resistor (using Table, look-up)
9. Nonlinear Resistor (using VCG as a function of through flow)
10. Nonlinear Function Generator (function of node voltage through TABLE, look-up)
11. Nonlinear Grounded Capacitor (using flow differencer and integrator)
12. Nonlinear Grounded Capacitor (using flow differencer, integrator and TABLE, look-up)
13. Nonlinear Capacitor Using Type 1 RC Mutator
14. Schematic of Type 1 RC Mutator as Capacitor
15. Nonlinear Capacitor (using Type 1 RC Mutator)
16. Nonlinear Inductor (using Type 1 RL Mutator)
17. Schematic of Type 1 RL Mutator as Inductor
18. Nonlinear Inductor (using Type 1 RL Mutator)
19. Switching Characteristic (actuated by node voltage and biased limiters)
20. Capillary (R, L, C Model)
21. Capillary (Linear L and C with measured linear resistance)
22. Capillary (Nonlinear R using TABLE, look-up)
23. Capillary (Nonlinear R using VCG)
24. Enclosed Volume (Grounded, Linear C)
25. Enclosed Volume (Grounded, Nonlinear C using integrated flow)
26. Enclosed Volume (Cylindrical volume with frequency dependence using ber - bei generator to control grounded RC).
27. Bellows (Pi networks with linear C's)
28. Diaphragm (Pi network with linear C's)
29. Diaphragm (Pi network with linear grounded C's and nonlinear point-to-point C, using Type 1 RC Mutator)
30. Laminar Proportional Amplifier (Linear, single-sided)
31. Laminar Proportional Amplifier (Nonlinear, two-sided)

LIST OF FIGURES (CON'T)

PAGE

- 32. Summing Junction
- 33. Distribution Junction
- 34. Lag Network
- 35. Lead Network with Bellows Module
- 36. Lead Network with Diaphragm Module
- 37. Lag-Lead Network with Bellows Module

LIST OF TABLES

PAGE

1. Features of SLIC, SCEPTRE, and NET-2.....
2. Standard Elements in SLIC.....
3. Standard Elements in NET-2.....

1. INTRODUCTION

The computer analysis and design of complex electronic circuits are highly developed techniques. Numerous methods have been developed using both analog and digital computers; and digital computer software facilitating the development and solution of circuit equations is extensive and well documented. It is therefore logical to apply these techniques to fluidic design problems.

To set a perspective for applying a circuit analysis to fluidic components, a brief statement of the analytical background is presented.

In making this application, the procedure has been to describe passive fluidic components analytically by employing the principles of fluid mechanics to specific internal flow problems. Rigorous analyses of these problems are performed by writing the governing equations (continuity equations, equations of motion, energy equations, and equations of state). Certain assumptions about a specific fluid problem reduce its complexity. For a specific set of simplifying assumptions, the governing fluidic equations are reduced to equations that are analogous to the circuit equations. These equations can then be stated in the form of equivalent circuits, which are the basic input for the computer programs.

Circuit equations may be solved manually or automatically with an analog or digital computer. Setting up the analog computer to simulate the circuit equation response presents several difficulties: (1) large numbers of analog components are needed to simulate large circuits, (2) scaling of numerical values must be performed, and (3) nonlinear circuit components sometimes preclude meaningful simulation. On the other hand, current digital computer methods are readily available and easily applied to solve the circuit equations. DSL/90 (ref 1)* and CSMP are two examples of available digital simulation languages.

When the circuit equations are linear, a digital computer solution is simple and straightforward. However, for circuits with nonlinear components, the user must correctly establish the sequence of the differential and algebraic equations to be solved.

Although much of this work relates equally well to hydraulics, the discussions in this paper are restricted to low-velocity pneumatics. The governing equations are simplified by assuming that the dynamic-pressure drop across any element is small compared with the static-pressure drop, i.e., that the fluid velocity is small compared to the speed of sound.

For these studies, the element variables are $q(t)$, which is the volume flow through an element, and $\Delta p(t)$, which is the total pressure drop across an element.

*Literature references are listed at end of this paper.

Static-pressure drop, which is more readily measurable than total-pressure, is, however, a more convenient choice for the across variable.

For steady incompressible flow if the cross-sectional area of a passage at two consecutive fluidic nodes is constant, then particle velocity is unchanged and the dynamic-pressure drop between the two nodes is zero so that the total pressure drop is equal to the static-pressure drop.

For such changes of cross-sectional area as in converging ducts, diverging ducts and sudden enlargements, dynamic-pressure drop generally must be included in the total-pressure drop.

However, in acoustics and hydraulics for passages with constant cross-sectional area, if the particle velocity is small compared with the acoustic velocity, total-pressure drop is approximately the static-pressure drop.

Many electronic components and devices, as well as many components and devices in nonelectronic technologies, (mechanics, pneumatics, hydraulics, thermodynamics), may be readily described in terms of equivalent circuits. The most basic circuit descriptions are passive, lumped, linear and one-dimensional. Certain modifications may be made for some problems to extend basic methods -- including equivalent circuits -- to more sophisticated studies of active, distributed, nonlinear and multi-dimensional configurations.

Several basic fluidic structures are modeled as equivalent circuits in section 3, both with and without taking into account the fact that the components are not purely resistive, capacitive, or inductive. Also, Section 3 discusses specific digital circuit analysis programs in relation to requirements for simulating the response of real pneumatic configurations based on equivalent circuit models.

This paper cites the pertinent basic programming manuals. Much of the material for coding fluidic equivalent circuits into a digital simulation program, DSL/90, and a simple circuit analysis program, SLIC, are given in their respective manuals. In section 4, DSL/90 is demonstrated for fluidic equivalent circuit problems. A handbook of new and modified subroutines in SLIC is given in section 5. However, neither DSL/90 nor SLIC can be modified to be as versatile as the powerful circuit analysis program, NET-2.

Because of the excellent versatility of NET-2 in performing fluidic circuit analysis compared with SLIC, the major part of this paper, section 6, is a fluidic NET-2 handbook. The improved fluidic version of NET-2 performs simultaneous solutions on equivalent circuits that include newly coded nonlinear resistances, nonlinear capacitors, nonlinear inductors, and switches.

Limitations relative to the circuit analysis approach and to digital computer codes are discussed in section 7. Conclusions are developed in section 8.

2. FLUIDIC STRUCTURES

The basic fluidic structures may be divided into: (1) energy sources, (2) energy sinks or drains, (3) fluid flow passages, (4) mechanical confining structures adjacent to the flow passages and (5) fluid distribution points (junctions). These basic fluidic structures are modeled as equivalent circuits composed of simple voltage sources, simple current sources, resistors, capacitors and inductors. For nonideal components, amplitude and frequency-dependent elements are introduced to extend modeling capability.

2.1 Fluid Flow Passages

The geometrical configuration through which the fluid passes between sources and sinks assumes many forms. Fluid flow passages of interest can be viewed as totally or partially surrounding the fluid. A geometrical configuration such as a tank, in which walls virtually surround the fluid, is described as an "enclosed volume". If part of the physical wall is not present, as in the case of a cavity on one side of the jet in a fluid amplifier, the configuration is described as an "almost enclosed volume". Air fluidic passage configurations of interest in this paper are (1) capillaries and (2) enclosed or almost-enclosed volumes. In each of these cases, reasonable assumptions lead to relatively simple equations that relate (1) differential pressure and flow, or (2) pressure and differential flow.

2.1.1 Capillary

Each segment of a capillary dissipates energy. Thus, a capillary is a resistor for a time-invariant (dc) flow. Schematically, it is



2.1.2 Enclosed or Almost-Enclosed Volume

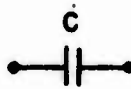
In pneumatics, potential energy may be stored by compressing a gas in a volume. Capacitance, which sets a value for the potential energy storage, is the circuit parameter that describes this structure.

The equivalent circuit representing an enclosed volume is a capacitor between a pressure node and ambient (ground). Schematically it is shown as



2.2 Mechanical Confining Structures

Ideally the confining structures should in no way influence the performance of the flow dynamics of fluidic components. These structures should be perfectly rigid and must be either perfect thermal conductors (for lossy devices) or perfect adiabatic walls (for lossless devices). These criteria may be approximately met in general. However, in selected cases rigidity may be specified at various finite rather than infinite values. Compliance (a mechanical capacitance) in the fluidic case is a ratio of the volume added by deflection of the confining structure to the difference between the internal and reference pressures. Bellows, diaphragms, and spring-loaded pistons are examples of confining structures and are used as point-to-point capacitors



2.3 Distribution Points

A node is a readily accepted concept in low-frequency electronics. No geometrical aspects are attributed to a pure node. An electronic node is described in terms of its voltage compared to a reference voltage.

A fluidic node is a junction, typically the meeting and branching point for several fluidic components. A pure node in fluidics is analogous to the electronic node so long as geometry need not be included in the description. Fluidic junctions are classed as pure nodes so long as dynamic pressure potential is small compared with static pressure potential.

A fluidic node connecting many branches may be physically designed if the static pressure is large compared with the dynamic pressure. A stilling chamber placed at the junction is sometimes included to convert dynamic pressure to static pressure.

Proper operation of pneumatic fluidic configurations in some cases is predicated on large dynamic pressures at certain nodes. In such cases pneumatic fluidic junctions are not pure nodes.

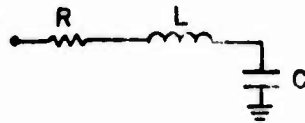
2.4 Impure Structures with Parasitics

Several of the components discussed above do not have physical properties that can be described in terms of pure concepts (only resistance, only capacitance, or only inertance). Instead the components are described as: (1) impure resistance, impure capacitance or impure inertance, each a function of either dependent or independent variables and each combining some other property with the primary property (e.g. inertance combined with resistance). Modified equivalent circuit models

are introduced (1) for a capillary, (2) for a mechanical capacitor, and (3) for a distribution point.

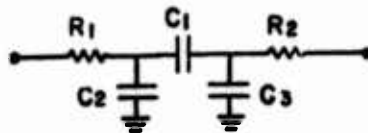
2.4.1 Capillary

Although capillaries are approximately resistive at low frequencies, for higher frequencies compressibility and inertia of the fluid introduce capacitance and inductance, respectively. As a first correction, the simple resistive capillary may be considered as one section of a lumped approximation of a fluid transmission line. An equivalent circuit is



2.4.2 Impure Mechanical Capacitor

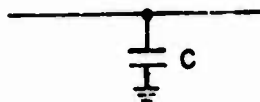
The mechanical devices included in this set of fluidic components are more complicated than purely point-to-point capacitors. In general, the cross-sectional area of the circuit must increase to the area of the deflecting devices (bellows or diaphragm) and then decrease. Line area increases and decreases add resistance, while the larger cross-sectional area of the circuit adds volume capacitance. Thus the equivalent circuit may be redrawn more accurately as



However, it is possible to reduce resistance values R_1 and R_2 by maintaining constant cross-sectional area and to reduce capacitance values C_2 and C_3 by adding as little volume as possible.

2.4.3 Impure Node

The fluid distribution points (junctions or nodes) ideally do not produce added energy losses or introduce added energy storage. However, as a stilling chamber at higher pressures or flows, the increased volume at the node introduces an added grounded fluid capacitor. The equivalent circuit of a node may then be a node and a shunt capacitor to ground:



3. EQUIVALENT CIRCUIT ANALYSIS

Although the equivalent circuits may be analyzed using conventional manual techniques, the digital computer makes the analysis much easier and quicker. Thus, steady-state dc analysis, time-dependent transient analysis, and small-signal steady-state ac analysis may be performed on a digital computer for passive and active circuits. Sensitivity analyses and design optimizations are also available using a digital computer.

A typical network is described with standard equivalent circuit nomenclature (fig. 1). R is a resistor, C is a capacitor, L is an inductor, and e is a voltage source. Currents i_R , i_L , and i_C flow in R, L, and C respectively.

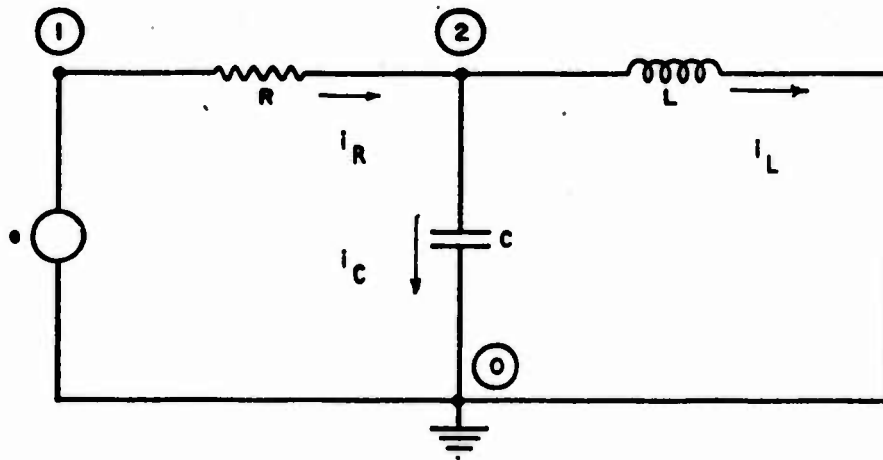


Figure 1: Schematic illustrating circuit terminology

Each component in the equivalent circuit constitutes one branch. For example, R is the branch between points (1) and (2) and C is the branch between points (2) and (0). The point in the circuit at which two or more branches connect is a node. There are three nodes in figure 1 -- (0), (1), and (2).

A circuit loop follows a complete, unbroken path starting at a node, following branches through one or more other nodes, and returning to the original node. One circuit loop starts at node (1), passes through branch R to node (2), passes through branch C to node (0), and returns to node (1) through branch e. Another circuit loop passes from (2) through branch L to (0) and through branch C back to (2).

3.1 Circuit Equation Method

A given equivalent circuit can be mathematically described as a set of algebraic and integral equations using one of several standard techniques. Two standard methods of forming a circuit are node/branch

analysis and node/loop analysis. Although they are not all-inclusive and do not apply to all circuits (ref 2), these two techniques are briefly described for completeness.

3.1.1 Node/Branch Analysis

In a node/branch analysis, the set of equations includes one equation for every non-grounded node and one equation for each branch.

Each fluidic node equation is a mathematical relationship that describes the physical principle of mass conservation at a node. For incompressible flow, the fluidic node equation describes conservation of volume flow, $q(t)$, at that node.

Each branch equation relates the across variable (voltage or pressure drop) to the through variable (current or volume flow) for each circuit component. For example, resistive, capacitive, and inductive branch relationships for figure 1 would be

$$\text{for a resistor } e(t) = Ri(t) \text{ or } \Delta p(t) = Rq(t)$$

$$\text{for a capacitor } e(t) = \frac{1}{C} \int i(t) dt \text{ or } \Delta p(t) = \frac{1}{C} \int q(t) dt$$

$$\text{and for an inductor } e(t) = L \frac{di(t)}{dt} \text{ or } \Delta p(t) = L \frac{dq(t)}{dt}$$

where

$$t = \text{time,}$$

$$e(t) = \text{voltage drop across branch,}$$

$$i(t) = \text{current through branch,}$$

$$\Delta p(t) = \text{pressure drop across branch,}$$

$$q(t) = \text{volume flow through branch.}$$

The components R , C , and L in the above equations may be (1) constant valued, (2) time-dependent, or (3) nonlinear functions of pressure drop or volume flow.

3.1.2 Node/Loop Analysis

Each fluidic loop equation is a mathematical description of the physical principle of conservation of energy in each loop. A loop equation for a fluidic circuit is the sum of potential drops (pressure drops, $\Delta p(t)$) around the loop.

In loop analysis mathematically independent loops are selected. Two fluidic loop equations for the fluidic equivalent circuit of figure 1 are

$$\Delta p(t) - Rq_R(t) - \frac{1}{C} \int q_C(t) dt = 0$$

$$\frac{1}{C} \int q_C(t) dt + L \frac{dq_L(t)}{dt} = 0$$

In addition for node/loop analysis as in node/branch analysis, conservation of volume flow must be described mathematically by fluidic node equations. For the fluidic equivalent of figure 1

$$q_R(t) - q_C(t) - q_L(t) = 0.$$

Components R, C, and L may take on the same forms as in node/branch analysis.

3.2 Computer Circuit Analysis

In determining the input/output response of a fluidic circuit by computer circuit analysis, the formulation and the solution of the circuit equations is performed by a numerical algorithm suitable for use on a digital computer algorithm; the user merely specified the component and connection functions and codes them as input into the digital computer program. For large or complicated circuits, this approach is convenient, fast and accurate. Once the user has drawn an equivalent circuit, many digital computer programs -- including SLIC, SCEPTRE, and NET-2 -- are available for the analysis. Circuit components and their connections are coded into the digital computer. The computer algorithm then determines the circuit response.

3.3 Sensitivity Analysis and Optimization

Additional features of some circuit analysis programs increase their general utility. For example, sensitivity analysis is available through subroutines in SLIC, and optimization is included in NET-2.

A fluidic sensitivity analysis computes the effect that an infinitesimal change of a fluidic circuit parameter makes on the input/output response. Thus, key parameters may be selected. Optimization automatically adjusts fluidic circuit parameters to extremize input/output response in terms of required specifications.

Both sensitivity analysis and optimization direct the solution of sets of circuit equations. Solutions of these equations are the parameter sensitivities and the optimum response, respectively.

4. COMPUTER-AIDED CIRCUIT ANALYSIS

Although circuit analysis may be readily performed with conventional manual techniques, the digital computer is rapidly supplementing the engineers' skills. Once the equivalent circuits are drawn, circuit analysis on a digital computer is of benefit in at least two ways. First, computer-aided circuit analysis contains organizational schemes through which the requisite equations are developed and solved. Second, the simplicity of defining the program makes computer-aided circuit design a valuable labor saving tool. Unlike analog simulation, a digital simulation does not require scaling of values.

There are a multitude of general and special-purpose circuit analysis programs including ECAP, CIRCUS, TRAC, NET-1, SCEPTRE, ECAP-II, SLIC, SPICE and NET-2. Each of these programs has specific attributes. Many of these programs were written and are being written to solve large electronic circuits that are subjected to electromagnetic and nuclear radiation.

Of the programs available to the author, SLIC (ref 3), SCEPTRE (ref 4), and NET-2 (ref 5) were considered possible choices to build on. A list of many available, required capabilities has been drawn up.

For completeness, these capabilities are tabulated for SLIC, SCEPTRE, and NET-2 in Table 1. There is a marked variation even among these three programs. SLIC lacks transient analysis and SCEPTRE lacks ac analysis, while NET-2 encompasses both. NET-2, which is still in development under HDL supervision, currently has the most versatility. NET-2 is much more sophisticated than either SLIC or SCEPTRE. Some modifications to SLIC and SCEPTRE may be introduced in FORTRAN subroutines. Although the basic NET-2 program is complicated, in-house modifications can be introduced within the user package.

Because of the existing in-house capabilities, many additional features that are possible with SLIC and SCEPTRE are designated as "can be". Since many of the more significant features in NET-2 will perform at a later date, they are categorized as "not at present".

No circuit analysis program has been written exclusively for fluidic components. To date, no single circuit analysis program has all the features necessary for directly implementing fluidic equivalent circuits.

The potential ability of one systems-simulation language (DSL/90) and two circuit analysis programs (SLIC and NET-2) for meeting the requirements of specific fluidic problems is examined in this paper. General circuit analysis programs can be applied to fluidic circuits to perform linear analyses for the dc, transient, and steady-state ac cases. However, it is necessary to develop fluidic circuit codes for amplitude dependent and frequency dependent components.

Basic computer programs are briefly outlined, existing fluidic equivalent circuit models are incorporated into the programs, circuit methods for several elementary fluidic configurations are demonstrated.

Fluidic versions of DSL/90, SLIC, and NET-2 are discussed in sections 5, 6, 7. To gain a comprehensive view of fluidic circuit analysis developed to date at HDL, this paper must be used in the light of the more general programs. Used in conjunction with the various general programming manuals (refs 2, 3, and 5), this serves as a reference and a handbook of current fluidic circuit analysis as applied to both elementary and sophisticated fluidic equivalent circuit models. No attempt is made to explain the underlying principles and assumptions upon which fluidic configurations are analyzed and equivalent circuits are synthesized.

TABLE 1: Features of SLIC, SCEPTRE, and NET-2

	(A) SLIC	(B) SCEPTRE	(C) NET-2 Through Release 8
1. Linear dc	Yes	Yes	Yes
2. Linear transient	No, but updated version (SPICE) can	Yes	Yes
3. Linear ac	Yes	No	Yes
4. Nonlinear dc	Yes; nonlinear resistor has been added at HDL by modifications.	Yes; nonlinear resistor has been added at HDL by new subroutine	Yes; voltage controlled conductance is set in a table to give resistance.
5. Nonlinear transient	No, but updated version (SPICE) can be modified.	Same as 4B	Same as 4c and a function generator has been defined at HDL for nonlinear capacitors.
6. Nonlinear ac	Same as 4A but only for small-signal analysis about computed dc operating point.	No	Same as 5c but only for small-signal analysis about computed dc operating point.
7. Frequency dependent components	Frequency dependent capacitor added at HDL in subroutines	No	Yes
8. Time dependent components	No, but updated versions (SPICE) can be modified.	Can be added if desired.	Yes
9. General functions for circuit parameters	Can be added in subroutine.	Can be added if desired.	No, if computational delay is unacceptable; however, any function of one or two variables can be coded as a one- or two-dimensional table, respectively.
10. Values defined	Numerically	Numerically and analytically	Numerically and analytically
11. Table look-up	Can be added	Can be added	Yes
12. General analog simulation blocks	No, but can be added	No, but can be added	Yes
13. Distributed parameter circuits	May be approximately represented in the frequency domain as phase shift in a lumped element.	May be approximately represented in the time domain as time delay in a lumped element or with Padé approximation.	NOT AT PRESENT Padé approximation for time delay in the complex frequency domain is applied both in small-signal ac and in transient analyses.
14. Sensitivity analysis	Yes, in updated version of SLIC	Can be added if desired	NOT AT PRESENT
15. Optimization	Can be added if desired	Can be added if desired	Yes
16. Simultaneity of solutions	No, solution uses value from last calculated operating point	No, solution uses value from last calculated operating point	Yes
17. Computer code in terms of fluidic variables and geometries	Can be added if desired	Can be added if desired	NOT AT PRESENT
18. Model hierarchy defining more complex models, based on simpler defined models	No	Yes	Yes
19. Computational speed	Adequate	Adequate	Very fast by comparison
20. Required size of computer	Moderate	Large (depends on the version)	Large
21. Interactive capability for user to control program as it computes	No	No	No

Reference 2 is a programming manual for DSL/90. Section 5 of this paper uses reference 2 as a guide in the development of the form of a DSL/90 program. No additional fluidic models are introduced into DSL/90 by the author. Two elementary fluidic configurations are computed as examples in section 5.

The general version of SLIC, (ref 3) is directly applicable to linear, passive circuits. However, a more complete fluidic version of SLIC has been extended at HDL to include nonlinear resistors and frequency dependent volumes. One simple fluidic configuration is analyzed using SLIC (sect. 6).

Simple fluidic circuit analysis is readily handled by a fluidic SLIC. However, a more sophisticated computational structure is required to analyze more complex configurations. Specifically, a general version of NET-2 will solve both active and passive linear fluidic circuits. Nonlinear fluidic functions have been included in the general version of NET-2 (sect. 7). For circuits described in terms of nonlinear fluidic functions, it was not at first possible to select digital computer models that could be transformed within the computer algorithm to a set of equations solved simultaneously at each solution point.

However, by selecting the proper structures for user-developed models (ref 3), the author has developed a fluidic version of NET-2 that allows the circuit equations to be solved simultaneously for fluidic structures modeled in terms of nonlinear resistors, nonlinear capacitors, nonlinear inductors, and switching characteristics.

The newly-added computer models make NET-2 extremely versatile in solving nonlinear fluidic equivalent circuits. Because NET-2 is far more sophisticated than the other two programs, many more complex and sophisticated fluidic component models have been modeled in NET-2. Therefore, a dominant portion of this paper contains fluidic models in NET-2. Six simple fluidic configurations are modeled in terms of NET-2.

The information that must be read into a computer by an engineer-user is quite similar, regardless of the circuit analysis program. The engineer-user:

- (1) Specifies the type of analysis
- (2) Defines the swept variable
 - (a) dc voltage range and increments
 - (b) time range and increments
 - (c) frequency range and increments
- (3) Defines equivalent circuit topology
 - (a) type and name of element
 - (b) names of connection nodes
 - (c) values of the parameters of the element
 - (d) special conditions required

- (4) Defines individual component topologies which are not stored
- (5) Defines constants and parameters.
- (6) Defines outputs formats.
- (7) Modifies and updates parameters and component parameters.

5. DSL/90

A standard systems simulation language such as DSL/90 (ref 2) may also be used for studying fluidic configurations that are modeled as circuits. Two simple circuits with nonlinear diaphragm components are set up for and coded into DSL/90 programs. In each nonlinear circuit, equations are appropriately represented and organized to assure solutions.

The following approach is described in terms of node and branch equations, organized so that a voltage or a current is equated to an algebraic or an integral function of other voltages and currents. For specific circuit topologies, one or more equations must be added (ref 1).

5.1 Lead Circuit Using Diaphragm Component Modeled as Nonlinear Capacitor in DSL/90

A lead network may be implemented with a diaphragm component (fig. 2).

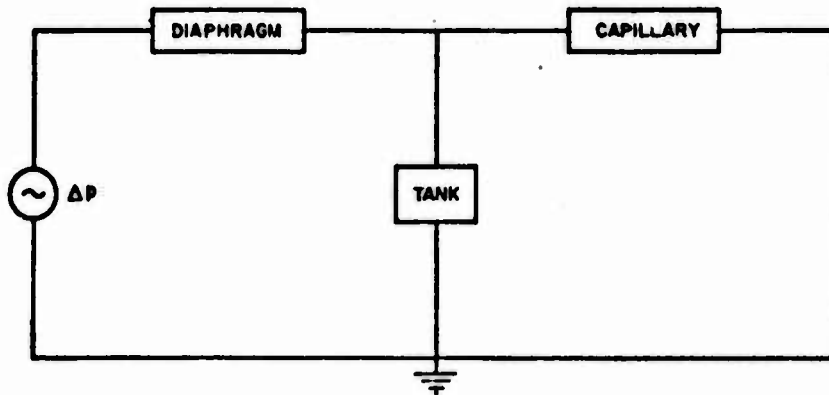


Figure 2: Lead Network with Diaphragm

This simple lead network may be converted into the equivalent circuit of the form in figure 3:

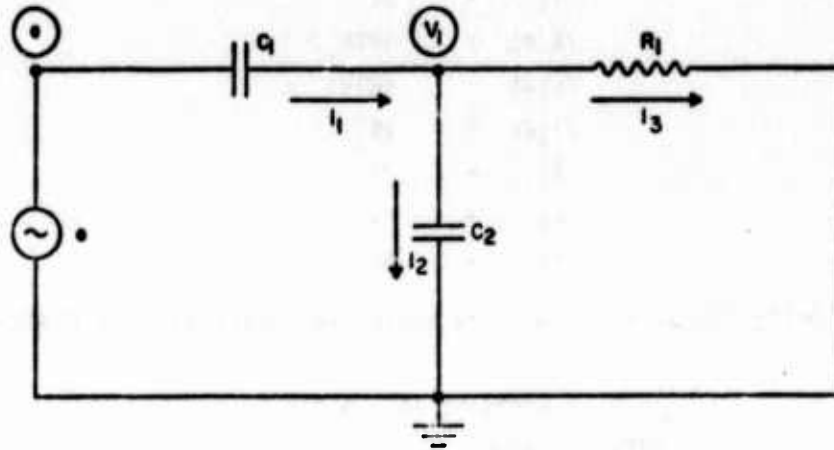


Figure 3: Equivalent Circuit for Lead Network with Diaphragm

The system of equations may be reduced to

$$\begin{cases} i_1 dt = \frac{1}{R_1} \int v_1 dt + C_2 v_1 \\ v_1 = e - \frac{1}{C_1} \int i_1 dt \end{cases}$$

The value of the capacitance of this diaphragm (ref 6) is expressed as

$$C_1 = \frac{K_1^3}{(\int i_1 dt)^2}$$

where K_1 is a constant.

Substituting C_1 into the system of equations

$$\begin{cases} \int i_1 dt = \frac{1}{R_1} \int v_1 dt + C_2 [e - (\int i_1 dt / K_1)^3] \\ v_1 = e - (\int i_1 dt / K_1)^3 \end{cases}$$

This system of equations may be solved simultaneously in DSL/90, using the INTRGL block and the IMPL function. A SINE function is used to produce the sinusoidal voltage source, e . These equations may be coded in DSL/90.

In DSL/90 it is possible to define variables in a notation close to that used in the actual systems equations. For this case, the following equivalences are defined:

e	→	E
v ₁	→	V1
i ₁	→	I1
∫E dt	→	INTE
∫v ₁ dt	→	INTV1
∫i ₁ dt	→	INTI1
R ₁	→	R1
C ₁	→	C1
K ₁	→	K1

The following DSL/90 equations are expressed essentially in FORTRAN format:

```

E = AMP*SINE (0., W,0.)
INTE = INTEGRAL (0.,E)
INTI1 = IMPL (0., .0001, FY)
FY = INTV1/R1 + C2* (E - (INTI1/K1)**3)
INTV1 = INTEGRAL (0., V1)
V1 = E - (INTI1/K1)**3

```

5.2 Lag-Lead Network with Diaphragm Shunted by Capillary in DSL/90

A lag-lead network with a diaphragm may be developed from the lead network (fig. 2) by shunting the diaphragm with a capillary (fig. 4).

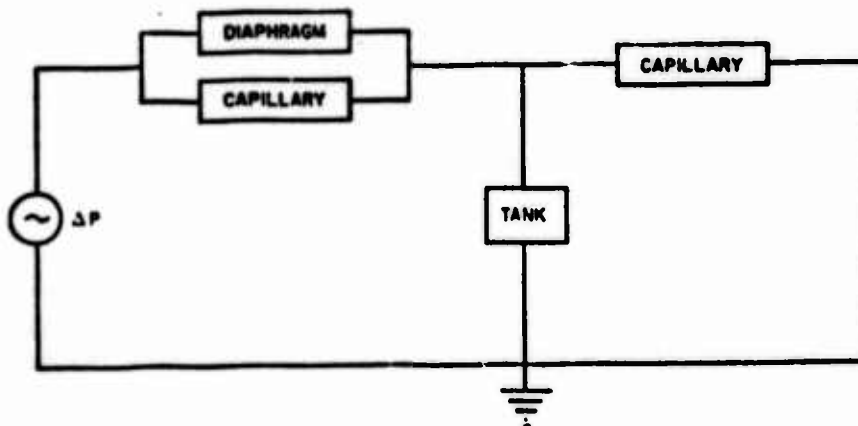


Figure 4: Lag-Lead Network

The equivalent circuit for this lag-lead network follows (fig. 5).

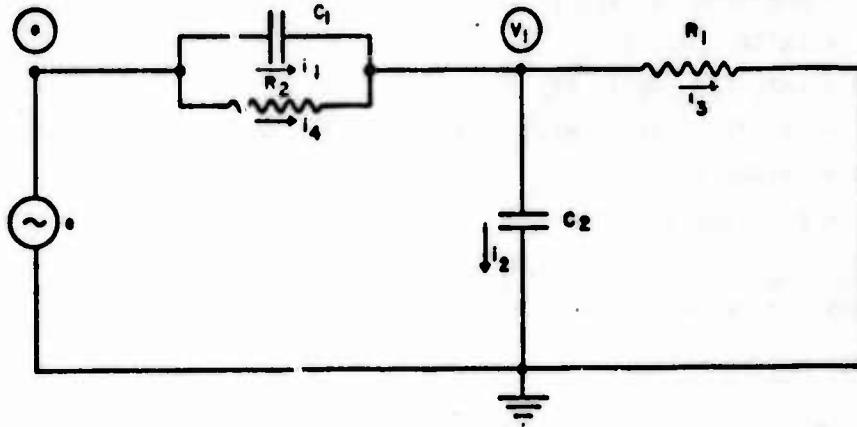


Figure 5: Equivalent Circuit for Lag-Lead Network

Setting up the circuit equations for DSL/90 yields

$$\begin{cases} i_1 dt = \left(\frac{1}{R_1} + \frac{1}{R_2}\right) v_1 dt + C_1 v_1 + \frac{1}{R_2} e dt \\ v_1 = e - \frac{1}{C_1} \int i_1 dt \end{cases}$$

where the nonlinear capacitance is again

$$C_1 = \frac{\int i_1^3 dt}{(\int i_1 dt)^2}$$

so that

$$\begin{cases} \int i_1 dt = \left(\frac{1}{R_1} + \frac{1}{R_2}\right) \int v_1 dt + C_2 \left[e - \left(\frac{\int i_1 dt}{K_1}\right)^3 \right] + \frac{1}{R_2} \int e dt \\ v_1 = e - \left(\frac{\int i_1 dt}{K_1}\right)^3 \end{cases}$$

The SINE function is again used to produce the sinusoidal input voltage, e .

In this case the equivalences between the systems equations and the DSL/90 notation are identical to the equivalences in section 5.1. One additional equivalence is

$$R_2 \rightarrow R2.$$

In DSL/90 the equations are coded as

```
E      = AMP*SINE (0.,W,0.)
INTE   = INTGRL (0., E)
INTI1  = IMPL (0, .0001, FY)
FY     = (1./R1+ 1./R2)*INTV1 + C2* (E - INTI1/K1)**3) - INTE/R2
INTV1  = INTGRL (0., V1)
V1     = E - (INTI1/K1)**3
```

If might be observed that if shunt resistor $R2 = \infty$, then the shunted case reduces to the unshunted case (sect. 5.1).

6. COMPUTER MODELS IN SLIC

SLIC (ref 3) is a simple, inexpensive program that is primarily a linear ac circuit analysis program. However, by modifying a few selected FORTRAN subroutines, it is possible to model (1) resistors with first-order dependence on volume flow and (2) resistors and capacitors with frequency dependence.

6.1 Standard Element Models in SLIC

The standard elements (table II) in SLIC, which are of concern in a fluidic circuit analysis package, are linear voltage sources, linear current sources, linear resistors, linear capacitors, and linear inductors.

TABLE II: Standard Elements in SLIC

Element		Card Format		
1. Voltage source	Vn	a	b	Value
2. Current source	In	a	b	Value
3. Resistor	Rn	a	b	x_r y_r z
4. Capacitor	Cn	a	b	x_c y_c z
5. Inductor	Ln	a	b	Value

where

a = input node number
b = output node number
n = alphanumeric name designating a particular element

and for

z = 0 (the linear case)
 x_r = linear value of resistance
 x_c = linear value of capacitance

and for

- $z = 1$ (the nonlinear resistive case)
- $x_r =$ linear value of resistance
- $y_r =$ coefficient of first-order term of resistance

and for

- $z = 2$ (the frequency-dependent case)
- $z_r = x_c$ and is the value of capacitance as frequency approaches zero
- $y_r = y_c$ and is the radius of a cylindrical enclosed volume.

6.2 Nonlinear Resistance in SLIC

In version C-3 of SLIC (ref 3), the values of the nonlinear resistors are computed directly as the elements of the admittance matrix is formed. In the subroutine DCANAL (for dc analysis) the nonlinear resistance, R , is of the form:

$$R = R_0 + R_1 q.$$

Using the general definition for resistance

$$R = \frac{\partial(\Delta P)}{\partial q}$$

where the nonlinear expression for R is given above, then $q(\Delta p, R_0, R_1)$ is found to be

$$q = -\frac{R_0}{R_1} + \sqrt{\left(\frac{R_0}{R_1}\right)^2 + \frac{2}{R_1} \Delta P}.$$

Substituting this into the nonlinear definition for R gives

$$R = \sqrt{R_0^2 + 2R_1 (\Delta p)}$$

SLIC is written to account for this type of nonlinearity (in terms of the voltage drop). It iteratively recalculates the value of R until the same value occurs for three successive calculations.

Nonlinear resistors are coded as data into SLIC through the resistor element card, which is of the form

$$Rn \ a \ b \ x \ y \ z$$

where n is an alphanumeric resistor name, a and b are the node numbers between which the resistor is connected, and

$$x = R_0,$$

$$y = R_1,$$

and

$$z = 1$$

where $z = 1$ indicates that the resistor is of the nonlinear form

$$R = R_0 + R_1 q.$$

6.3 Frequency-Dependent Capacitance in SLIC

The frequency-dependent capacitor is implemented in new subroutines called by the subroutine ACANAL (for ac analysis) of the SLIC program. The cylindrical frequency-dependent enclosed volume is shown to be a capacitor shunted by a resistor (ref 7)

$$C = C_r,$$
$$R = \frac{1}{\omega C_i},$$

where C_r and C_i are the real and imaginary parts of Katz's complex expression for capacitance (ref 8).

The frequency response analysis is initiated in the subroutine ACANAL as the desired frequency range is swept. If the capacitor-resistor pair is frequency dependent, then the values (C_r and C_i) are calculated in special fluidic subroutines FDVLC and FDVLR respectively.

The frequency-dependent capacitor-resistor pair is coded into SLIC as data on a capacitor card and a resistor card of the form

Cm a b x y z

Rn a b x y z

where m and n are alphanumeric names of the capacitor and resistor, respectively; a and b are the numbers of the nodes between which the parallel capacitor resistor pair are connected; x is the capacitance value of an identical capacitor for the adiabatic case

$$x = \frac{v}{\gamma p_0}$$

y is the radius of the cylindrical volume; and z is 2. Here, v is the volume of the cylindrical volume, p_0 is the reference static pressure, and γ is the ratio of specific heats.

When $z = 2$, the SLIC program treats the capacitance and resistance as frequency-dependent components.

6.4 Lead-Lag Network in SLIC

A simple lead-lag network is represented as an equivalent circuit in figure 6.

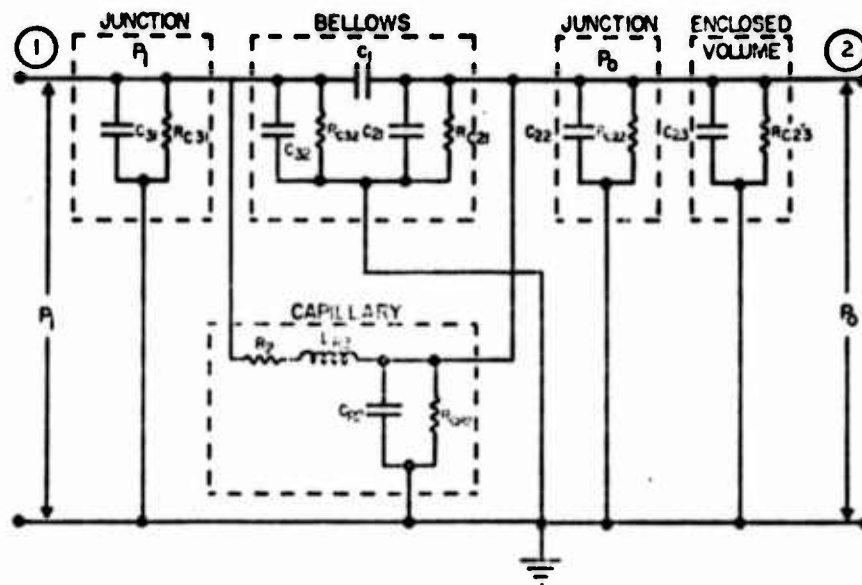


Figure 6: Lead-Lag Network.

To implement the lead-lag circuit (fig. 6) in SLIC, the following steps are taken:

- (1) The pressure source, p_i , is simulated by VI between nodes 1 and 0 in figure 7.
- (2) Capacitors, which shunt the pressure source, are taken as part of the pressure source. Therefore, elements C_{31} , R_{C31} , C_{32} , R_{C32} do not appear in figure 7.
- (3) An RLC model of a load capillary and a small resistor, R_B , are added between nodes 2 and 0. Only R_B , R_1 and L_{R1} appear in figure 7.
- (4) Remaining parallel resistors and parallel capacitors are combined as equivalent resistors and capacitors evaluated as

$$R_{C2} \equiv \frac{1}{\frac{1}{R_{C21}} + \frac{1}{R_{C22}} + \frac{1}{R_{C23}}}$$

$$C_2 \equiv C_{21} + C_{22} + C_{23}.$$

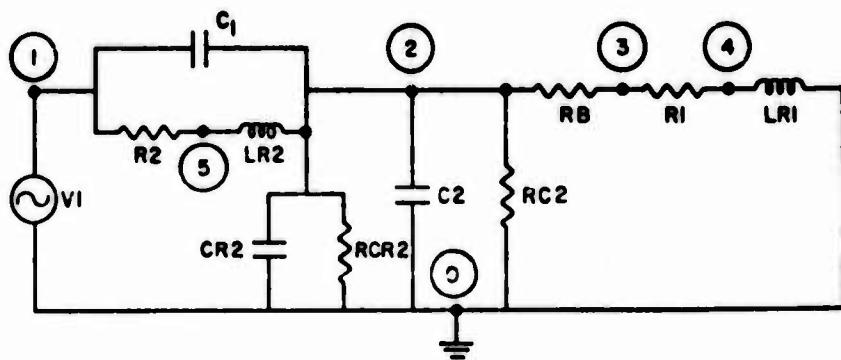


Figure 7: Lead-Lag Network Prepared for SLIC Program

Considering nonlinearities in the capillaries and frequency dependence in the enclosed volumes within the bellows, enclosed volume, junctions, and capillary, the SLIC input program is of the form:

```

GAIN  02 00 01 00 AC
FREQ  fn f1 f2
V1    01 00      (value of voltage)
C1    01 02      (value of capacitance)
C2    02 00      (value of capacitance) (radius)          2.
RC2   02 00      (value of capacitance) (radius)          2.
R2    01 05      (linear coefficient) (first-order coefficient) 1.
LR2   05 02      (value of inductance)
CR2   02 00      (value of capacitance) (radius)          2.
RCR2  02 00      (value of capacitance) (radius)          2.
RB    02 03      (small value, e.g. .001)
R1    03 04      (linear coefficient) (first-order coefficient) 1.
LR1   04 00      (value of inductance)
END

```

7. NET-2

NET-2 (ref 5) is more convenient and versatile for studying fluidic circuits than any other circuit analysis program. Three factors contribute to its convenience and versatility. First, nonlinear components may be described in NET-2, so that all response calculations are simultaneous solutions. Second, the values of the elements in the equivalent circuit models may be entered as numbers, as parameters, as algebraic expressions or as tables. Third, a modular hierarchy may be established with defined models and stored models. In the hierarchy of models, large models may be assembled from both individual element representations and basic models.

In this section, standard NET-2 elements are listed. Basic nonlinear resistors, nonlinear capacitors, and nonlinear inductors are built up. Basic models of fluidic capillaries, enclosed volumes, bellows/chambers, diaphragm/chambers, and laminar proportional amplifiers are described. Finally, a few simple networks are set up in NET-2.

It is important to recognize that while NET-2 can solve sophisticated network problems, computational costs of this system reflect both the amount of core memory and the running time it requires. No direct checks have yet been run on comparative costs between NET-2 solutions to fluidic networks and solutions used with other programs, including SLIC. In general, it may be assumed that NET-2 runs a problem faster. However, the greater sophistication of NET-2 might be used when less sophisticated models would be adequate. The use of sophisticated models may increase the relative cost of NET-2 solutions, for example, over SLIC solutions by factors from 1.5 to 10.

7.1 Standard Elements in NET-2

A total of 16 elements of current interest are available in release 8 of NET-2 (ref 5). Each of the following standard elements is designated both by a type name and by a number for that type. The nodes to which it is connected and its value are specified. Table III summarizes the standard NET-2 elements.

TABLE III: Standard Elements in NET-2

1. Voltage source	Vn	a b Value, r
2. Current source	In	a b Value
3. Resistor	Rn	a b Value
4. Capacitor	Cn	a b Value
5. Inductor	Ln	a b Value
6. Switch	Sn	a b Value
7. Gain block	GAINn	a b Value
8. Summer	SUMn	b $\pm a_1 \pm a_2 \dots$
9. Integrator	INTn	a b g
10. Differentiator	DERIVn	a b
11. Multiplier	MULTn	b $\pm a_1 \pm a_2 \dots$
12. Limiter	LIMn	a b Value
13. Voltage controlled conductance	VCGn	e f a b g
14. Voltage controlled voltage source	VCVSn	e f a b g, r
15. Voltage controlled current source	VCCSn	e f a b g
16. Voltage controlled conductance defined by table look-up	XMODn	8 1 a b //TABLEm

where

- a, a_1 are input node names
- b is an output node name
- e, f are differential control node pairs
- g is a gain value
- m is a number designating a particular table
- n is a number designating a particular element
- r is the value of internal resistance

7.2 Basic Nonlinear Components in NET-2

In NET-2, nonlinearities may be written directly into the expressions that define "value" of the components. In NET-2 (release 8), if the "value" is defined by a nonlinear expression (in terms of a dependent response variable), simultaneity of solution will be sacrificed.

However, by using the simulation elements (7-12, Table III) and the table look-up in conjunction with the voltage controlled elements (13-16, Table III), the nonlinear expressions may be rephrased so that simultaneous solutions are obtained.

For the fluidic components described in succeeding sections, it is necessary to develop nonlinear resistors, nonlinear capacitors and nonlinear inductors. Two nonlinear resistors, two nonlinear capacitors and one nonlinear inductor are described and modeled below. In addition, a nonlinear function generator and a switching characteristic are introduced.

Exact solutions at each point in the response calculations can be assured by appending these more sophisticated models to the existing NET-2 element models.

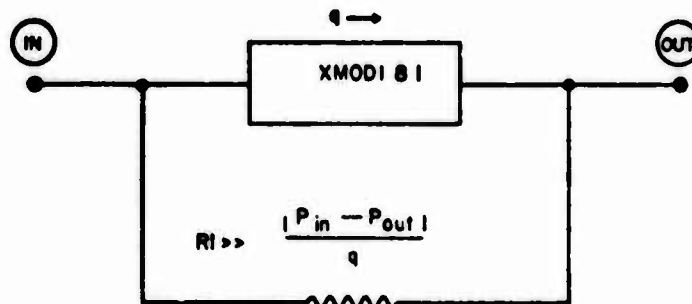


Figure 8. Nonlinear Resistor (using TABLE lookup)

NET-2 Listing

```

DEFINE  RNL1      IN  OUT
XMOD1   B 1      IN  OUT//TABLE1
R1      IN  OUT  ***LARGE SHUNTING RESISTANCE, E.G., 10+10***
TABLE1
***VALUE OF VOLTAGE***  ***VALUE OF CURRENT***

```

7.2.1 Nonlinear Resistor (general nonlinearity through table look-up)

A general nonlinear resistance value is set up with a voltage controlled conductance in conjunction with a table look-up. A table look-up is implemented with a special block, currently designated as XMODn (eXternal computer MODel). This particular XMOD is a nonlinear resistor in which voltage and current are tabular functions that are defined in TABLEm. The schematic is shown in figure 8. A resistor, R1, shunts XMOD1 to maintain a finite total resistance. The conductance of VCG1 is defined in TABLE1, in which the differential voltage ($V_{IN} - V_{OUT}$) is entered and the current q selected. (Note that the voltage difference, which is the independent variable, is arranged monotonically from smaller to larger values). A typical defined model, designated as RNL (Resistance, Non-Linear with a Table look-up) is given in figure 8.

7.2.2 Nonlinear Resistor (with flow nonlinearity using VCG)

A nonlinear resistance value that occurs frequently in fluidic components has the form

$$r = f(q).$$

A resistor of this form is implemented computationally in NET-2 with a voltage-controlled conductance (VCG). The schematic is given in figure 9.

Resistance is established in VCG1. The flow is metered in R1 and evaluated at node 3. Nonlinear functions are introduced at node NL. The conductance, calculated and evaluated at node 10, is applied to VCG1 between node pairs 10 and 0.

A typical defined model, designated as RNLVCG (Resistance, Non-Linear with a VCG), is shown in figure 9.

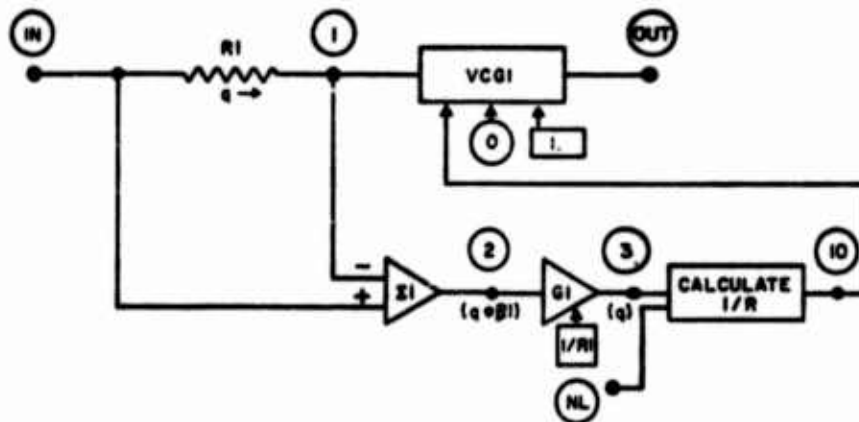


Figure 9. Nonlinear Resistor (using VCG as a function of through flow)

NET-2 Listing

```
DEFINE      RNLVCG      IN  OUT  0      NL
R1         IN      1      ***SMALL METERING RESISTANCE, E.G., .001***
VCG1      10      0      1      OUT, 1.
SUM1       2      +IN    -1
GAIN1      2      3      1./R1
```

7.2.3 Nonlinear Function Generator (general nonlinearities through table look-up)

To implement many of the nonlinear functions, a general nonlinear function generator is needed. In release 8 of NET-2, the sole mechanism for producing a general nonlinear relationship (while maintaining simultaneous solutions) is the use of a table look-up. By incorporating the table look-up with the voltage-controlled conductance in the XMOD form (an ex computer model in NET-2) a general nonlinear function generator is modeled. A schematic of the model is shown in figure 10.

The input function is given at node IN. It is necessary to generate a specific function at node OUT so that

$$V_{OUT} = f(V_{IN}) .$$

A voltage-controlled conductance of the form, XMOD1, has approximately the voltage drop, V_{IN} , across it. TABLE1 defines the current, i , through XMOD1 so that the numerical value of i is equal to the required value $V_{OUT} = f(V_{IN})$.

A metering resistor, R_1 (fig. 10), is defined to be much smaller than any resistance attained in XMOD1.

$$R_1 \ll R(XMOD1) .$$

Current i , through XMOD1 is approximately given as

$$i(XMOD1) = \frac{V_{IN} - V_1}{R_1} .$$

Elements SUM1 and GAIN1 set the voltage at node OUT numerically equal to the current (the desired functional relationship), through the voltage-controlled conductance. This nonlinear function generator, defined as FGFLT (Function Generator, NonLinear with a Table look-up), is given in NET-2 in figure 10.

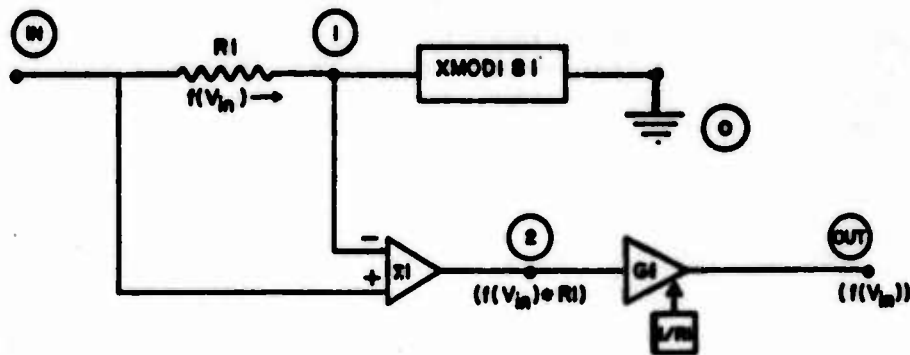


Figure 10. Nonlinear Function Generator (function of node voltage through TABLE lookup)

NET-2 Listing

```

DEFINE  FGNL      IN  OUT
R1      IN      1    ***SMALL METERING RESISTANCE, E.G., .001***
XMOD1  8      1    1    O//TABLE1
SUM1    2      +IN  -1
GAIN1   2      OUT  1./R1
TABLE1
***VALUE OF VIN***    ***VALUE OF F(VIN)***

```

7.2.4 Nonlinear Grounded Capacitor (using flow differencer and Integrator)

A nonlinear grounded capacitor is modeled with a flow differencer and an integrator. For grounded capacitors in fluidics, the relationship between the pressure drop, Δp , (compared to a reference pressure) and the volume flow, q , is of the form: (ref 9)

$$\Delta p \equiv p - p_0 = \frac{1}{C} \int \Delta q dt.$$

When C is a nonlinear function of the nodal pressure, a nonlinear approach is useful. The differential flow is found by subtracting the flow passing out of the capacitor from the flow entering the capacitor. The model that implements the nonlinear grounded capacitor is shown in figure 11.

Resistors R_1 and R_2 meter the input and output flows, respectively. With summers and gain blocks, the voltage at node 5 is equal to the output flow to ground ($q_1 - q_2$). Node 6 is the integrated value of node 5. A nonlinear function for C is introduced at node NL. The pressure at node MID is computed. The NET-2 listing is shown in figure 11. Here, the non-

linear grounded capacitor is defined in the model CNLG (Capacitance, Non-Linear Grounded).

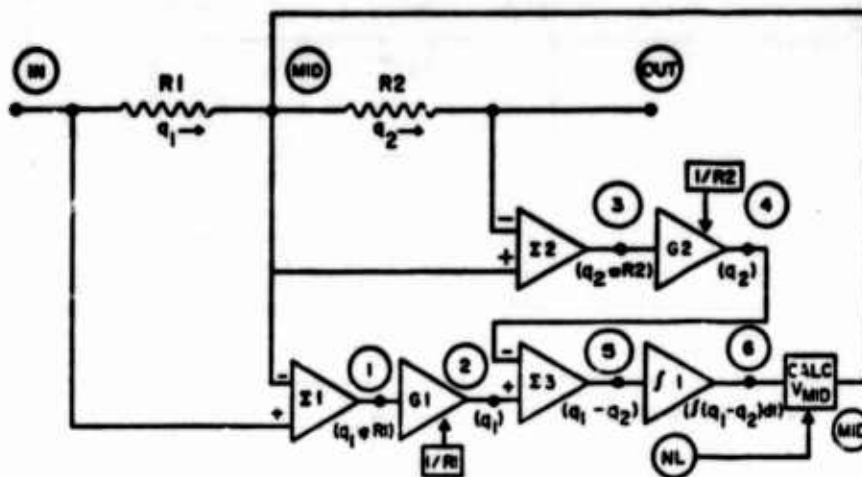


Figure 11. Nonlinear Grounded Capacitor (using flow differencer and integrator)

NET-2 Listing

```

DEFINE  CNLG      IN  OUT  D  NL
R1      IN  MID  ***SMALL METERING RESISTANCE, E.G., .J01***
R2      MID  OUT  ***SMALL METERING RESISTANCE, E.G., .J01***
SUM1    1      +IN  -MID
GAIN1   1      2    1./R1
SUM2    3      +MID -OUT
GAIN2   3      4    1./R2
SUM3    5      +2   -4
INT1    5      6

```

7.2.5 Nonlinear Grounded Capacitor (using flow differencer, Integrator and table look-up)

The nonlinear capacitor discussed above may be used in conjunction with a table look-up through the nonlinear function generator (sect. 7.2.3). The schematic of this simulation is shown in figure 12. The computation is identical to the more general model, CNLG, as far as the output of INT1 (node 6). The function generator with table look-up (FGNL) is connected at node 6. The output of the nonlinear function generator establishes the voltage at node MID.

The NET-2 listing for this nonlinear capacitor (CNLGT-Capacitor, NonLinear Grounded with Table look-up) is shown in figure 12.

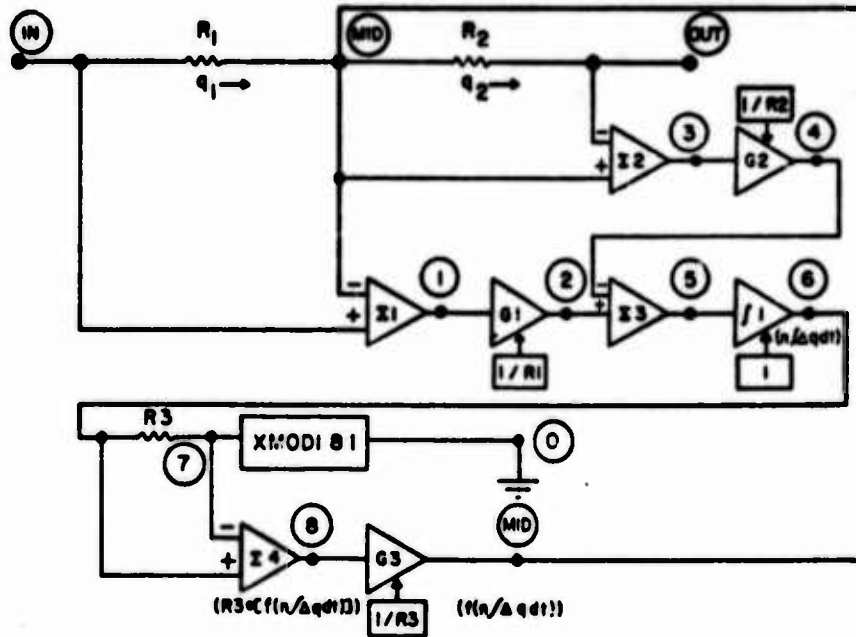


Figure 12. Nonlinear Grounded Capacitor (using flow differencer, integrator, and TABLEm lookup)

NET-2 Listing

```

DEF INE  CNLGT      IN  OUT  0
P1      ***VOLUME***
PI35    ***POLYTROPIC COEFFICIENT***
R1      IN  MID  ***SMALL METERING RESISTANCE, E.G., .001***
R2      MID  OUT ***SMALL METERING RESISTANCE, E.G., .001***
SUM1    1      +IN  -MID
GAIN1   1      2      1./R1
SUM2    3      +MID -OUT
GAIN2   3      4      1./R2
SUM3    5      +2    -4
INT1    5      6      PI35
R3      6      7      ***SMALL METERING RESISTANCE, E.G., .001
XMOD1   8      1      7      O//TABLE1
SUM4    8      +6    -7
GAIN3   8      MID  1./R3
TABLE1
***N*(INT(QIN-QOUT)DT)***      F(N*(INT(QIN-QOUT)DT))***

```

7.2.6 Nonlinear Point-to-Point Capacitor (using type -1 RC mutator)

A nonlinear point-to-point capacitor is modeled with a type -1 RC mutator (Chua, ref 10). The approach used above for the grounded capacitor is unsatisfactory because neither the input nor the output of a point-to-point capacitor is at the reference pressure. A mutator is in the class of a more general two-port (four-terminal) device--the gyrator. In essence, voltage and current functions may be interchanged within the gyrator.

To form a nonlinear point-to-point capacitor, C , with the same value as $\frac{k}{R}$ (where $k = 1$ in units of time), a type-1 RC mutator is used. A nonlinear resistor, R , is used, as well as controlled-voltage sources and controlled-current sources. The RC mutator is a two-port black box (fig. 13).

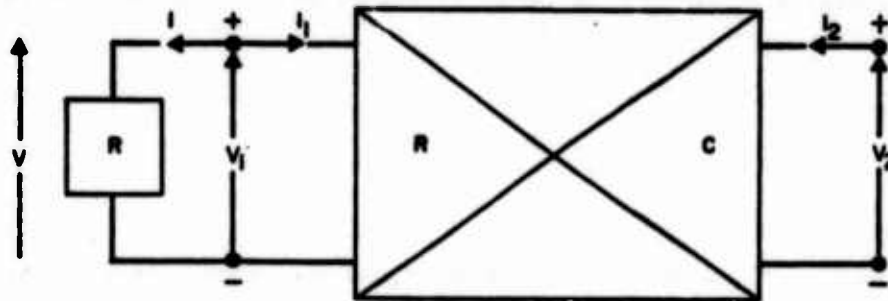


Figure 13. Nonlinear Capacitor Using Type-1 RC Mutator

For the resistor, R , Ohm's law gives

$$v = Ri$$

where

$$v \equiv v_1$$

and

$$i \equiv -i_1$$

so that

$$v_1 = -Ri_1$$

A capacitance-type relationship between v_2 and i_2 is required so that

$$v_2 = \frac{1}{C} \int i_2 dt .$$

Equating $\frac{1}{C}$ and $\frac{R}{k}$

$$\frac{1}{C} \equiv \frac{R}{k}$$

and substituting for $\frac{1}{C}$ from the differential equation and R from Ohm's law:

$$\frac{v_2}{\int i_2 dt} = \frac{v_1}{-ki_1} .$$

Then the numerators may be equated and the denominators may be equated:

$$\begin{cases} v_2 = v_1 \\ \int i_2 dt = -ki_1 \end{cases} .$$

Differentiating the second equation with respect to t gives the pair of equations:

$$\begin{cases} v_1 = v_2 \\ i_2 = -k \frac{di_1}{dt} \end{cases} .$$

Thus, relationships for a type -1 RC mutator have been derived. In figure 14, R can be driven by a controlled-voltage source, $v_1 = v_2$, and $\frac{1}{C}$ can be driven by a controlled-current source, $i_2 = -k \frac{di_1}{dt}$.

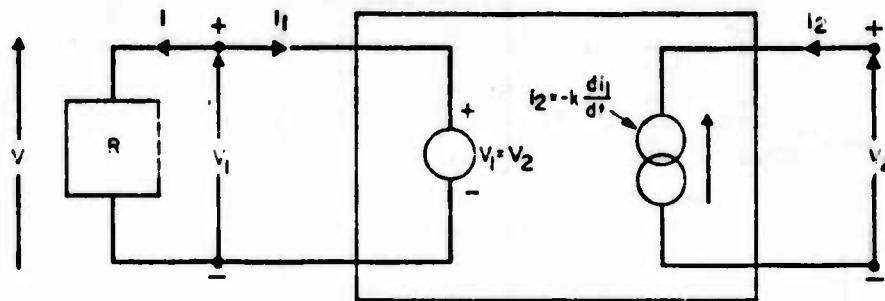


Figure 14. Schematic of Type-I RC Mutator as Capacitor

The value of $\frac{1}{C}$ can thus be set equal to the value of $\frac{R}{k}$ (where $k = 1$).

The NET-2 model that simulates this nonlinear capacitor is shown in figure 15. The main body of this RC mutator is the voltage-controlled voltage source, VCVS1, and the voltage-controlled current source, VCCS1. The calculated nonlinear capacitance value, C, is introduced at node NL. The voltage-drop relationship between V_{IN} and V_{OUT} is implemented as the output of SUM1 at node 1 (referenced to ground) controls VCVS1. The relationship between i_1 and i_2 is set up by metering the input current into VCVS1 with resistor R_1 , calculating i_1 with SUM2 and GAIN1, and differentiating it in DERIV1. Node 6 at the output of DERIV1 (referenced to ground) controls VCCS1.

The element VCCS1 in this mutator serves as the nonlinear capacitor. In figure 15, the nonlinear point-to-point capacitor (defined as a model in NET-2) is called CNLPP (Capacitance, NonLinear Point-to-Point).

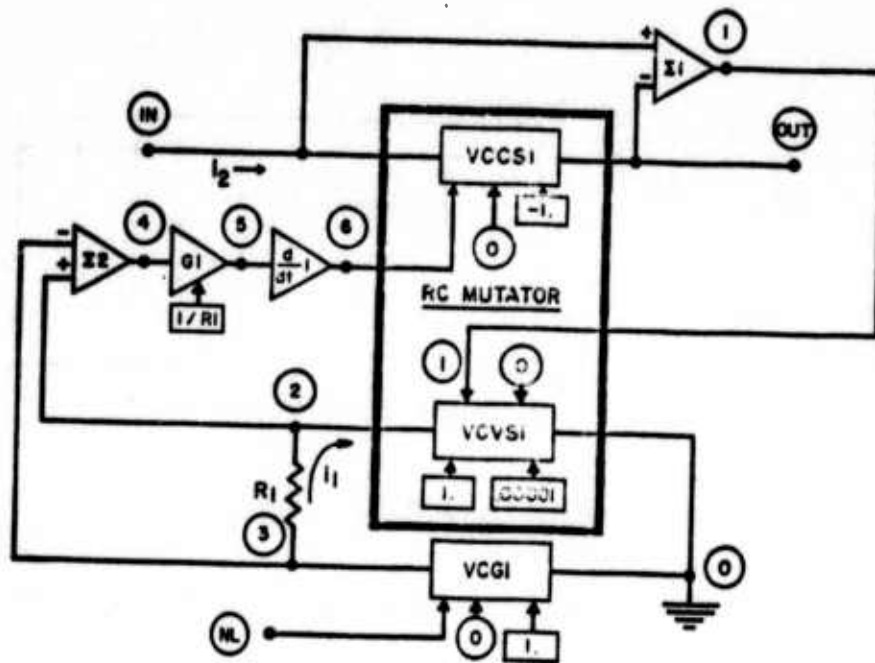


Figure 15. Nonlinear Capacitor (using Type-1 RC mutator)

NET-2 Listing

```

DEFINE  CNLPP  IN  OUT  0  NL
VCCS1  6  0  IN  OUT  -1.
SUM1  1  +IN  -OUT
VCG1  NL  0  3  0  1.
VCSV1  1  7  2  0  1.  ***SMALL INTERNAL RESISTANCE,
                               F.G., .00001***

R1  2  3  ***SMALL METERING RESISTANCE, E.G., .001***
SUM2  4  +2  -3
GAIN1  4  5  1./R1
DERIV1  5  6

```

7.2.7 Nonlinear Inductor (using type-1 RL mutator)

As in the case of the nonlinear point-to-point capacitor, a nonlinear inductor is modeled with a mutator. For the nonlinear inductor, a type-1 RL mutator (Chua, ref 10) is modeled. Starting with a nonlinear resistor, R , and using the type-1 RL mutator, a nonlinear inductor, L , equal to kR (where k is unity in units of time) is to be constructed. The RL mutator is considered as a two-port block box (fig. 16).

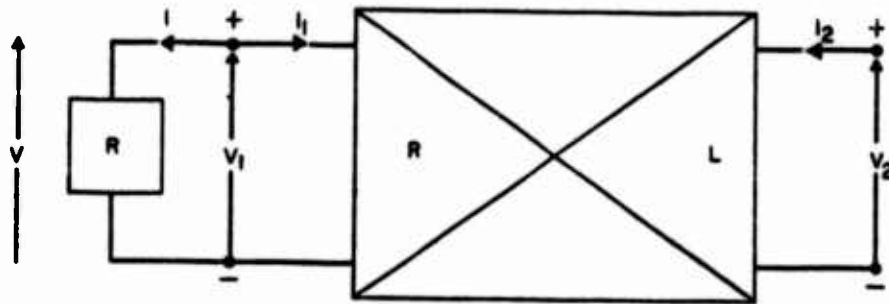


Figure 16. Nonlinear Inductor Using Type-1 RL Mutator

An Ohm's law relationship between the voltage drop, v , and the current, i , is

$$v = Ri$$

where

$$v \equiv v_1$$

and

$$i \equiv -i_1$$

so that

$$v_1 \equiv -Ri_1$$

The RL mutator must be designed to develop an inductive type relationship between v_2 and i_2 , as

$$v_2 = L \frac{di_2}{dt}$$

or

$$\int v_2 dt = L i_2$$

where L and kR have the same value

$$L \equiv kR .$$

Substituting for R from Ohm's law and for L from the integral equation:

$$\frac{\int v_2 dt}{i_2} = - \frac{kv_1}{i_1} .$$

Both the numerators may be equated and the denominators may be equated

$$\begin{cases} \int v_2 dt = kv_1 \\ i_2 = -i_1 \end{cases}$$

Differentiating the first equation with respect to t gives the pair of equations

$$\begin{cases} v_2 = k \frac{dv_1}{dt} \\ i_1 = -i_2 \end{cases}$$

This gives the necessary relationships for a type -1 RL mutator. As shown in figure 17, R can be driven by a controlled-current source, $\frac{dv_1}{dt}$, $i_1 = -i_2$, while L can be driven by a controlled voltage source, $v_2 = k \frac{dv_1}{dt}$.

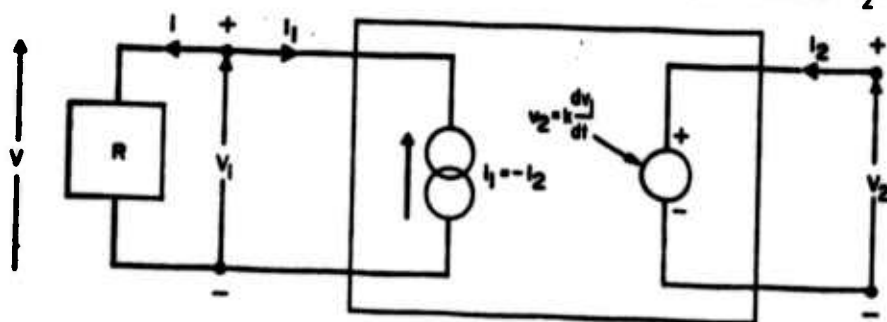


Figure 17. Schematic of Type-1 RL Mutator as Inductor

The value of L can therefore be equated to the value of R (where $k = 1$). A NET-2 simulation model of this nonlinear inductor is shown in figure 18.

The mutator itself is a voltage-controlled voltage source, VCVS1, and a voltage-controlled current source, VCCS1. Node NL is set at a voltage corresponding to the reciprocal of the value of the nonlinear inductor, $1/L$. The value of i_1 is set by metering the current i_2 through R_1 with SUM1 and GAIN1. Node 3 at the output of GAIN1 controls VCCS1, which has the gain of -1.0 . The relationship between V_2 and V_1 is calculated with DERIV1, the output of which (node 5) controls VCVS1. In this mutator, VCVS1 serves as the nonlinear inductor.

In NET-2, the nonlinear inductor (fig. 18) is defined as the model, LNL (for Nonlinear inductor).

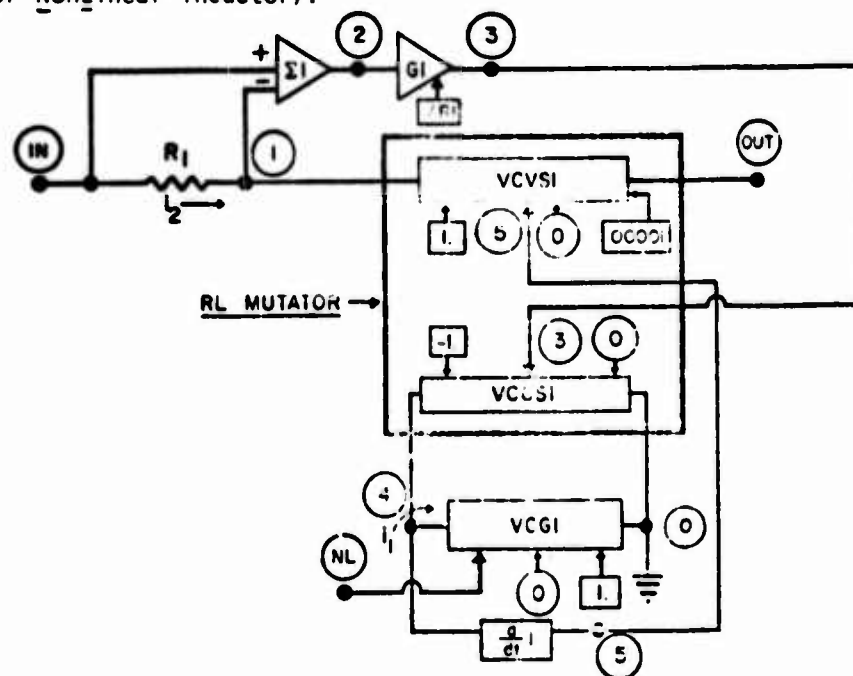


Figure 18. Nonlinear Inductor (Using type-1 RL Mutator)

NET-2 Listing

DEFINE	LNL	IN	OUT	0	NL
R1	IN	1	***SMALL METERING RESISTANCE, E.G., .001***		
SUM1	2	IN	-1		
GAIN1	2	3	1./?1		
VCVS1	5	0	1	0	1. ***SMALL INTERNAL RESISTANCE, E.G., .00001***
VCCS1	3	0	4	0	-1.
VCGI	NL	0	4	0	1.
DERIV1	4	5			

7.2.8 Switching Characteristic (actuated by node voltage using biased limiters)

When the response variables are introduced into the standard NET-2 switch element, the solution simultaneity breaks down. Therefore the following approach is useful for preserving simultaneity. A typical switching characteristic from low to high is shown in figure 19--when the independent variable x (in this case, a node voltage) equals x_1 , the value of y is switched from y_1 to y_2 .

A simulation schematic is diagrammed in figure 19. The difference between the voltage x at node IN and the switching value x_1 at node 1 are obtained in SUM1 at node 2. The difference $(x-x_1)$ is amplified with a high positive gain in GAIN1 and limited at $\pm(y_2 - y_1)/2$ in LIM1. Thus at node 4, y switches between $\pm(y_1 - y_2)/2$ at $x = x_1$. Then the level can be set by adding $(y_1 + y_2)/2$ at node 5 to node 4 in SUM2 to give the output at node OUT.

The NET-2 listing for this model, called SWITCH, is given in figure 19. To switch from high to low, the slope is made negative either by performing the difference $(x_1 - x)$ or using a high negative gain in GAIN1.

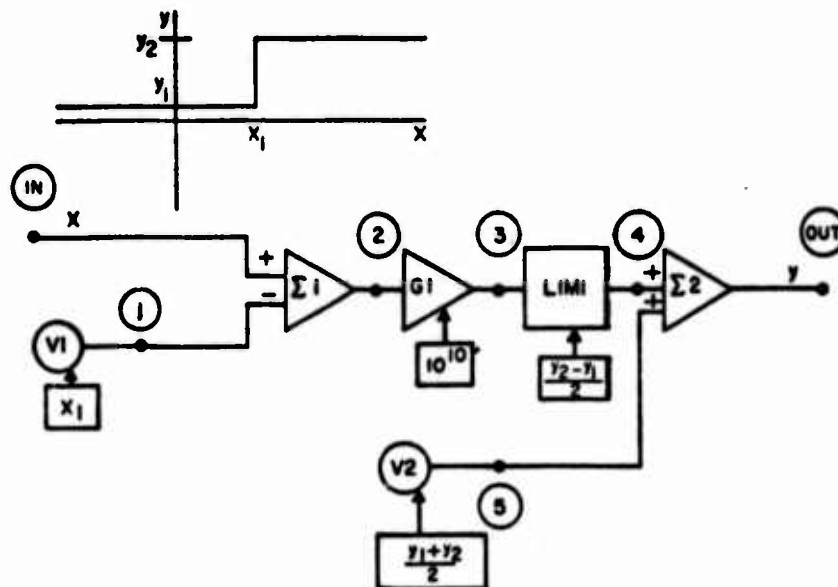


Figure 19. Switching Characteristic (actuated by node voltage and biased limiters)

NET-2 Listing

```
DEFINE      SWITCH      IN      OUT
V1          1           0      ***VALUE OF X1***
SUM1        2           +IN    -1
GAIN1       2           3      ***HIGH GAIN, E.G., 10+10***
LIM1        3           4      ***VALUE OF (Y2-Y1)/2.***
V2          5           0      ***VALUE OF (Y1+Y2)/2.***
SUM2 (OUT)  +4          +5
```

7.3 Basic Fluidic Components in NET-2

The basic fluidic components are defined in NET-2. Using the standard forms of the NET-2 elements as well as the nonlinear simulations described in section 7.2, several computational models of the capillary, enclosed volume, bellows, diaphragm, and laminar proportional amplifier components are constructed.

The values of the elements in the components are defined parametrically in expressions. In NET-2 all parameters are designated in the form "Pn", where n takes on a different integral value for each parameter. Certain fluid parameters are included in the several component models. These are designated as

P101 $\pi = 3.14159$
P102 ρ , mass density
P103 μ , dynamic viscosity
P104 ν , kinematic viscosity
P106 p_0 , ambient static pressure
P107 $\begin{cases} 0 \\ 1 \end{cases}$, dummy variable for $\begin{cases} \text{static case} \\ \text{dynamic case} \end{cases}$
P108 β , inertance coefficient

7.3.1 Capillary Component with Linear Resistance, Inertance, and Capacitance

The capillary component is a bundle of N identical, parallel, circular capillaries. A possible low-frequency equivalent circuit is one lump of a transmission line (ref 11) shown in figure 20. The linear values (ref 12) of the Poiseuille Law resistance, R, (where $l/r > 100$), for the slug inertance, L, and of the compressibility capacitance, C, of a perfect gas are

$$R = \frac{8\mu l}{N\pi r^4}$$

$$L = \frac{\beta \rho l}{N\pi r^2}$$

$$C = \frac{N\pi r^2 l}{n p_0}$$

where r and l are the radius and length, respectively, for each capillary in the bundle. The constant, β , (ref 12) goes from $4/3$ at low frequencies to 1 at frequencies above 500 Hz. The polytropic coefficient, n , (ref 8) for air goes from 1.0 at low frequencies to 1.4 at high frequencies. Additional parameters in a NET-2 model are the capillary radius, P1; the capillary length, P2; and the number of parallel capillaries, P3. The nodes are called IN, MID, OUT and 0 (ground). When the capillaries are considered simple resistors, parameter P107 is 0, so that the inertance and capacitance are zero. For cases in which the dynamics are desired, P107 is set to 1. The linear, dynamic model of the capillary component in NET-2 is defined as TUBEDY (capillary with Dynamics) in figure 20.

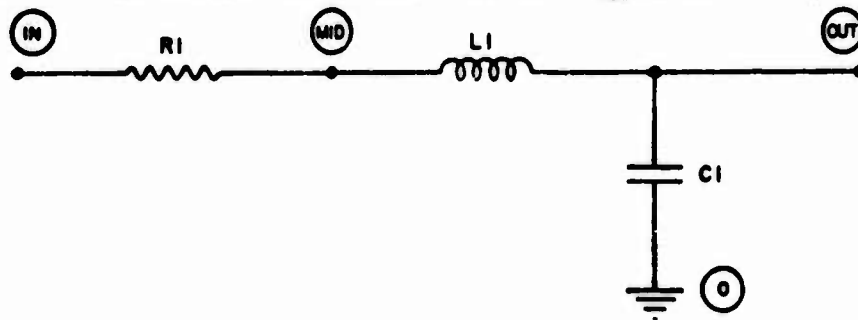


Figure 20. Capillary (Linear R, L, C Model)

NET-2 Listing

```

DEFINE  TUBEDY  IN  OUT  0
P1      ***RADIUS***
P2      ***LENGTH***
P3      ***NUMBER***
P101    ***   ***
P102    ***MASS DENSITY***
P103    ***DYNAMIC VISCOSITY***
P106    ***REFERENCE PRESSURE***
P107    ***ON-OFF SWITCH FOR DYNAMICS (0 = OFF, 1 = ON)***
P108    ***INERTANCE COEFFICIENT***
R1      IN  MID  8.*P103*P2/(P101*P1**4*P3)
L1      MID  OUT  P108*P102*P2/(P101*P1**2*P3)*P107
C1      OUT  0   P101*P1**2*P3/(P105*P106)*P107

```


7.3.2 Capillary Component with Inertance, Capacitance, and Measured Resistance

The dimensions of the capillary are critical in the calculation of the linear values of R, L, and C. Resistance is the most critical value because it is inversely proportional to the fourth power of the small and irregular capillary radius. It is often more precise to measure resistance experimentally and to use the measured numerical quantity for the defined value.

For the circuit shown in figure 21, the measured value of resistance is used in the defined NET-2 model called TUBEMR (capillary with Measured Resistance). The value of the measured dc resistance is given as P4.

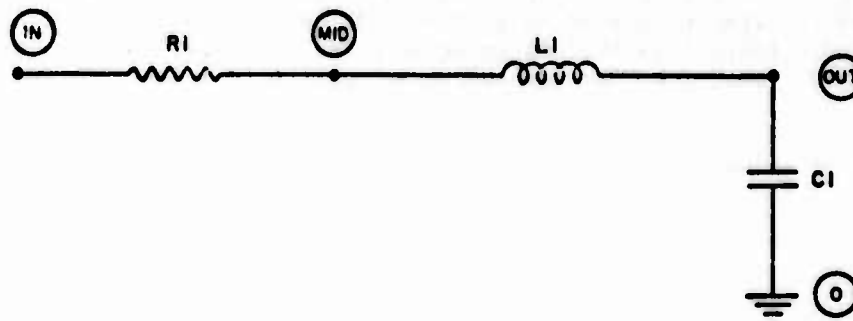


Figure 21. Capillary (Linear L and C with measured linear R model)

NET-2 Listing

```

DEFINE      TUBEMR      IN      OUT      0
P1          ***RADIUS***
P2          ***LENGTH***
P3          ***NUMBER***
P4          ***MEASURED VALUE OF RESISTANCE***
P101       ***   ***
P102       ***MASS DENSITY***
P103       ***DYNAMIC VISCOSITY***
P105       ***POLYTROPIC COEFFICIENT***
P106       ***REFERENCE PRESSURE***
P107       ***ON-OFF SWITCH FOR DYNAMICS (0 = OFF, 1 = ON)***
P108       ***INERTANCE COEFFICIENT***
R1          IN      MID      P4
L1          MID      OUT      P108*P102*P2/(P101*P1**2*P3)*P107
C1          OUT      0       P101*P1**2*P3/(P105*P106)*P107
  
```

7.3.3 Capillary with Nonlinear Resistance

If the capillary has a small length-to-diameter ratio, the end effects contribute a nonlinear term to the resistance value. According to the formulation by White (ref 13), the resistance of a capillary is expressed as

$$R = \frac{8\mu L}{N\pi r^4} + \frac{7}{6} \frac{p}{N^2 \pi^2 r^4} q$$

where q is the volume flow.

The simulation schematic and the NET-2 listing for TUBERT (capillary with Resistance given in Table look-up) are shown in figure 22. The nonlinear resistor simulated in section 7.2.1 and designated RNL1, in NET-2, is used. TABLE 1 in RNL1 is coded as pairs of values (of pressure drops, Δp_i , and flows, q_i), for the nonlinear resistor. Since $R_i = \frac{\Delta p_i}{q_i}$,

pairs of values ($\Delta p_i, q_i$) are coded into the two columns of TABLE 1.

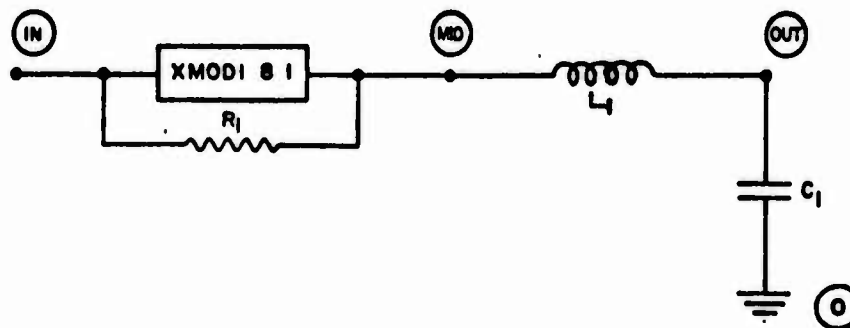


Figure 22. Capillary (Nonlinear R using TABLEm lookup)

NET-2 Listing

```
JF INF      TUBEPT      IN      OUT      0
P1          ***RADIUS***
P2          ***LENGTH***
P3          ***NUMBER***
PI01       ***
PI02       ***MASS DENSITY***
PI03       ***DYNAMIC VISCOSITY***
PI05       ***POLY TROPIC COEFFICIENT***
PI06       ***REFERENCE PRESSURE***
PI07       ***ON-OFF SWITCH FOR DYNAMICS (0 = OFF, 1 = ON)***
PI08       ***INERTANCE COEFFICIENT***
XMODL 6     1     IN     MID//TABL1
R1       IN     MID     ***LARGE SHUNTING VALUE, 100 TIMES THE LINEAR
                        PART OF R***
L1       MID     OUT     PI05*PI02*P2/(PI01*PI4*2*P3)*PI07
C1       OUT     0     PI01*PI4*2*P3/(PI05*PI06)*PI07
TABLE1
***PRESSURE DROP***          ***VOLUME FLOW***
```

7.3.4 Capillary with Nonlinear Resistance Using VCG

When the values of resistance are expressed in terms of relatively simple functions of the dependent variable (pressure drop or volume flow), the approach using a VCG is applicable.

The nonlinearity given in White's expression (ref 13) may be simulated in the schematic shown in figure 23. A NET-2 listing is given for TUBERV (capillary with a nonlinear Resistance expressed with a Voltage-controlled conductance). This approach utilizes the nonlinear form of resistance developed as the model RNLVCG (section 7.2.2).

The constant term in the resistance is calculated at node 6. The flow-dependent term is generated at node 4. The resistance is formed from the constant and flow-dependent terms that are summed in SUM2. Resistance is inverted in MULTI at node 8, which controls VCG1.

7.3.5 Enclosed Volume Component with Linear Capacitance

The enclosed volume component is a tank. The simplest equivalent circuit for the enclosed volume is a grounded, linear capacitor, shown schematically in figure 24. The linear value of capacitance (ref 8) is approximated as

$$C = \frac{v}{np_0}$$

where v is its volume. The only additional parameter required in NET-2 is $P1$, the volume. Here the input node is designated as IN . The linear model of the enclosed volume is defined in NET-2 as TKL (TanK with Linear capacitance).

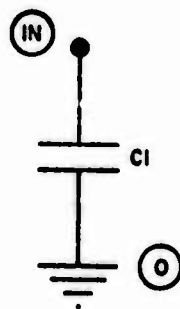


Figure 24. Enclosed Volume (Grounded, Linear C)

NET-2 Listing

```
DEFINE    TKL  IN  0
          P1   ***VOLUME***
          P105 ***POLYTROPIC COEFFICIENT***
          P106 ***REFERENCE PRESSURE***
          C1   IN  0   P1/(P105*P106)
```

7.3.6 Enclosed Volume Component (Grounded Linear C Using Integrated Differential Flow)

In working toward more complex models of the enclosed volumes, the nonlinear grounded capacitor (CNLG in section 7.2.4) is used. As a demonstration, the linear capacitance may be introduced in the form: (ref 9)

$$C = \frac{f q dt}{\Delta p}$$

The schematic (fig. 25) shows that INT1 is given a gain of the reciprocal of capacitance. The output of INT1 is a voltage at node MID. The NET-2 listing for TKINTL (TanK with INtegrator and LInear capacitance) is also given in figure 25.

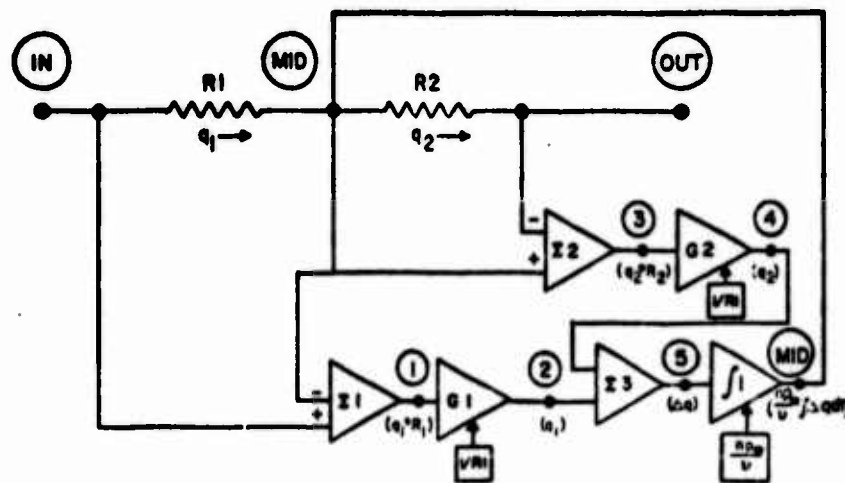


Figure 25. Enclosed Volume (grounded, nonlinear C using integrated flows)

NET-2 Listing

```

DLFINE  TRINTL  IN  OUT  0
P1      ***VOLUME***
P105    ***POLYTROPIC COEFFICIENT***
P106    ***REFERENCE PRESSURE***
R1      IN  MID  ***SMALL METERING RESISTANCE, E.G., .001***
R2      MID  OUT ***SMALL METERING RESISTANCE, E.G., .001***
SUM1    1    +IN  -MID
GAIN1   1    2    1./R1
SUM2    3    +MID -OUT
GAIN2   3    4    1./R2
SUM3    5    +2   -4
INT1    5    MID  P105*P106/P1
    
```

7.3.7 Enclosed Volume Component (grounded, linear, frequency-dependent RC)

If the frequency dependence of the polytropic coefficient in a cylindrical tank is accounted for (as by Katz, ref 8), the equivalent circuit of the enclosed volume is modeled as a grounded parallel resistor-capacitor pair. A simple simulation circuit (fig. 26) uses a voltage-controlled conductance (VCG1) for the resistor. The capacitance is represented by the linear grounded capacitor, in the form of the model CNLG. The analytic results lead to the frequency-dependent values of resistance and capacitance being represented as

$$R = \left[\frac{p}{\omega U} \frac{\gamma-1}{\gamma} \frac{\sqrt{2}}{\sqrt{\frac{\omega p C}{\kappa}} r_o} \frac{R_o R_o + I_o I_o - R_o I_o + R_o I_o}{R_o^2 + I_o^2} \right]^{-1}$$

$$C = \left[\frac{U}{p} \frac{1}{\gamma} - \frac{\gamma-1}{\gamma} \frac{\sqrt{2}}{\sqrt{\frac{\omega p C}{\kappa}} r_o} \frac{R_o R_o + I_o I_o + R_o I_o - R_o I_o}{R_o^2 + I_o^2} \right]$$

where

$$R_0 = \text{ber}_0 \sqrt{\frac{\omega p C}{\kappa}} r_0, \quad I_0 = \text{bei}_0 \sqrt{\frac{\omega p C}{\kappa}} r_0$$

$$R_1 = \text{ber}_1 \sqrt{\frac{\omega p C}{\kappa}} r_0, \quad I_1 = \text{bei}_1 \sqrt{\frac{\omega p C}{\kappa}} r_0$$

$$\text{ber}_i \sqrt{\frac{\omega p C}{\kappa}} r_0 = \text{Re} \left\{ J_i \left(j^{3/2} \sqrt{\frac{\omega p C}{\kappa}} r_0 \right) \right\}$$

$$\text{bei}_i \sqrt{\frac{\omega p C}{\kappa}} r_0 = \text{Im} \left\{ J_i \left(j^{3/2} \sqrt{\frac{\omega p C}{\kappa}} r_0 \right) \right\}$$

Im is the imaginary part of the argument

Re is the real part of the argument

J_i is the i th order Bessel function

i is 0, a positive integer or a negative integer

$$j \equiv \sqrt{-1}$$

ω = frequency in radians per sec

p = internal pressure

C_p = specific heat at constant pressure

γ = ratio of specific heats

κ = thermal conductivity

r_0 = radius of the cylinder

v = volume of the cylinder

The ber and bei functions are computed as series expansions. The functions ber_0 , bei_0 , ber_1 , and bei_1 are introduced at nodes 1, 2, 3 and 4, respectively. The reciprocal of resistance, $1/R$, is calculated at node 42, which controls VCG1. The reciprocal of capacitance, $1/C$, is calculated at node 36. The value of $1/C$ multiplies the integral of differential flow (the output of INT1 at node 17) in MULT10. The output of MULT10 is the voltage of the capacitor applied at node 11.

A listing of the defined NET-2 routine, TKFD (TanK, Frequency Dependent) is also given in figure 26.

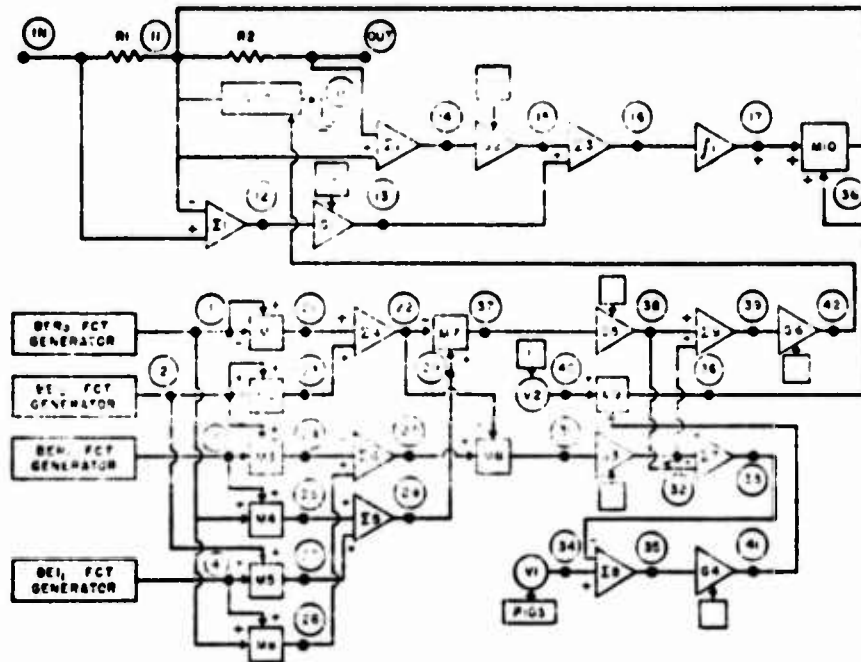


Figure 26. Enclosed Volume (cylindrical volume with frequency dependence using ber-bei generator to control grounded RC)

NET-2 Listing

```

DEFINE      TKFD IN  OUT  0
P1          ***HEIGHT OF CYLINDER***
P3          ***RADIUS OF CYLINDER***
PI01       *** **
PI05       ***RATIO OF SPECIFIC HEATS***
PI06       ***REFERENCE PRESSURE***
PI07       ***(MASS DENSITY)*(SPECIFIC HEAT AT P=CONST)/(THERMAL
CONDUCTIVITY)***

R1  IN  11  ***SMALL METERING RESISTANCE, E.G., .001***
R2  11  OUT ***SMALL METERING RESISTANCE, E.G., .001***
VCG1 42  0  11  0  1.
SUM1 12  +IN -11
GAIN1 12  13  1./R1
SUM2 14  +11 -OUT
GAIN2 14  15  1./R2
SUM3 16  +13 -15
INT1 16  17  1.
MULT10 11 +17 +3r

```

Continued on Next Page

```

***BERO FUNCTION GENERATOR CONNECTED TO (1)***
***BEID FUNCTION GENERATOR CONNECTED TO (2)***
***BERI FUNCTION GENERATOR CONNECTED TO (3)***
***BELL FUNCTION GENERATOR CONNECTED TO (4)***
MULT1 21  +1  +1
MULT2 23  +2  +2
SUM4  22  +21 +23
MULT3 24  +2  +3
MULT4 25  +1  +3
MULT5 28  +2  +4
SUM5  29  +25 +28
MULT6 26  +1  +4
SUM6  27  -24 +26
MULT7 37  -22 +24
MULT9 31  -22 +27
GAIN3 31  32  (P105-1.)/P105*SQRT(2./FREQ)/(P109*P3)
SUM7  33  -33  +38
V1    34  0    1./P105, ***SMALL INTERNAL RESISTANCE,
                                     E.G., .00001***

SUM8  35  +34  -33
GAIN4 35  41  P101*P3**2*P1/P106
V2    40  0    1., ***SMALL INTERNAL RESISTANCE,
                                     E.G., .00001***

MULT9 36  +40  -41
GAIN5 37  38  (P105-1.)/P105*SQRT(2./FREQ)/(P109*P3)
SUM9  39  +32  +38
GAIN6 39  42  2.*P101*FREQ*(P101*P3**2*P1)/P106

```

7.3.8 Bellows Module (linear array of C's)

The bellows module is a bellows in a small volume or confining cylinder. Its equivalent circuit (fig. 27) is a Pi network of capacitors.

The bellows is modeled as a point-to-point capacitor, C_1 , expressed as

$$C_1 = \frac{A^2}{k}$$

where A is the area of the circular end of the bellows and k is the spring constant of the bellows.

The volumes of the chambers adjacent of the bellows are modeled as capacitors, representing standard enclosed volumes. Their linear description is again

$$C_2 = \frac{v_{out}}{np_0}$$

$$C_3 = \frac{v_{in}}{np_0}$$

where v_{in} is the volume inside the bellows and v_{out} is the volume between the bellows and the confining cylinder. The bellows displaces very little volume, v_{out} and v_{in} . Hence, they are approximately constant in this mode.

A NET-2 listing called BELLOW is shown in figure 27. The following parameters are defined: P1 is the spring constant of the bellows; P2 and P4 are the inner radius and length of the bellows, respectively; P5 and P6 are the inner radius and height of the confining cylinder, respectively.

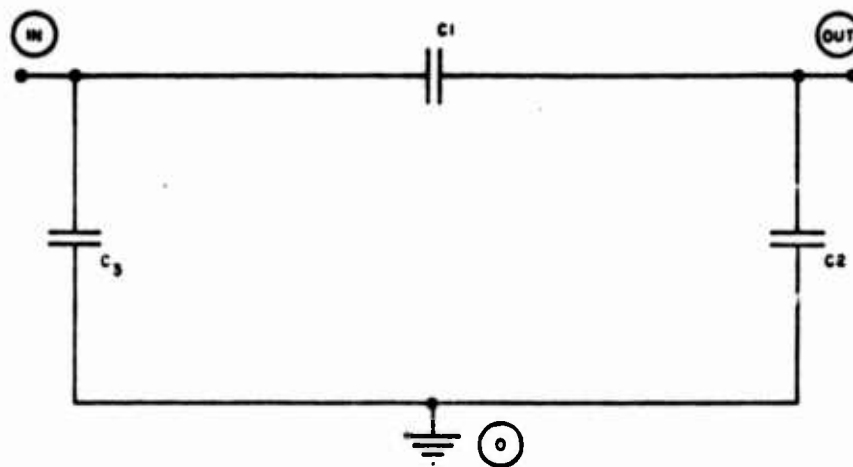


Figure 27. Bellows (Pi network with linear C's)

NET-2 Listing

```
DEFINE BELLOW IN OUT 0
P1 ***SPRING CONSTANT OF BELLOWS***
P2 ***INNER RADIUS OF BELLOWS***
P3 ***OUTER RADIUS OF BELLOWS***
P4 ***LENGTH OF BELLOWS***
P5 ***RADIUS OF CONTAINER***
P6 ***HEIGHT OF CONTAINER***
P101 *** **
P105 ***POLYTROPIC COEFFICIENT***
P106 ***REFERENCE PRESSURE***
C1 IN OUT (P101*P2**2)**2/P1
C2 OUT 0 P101*(P5**2*P6-P3**2*P4)/(P105*P106)
C3 IN 0 P101*(P3**2*P4)/(P105*P106)
```

7.3.9 Diaphragm Module (linear array of C's)

The diaphragm module is a circular membrane set between two volumes. As in the case of the bellows module, the diaphragm component (modeled in fig. 28) is a Pi network of capacitors. The diaphragm is a point-to-point capacitor expressed by Katz (ref 6) as

$$C_1 = \frac{0.362 r_o^{10/3}}{(Eh)^{1/3}} f(p).$$

where r_o , E and h are the radius, modulus of elasticity, and thickness of the diaphragm, respectively. The factor $f(p)$, a nonlinear function of the pressure drop Δp across the diaphragm, is of the form

$$f(p) = (\Delta p)^{-2/3}.$$

For simplicity, a linear constant average value can be computed for $f(p)$.

The volumes of the chambers adjacent to the diaphragm are modeled as enclosed volumes that exhibit capacitance of the form

$$C_2 = \frac{v_{out}}{np_o}$$

$$C_3 = \frac{v_{in}}{np_0}$$

where v_{in} and v_{out} are the volumes on the output and input sides of the diaphragm, respectively. As in the case of the bellows module (sect 7.3.8), volumes v_{out} and v_{in} are approximated as constants.

A NET-2 listing (fig. 28) is called DPL (DiaPhragm, Linear). The following parameters are used: P1, P2, and P3 are the radius, modulus of elasticity, and thickness of the diaphragm, P4 is the volume of the adjacent chambers, and PB is the linearization factor.

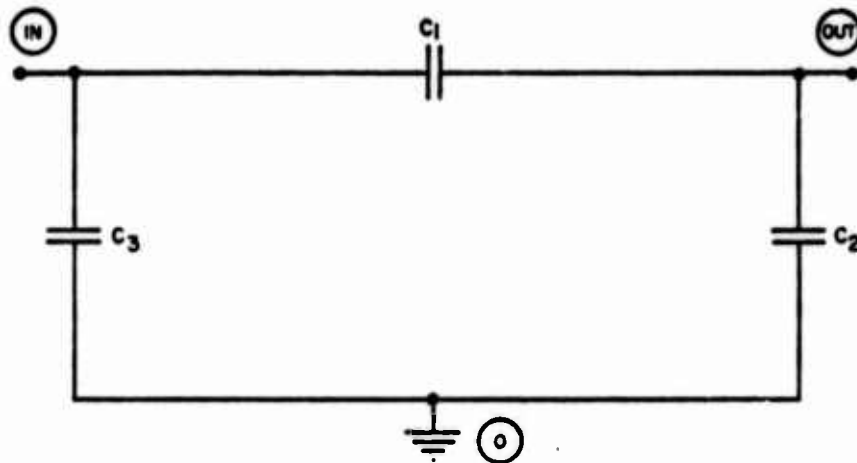


Figure 28. Diaphragm (Pi network with linear C's)

NET-2 Listing

```

DEFINE CPL IN OUT 0
P1 ***RADIUS OF DIAPHRAGM***
P2 ***MODULUS OF ELASTICITY OF DIAPHRAGM***
P3 ***THICKNESS OF DIAPHRAGM***
P4 ***VOLUME OF ADJACENT CHAMBER***
PB ***LINEARIZATION FACTOR***
P105 ***POLYTROPIC COEFFICIENT***
P106 ***REFERENCE PRESSURE***
C1 IN OUT 0.362*P1**((10./3.1)*((P2*P3)**(-1./3.1))*PB
C2 OUT 0 P4/(P105*P106)
C3 IN 0 P4/(P105*P106)

```

7.3.10 Diaphragm component (linear volume C's and nonlinear point-to-point C using type I, RC mutator)

In section 7.3.9, the linearized diaphragm model DPL uses an approximation for the factor $(\Delta p)^{-2/3}$. For the full nonlinear version of the diaphragm component, the nonlinear point-to-point capacitor model (CNLPP) is used. The schematic of the nonlinear diaphragm component is shown in figure 29. A nonlinear function of the form $(\Delta p)^{-2/3}$ is formed with the nonlinear function generator FGNL (using a table look-up).

The NET-2 listing for the block, called DPNL (DiaPhragm, NonLinear), is given in figure 29. Parameter P4 is the volume of the chambers adjacent to the diaphragm membrane.

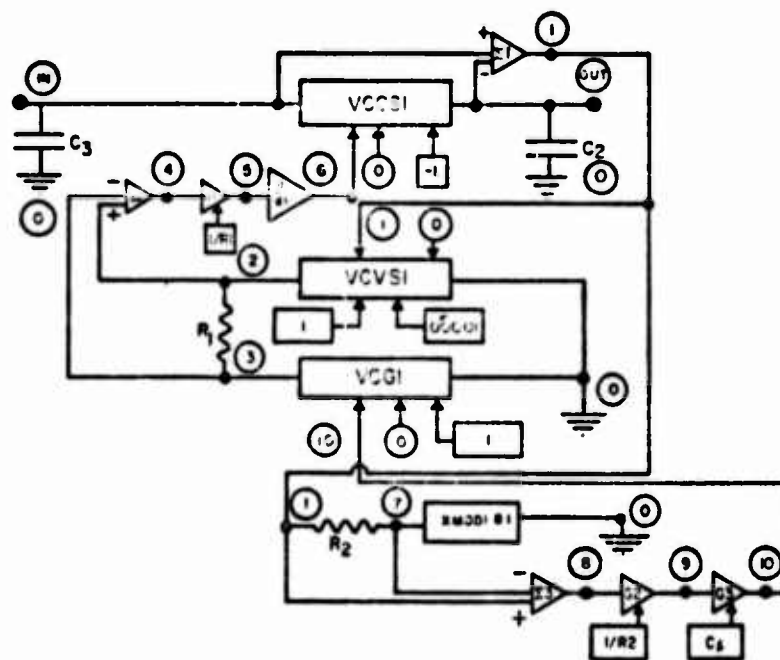


Figure 29. Diaphragm (PI network with linear grounded C's and nonlinear point-to-point C using type I RC mutator)

NET-2 Listing

```

DEFINE      DPNL      IN      OUT      J
P4          ***VOLUME OF ADJACENT CHAMBER***
P105       ***POLYTROPIC COEFFICIENT***
P106       ***REFERENCE PRESSURE***
VCCS1 6    0          IN      OUT      -1.
SUM1 1     +IN      -OUT
VCC1 10    0          2      0      1.
VCVS1 1    0          2      0      1., ***SMALL INTERNAL RESISTANCE,
                                     E.G., .00001***
R1 2       3          ***SMALL METERING RESISTANCE, E.G., .001***
SUM2 4     +2      -3
GAIN1 4     5          1./R1
DERIV1 5    6
R2 1       7          ***SMALL METERING RESISTANCE, E.G., .001***
XNDD1 6     1          7      0//TABLE1
SU43 H     +3      -7
GAIN2 8     9          1./R2
GAIN3 9     10         ***CONSTANT PART OF C***
C2      OUT  0          P4/(P105*P106)
C3      IN  0          P4/(P105*P106)
TABLE1
***PRESSURE DROP***          ***[PRESSURE DROP]**(-2./3.)***

```

7.3.11 Laminar Proportional Amplifier (Linear single-sided)

Each fluidic component defined to this point in NET-2 is a passive component. The simulation procedures have utilized various sources and gain blocks solely for computational ease. In simulating active components such as proportional amplifiers, gain blocks are used as part of the physical circuitry.

The schematic of the linear single-sided amplifier (ref 14) is shown in figure 30. The model may be used for a one-sided amplifier or a push-pull amplifier described in terms of differential quantities. The values of resistances, inductances, capacitances and gains are linear.

The NET-2 listing is shown in figure 30. This define block is called AMPLS (Amplifier, Linear Single-sided).

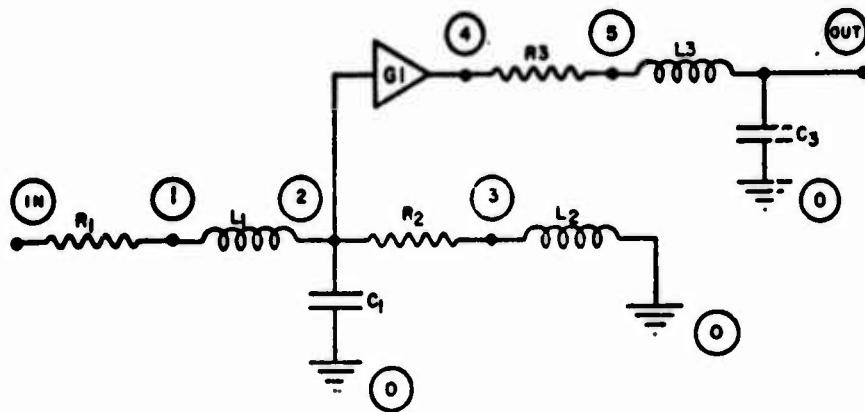


Figure 30. Laminar Proportional Amplifier (Linear Single-sided)

NET-2 Listing

OFFINE	AMPLS	IN	OUT	0
R1	IN	1	***VALUE***	
L1	1	2	***VALUE***	
C1	2	0	***VALUE***	
R2	2	3	***VALUE***	
L2	3	0	***VALUE***	
GAIN1	2	4	***VALUE***	
R3	4	5	***VALUE***	
L3	5	OUT	***VALUE***	
C3	OUT	0	***VALUE***	

7.3.12 Laminar Proportional Amplifier (Nonlinear two-sided)

More sophisticated models of the laminar proportional amplifier have been investigated by Manion and Mon (ref 14). In these models of the amplifier (fig. 31), the major complexities that are added to the linear model are: (1) nonlinear vent components--RNLV1, RNLV2, LNL1, and LNL2, (2) a jet position generator, (3) entrainment-flow generators, and (4) signal saturation generators.

Considering the upper half of the symmetric schematic, the voltage at node 12 (control region pressure) sets the jet position at nodes 31, 32 and 33. Amplifier gain is controlled by multiplying nodes 31 and 12 in MULT11. The jet position controls the entrainment-flow generator

connected to node 12. The jet position also sets node 33, to which saturation characteristics are applied to give the nonlinear vent resistance and inductance, which are set at nodes 15 and 16 respectively. The lower half is treated similarly. A NET-2 listing is given in figure 31 for this block, defined as AMPNL (Amplifier, NonLinear).

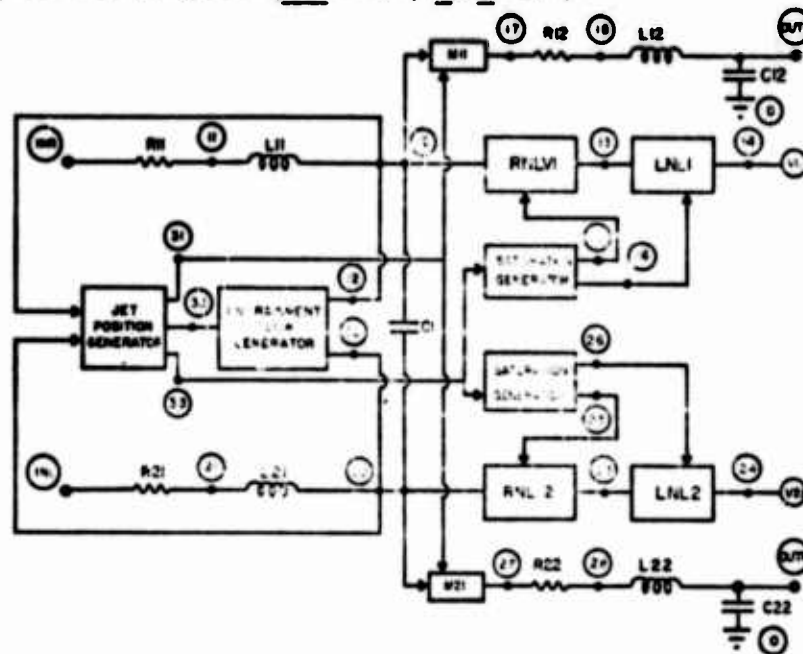


Figure 31. Laminar Proportional Amplifier (Nonlinear two sided)

NET-2 Listing

```

DEFINE  AMPNL  INF  OUTL  INL  OUTR  0
R11  INK  11  ***VALUE OF INPUT R***
L11  11  12  ***VALUE OF INPUT L***
RNLV1 12  13  15
LNL1  13  14  16
V11  14  0  ***VALUE OF VENT PRESSURE***
MULT11 17  +12  +33
***SATURATION GENERATOR FROM (33) TO (15,16)***
R12  1  1  ***VALUE OF OUTPUT R***
L12  18  OUTL ***VALUE OF OUTPUT L***
C12  OUTL 0  ***VALUE OF OUTPUT C***
***JET POSITION GENERATOR FROM (12,22) TO (31,32,33)***
***ENTRAINMENT FLOW GENERATOR FROM (32) TO (34,35)***
C1  12  22  ***VALUE OF JET C***
R21  INL  21  ***VALUE OF INPUT R***
L21  21  22  ***VALUE OF INPUT L***
RNLV2 22  23  25
LNL2  23  24  26
V21  24  0  ***VALUE OF VENT PRESSURE***
MULT21 2  +22  +33
***SATURATION GENERATOR FROM (33) TO (25,26)***
R22  27  28  ***VALUE OF OUTPUT R***
L22  28  OUTR ***VALUE OF OUTPUT L***
C22  OUTR 0  ***VALUE OF OUTPUT C***

```

7.4 Networks in NET-2

With the flexibility of expressing the nonlinearities for both the passive and active components in NET-2, it is possible to analyze and to design fluidic network configurations. When the real fluidic devices are modeled accurately, the computer studies are very meaningful. A significant feature of NET-2 is the modular hierarchy of components built from circuit elements, simulation elements, defined models and stored models (including fluidic models). All of the elements and models described in sections 7.1, 7.2 and 7.3 can be used in modeling more complex fluidic components and systems.

7.4.1 Circuit Analysis in NET-2

To complete the NET-2 programming picture for fluidic analysis, the means of setting up frequency-response and transient-response programs must be described.

7.4.1.1 Frequency Response in NET-2

A frequency-response program in NET-2 includes a listing of each element and each model. The required frequency-response calculations for a circuit are described in STATE solutions of the form:

STATES

FREQ f_1 (f_n) f_2

PRINT A(a-b / c-d) B(a-b / c-d) Y(a-b / c-d) Z(a-b / c-d)

PLOT A(a-b / c-d) B(a-b / c-d) Y(a-b / c-d) Z(a-b / c-d)

where f_1 is the initial value of frequency,

f_2 is the final value of frequency,

f_n is the number of equally spaced intervals between f_1 and f_2 ,

A is the complex voltage gain to be output,

B is the complex current gain to be output,

Y is the admittance to be output,

Z is the impedance to be output,

a, b are the differential output node pair (node a is referenced to node b),

c, d are the differential input node pair (node c is referenced

to node d),

s is the number assigned to the state solution.

7.4.1.2 Transient Response in NET-2

For transient response, the NET-2 program also includes a listing of each element and each model. A transient signal generator of the form VI (below) is used as a driver. Additional statements include MAXSTEP and TERMINATE. The form of the STATE solution for transient response is:

```
VI 1 0 f(TIME)
MAXSTEP (the maximum size of the integration step)
TERMINATE (an algebraic expression in an independent or a dependent
variable, which when reached, stops the transient response
calculation).
```

STATES

```
TIME t1 (tn) t2
PRINT N(n) V(v) I(i) Rm Cm Lm
PLOT N'(n) V(v) I(i) Rm Cm Lm
```

where f(TIME) is the value of the voltage (or current) from the transient signal generator

t₁ is the initial value of time,

t₂ is the final value of time,

t_n is the number of equally spaced intervals between t₁ and t₂,

N(n) is the node voltage n to be output

V(v) is the voltage of element v to be output,

I(i) is the current of element i to be output,

Rm is the resistor value to be output,

Cm is the capacitor value to be output,

Lm is the inductor value to be output,

s is the number assigned to the state solution.

7.4.1.3 Sine Generator

In several of the experimental studies related to these computer studies, the test signal is a sinusoid of finite amplitude. A sine wave driver in NET-2 is shown below:

P101 3.14159

P110 (input pressure amplitude)

P111 (input frequency in Hz)

V1 1 0 P110* (SIN(2.*P101 * P111 * TIME + .0001))

The term .0001 is added to facilitate the initial calculations at TIME = 0.

7.4.2 Fluidic Network Design in NET-2

Both frequency-response and transient-response programming procedures in NET-2 have been discussed above. Much of the power of NET-2 as a circuit response program lies in its capability of handling design problems, including those arising in fluidics. All elements and models (including the fluidic models developed in sect. 7.3) are available for designing fluidic networks.

In design problems not only are circuit responses computed, but also forms and values of the circuits are selected to give the best performance of the configuration as specified in the design requirements. The NET-2 design approach is couched in terms of OPTIMIZE routines. The form of OPTIMIZE is

OPTIMIZE n

STATE

OBJ = f VS CURVE m 1.

g_1 a_1 b_1

g_2 a_2 b_2

where f is the function to be compared to a specified data curve,

g_i is the parameter or variable to be chosen in minimizing the objective function,

a_i is the lower limit of the value of the variable g_i ,

b_i is the upper limit of the value of the variable g_i ,

n is the number assigned to the optimize solution,

m is the number assigned to the specified data curve.

By first specifying the form (topology) of the circuit and its values, one or more parameters or variables may be selected (through specifications in the OPTIMIZE procedure) to extremize the required design characteristics.

7.4.3 Simple Fluidic Networks in NET-2

Several passive fluidic networks are being investigated in the laboratory. Their experimental responses are being compared to the calculated responses from NET-2 models described for several components. NET-2 programs for six simple configurations, using only simple models, are described in the following sections. A summing, (fig. 32), a distribution junction, (fig. 33), a lag circuit (fig. 34), two lead circuits (figs. 35 and 36), and a lag-lead circuit (fig. 37) are presented.

A line drawing of each of the simple test configurations, along with simple equivalent circuits, and partial NET-2 listings are given (figs. 32-37). The simple equivalent circuits for the passive components of each configuration and the selected NET-2 models are tabulated below.

	<u>Fluidic Component</u>	<u>Equivalent circuit</u>	<u>NET-2 model</u>
(1)	Capillary	Resistor	TUBEDYNnwith PI07=0, 1
(2)	Summing junction	Grounded capacitor	TKLn
(3)	Distribution Junction	Grounded capacitor	TKLn
(4)	Enclosed volume	Grounded capacitor	TKLn
(5)	Bellows module	Pi network of capacitors	BELLOWn
(6)	Diaphragm module	Pi network of capacitors	DPLn
(7)	Signal generator	Voltage source	Vn

It should be noted that the capacitors denoted as C_4 and C_5 (figs. 35, 36, and 37) are in direct shunt across the pressure source.⁵ These capacitors appear as part of the pressure source generator. These capacitors must be eliminated from the computation. Capacitance values for C_4 and C_5 are therefore set to zero in the models of TKLn, BELLOWn, and DPLn.

8. Limitations of the Computer Approach

The limitations of the computer approach described in this paper fall into two classes: (1) limitations in synthesizing an equivalent circuit, and (2) limitations in using the digital computer to determine the response of the equivalent circuit.

SUMMING JUNCTION

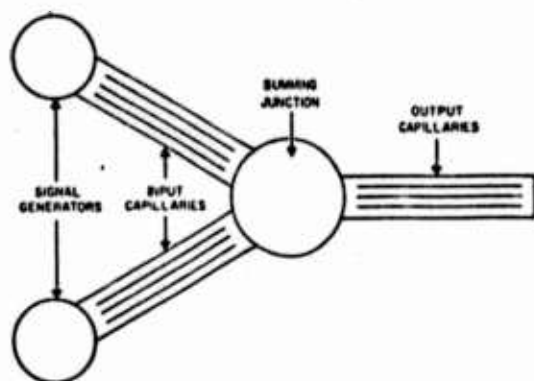


Figure 32a. Test Configuration of Summing Junction

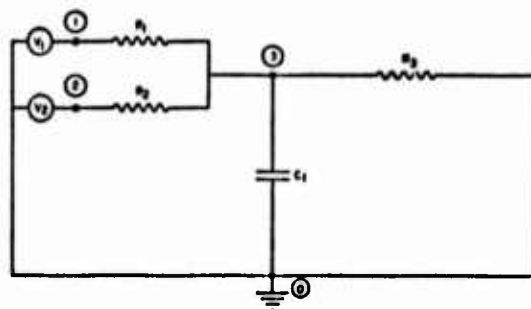


Figure 32b. Simple Equivalent Circuit of Summing Junction

Partial NET-2 Listing

```

* SUMMING JUNCTION - PARTIAL LISTING
V1      1      0      ***VALUE OF AMPLITUDE OF PRESSURE SIGNAL-1***
V2      2      0      ***VALUE OF AMPLITUDE OF PRESSURE SIGNAL-2***
TUBEDY1 1      3      0
TUBEDY2 2      3      0
TKL1    3      0      0
TUBEDY3 3      0      0
PARAMETER
    TUBEDY1.P107      1
    TUBEDY2.P107      1
    TUBEDY3.P107      1
DEFINE  TUBEDY      IN      OUT 0
    R1      IN      MID      8.*P103*P2/(P105*P1**4*P3)
    L1      MID      OUT      P106*P102*P2/(P101*P1**2*P3)*P107
    C1      OUT      0        P101*P1**2*P3/(P105*P106)*P107
DEFINE  TKL         IN      0
    C1      IN      0        P1/(P105*P106)
END
    
```

DISTRIBUTION JUNCTION

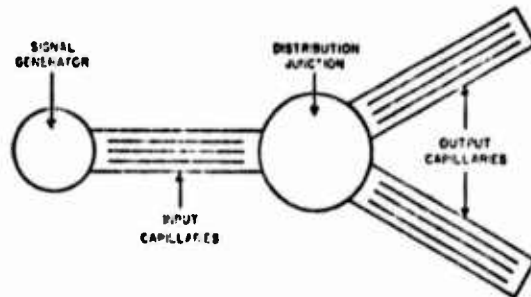


Figure 33a. Test Configuration of Distribution Junction

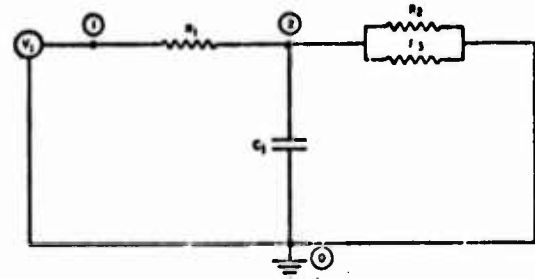


Figure 33b. Simple Equivalent Circuit of Distribution Junction

Partial NET-2 Listing

```

* DISTRIBUTION JUNCTION - PARTIAL LISTING
VI          1    0    ***VALUE OF AMPLITUDE OF PRESSURE SIGNAL***
TUBEDY1    1    2    0
TKL1       2    0    0
TUBEDY2    2    0    0
TUBEDY3    2    0    0
PARAMETER
  TUBEDY1.P107    1
  TUBEDY2.P107    1
  TUBEDY3.P107    1
DEFINE TUBEDY    IN    OUT    0
  RL    IN    MID    8.*P103*P2/(P101*P1**4*P3)
  LL    MID    OUT    P108*P102*P2/(P101*P1**2*P3)*P107
  CL    OUT    0    P101*P1**2*P3/(P105*P106)*P107
DEFINE TKL       IN    0
  CL    IN    0    P1/(P105*P106)
END
  
```

LAG NETWORK

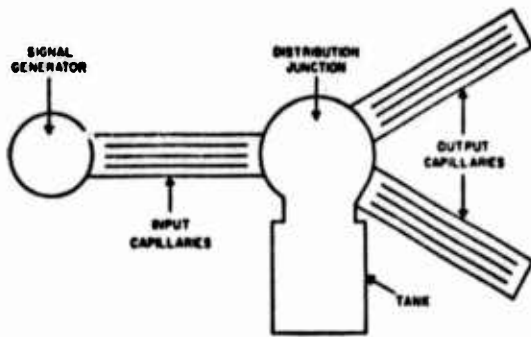


Figure 34a. Test Configuration of Lag Network

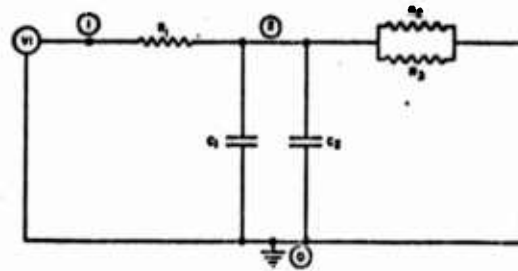


Figure 34b. Simple Equivalent Circuit of Lag Network

Partial NET-2 Listing

```

* LAG NETWORK - PARTIAL LISTING
V1      1      0      ***VALUE OF AMPLITUDE OF PRESSURE SIGNAL***
TUBEDY1 1      2      0
TKL2    2      0
TKL1    2      0
TUBEDY2 2      0      0
TUBEDY3 2      0      0
PARAMETER
    TUBEDY1.P107      1
    TUBEDY2.P107      1
    TUBEDY3.P107      1
DEFINE  TUBEDY      IN      OUT      0
    R1      IN      MID      8.*P103*P2/(P101*P1**4*P3)
    L1      MID      OUT      P109*P102*P2/(P101*P1**2*P3)*P107
    C1      OUT      0      P101*P1**2*P3/(P105*P106)*P107
DEFINE  TKL        IN      0
    C1      IN      0      P1/(P105*P106)
END
    
```


LEAD NETWORK USING BELLOWS COMPONENTS

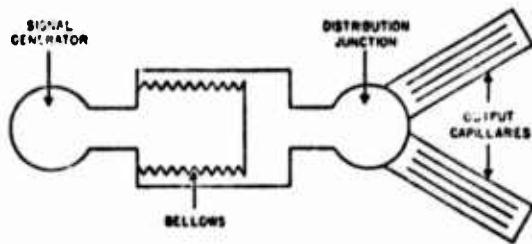


Figure 35a. Test Configuration of Lead Network with Bellows

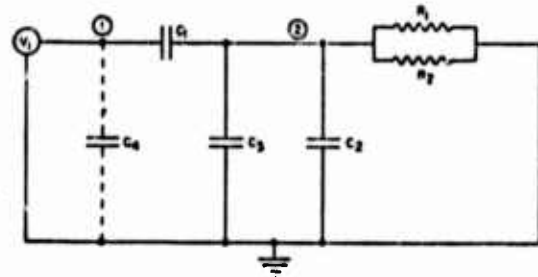


Figure 35b. Simple Equivalent Circuit of Lead Network with Bellows

Partial NET-2 Listing

```

* LEAD NETWORK - PARTIAL LISTING
V1      1      0      ***VALUE OF AMPLITUDE OF PRESSURE SIGNAL***
BELLOW1 1      2      0
TKL1    2      0
TUBEDY1 2      0      0
TUBEDY2 2      0      0
PARAMETER
PARAMETER
    TUBEDY1.P107      1
    TUBEDY2.P107      1
DEFINE   TUBEDY      IN      OUT  0
    R1     IN      MID  8.*P103*P2/(P101*P1**4*P3)
    L1     MID     OUT  P105*P102*P2/(P101*P1**2*P3)*P107
    C1     OUT     0    P101*P1**2*P3/(P105*P106)*P107
DEFINE   TKL         IN      0
    C1     IN      0    P1/(P105*P106)
DEFINE   BELLOW      IN      OUT  0
    C1     IN      OUT  (P101*P2**2)**2/P1
    C2     OUT     0    P101*(P5**2*P6-P3**2*P4)/(P105*P106)
    C3     IN      0    P101*(P3**2*P4)/(P105*P106)
END
    
```

LEAD NETWORK USING A DIAPHRAGM COMPONENT

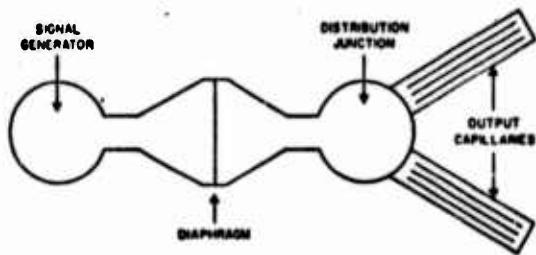


Figure 36a. Test Configuration of Lead Network with Diaphragm

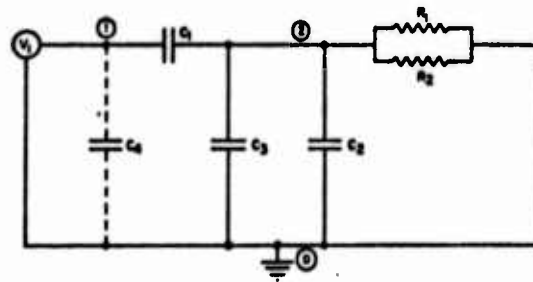


Figure 36b. Simple Equivalent Circuit of Lead Network with Diaphragm

Partial NET-2 Listing

```

* LEAD NETWORK USING DIAPHRAGM COMPONENT - PARTIAL LISTING
V1      1      0      ***VALUE OF AMPLITUDE OF PRESSURE SIGNAL***
DPL1    1      2
TKL1    2      0
TUBEDY1 2      0      0
TUBEDY2 2      0      0
PARAMETER
  TUBEDY1.P107      1
  TUBEDY2.P107      1
DEFINE  TUBEDY      IN  OUT  0
  R1     IN  MID    8.*P103*P2/(P101*P1**4*P3)
  L1     MID  OUT    P108*P102*P2/(P101*P1**2*P3)*P107
  C1     OUT  0      P101*P1**2*P3/(P105*P106)*P107
DEFINE  TKL         IN  0
  C1     IN  0      P1/(P105*P106)
DEFINE  DPL         IN  OUT  0
  C1     IN  OUT    0.362*P1**((10./3.)*(P2*P3)**(-1./3.))*P8
  C2     OUT  0      P4/(P105*P106)
  C3     IN  0      P4/(P105*P106)
END
  
```

Reproduced from
best available copy.

LAG-LEAD NETWORK USING BELLOWS COMPONENT

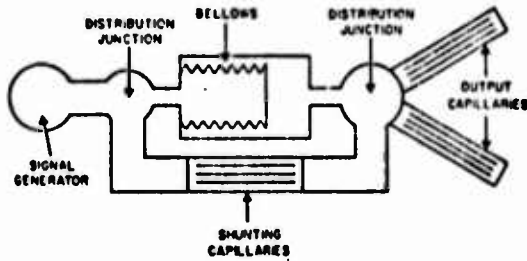


Figure 37a. Test Configuration of Lag-Lead Network

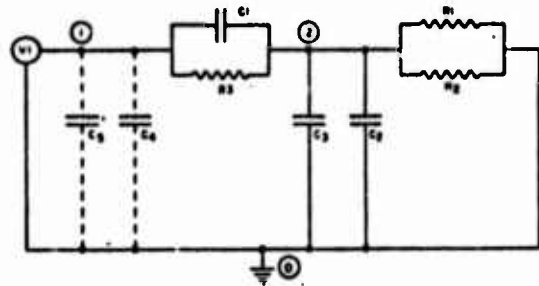


Figure 37b. Simple Equivalent Circuit of Lag-Lead Network

Partial NET-2 Listing

```

* LAG-LEAD NETWORK USING BELLOWS COMPONENT - PARTIAL LISTING
V1      1      0      ***VALUE OF AMPLITUDE OF PRESSURE SIGNAL***
TKL2    1      0
BELLOW  1      2      0
TUBEDY3 1      2      0
TKL1    2      0
TUBEDY1 2      0      0
TUBEDY2 2      0      0
PARAMETER
TUBEDY1.P107 1
TUBEDY2.P107 1
TUBEDY3.P107 1
DEFINE TUBEDY IN OUT 0
R1     IN  MID  5.*P103*P2/(P101*P1**4*P3)
L1     MID  OUT  P104*P102*P2/(P101*P1**2*P3)*P107
C1     OUT  0   P101*P1**2*P3/(P105*P106)*P107
DEFINE TKL IN 0
C1     IN  0   P1/(P105*P106)
DEFINE BELLOW IN OUT 0
C1     IN  OUT (P101*P2**2)**2/P1
C2     OUT  0   P101*(P5**2*P6-P3**2*P4)/(P105*P106)
C3     IN  0   P101*(P3**2*P4)/(P105*P106)
END

```

It is important to recognize that fluidic configurations of current interest may not have completely equivalent electrical analogs. It is equally important to see that equivalent circuits describe a significant range of components with adequate accuracy. However, the mathematics, in many cases, become nonlinear.

Limitations within digital computation may be defined as

(1) Inability to obtain a solution - a limitation that depends on the form of the nonlinear equations and the iteration routines to assure convergence in each solution.

(2) Inability to obtain accurate solutions - a limitation that depends on the error generated in each iteration. Since errors can occur with each calculation, depending upon the use of one solution in performing the next, errors can be greatly compounded as solutions are computed point by point. Simultaneous solutions at each point avoid this limitation.

(3) Allowable forms of circuit models - a limitation in the type of analytic and experimental models that may be introduced into the equivalent circuit format. To avoid this limitation, it may be necessary to simplify the form of the model so that computational techniques may be applied.

(4) Form of response - a limitation in the response of certain programs. A circuit analysis program must be selected to calculate the desired form of response; i.e., (a) steady state or dynamic, (b) time-domain or frequency-domain.

(5) Difficulty in programming - a limitation that might dictate the program used. Some considerations include (a) writing correct circuit equations or interconnecting the elements correctly for circuit analysis, (b) writing parametric equations or numerical values for elements, and (c) writing functional forms or computing the forms.

The limitations that relate to the digital computer may eventually be eliminated or avoided by incorporating both greater computational capability and user-oriented flexibility into existing programs.

Cost is of primary importance when developing solutions valid over all ranges. Keeping the cost in mind, it is usually necessary to trade off the complexity of the model against the accuracy of the response.

9. Conclusions

Electronic equivalent circuits can be adapted to represent many of the fluidic circuits in the current ranges of interest. Circuit

synthesis procedures are readily available for carrying an analytical or experimental model over into an equivalent circuit.

The available computer technology presents two types of computer programs--one for solving circuit equations and one for performing circuit analysis. Studies reported in this paper have been based on DSL/90 as an example of a program to solve circuit equations, and on SLIC and NET-2 to perform circuit analysis.

This paper is mainly a catalog of computer models that have been incorporated into fluidic versions of SLIC and NET-2. Because of the allowable sophistication in NET-2, most of the computer models have been developed for NET-2.

If a problem is run with overly sophisticated models, the cost may not be warranted. The accuracy of the solution (a function of the sophistication of the model) must be traded off against cost. The added accuracy of the solution should be used as a criterion to justify the cost of selecting sophisticated circuit models.

At present no technique has been attached to the response errors that are generated when solutions are not computed simultaneously. But, in general, a lack of simultaneity of solution can be disastrous; i.e., solutions are not valid. NET-2 is the only one of these programs that insures solution simultaneity.

Observing cost, model complexity, types of solutions, optimization, and ease of programming the following conclusions are made for SLIC, NET-2, and DSL/90. NET-2 is the most costly program, while SLIC is the least costly. Both NET-2 and DSL/90 can handle the most complex problems. SLIC handles only steady-state dc and ac problems. DSL/90 handles nonlinear, transient studies. NET-2 treats nonlinear, transient studies as well as steady-state dc and steady-state ac problems. NET-2 is the only one of the three that can locate optimum solutions within specified parameter ranges.

Because of their self-organizing capabilities, the two circuit analysis programs, SLIC and NET-2, are far easier to program. DSL/90 is not self-organizing. Fluidic expressions for such parameters as resistance, capacitance, inertance, or gain can be readily entered into both NET-2 and DSL/90. Numerical values, instead of expressions, must be entered for SLIC.

When all of these points are considered, the following uses of the three programs are visualized:

- Use SLIC for simple, linear or nonlinear, dc or ac analyses.
- Use DSL/90 for simple, nonlinear transient analyses when the form of the model does not easily fit into a circuit analysis program.
- Use NET-2 when sophisticated nonlinear problems are represented in the framework of circuit analyses. However, keep in mind that NET-2 may be too costly for many simpler problems.

Within the framework of circuit analysis, this paper serves as a handbook for implementing computer solutions for amplitude-dependent and frequency-dependent fluidic equivalent circuits. In conjunction with users' manuals for DSL/90, SLIC, or NET-2, this paper makes it possible to readily program, solve, and design many complex fluidic circuit configurations of current interest.

10. Literature Cited

- (1) Bloom, H.M., HDL-TM-71-13, DSL/90 Programming Manual, October 1971.
- (2) Hausner, Arthur, Analog and Analog/Hybrid Computer Programming, Prentice Hall Inc., Englewood Cliffs, NJ, 1971.
- (3) Kop, Harold M., An Improved Version of SLIC, Electronics Research Laboratory, College of Engineering, University of California, Berkeley, August 1972.
- (4) Mathers, Harry W., Stephen R. Sedore, John R. Sents, SCEPTRE Support, Volume 1: Revised SCEPTRE User's Manual, Technical Report No. AFWL-TR-67-124, Vol. 1., Air Force Weapons Laboratory, Kirtland AFB, N.M., April 1968.
- (5) Malmberg, Allan F., Preliminary User's Manual, NET-2, Network Analysis Program, Harry Diamond Laboratories, September 1972
- (6) Katz, Silas and Edgar Hastie, "Pneumatic Passive Lead Networks for Fluidic Systems," Joint Automatic Control Conference, St. Louis, 1971.
- (7) Iseman, Joseph M., HDL State of the Art Fluidics Symposium, A Circuit Analysis Approach to the Solution of Passive Pneumatic Fluidic Compensation Networks, 30 Sept - 3 Oct 1974.
- (8) Katz, Silas and Edgar Hastie, HDL-TM-71-35, "Fluerics 31. The Transition from Isothermal to Adiabatic Capacitance in Cylindrical Enclosures," 1971.

9. Alexander, J. Eugene and J. Milton Bailey, Systems Engineering Mathematics, Prentice-Hall, Englewood Cliffs, New Jersey, 1962.
10. Chua, Leon O., Introduction of Nonlinear Network Theory, McGraw-Hill New York, 1969.
11. Reid, Karl N., "Fluid Transmission Lines", School of Mechanical and Aerospace Engineering, Oklahoma State University, Stillwater, Oklahoma, July - August 1968.
12. Rohmann, C.P. and E. C. Grogan, On the Dynamics of Pneumatic Transmission Lines, Transactions of the ASME, pp. 853-874, May 1957.
13. White, Harry W., Analysis of the Steady-Flow Pneumatic Resistance of Parallel Capillaries, Proceedings of the Fluidic Amplification Symposium, Volume 1, HDL, Washington, D.C., October 1965.
14. Manion, Francis M. and George Mon, HDL-TR-1608, "Fluerics 33. Design and Staging of Laminar Proportional Amplifiers," September 1972.

A CIRCUIT ANALYSIS APPROACH TO THE SOLUTION OF PASSIVE
PNEUMATIC FLUIDIC COMPENSATION NETWORKS

by

JOSEPH M. ISEMAN

HARRY DIAMOND LABORATORIES
WASHINGTON, D.C. 20438

Preceding page blank

ABSTRACT

This paper summarizes circuit models of passive pneumatic fluidic components, and demonstrates the feasibility of a circuit approach for designing passive fluidic control system circuits. It is a first attempt at tying passive fluidics device research to actual hardware design.

Starting with a set of fluidic components--capillaries, enclosed volumes, bellows modules, and diaphragm modules--circuit models are synthesized from an analytical-experimental-computational approach. Simple, ideal electronic circuit models that are linear and frequency independent are extended to models that are nonlinear and frequency dependent. These circuit models are described by analytic expressions. Relative errors arising from model simplifications are also expressed analytically.

A few test configurations were built and their responses were measured using existing hardware. Simulation for these configurations was performed with digital computer programs. Comparisons between the test data and simulated models were made and qualitatively evaluated; these data were, generally, in agreement over the ranges tested.

The most often selected linear models in the studies to date include RLC models of the capillary (with an experimentally measured d-c resistance) and frequency-dependent models of capacitance and inductance.

A seven-step design approach, based on a catalog of available circuit models, is presented for passive fluidic circuits.

The study described in this paper deals with several fluidic components, connected in simple junction and compensation arrays. Comparisons of simulated and experimental frequency responses on limited a-c testing over specific frequency ranges are given. Frequency ranges are given in which the magnitude ratio of the simulated response is within ± 10 percent of the experimental response and in which the phase difference for the simulated response is within ± 10 deg. of the experimental response.

ACKNOWLEDGEMENTS

The author expresses his gratitude to the following individuals:
Prof. Karl N. Reid, Jr. (Oklahoma State University) and Albert I. Talkin for proposing and encouraging these studies.

Kenji Toda for helping to design the experimental hardware and helping to specify the experimental equipment.

Robert O. Talbot for assisting in the design and constructing the experimental hardware.

Dyrull V. White for assisting in checking out and calibrating the equipment and for running the tests on some experimental configurations.

LIST OF FIGURES

Page

1.	Static equivalent circuit model of capillary	
2.	Simple dynamic equivalent circuit models of capillary	
3.	Simple loaded dynamic equivalent circuit models of capillary	
4.	Simple dynamic equivalent circuit models for bundles of N parallel capillaries	
5.	Equivalent circuit model of simple enclosed volume	
6.	Equivalent circuit of frequency dependent cylindrical volume	
7.	Frequency dependent resistance and capacitance for enclosed cylinder	
8.	Simple equivalent circuit model for bellows module	
9.	Sophisticated equivalent circuit model for bellows module ..	
10.	Simple equivalent circuit for diaphragm module	
11.	Sophisticated equivalent circuit for diaphragm module	
12.	Simple equivalent circuit for pneumatic node	
13.	Passive summing junction in system	
14.	Passive summing junction	
15.	Simple equivalent circuit for passive summing junction	
16.	Passive distribution junction in system	
17.	Simple equivalent circuit for passive distribution junction.	
18.	Static test stand	
19.	Static calibration curves for capillaries	
20.	Schematic of AC test stand	
21.	Shaker table signal generator	
22.	Speaker cone signal generator	
23.	Straight microphone probe holder	
24.	Tee microphone probe holder	
25.	Simple equivalent circuit of passive summing junction	
26.	Modified air cylinder as an enclosed volume	
27.	Improved enclosed volume	
28.	Test configuration for passive summing junction	
29.	Bode plot for summing junction	
30.	Simple equivalent circuit of passive distribution junction	
31.	Test configuration for passive distribution junction	
32.	Bode plot for distribution junction	
33.	Phase lead compensation	
34.	Phase lag compensation	
35.	Lag-lead compensation	
36.	Schematic of simple lag network	
37.	Test configuration for lag network	
38.	Resistive circuit model of experimental lag network	
39.	Resistive and inductive circuit model of experimental lag network	
40.	Added linearized phase shift in lag network	

41. Bode plot for lag network
42. Schematic of simple lead network
43. Fluidic lead network with bellows module
44. Circuit of experimental lead network
45. Bellows
46. Bellows Module
47. Bode plot for lead network with bellows
48. Schematic of simple lag-lead network
49. Fluidic lag-lead network with bellows module
50. Circuit of experimental lag-lead network with bellows
module
51. Bode plot for lag-lead network with bellows
52. Fluidic lead network with diaphragm module
53. Diaphragm module
54. Circuit of experimental lead network with diaphragm module .
55. Bode plot for lead network with bellows
56. Flow chart for design approach

LIST OF TABLES

Page

I.	Lead Network Response	
II.	Percentage Changes from Simple Linear, Frequency Independent Lead Network	
III.	Lag-Lead Network Response	
IV.	Percentage Changes from Simple Linear, Frequency Independent Lag-Lead Network	
V.	Error Ranges for Models of Subsystems--10percent, 10 deg ...	

NOMENCLATURE

A	- area (m ²)
C	- capacitance (m ⁴ sec ² /kg)
C _p	- specific heat capacity at constant pressure (m ² /sec ² °C)
d	- diameter (m)
D(ω)	- frequency dependent energy dissipation (kg/m ⁴ -sec)
E	- modulus of elasticity (kg/m sec ²)
F	- force (kg m/sec ²)
g _i	- gain in transfer functions (section 7.1) (-)
G	- magnitude ratio, or gain (-)
h	- height or thickness (m)
Im	- Imaginary part of a function
J _n	- Bessel function of nth order
k	- spring constant (kg/m ² sec ²)
k ₁	- constant in equation (5.1) (m ⁴ sec/kg)
K	- constant in point-to-point capacitance of diaphragm defined in equation (39) (m ⁴ sec ² /kg)
K ₁	- constant for capillary in sensitivity analysis (section 7.3.2) (Pa)
K ₂	- constant for enclosed volume in sensitivity analysis (section 7.3.2) (kg/m ⁵)
ℓ	- length (m)
L	- inductance (inertance) (kg/m ⁴)
n	- polytropic coefficient (-)
N	- number of tubes in a capillary module (-)
N _R	- Reynolds number $N_R = \left(\frac{U}{\nu}\right) \times (\text{characteristic dimension})$
p	- static pressure (Pa)
p ₁	- pressure fluctuation (Pa)
Δp	- pressure drop (Pa)
P _i	- input pressure (section 7.1) (Pa)
P _o	- output pressure (section 7.1) (Pa)
P _∞	- ambient or reference pressure (Pa)
Q	- volume flow (m ³ /sec)
ΔQ	- net volume inflow (m ³ /sec)
r	- radius (m)
r _o	- radius of diaphragm (m)
R	- resistance (kg/m ⁴ sec)
R	- universal gas constant (kg m ² /sec ² - mole ⁻¹ °K)
Re	- real part of a function
s	- Laplace variable (1/sec)
t	- time (sec)
T _i	- time constant (sec)
$\overline{\Delta T}$	- average temperature change (°K)

- u - velocity (m/sec)
- V - volume (m³)
- ΔV - added volume as a result of deflection (m³)
- w - width of chamber in enclosed pneumatic volume (m)
- x - deflection (m)
- X_C - capacitive reactance (kg/m⁴-sec)
- X_L - inductive reactance (kg/m⁴-sec)
- Y - admittance (m⁴ sec/kg)

Greek Symbols

- $\alpha = \sqrt{\frac{\omega \rho c_p}{\kappa}} r$ (defined in equation (3.20d)) (-)
- γ - ratio of specific heats (-)
- Γ - ratio of weights of input signals to summing junction (-)
- κ - thermal conductivity (kg m/sec²- °C)
- λ - factor in inertance (section 3.1) (-)
- μ - dynamic viscosity (kg/m sec)
- ν - kinematic viscosity (m²/sec)
- ρ - mass density (kg/m³)
- ϕ - phase difference (°)
- ω - frequency (Hz)

Subscripts

- dt. - decibel, e.g., G_{db}
- i - input
- ℓ - linear
- L - load
- max - maximum
- n - node
- N - number
- n ℓ - nonlinear
- o - output
- v - volume

1. INTRODUCTION

In its simplest form, a fluidic system is conceptually identified as an array of interconnected flow paths within rigid or semirigid walls. Mathematical models for analysis and design of fluidic systems are based on this concept tempered by well-chosen assumptions.

In general, flow paths in the overall fluidic system are conceptually, if not physically, divided into a set of connected system components including capillaries, orifices, tanks and other enclosed volumes, bellows, diaphragms, lines, transmission lines, junctions, area changes, amplifiers and sensors. Many mathematical models of these components have been analyzed previously in the context of both an internal flow field approach from fluid mechanics (ref 1 through 8) and a black-box approach from systems analysis (ref 9, 10)¹.

In either a fluid mechanics or black-box approach, individual component models are synthesized to demonstrate first-order effects (and perhaps higher) in each component. Usefulness of the models rests in the ability of engineers to describe physical processes over sufficiently wide operating ranges so that each model can accurately predict the response of the physical component that it represents.

In the fluid mechanics approach, the general governing equations may be applied to fluid processes in special cases such as potential flow, viscous flow, acoustics, gas dynamics, or jet flow. In such cases, the predominant fluid processes are isolated by applying appropriate simplifying assumptions and boundary conditions.

In a systems approach (ref 1), a complicated fluidic system is resolved into simpler components; each individual component is modeled as a black box (by isolating it to determine its output as a function of arbitrary inputs); and then the individual component models are recombined to describe the total system.

Despite rather extensive academic fluidic studies, as is borne out by the mass of literature in fluidics bibliographies such as reference 11, very little effort has been expended to develop consistent and comprehensive models of fluidic devices. Instead, the models cover different ranges of amplitude and frequency, and lead to solutions with different degrees of precision. An organized approach for modeling and evaluating fluidic configurations is necessary for relating research programs to hardware designs.

For many special conditions, the form of component models leads to descriptions of fluidic systems as fluidic circuits. A circuit description of a fluidic system is analogous to circuit models in

¹Literature references are listed at the end of this paper.

electronics and several other technical fields such as heat transfer, mechanics, hydraulics, and pneumatics. Even though they are relatively simple to implement, circuit analyses are still nonetheless powerful techniques for determining the performance of devices.

In fluidics as well as in electronics, circuit analyses are simplified and approximate forms of field analyses for solving the fluid governing equations. It is well to note that general field equations are rarely easy to solve because they are dependent on a time variable as well as on three spatial variables. Circuit analyses in fluidics as well as in other disciplines, however, are more convenient representations than field analysis. Field equations can sometimes be reduced, all or in part, to circuit models that account for essential internal processes of components and that can be represented in terms of variables that are available at external terminals.

When component dimensions are small with respect to signal wavelengths, field analysis completely carries over into circuit analysis, pertaining to familiar element models described as equivalent circuits. In an equivalent circuit, the essential internal fluidic energy processes are taken as integrated effects or lumped properties (ref 12) of energy supply, energy storage, or energy dissipation. Values of the lumped properties are assigned to the elements in the circuit. Mathematical laws for interconnecting equivalent circuit models in a system are summarized as a circuit topology (ref 13), which is a circuit connection diagram.

With regard to circuit analysis techniques, two important questions arise: Can circuit analysis be applied successfully to the ranges of interest for fluidic configurations? and, if it can, how must equivalent circuit models be modified to account for the unique features of fluidic devices? These two questions fortunately are partially answered in favor of a fluidic circuit analysis. One of the best documented studies involving fluidic circuits is by Belsterling (ref 9). His recent book demonstrates that not only devices but also circuit modeling techniques are currently available for designing quite sophisticated fluidic systems. However, his approach relies heavily on viewing fluidic components from external terminals, thus failing to apply much of the available internal flow analytic background to circuit modeling.

A good base for applying the circuit approach to fluidics seems available within the current literature. Thus, we question: Is it possible to synthesize valid fluidic circuit models? and what procedures are available for evaluating and improving fluidic circuit models? These questions are answered in the following sections outlining the purpose and approach of this paper.

1.1 Purpose

The overall study is intended to answer the above questions about circuit analysis with regard to designing passive pneumatic fluidic control circuitry. In this regard, four specific tasks can be identified:

- (1) To synthesize circuit models of passive pneumatic fluidic components.
- (2) To simulate the response of fluidic circuits.
- (3) To evaluate individual and interconnected fluidic circuit models in light of the performance of physical test configurations.
- (4) To develop approaches for designing fluidic control systems, using circuit models, circuit programs, and evaluation procedures.

In section 3 of this paper, task (1) is performed by synthesizing one or more models of capillary modules, enclosed volumes, bellows modules, diaphragm modules, and junctions. Task (2) is described by Iseman in reference 14. Task (3) is performed in sections 6 and 7 in a nonsophisticated way by evaluating a few circuit models in simple fluidic subsystems. Task (4) is outlined in section 8 but is not directly implemented.

1.2 Approach

This study ties together developments in pneumatic fluidics and improves existing linear and almost linear passive fluidic models. It is limited to a lumped parameter range (low frequencies) and a quasi-linear range (low signal and low-power levels to maintain low pressures and low velocities) in which a wide dynamic range may be achieved.

Modeling fluidic components and evaluating these models within an equivalent circuit framework is investigated in this paper by combined analytical, computational, and experimental methods. In the past few years, there have been numerous analyses performed in developing models of passive pneumatic fluidic components (ref 2 through 8). To synthesize circuit models, the most meaningful analytical models are selected and defined over the ranges of interest.

Circuit response may be calculated analytically. Many analytic methods have been coded into circuit-analysis programs on the digital computer. Fluidic circuit models are incorporated into a few of these existing programs (ref 14). The response of fluidic system models as equivalent circuits is then determined by computer analysis techniques.

Experimental aspects of this study are based on the state-of-the-art. In this study (sect 5), d-c and a-c experiments are designed with new hardware and instrumentation to give accurate measurements

in validating the synthesized circuit models and their ranges of applicability. To demonstrate the use of synthesized circuit models of individual fluidic components, a few simple passive fluidic junctions and compensation networks are studied in sections 6 and 7.

The validity of the synthesized circuit models is considered briefly by comparing simulated circuit response data and experimental response data. Succeeding studies will continue to examine techniques to optimize performance criteria (such as minimum error) and to improve circuit models by adjusting (1) expressions for element values in the circuit, and (2) circuit topology (the arrangement of circuit elements).

2. TERMINOLOGY AND DEFINITIONS

In developing an analysis of fluidic systems based on a circuit analysis approach, many definitions from circuit theory are first clarified with respect to pneumatic fluidics.

Circuit theory (ref 15) describes the transfer of energy from a source or supply to devices that employ energy in gaining useful results. A circuit is composed of elements that supply and receive energy and may either convert it to heat or store it. Two types of elements can be classified: an element that supplies energy is an *active* element, an element that receives energy (with subsequent energy storage) is a *passive* element. Four fundamental types of fluidic elements are treated in the paper: an *energy-supply element*, an *energy-dissipation element* and two types of *energy-storage elements*.

The energy processing elements are integral to circuit theory. A *circuit* or *network* (ref 15) is any arrangement of passive or active elements that form closed paths. Each element is connected to one or more elements at two or more circuit nodes. A *branch* is a section of a circuit between nodes at which three or more circuit elements are connected.

A fluidic component is modeled as one or more passive elements if the fluidic signals interact only with other signals, the constraining geometry, and the fluid environment.

A fluidic component is modeled as one or more active and passive elements if additional energy sources are integral parts of the components. In some active components (amplifiers), fluidic signals are directed to influence auxiliary energy supplies.

The simplest lumped fluidic elements have two external terminals at which energy is interchanged. Such elements are termed two-terminal elements or one-port elements.

Fluidic energy (ref 12) in a lumped system is described by

two related physical variables. A through variable (volume flow, analogous to electric current) has the same value at both of its two terminals (or external nodes). An across variable (static-pressure drop, analogous to electric voltage) changes between the two terminals (nodes) of a two-terminal element.

Circuit models are the models used to characterize the fluid mechanical processes in fluidic systems. Fluidic system components are approximated in this paper as two-terminal sources, dissipators, and storers of energy. Only one energy process is considered in each model.

A fluidic energy supply or source (ref 12) is capable of delivering energy continuously to a system. The source static pressure, p , is a specific function of time,

$$p = F(t) . \quad (1)$$

A volume flow source (ref 12) is defined with volume flow, Q , as a specified function of time,

$$Q = F(t) . \quad (2)$$

A d-c fluidic resistor and an a-c fluidic dissipator both dissipate energy. Energy dissipation (ref 12) is described by some algebraic relationship between the through variable (volume flow, Q) and the across variable (static-pressure drop, Δp),

$$Q = f(\Delta p) \quad (3a)$$

and

$$\text{sign}(Q) = \text{sign}(\Delta p), \quad (3b)$$

where $Q = 0$ when $\Delta p = 0$.

A fluid capacitor (ref 12) is an element in which the energy stored is a function of the static pressure. In a pneumatic tank, fluidic energy is stored because of the compressibility of the fluid.

Capacitance of a fluidic system is also attributable to the volume change due to the mechanical spring constant or mechanical elasticity of the walls.

In both cases, a fluidic element is a capacitance when it is described by a functional relationship between the increased fluid volume, ΔV (the integral of the change of volume flow, ΔQ), and the pressure drop,

$$\int \Delta Q \, dt = f(\Delta p) . \quad (4)$$

A fluid inductor (ref 12) is an element in which energy is stored as kinetic energy in the fluid. The fluid acquires energy from the force required to accelerate it. An inertance is described mathematically by a functional relationship between the integral of the pressure drop and the volume flow,

$$\int \Delta p dt = f(Q). \quad (5)$$

The approach to represent fluidic components with pure lumped elements, described in terms of a through variable (volume flow) and an across variable (static pressure drop), measured at external terminals is called an equivalent circuit approach.

In both acoustics and hydraulics, under certain circumstances the fundamental governing equations may be reduced to linear ordinary differential equations that fit directly into an equivalent circuit approach. Solutions can then be obtained for steady-state dc, as well as in the time domain and in the complex frequency domain.

2.1 Signal-Amplitude Dependence

To consider a wide dynamic range--perhaps as large as 1000 (60 dB)--it is necessary to cover the range from small amplitude signals (in the acoustic range) to large, finite amplitude signals. Signal amplitude is the magnitude of the static-pressure excursion or of the volume flow. At larger pressure amplitudes, if momentum flux is of the same order as static-pressure forces, then the value of an element may become a function of the signal amplitude. In general, a linear-circuit representation of the actual fluidic component will be incorrect at higher signal levels. For example, a long cylindrical capillary (ref 2) with a small static-pressure drop follows Poiseuille's law in which resistance is constant. However, as the static-pressure drop is increased across the same capillary (ref 3, 4), a greater fraction of its length is needed to produce fully-developed laminar flow. Resistance is then a function of the differential static pressure.

2.2 Signal-Frequency Dependence

Signal frequency in the complex frequency domain and time rate of change in the time domain are considered in the development of circuit models. There are three aspects of circuit analysis that are related to the signal frequency: (1) validity of lumped element models, (2) topology of the circuit, and (3) values of circuit elements.

An element may be described by a lumped model when there is little signal phase shift as a function of position within the element. A distributed model is applied if the lumped model is not valid. Lumped models are usually considered valid if physical dimensions are less than 0.10 wavelengths (ref 16). The product of signal frequency and component size determines acceptance or rejection of the lumped-circuit approach

for modeling components. As the ratio of component size to fundamental wavelength (wave velocity/frequency) gets much smaller than unity, lumped-element models are valid.

In a circuit approach, fluidic components are modeled as topological arrays of lumped elements. Topology of circuit models is determined from the relationships among resistance, inductive reactance, and capacitive reactance. For example, at frequencies close to dc, a capillary is modeled as a pure lumped resistive element. As frequency increases, dynamic effects increase in significance and an array of resistive, inductive, and capacitive elements (ref 5) more adequately represents a capillary.

An example related to both amplitude and frequency dependence is a fluidic junction into which three or more fluidic components are connected. For small amplitude signals, a junction is purely a node. For finite amplitude signals, the ratio between dynamic pressure and the absolute pressure is no longer negligible, so that the junction is not a pure node; it therefore fails to be one dimensional and becomes directional.

Directionality in a junction can be virtually eliminated for large ratios of dynamic pressure to absolute pressure by redesigning the junction into a stilling chamber (ref 6) to reduce dynamic pressure. However, capacitive dynamics are added by converting the junction into a stilling chamber (an enclosed volume).

Values of the elements in some circuit models are also related to frequency. In the case of an enclosed volume, a polytropic coefficient associated with the thermodynamic processes occurring in a gas is a function of the signal frequency. Hence, since the capacitance and a-c dissipation of an enclosed volume are functions of the polytropic coefficient, they are thus functions of frequency. Katz and Hastie (ref 7) show that the impedance of an enclosed volume is equivalent to a grounded frequency-dependent capacitor shunted by a frequency-dependent energy dissipation element.

3. MODELS OF FLUIDIC COMPONENTS

Five types of passive components that are commonly used in fluidic networks are (1) a capillary module, (2) an enclosed volume, (3) a bellows module, (4) a diaphragm module, and (5) a junction. Each of these fluidic components is studied individually in this section. In sections 6 and 7, these components are studied as parts of larger systems.

This section describes each component as one or more typical algebraic expressions valid over different operating ranges, and one or more equivalent circuit topologies valid over different operating ranges.

3.1 Capillary Module

Consider, as the simplest case, a circular capillary with a steady, dc pressure drop and through volume flow.

For a sufficiently long cylindrical capillary, pressure drop is produced in opposing the dissipative viscous shear losses. For laminar flow, Poiseuille's law (ref 2, p. 58) gives the pressure drop, Δp , as a function of the volume flow, Q ,

$$\frac{\Delta p}{Q} = \frac{8\mu\ell}{\pi r^4} \quad (6)$$

where r and ℓ are the radius and length of the capillary, and μ is the dynamic viscosity of the fluid.

Fluidic resistance, R , is defined (ref 17) as rate of change of pressure drop, Δp , as a function of volume flow, Q ,

$$R = \frac{d(\Delta p)}{dQ} \quad (7)$$

For the linear relationship between Δp and Q in equation (6), resistance for a single long capillary is a constant,

$$R_{\ell,1} = \frac{8\mu\ell}{\pi r^4} \quad (8)$$

By placing a bundle of N identical capillaries in parallel, the total linear resistance, $R_{\ell,N}$, of a capillary module is reduced by a factor of N to

$$R_{\ell,N} = \frac{8\mu\ell}{N\pi r^4} \quad (9)$$

For shorter capillary tubes, the steady-state pressure drop opposes not only the viscous losses but also (as in ref 3) kinetic energy increases due to velocity profile changes in the entrance and along the velocity profile development length. In reference 3, a bundle of N parallel capillaries is described as a nonlinear resistance, $R_{n\ell,N}$, by adding a flow dependent resistive term to the viscous dissipation term in equation (9),

$$R_{n\ell,N} = \frac{8\mu\ell}{N\pi r^4} + \frac{7}{6} \frac{\rho}{N^2\pi^2 r^4} Q \quad (10)$$

where ρ is the mass density of the fluid.

The ratio of the flow-dependent term to the flow-independent term is

$$\frac{R_{n\ell,N} - R_{\ell,N}}{R_{\ell,N}} = \frac{28\pi}{3} \frac{\rho N}{\mu \ell} Q \quad (11)$$

This ratio is directly proportional to $\rho N Q$, inversely proportional to $\mu \ell$, and independent of the radius, r . According to Merritt (ref 4), in the laminar flow regime the amount of error in accepting a linear formulation for the resistance of the capillary is within 10 percent of a constant value if the ratio of length to diameter, ℓ/d , is related to the Reynolds number, N_R , by the inequality,

$$\frac{\ell}{d} \geq 0.434 N_R \quad (12)$$

Merritt (ref 4) suggests that as a rule of thumb $\ell/d \geq 400$ to assure linearity within 10 percent. However, as Reynolds number is lowered, error is reduced if length is held fixed; or the minimum ℓ/d ratio is reduced if error is kept within the same limits.

For steady flow through a bundle of capillaries, resistance alone describes the physical process. Hence, an equivalent circuit representing a capillary with steady flow is a pure resistor (fig. 1).



Figure 1. Static-equivalent circuit model of capillary

When a time-varying pressure drop is applied across the capillary, compressibility or inertial phenomena produce dynamic effects. The output pressure may lead the input pressure as well as be attenuated. As a first-order dynamic correction, each capillary is assumed to be a short segment of a circular transmission line. In reference 5, the transmission line is made up of a Poiseuille law resistance, a constant* linear capacitance, and a constant inductance (inertance). For a single capillary, linear capacitance, $C_{\ell,1}$, and linear inductance, $L_{\ell,1}$, are

$$C_{\ell,1} = \frac{\pi r^2 \ell}{n p_{\infty}} \quad (13a)$$

*A more accurate representation (discussed subsequently) takes into account the variation of capacitance with frequency.

where n is the polytropic coefficient, and p_∞ is the ambient absolute pressure; and

$$L_{\ell,1} = \frac{\lambda \rho \ell}{\pi r^2} \quad (13b)$$

where, from reference 5, λ is approximated as

$$\lambda = 1 + \frac{1}{3} \exp\left(\frac{\omega r^2}{32\pi\nu}\right) \quad (13c)$$

For higher frequencies,

$$\omega \geq \frac{100\nu}{r^2}, \quad \lambda = 1; \quad (13d)$$

and for lower frequencies,

$$\omega \leq \frac{10\nu}{r^2}, \quad \lambda = \frac{4}{3} \quad (13e)$$

The ratio of linear inductive reactance, X_L , to linear resistance is determined from equations (13b) and (9),

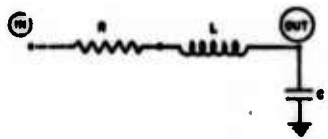
$$\frac{X_L}{R_\ell} = \frac{\lambda \omega r^2}{8\nu} \quad (14)$$

where ω is the radian frequency and ν is the kinematic viscosity. The ratio of linear capacitive reactance, X_C , to linear resistance is determined from equations (13a) and (14),

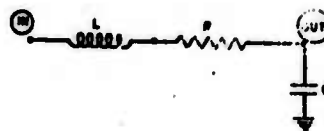
$$\frac{X_C}{R_\ell} = \frac{n p_s r^2}{8 \omega \mu \ell^2} \quad (15)$$

As the frequency increases, the inductive reactance increases and the capacitive reactance decreases relative to resistance.

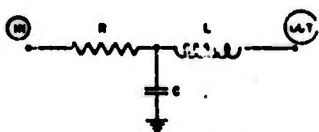
A dynamic equivalent circuit model of the capillary therefore includes resistance, capacitance, and inductance. Resistance and inductance are defined for through flow. Figure 2 shows six possible circuit models; in each model, resistance and inductance are in series between the input and output. Because pneumatic capacitance describes an energy storage process due to gas compressibility, and is made relative to a reference pressure, pneumatic capacitance is therefore in shunt to ground.



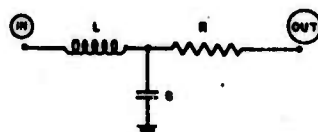
RLC model



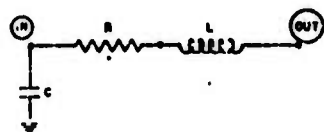
LRC model



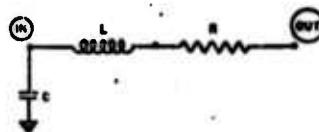
RCL model



LCR model



CRL model



CLR model

Figure 2. Simple dynamic equivalent circuit models of capillary

The six possible configurations in figure 2 are suggested by reference 16 which describes several lumped approximations to a lossless transmission line. Included in reference 16 are a lossless LC model and a lossless CL model. Responses of the different circuit models in figure 2 are expected to have better agreement over various ranges of real conditions as different combinations of values of R, L, C and external circuit conditions are tried.

To gain further insight, let us consider three linear circuit models of a capillary: RCL (fig. 2a), RLC (fig. 2c), and CRL (fig. 2e). Each circuit is driven by a sinusoidal pressure source p and loaded by Z . The three loaded circuits are shown in figure 3.

In figure 3c, capacitor C shunts pressure source p . To obtain a solution C must be considered as part of p and, hence, is shown dashed to indicate that it must be eliminated from this circuit.

Based on an assumption of linear components, transfer functions, $\frac{P_{out}}{P_{in}}(s)$, for the loaded RLC, RCL, and CRL circuits are derived as

$$\frac{RLC}{P_{in}} \frac{P_{out}}{P_{in}}(s) = \frac{1}{(1 + \frac{R}{Z}) + (RC + \frac{L}{Z})s + LCs^2} \quad (15a)$$

$$\frac{RCL}{P_{in}} \frac{P_{out}}{P_{in}}(s) = \frac{1}{(1 + \frac{R}{Z}) + (RC + \frac{L}{Z})s + \frac{R}{Z}LCs^2} \quad (15b)$$

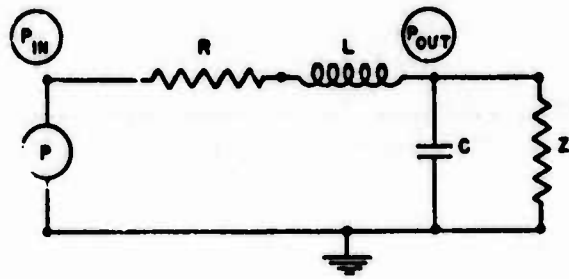
$$\frac{CRL}{P_{in}} \frac{P_{out}}{P_{in}}(s) = \frac{1}{(1 + \frac{R}{Z}) + \frac{L}{Z}s} \quad (15c)$$

To simplify the problem, assume Z is purely resistive so that

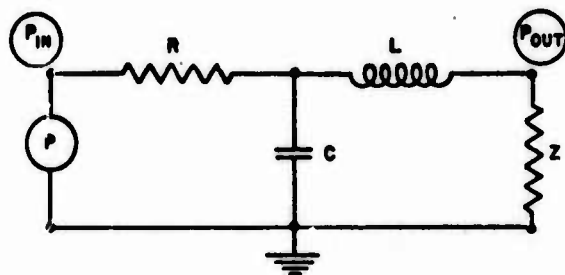
$$Z \equiv R_L$$

Then equation 15 becomes

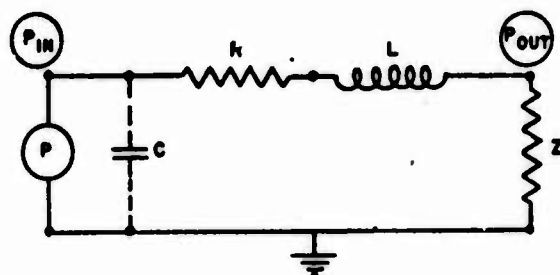
$$\frac{RLC}{P_{in}} \frac{P_{out}}{P_{in}}(s) = \frac{1}{(1 + \frac{R}{R_L}) + (RC + \frac{L}{R_L})s + LCs^2} \quad (16a)$$



(a) Loaded RLC circuit



(b) Loaded RCL circuit



(c) Loaded CRL circuit

Figure 3. Simple loaded dynamic equivalent circuit models of capillary

$$\frac{RCL}{P_{in}} \frac{P_{out}}{P_{in}} = \frac{1}{\left(1 + \frac{R}{R_L}\right) + \left(RC + \frac{L}{R_L}\right) s + \frac{R}{R_L} LC s^2} \quad (16b)$$

$$\frac{CRL}{P_{in}} \frac{P_{out}}{P_{in}} (s) = \frac{1}{\left(1 + \frac{R}{R_L}\right) + \frac{L}{R_L} s} \quad (16c)$$

The magnitude ratios $G \left[\frac{P_{out}}{P_{in}} (j\omega) \right]$ and phase difference $\phi \left[\frac{P_{out}}{P_{in}} (j\omega) \right]$ for each of the three models are tabulated below.

Model	$G \left[\frac{P_{out}}{P_{in}} (j\omega) \right]$	$\phi \left[\frac{P_{out}}{P_{in}} (j\omega) \right]$
RLC	$\frac{1}{\sqrt{\left(1 + \frac{R}{R_L} - LC\omega^2\right)^2 + \left(RC + \frac{L}{R_L}\right)^2 \omega^2}}$	$-\arctan \left[\frac{\left(RC + \frac{L}{R_L}\right)\omega}{1 + \frac{R}{R_L} - LC\omega^2} \right]$
RCL	$\frac{1}{\sqrt{\left(1 + \frac{R}{R_L}(1 - LC\omega^2)\right)^2 + \left(RC + \frac{L}{R_L}\right)^2 \omega^2}}$	$-\arctan \left[\frac{\left(RC + \frac{L}{R_L}\right)\omega}{1 + \frac{R}{R_L}(1 - LC\omega^2)} \right]$
CRL	$\frac{1}{\sqrt{\left(1 + \frac{R}{R_L}\right)^2 + \left(\frac{L}{R_L}\right)^2 \omega^2}}$	$-\arctan \left[\frac{\frac{L}{R_L} \omega}{1 + \frac{R}{R_L}} \right]$

Consider typical values of R , L , C and R_L for the capillaries discussed in this paper,

$$R = 10^8 \frac{\text{kg}}{\text{m}^4 \text{sec}},$$

$$L = 10^5 \frac{\text{kg}}{\text{m}^4},$$

$$C = 10^{-12} \frac{\text{m}^4 \text{sec}^2}{\text{kg}},$$

$$R_L = 10^8 \frac{\text{kg}}{\text{m}^4 \text{sec}}.$$

To get some further feel for the three models without making any generalizations, choose $R_L \equiv R = \frac{8\mu\ell}{\pi r^4}$. (This assumption about the values of R in no way says that a real R of this form exists without L and C.) Above, it should be noted that when $R_L \equiv R$, the transfer functions for the RLC model (equation 16a) and the RCL model (equation 16b) are the same, as are the tabulated expressions for G and ϕ .

Substituting typical values for R, L, C, and R_L into the expressions for magnitude ratios and phase differences

Model	$G\left[\frac{P_{out}}{P_{in}}(j\omega)\right]$	$\phi\left[\frac{P_{out}}{P_{in}}(j\omega)\right]$
RLC	$\sqrt{\frac{1}{4-3.6 \times 10^{-7}\omega^2+10^{-14}\omega^4}}$	$\left[-\arctan \frac{2 \times 10^{-4}\omega}{2-10^{-7}\omega^2}\right]$
RCL	$\sqrt{\frac{1}{4-3.6 \times 10^{-7}\omega^2+10^{-14}\omega^4}}$	$\left[-\arctan \frac{2 \times 10^{-4}\omega}{2-10^{-7}\omega^2}\right]$
CRL	$\sqrt{\frac{1}{4+10^{-8}\omega^2}}$	$\left[-\arctan \frac{10^{-4}\omega}{2}\right]$

Now if the frequency $\omega < 10^3$ (< 160 Hz), G and ϕ are monotonic. Using $\omega = 10^3$, the comparison of G and ϕ is tabulated below.

Model	$G\left[\frac{P_{out}}{P_{in}}(j\omega)\right]$	$\phi\left[\frac{P_{out}}{P_{in}}(j\omega)\right]$
RLC	.523	- 6.09 deg
RCL	.523	- 6.09 deg
CRL	.499	- 2.86 deg

Thus, for linear models loaded with an equal resistance ($Z \equiv R_L$), the CRL model has about the same frequency response (G and ϕ) as the RLC and RCL models up to 160 Hz. These results may be extended somewhat. Consider a resistor loading the capillary. Then for linear models, the geometry and fluid parameters determine the values of RC, LC, R/R_L and L/R_L used in computing G and ϕ for a loaded capillary.

$$RC = \frac{8\mu\ell}{\pi r^4} \frac{\pi r^2 \ell}{np_\infty} = \frac{8\mu}{np_\infty} \frac{\ell^2}{r^2} \quad (17a)$$

$$LC = \frac{\beta\rho\ell}{\pi r^2} \frac{\pi r^2\ell}{np_\infty} = \frac{\beta\rho}{np_\infty} \ell^2 \quad (17b)$$

$$\frac{R}{R_L} = \frac{8\mu\ell}{\pi r^4} \frac{\pi r_L^4}{8\mu\ell_L} = \left(\frac{r_L}{r}\right)^4 \frac{\ell}{\ell_L} \quad (17c)$$

$$\frac{L}{R_L} = \frac{\beta\rho\ell}{\pi r^2} \frac{\pi r_L^4}{8\mu\ell_L} = \frac{\beta\rho}{8\mu} \left(\frac{r_L}{r}\right)^2 \frac{\ell}{\ell_L} \quad (17d)$$

For other than resistive loads and linear component models, the above discussion gives only an approximate method for comparing models of the capillary. A more detailed discussion is presented in reference 18.

For a bundle of N parallel capillaries consider each of the six individual circuits placed in parallel as in figure 4.

The N identical capacitors, placed at node OUT (fig. 4a, b) and node IN (fig. 4e), are in parallel so that from equation (13a)

$$C_{\ell,N} = \sum_{i=1}^N C_{\ell,i} = \sum_{i=1}^N \left(\frac{\pi r^2 \ell}{np_\infty} \right) = \frac{N\pi r^2 \ell}{np_\infty} \quad (18a)$$

However only if the pressures at all three nodes MID1, MID2 and MID3 are equal, equation (18a) will apply for figure 4 (c, d). Also for equal pressures at MID1, MID2, and MID3, not only N identical resistors will be in parallel so that equation (9) holds, but also N identical inductors will be in parallel so that from equation (13b),

$$L_{\ell,N} = \sum_{i=1}^N L_{\ell,i} = \sum_{i=1}^N \left(\frac{\lambda\rho\ell}{\pi r^2} \right) = \frac{\lambda\rho\ell}{N\pi r^2} \quad (18b)$$

3.2 Enclosed Pneumatic Volume

A tank and a cavity with almost closed surfaces are the structures described as enclosed volumes. In this section, the dynamics of enclosed volumes are represented in an equivalent circuit framework. As mentioned briefly in section 3.1, an enclosed pneumatic volume stores energy through the compressibility process.

Static absolute pressure, p , in the enclosed volume may be written as

$$p = p_\infty + p_1 \quad (19a)$$

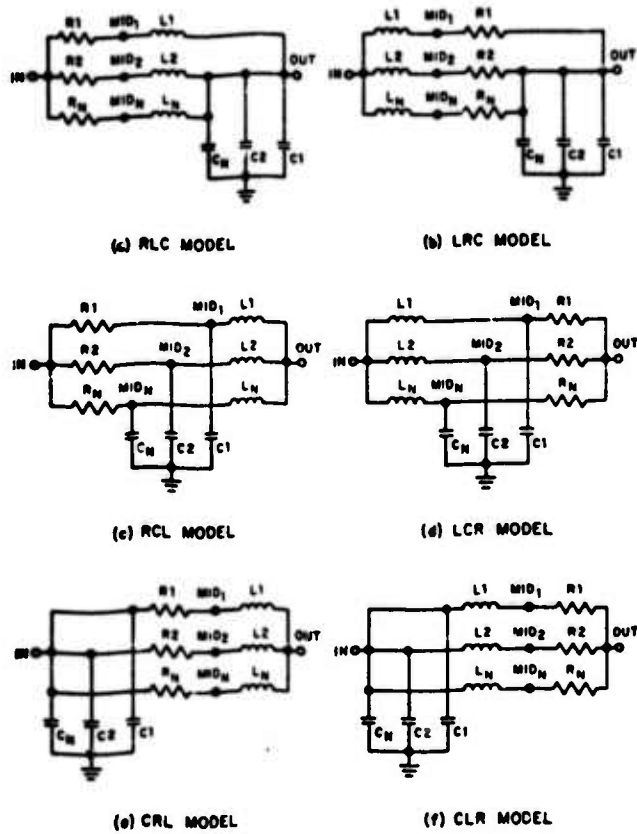


Figure 4. Simple dynamic equivalent circuit models for bundles of N parallel capillaries

where p_∞ is a steady-state reference pressure and p_1 is a small fluctuation about p_∞ . In a small signal analysis,

$$p_\infty = \text{constant}, \quad (19b)$$

$$p_1 \ll p_\infty, \quad (19c)$$

so that

$$p = p_\infty, \quad (19d)$$

and

$$\frac{dp}{dt} = \frac{dp_1}{dt}. \quad (19e)$$

Pressure in an enclosed pneumatic volume may be expressed in differential form (ref 2) in terms of the net volume inflow, ΔQ , as

$$\frac{dp}{dt} = \frac{n}{V} \Delta Q, \quad (20a)$$

where V is the volume and n is the polytropic coefficient. In integral form for constant n and constant volume, V ,

$$p_1 = p_\infty \frac{n}{V} \int_0^t (\Delta Q) dt. \quad (20b)$$

Linear fluidic capacitance, C_L , is defined as a ratio of the change of gas volume (the time integrated volume flow) to the static pressure drop developed across the enclosed volume (ref 19),

$$C_L = \frac{\Delta V}{\Delta p}; \quad (21a)$$

or

$$C_L = \frac{\int_0^t (\Delta Q) dt}{p - p_\infty}. \quad (21b)$$

In this simple linear model, linear capacitance, C_L , is found from equations (20b) and (21b) to be

$$C_L = \frac{V}{np_\infty}. \quad (22)$$

The simple definition for linear capacitance in equation (22) fails to account for several factors:

- (1) Large changes in pressure, p_1 , about steady state (not as small as indicated in equation 19c).
- (2) Variable polytropic coefficient, n , as a function of the pressure change.
- (3) Shape of the enclosed volume that affects the value of capacitance.
- (4) Energy dissipation as well as energy storage processes.

Case (1) occurs for finite pressure perturbations, in which p_1 is of order p_∞ , for which a pneumatic enclosed volume operates in a nonlinear range. Then the nonlinear equivalent of equation (20b) relating the static pressure to the time integrated volume flow, is derived from the continuity equation and the polytropic equation of state as equation (23),

$$p = p_\infty \exp \left(\frac{n}{V} \int \Delta Q dt \right) \quad (23)$$

The use of two linear circuit equations (conservation of mass and conservation of energy) as approximations for the nonlinear fluid equations for conservation of mass, energy, and momentum is not warranted for large perturbations. Our purpose here is to obtain an indication of the range of validity of the linear approximation for capacitance.

It is possible to approximate the error in assuming a linear model of capacitance in equation (22) instead of the nonlinear functional relationship in equation (23) by expanding equation (23) in a series,

$$p = p_\infty \left(1 + \left(\frac{n}{V} \right) \int^t \Delta Q dt + \frac{1}{2} \left(\frac{n}{V} \right)^2 \int^t \Delta Q dt^2 + \frac{1}{6} \left(\frac{n}{V} \right)^3 \int^t \Delta Q dt^3 + \dots \right) \quad (24)$$

Now if the quantity $(p - p_\infty)$ is formed from equation (24), the reciprocal taken, and the result rearranged in the form of the definition of capacitance in equation (21b), then equation (25) yields the desired result for nonlinear capacitance.

$$c = \frac{\int^t \Delta Q dt}{p - p_\infty} = \frac{V}{np_\infty} \left(1 - \frac{1}{2} \left(\frac{n}{V} \right) \int^t \Delta Q dt + \frac{1}{6} \left(\frac{n}{V} \right)^2 \left[\int^t \Delta Q dt \right]^3 + \dots \right) \quad (25)$$

If the higher order terms of the series are small, equation (25) is identical with the linear definition of capacitance in equation (22). The relative importance of the second term of the series in equation (25) may be judged by taking the absolute value of the ratio of the second and first terms of the series as

$$\frac{1}{2} \frac{n}{V} \int^t \Delta Q dt .$$

It is usually desirable that this quantity be less than 0.05.

The dynamic properties of the enclosed volume are described as a grounded capacitor as shown in figure 5.



Figure 5. Equivalent circuit model of simple enclosed volume

As cited in case (2) above, when the polytropic coefficient is nonconstant, a better model may be made. Katz and Hastie (ref 7) investigate this problem and approximate n as

$$n = \frac{1}{1 - \rho R \frac{\Delta T}{\Delta p}}, \quad (26)$$

where R is the universal gas constant. The ratio of average temperature change to pressure change $\frac{\Delta T}{\Delta p}$ (developed by Daniels, ref 20 for several specific structures) may be expressed for an infinitely long cylinder as

$$\frac{\Delta T}{\Delta p} = 1 - \frac{2 J_1 (j^{3/2} \sqrt{\frac{\omega \rho C_p}{\kappa}} r)}{j^{3/2} \sqrt{\frac{\omega \rho C_p}{\kappa}} r J_0 (j^{3/2} \sqrt{\frac{\omega \rho C_p}{\kappa}} r)} \quad (27)$$

where

J_0 and J_1 are zeroth and first-order Bessel functions,
 ω is the frequency,
 C_p is the specific heat capacity at constant pressure, and
 κ is the thermal conductivity.

No correction is made for the end effects of a cylinder of finite length.

In case (3), linear capacitance for a cylinder that operates in a frequency range having a varying polytropic coefficient is calculated from equations (21'), (26), and (27).

$$C_L = \frac{V}{p} [\operatorname{Re} \left(\frac{1}{n} \right) - j \operatorname{Im} \left(\frac{1}{n} \right)], \quad (28a)$$

where the real and imaginary parts of $\frac{1}{n}$ are given as

$$\operatorname{Re} \left(\frac{1}{n} \right) = \left[\frac{1}{Y} - \frac{Y-1}{Y} \frac{\sqrt{2}}{\alpha} \frac{\operatorname{ber}_0 \alpha \operatorname{ber}_1 \alpha + \operatorname{bei}_0 \alpha \operatorname{bei}_1 \alpha - \operatorname{ber}_0 \alpha \operatorname{bei}_1 \alpha + \operatorname{ber}_1 \alpha \operatorname{bei}_0 \alpha}{\operatorname{ber}_0^2 \alpha + \operatorname{bei}_0^2 \alpha} \right] \quad (28b)$$

$$\operatorname{Im} \left(\frac{1}{n} \right) = \left[\frac{Y-1}{Y} \frac{\sqrt{2}}{\alpha} \frac{\operatorname{ber}_0 \alpha \operatorname{ber}_1 \alpha + \operatorname{bei}_0 \alpha \operatorname{bei}_1 \alpha + \operatorname{ber}_0 \alpha \operatorname{bei}_1 \alpha - \operatorname{ber}_1 \alpha \operatorname{bei}_0 \alpha}{\operatorname{ber}_0^2 \alpha + \operatorname{bei}_0^2 \alpha} \right] \quad (28c)$$

where

$$\alpha = \sqrt{\frac{\omega C}{p}} \frac{r}{r} \quad (28d)$$

and where the ber and bei functions are Bessel functions of zero and integer orders and with arguments that are functions of $j^{3/2}$.

Admittance, Y , of a capacitor is written as

$$Y = j\omega C \quad (29)$$

Combining equations (28a) and (29), the admittance of the cylindrical volume becomes

$$Y = \frac{V\omega}{p} \operatorname{Im} \left(\frac{1}{n} \right) + j \frac{V\omega}{p} \operatorname{Re} \left(\frac{1}{n} \right) \quad (30a)$$

Admittance in equation (27a) has a form

$$Y = \frac{1}{D(\omega)} + j\omega C, \quad (30b)$$

where $D(\omega)$ is a-c dissipation.

According to Shearer et al (ref 12), the form of the admittance in equation (30b) defines the equivalent circuit of an enclosed volume as

a parallel (fig 6) array of a frequency-dependent capacitor and a frequency-dependent energy dissipating element, $D(\omega)$, that dissipates energy as a function only of the a-c pressure at node (IN). Its d-c impedance is infinite.

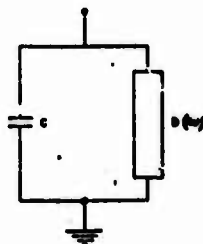


Figure 6. Equivalent circuit of a frequency dependent cylindrical volume

As noted in case (4) above, energy storage and energy dissipation for a cylindrical volume are defined in equations (30a, b).

$$\frac{1}{D(\omega)} = \frac{V\omega}{p} \operatorname{Im} \left(\frac{1}{n} \right), \quad (31a)$$

$$C = \frac{V}{p} \operatorname{Re} \left(\frac{1}{n} \right). \quad (31b)$$

In terms of the argument, α , it can be shown that

as $\alpha \rightarrow 0$

$$C = \frac{V}{p} \operatorname{Re} \left(\frac{1}{n} \right) \rightarrow \frac{V}{p}, \text{ the isothermal case;} \quad (32a)$$

as $\alpha \rightarrow \infty$

$$C = \frac{V}{p} \operatorname{Re} \left(\frac{1}{n} \right) \rightarrow \frac{V}{\gamma p}, \text{ the adiabatic case;} \quad (32b)$$

and also as $\alpha \rightarrow 0$, and $\alpha \rightarrow \infty$

$$D(\omega) = \frac{p}{V\omega} \frac{1}{\operatorname{Im} \left(\frac{1}{n} \right)} \rightarrow \infty \quad (32c)$$

Capacitance and frequency-dependent energy dissipation for a cylindrical volume are plotted in figure 7. Frequency dependent energy dissipation has approximately a minimum value when argument $\alpha = 3$. Below a value $\alpha = .52$ and above a value $\alpha = 40$, energy dissipation is at least an order of magnitude greater than that of its minimum value.

Capacitance is within 1 percent of its isothermal value for values of $\alpha < 1$ and within 1 percent of its adiabatic value for $\alpha > 50$.

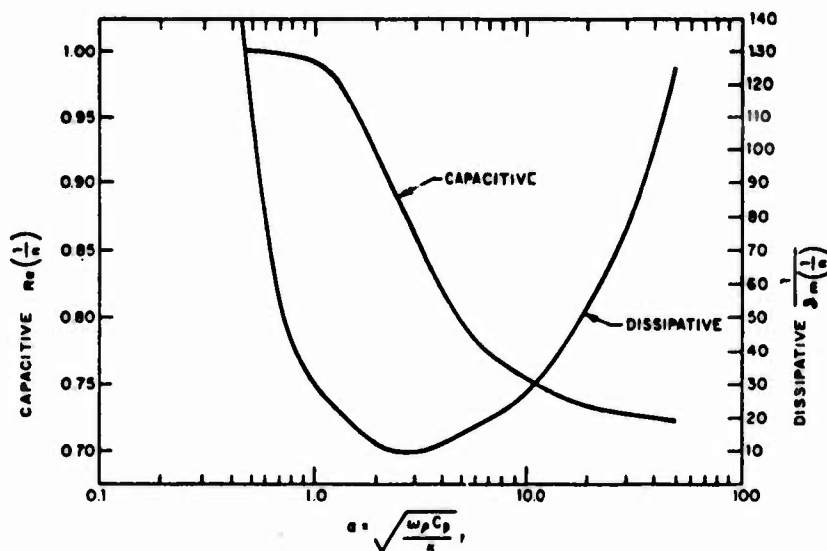


Figure 7. Frequency dependent dissipation and capacitance for enclosed cylinder

3.3 Mechanical Confining Structures

The bellows module and the diaphragm module are mechanical, moving parts devices introduced into no-moving-parts fluidic circuits to provide point-to-point capacitance functions.

3.3.1 Bellows Module

The energy storage process in the bellows module occurs through the deflection of its moving member and the gas compressibility. The deflection process is analogous either to mechanical energy being stored in the deflection of a spring or to electrical energy being stored in an electrical capacitor.

The bellows operates approximately in a linear mode as long as its maximum deflection, x_{\max} , is not exceeded. To determine the relation between pressure difference and deflection, consider that in a linear mode, Hooke's law gives the restoring force, F , as

$$F = -kx, \quad (33a)$$

where k is the spring constant.

From equation (33a), the pressure difference, Δp , across the bellows is determined to be

$$\Delta p = \frac{kx}{A}, \quad (33b)$$

where A is the cross-sectional area of the bellows.

Writing the deflection in terms of a volume change, ΔV , then equation (33b) may be rewritten as

$$\Delta p = \frac{k\Delta V}{A^2}. \quad (33c)$$

Volume change, ΔV , is equivalent to $(\int \Delta q \, dt)$ so that from equation (33c) it is possible to write

$$\Delta p = \frac{k}{A^2} \int \Delta Q \, dt. \quad (33d)$$

Comparing equation (33d) with a definition of capacitance in equation (21b), a formula for the point-to-point capacitance of the pneumatic bellows module without compressibility effects is

$$C = \frac{A^2}{k}. \quad (34)$$

Thus, as desired, a simple equivalent circuit model of the dynamic process (eq 34) in the bellows module is a point-to-point capacitor (fig. 8).

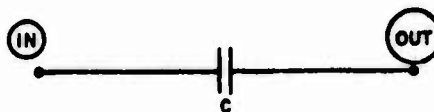


Figure 8. Simple equivalent circuit for bellows module

However, these mechanical modules are more complicated than those of pure point-to-point capacitors. In the expanded equivalent circuit (fig. 9), two capacitors, two resistors, and two inductors are added to the simplest equivalent circuit (fig. 8) of a point-to-point capacitor, C_1 , between nodes IN and OUT.

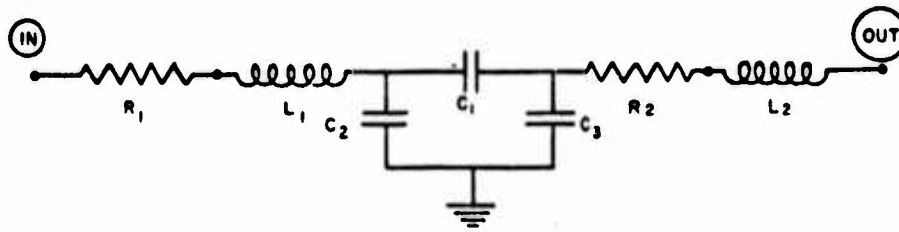


Figure 9. Sophisticated equivalent circuit for bellows module

Resistors, R_1 and R_2 , and inductors, L_1 and L_2 , are the expansions to and the contractions from the cross-sectional area, A , of the bellows. The increased cross-sectional area also introduces added volumes, represented by capacitors, C_2 and C_3 , for each side of the bellows to account for compressibility.

3.3.2 Diaphragm Module

The diaphragm module, a second mechanical point-to-point capacitor, has been studied by Katz and Hastie (ref 8). In this section, its dynamic processes are modeled within the equivalent circuit framework.

The diaphragm module stores energy in a diaphragm (membrane), through a deflection process similar to that of a bellows. The deflection, $x(r)$, of a circular diaphragm membrane is shown by Katz and Hastie (ref 8) to be a function of the radial position, r , in terms of the modulus of elasticity of the diaphragm, E , the diaphragm thickness, h , the diaphragm radius, r_0 , and the pressure difference, Δp , across the diaphragm as

$$x(r) = 0.662 r_0^{4/3} \left(\frac{p_1 - p_2}{Eh} \right)^{1/3} \left(1.0 - 0.9 \frac{r^2}{r_0^2} - 0.1 \frac{r^5}{r_0^5} \right), \quad (35)$$

where

$$p_1 > p_2$$

The volume displaced, ΔV , in diaphragm deflection is determined by integrating equation (35) yielding,

$$\Delta V(r) = 0.362 \left(\frac{p_1 - p_2}{Eh} \right)^{1/3} r_0^{10/3}. \quad (36)$$

The displaced volume, $\Delta V(r)$, is substituted into the definition of fluidic capacitance in equation (21a) so that capacitance, C , for the circular diaphragm is given as

$$C = 0.362 \frac{r_o^{10/3}}{(Eh)^{1/3}} |p_1 - p_2|^{-2/3} \quad (37)$$

The mechanical capacitance of the diaphragm is nonlinear because of its functional dependence upon the pressure difference, $p_1 - p_2$, across the diaphragm. When the difference is zero, equation (37) indicates that capacitance, C , becomes infinite. According to reference 8, however, a d-c bias pressure may be applied across the diaphragm. Then for small amplitude signals, the pressure changes in equation (37) remain approximately constant and the capacitance, C , is fairly linear for small signals.

The value of the linearized capacitance (about a d-c operating point) is calculated from equation (37) and rewritten as

$$C = K |p_1 - p_2|^{-2/3} \quad (38)$$

where

$$K = \frac{0.362 r_o^{10/3}}{(Eh)^{1/3}} \quad (39)$$

Therefore from equation (38), the simplest equivalent circuit model of the energy processes in a diaphragm module is a point-to-point capacitor (fig. 10).

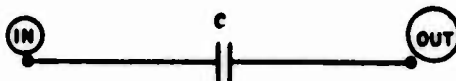


Figure 10. Simple equivalent circuit for diaphragm module

As discussed in section 3.3.1 for the bellows modules, additional energy processes are included in more sophisticated equivalent circuits (fig. 11) to account for losses and inductance in the inlets/outlets,

and added capacitance due to the fixed volumes on each side of the diaphragm.

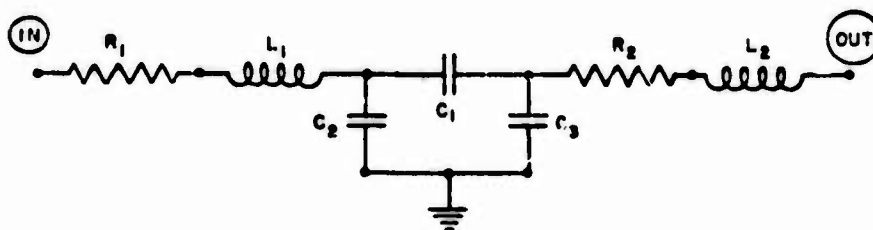


Figure 11. Sophisticated equivalent circuit for diaphragm module.

A point-to-point capacitor, C_1 , is placed between nodes IN and OUT. The equivalent circuit model for expansions and constrictions includes in addition both energy dissipation in two resistors, R_1 and R_2 , and energy storage in two inductors, L_1 and L_2 . In addition energy storage in the two chambers (adjacent to the diaphragm) is modeled as two capacitors C_2 and C_3 .

3.4 Fluidic Junction

The foregoing sections have described equivalent circuit models for several passive components--capillaries, enclosed volumes and mechanical capacitors. Each of these passive components forms a branch of a fluidic configuration. Fluidic junctions, at which these components are joined, are discussed in this section.

Fluidic junctions may be as simple as connection points where two or more fluidic components are joined. For example, the connection point for two components is a union. For three components or branches meeting at one point, the connection points are tees and Y's while for four components they are X's. More complicated configurations with multiple fittings such as tanks and stilling chambers are also considered as junctions.

The flow in the ideal fluidic junction is one dimensional and the junction offers zero impedance that is, no energy losses and no energy storage. An ideal fluidic junction is analogous to the voltage node in electronics. However, when considering an actual fluidic junction that must cover a wide bandwidth and a wide dynamic range, a tradeoff between directional (momentum) effects and zero impedance must generally be made.

Impedance of fluidic junctions is minimized by keeping passages

short and by not expanding into large chambers. On the other hand, directionality in fluidic junctions is minimized by expanding into large chambers to convert directional dynamic pressure into a uniform static pressure. A junction of three or more fluidic components may be considered to be a pure node if energy is neither dissipated nor stored at the junction and if all the energy is in the form of potential energy. Pneumatic nodes are usually designed by minimizing the ratio of kinetic to potential energies at the expense of added impedance. The simplest equivalent circuit that represents a pneumatic node is a capacitor, C , from the connection point, IN, to ground (fig. 12). Capacitance is minimized if the volume is kept small.



Figure 12. Simple equivalent circuit for pneumatic node

At higher velocities, the nodal connection point may be actually converted into a stilling chamber to guarantee that static pressure drop instead of total pressure drop is developed.

The pneumatic fluidic junction discussed above may also be used to perform other functions in fluidic circuits. For example, in systems applications, this fluidic junction may be used as a passive fluidic summing junction and as a passive fluidic distribution junction, which will be discussed in the following sections.

3.4.1 Passive Fluidic Summing Junction

Passive fluidic summing junctions have the same configurations (tees, Y's, x's, and stilling chambers) as junctions of three or more fluidic components (sect 3.4). Consider now the passive junction connecting linear resistors (fig. 13), where an output pressure, p_o , is a function of the sum of input pressures p_1 and p_2 , so that

$$p_o = f(p_1 + p_2). \quad (41)$$

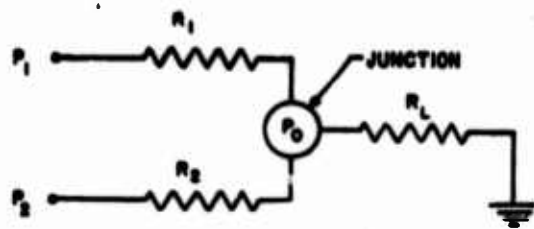


Figure 13. Passive summing junction in system.

The general expression for the output pressure, p_o , at the junction may be written in terms of the input pressures, p_1 and p_2 , the input resistances, R_1 and R_2 , and the load resistance, R_L ,

$$p_o = \frac{\frac{p_1}{R_1} + \frac{p_2}{R_2}}{\frac{1}{R_1} + \frac{1}{R_2} + \frac{1}{R_L}} \quad (42a)$$

Multiplying top and bottom by R_1 and letting $R_2/R_1 = \Gamma$ leads to

$$p_o = \frac{p_1 + \frac{p_2}{\Gamma}}{(1 + \frac{1}{\Gamma}) \frac{R_1}{R_L}} \quad (42b)$$

If the input resistors R_1 and R_2 are much less than R_L , then the pressure at the junction is

$$p_o = \frac{p_1 + \frac{p_2}{\Gamma}}{1 + \frac{1}{\Gamma}} \quad (42c)$$

If $R_1 = R_2$, then $\Gamma = 1$ and the junction pressure is approximately

$$p_o = \frac{p_1 + p_2}{2} \quad (42d)$$

Thus, by letting $R_1 = R_2 \ll R_L$, the half sum (average) of the input pressure p_1 and p_2 is produced independently of the exact values of R_1 , R_2 , and R_L . If $R_1 = R_2 = R_L$ then $p_o = (p_1 + p_2)/3$. The same type of configuration used in the fluidic node may also be used as a passive fluidic summing junction. Tradeoffs must also be made between the impedance and the one dimensionality of the passive fluidic summing junction.

Turnquist (ref 6) uses a stilling chamber in constructing a passive summing junction (fig. 14). Capillaries can then be simply connected as branches to the passive summing junction.

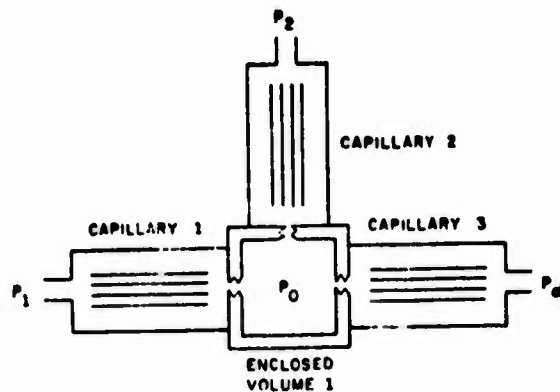


Figure 14. Passive summing junction

Junctions used in the present studies are the enclosed volumes (discussed in section 3.2). The simplest equivalent circuit for a passive summing junction is identical with a simple model of a node. It is a capacitor, C , between the connection point, IN, and ground (fig. 15).

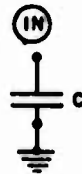


Figure 15. Simple equivalent circuit for passive summing junction

3.4.2 Passive Fluidic Distribution Junction

The passive fluidic distribution junction is a device that receives an input pressure p_1 and applies a reduced part of it to two

or more output loads. In such a manner, the same output driving pressure can be applied to each of the loads, regardless of the geometry and the pressure level. As in the consideration of a fluidic junction, tradeoffs between momentum effects and the impedance must be made in certain cases.

The passive distribution junction may be viewed as a passive junction in conjunction with linear resistors (fig. 16).

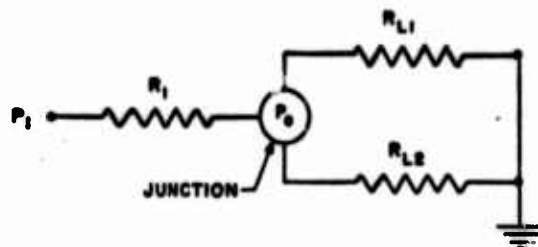


Figure 16. Passive distribution junction in system

The simple equivalent circuit for the passive fluidic distribution junction is also identical with a simple model of a node (fig. 17). It is a capacitor, C , between the connection point, IN , and ground (fig. 17).

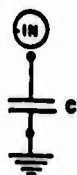


Figure 17. Simple equivalent circuit for passive distribution junction

4. COMPUTER-AIDED CIRCUIT ANALYSIS

To complement the circuit models that have been developed in section 3, methods are required for computing the response of these models, for evaluating these models, and for selecting the best models in network designs. This section cites a few methods of computing the response of circuit models. Useful methods include manual techniques, analog computer techniques, and digital computer algorithms.

The digital computer is useful in at least two ways for performing

circuit analysis. First, input format to the circuit analysis program of the digital computer is extremely easy to code. Second, self-organizing schemes allow circuit equations to be formed and solved internally by the computer when only component values and interconnections are provided.

Many circuit analyses programs including CIRCUS, ECAP, ECAP II, NET-1, NET-2, SCEPTRE, SINC, SLIC, SPICE, and TRAC are currently available at HDL. Most of these have been written for solving large electronic circuits. To date, no single circuit analysis program has been written solely for fluidic circuits. Reference 14 gives a detailed description of two programs--SLIC (ref 21) and NET-2 (ref 22)--that have been converted for fluidic circuit analyses. If self-organizing schemes for equations are not desired, then circuit equations may be solved with such programs as DSL/90 (ref 23) or even simply in FORTRAN.

Steady-state d-c analyses, small signal steady-state a-c analyses, and time dependent analyses may be performed on a digital computer for both passive and active circuits. Also, sensitivity analyses and optimization routines are available in many digital computer schemes.

In reference 14, general passive circuit analyses are implemented in SLIC and NET-2 so that both amplitude and frequency-dependent fluidic circuits may be solved. Simultaneity of solutions is assured at each operating point for both of these programs. In both SLIC and NET-2, the computational approach is designed to solve the complete set of circuit equations simultaneously at each selected operating point. Initial guesses, usually based on previous results, are used to start iterative calculations. Then the iteration process is performed until the difference between successive solutions is minimized within an allowable error.

Less sophisticated approaches do not use as much care in calculating circuit response. Instead, accuracy of response variables is traded off against complexity and computer cost.

In cases where circuit equations are not solved simultaneously, if starting approximations are good because computational points are taken close together, results can be very good. However, in general when a system of circuit equations lacks simultaneity of solution, response errors can compound significantly as successive guesses are based on increasingly less valid starting values.

5. EXPERIMENTAL STUDIES

The next objective discussed is the evaluation of equivalent circuit models of fluidic components. Evaluation, in the context of this study, is a qualitative assessment of the agreement between the measured response of the fluidic network and the calculated response of several circuit models. The evaluation procedure shows how changes in

the models improve agreement relative to changes of the structure of the expressions for component values and of equivalent circuit topology.

As a basis for evaluating models of various passive fluidic components, experimental studies have been run in the laboratory on individual components and on components connected as subsystems. Both dc- and ac-response tests were run in these studies. The dc tests were run on capillaries. The tests were run on summing and distribution junctions and on compensation networks, including lead, lag, and lag-lead subsystems. The a-c tests were not conducted on individual components in this study.

Fluidic components have been selected that would be typically used in fluidic systems. The hardware discussed in sections 5, 6, and 7 are four types of modular components: (1) capillary modules, (2) enclosed volumes, (3) bellows modules, and (4) diaphragm modules. Each of the individual hardware components is designed to be compatible both with the others, to assure interchangeability among various subsystems, and with other fluidic hardware, including pressure transducers.

Modules are made of a variety of materials including brass, aluminum, plexiglass and porcelain. Most connectors use teflon seals on the threads to prevent leaks.

All measurements presented herein represent data using air at 20°C as the working fluid.

5.1 DC-Response Measurements

The dc-response measurements were made on components that dissipate energy. For these components both steady-state pressure drops between nodes and through flows were measured on a static-test stand (fig. 18). In the static tests a pressure differential was established between a regulated pressure source and ambient pressure. One end of the test element was connected to the source and the other was exhausted through a flow meter to ambient.

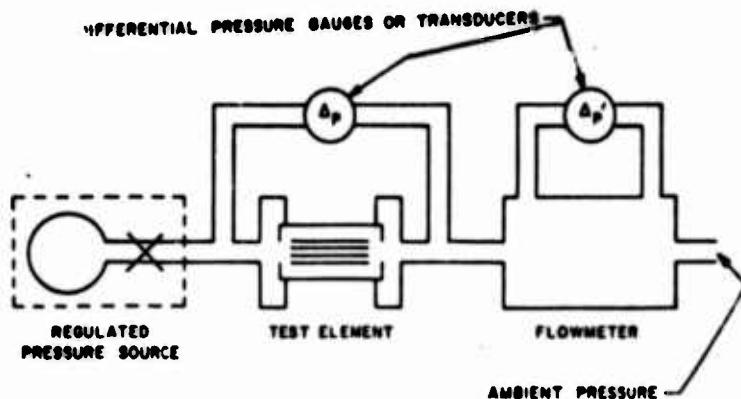


Figure 18. Static-test stand

A plot of pressure drop versus volume flow was obtained by sweeping the regulated pressure source slowly enough through a range to provide repeatability when the motor first opens and then closes the pressure regulator.

The steady-state pressure drop, Δp , across the component was measured either on a pressure gauge or with a low frequency differential pressure transducer, such as an electronic manometer. At low-flow rates, volume flow, Q , was measured with a laminar flow meter. Volume flow, Q , was indicated as a pressure drop, $\Delta p'$, proportional to Q so that

$$Q(\Delta p') = k_1 \Delta p' , \quad (5.1)$$

where k_1 is the proportionality constant. This pressure drop, $\Delta p'$, may also be measured either on a pressure gage or with a low-frequency pressure transducer.

The resultant data, static-pressure drop, Δp , was plotted as a function of the volume flow, Q , on an x-y plotter. The instantaneous slope of Δp versus Q is the resistance, R , of the component being tested,

$$R = \frac{\partial(\Delta p)}{\partial Q} \quad (5.2)$$

If the plot of Δp versus Q is a straight line through the origin and the slope is constant, the resistance has a constant value,

$$R = \frac{\Delta p}{Q} \quad (5.3)$$

The d-c response for several bundles of capillaries used in the various configurations was measured on the static-test stand. Several porcelain capillary modules with either 8 or 25 parallel cylindrical capillaries were selected. Each capillary has an internal radius of approximately 1.525×10^{-4} m. Capillary modules were cut from sections that are approximately 0.3 m in length. The diameter of each module is approximately 2.5×10^{-3} m. By individually fitting teflon sleeves over each porcelain module, a single outside diameter can be produced to assure good seals with brass capillary holders in forming overall capillary modules.

Typical pressure drop versus flow curves are shown in figure 19 for three such bundles. In each case, they all have approximately a constant resistance.

5.2 AC-Response Measurements

Steady-state a-c tests were run on several fluidic components and subsystems involving storage devices. For each test configuration, the source and load were kept reasonably isolated from one another.

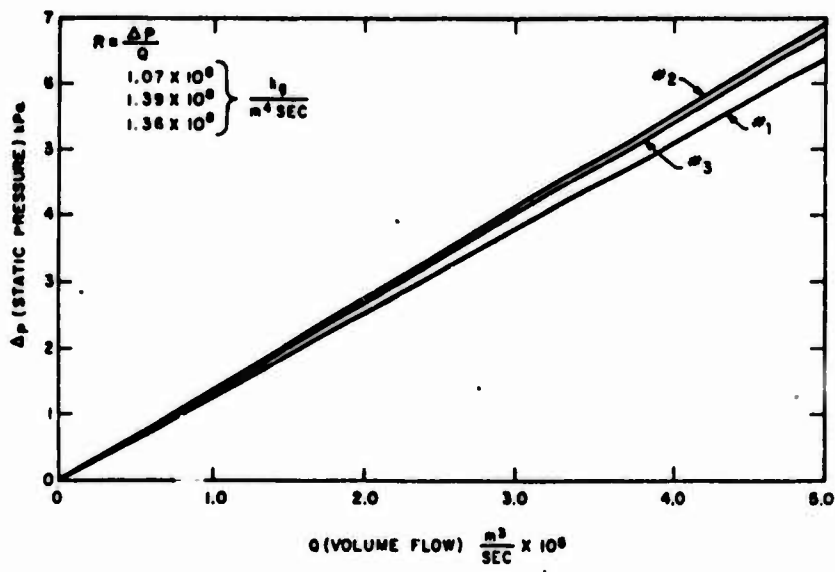


Figure 19. Static response curve for capillaries

The pressure source was a variable frequency, sinusoidal pressure generator which has very low impedance so that the load circuit would have approximately an infinite impedance relative to the test configuration. A pair of small, low-frequency, low-pressure microphones were placed at two pressure nodes in the test configuration to monitor the pressures. When the signal generator was swept through a range of frequencies, Bode plots (magnitude ratio versus frequency and phase difference versus frequency) were obtained.

For linear components, since ratios of nodal response amplitudes are independent of the source amplitude, any source amplitude is permissible; but for nonlinear components, by restricting a-c tests to small signal amplitudes, linearized response about some mean level is measured.

A-c tests were run around ambient pressure level with no through flow. The frequency range is from about 1 to 200 Hz and the input pressure amplitude range is from about 0.02 kPa (0.003 psi) rms to 10 kPa (1.5 psi) rms.

The remaining section discusses the experimental apparatus (fig. 20) which consists of (1) a fluidic signal generator, (2) a fluidic test configuration, (3) a pressure transducer system, and (4) a computation and output system. Calibration of the actual system and a very brief introduction to the experimental measurements on the fluidic configurations are also discussed.

5.2.1 Fluidic Signal Generator

The fluidic signal generator shown in figure 20 consists of two parts -- one part develops a periodic electronic signal that may be swept through a frequency range and another part converts the electronic signal into a pneumatic test signal. Both the frequency and the amplitude of the signal can be adjusted within the electronic equipment. For most cases, the equipment generates a sinusoidal signal that is swept through a frequency range.

Two sinusoidal pressure generators are used. One is a shaker table that drives a piston in an air cylinder (fig. 21); the second is a speaker cone used as a flapper to modulate a fluidic diffuser nozzle (fig. 22).

The shaker table signal generator produces a sinusoidal pressure signal, oscillating about ambient pressure. Two piston/cylinder configurations are used: (1) a piston with an O-ring seal, and (2) a piston with an integral rolling diaphragm seal. Because there is no leakage around the latter cleaner signals can be produced at lower frequencies than with the O-ring seal generator.

No external pressurized air source was used; hence, the net d-c flow was essentially zero. Unfortunately, at low frequencies the

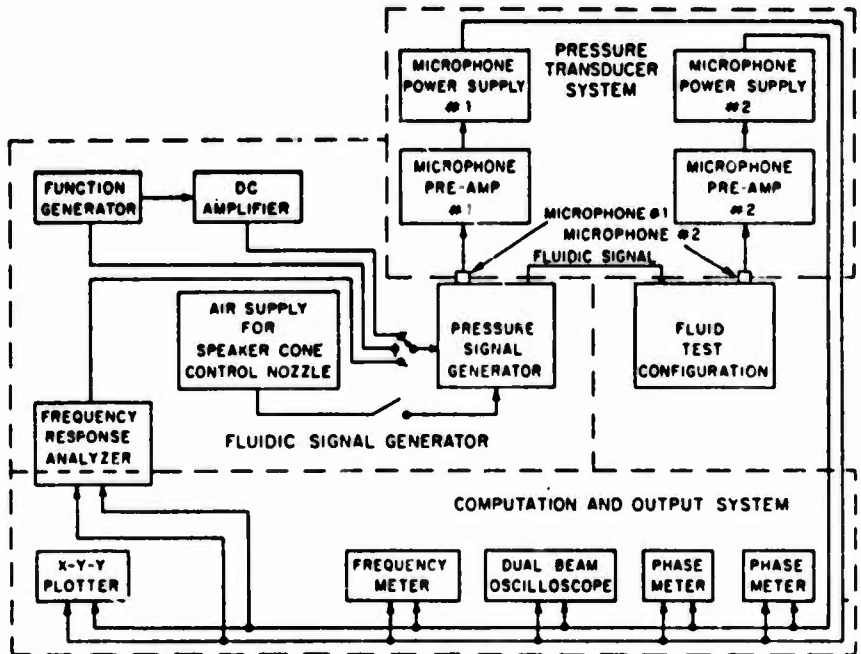


Figure 20. Schematic diagram of a-c test stand

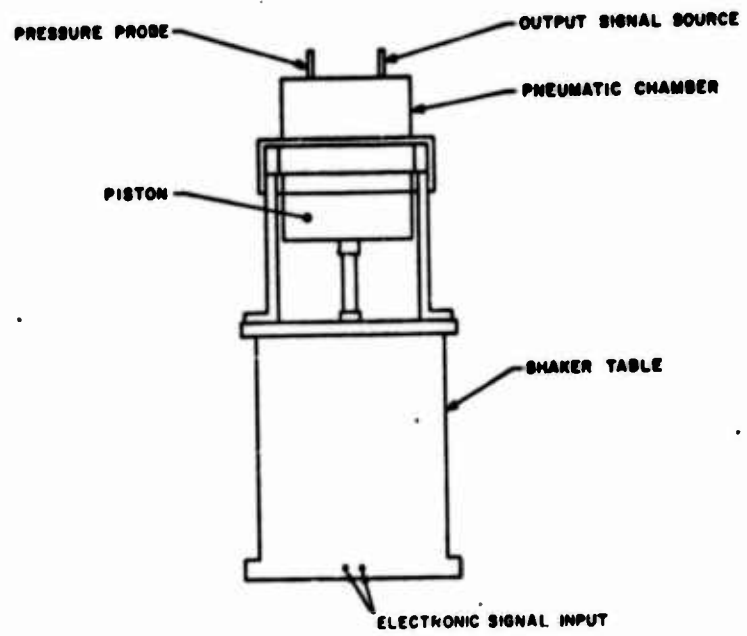


Figure 21. Shaker table signal generator

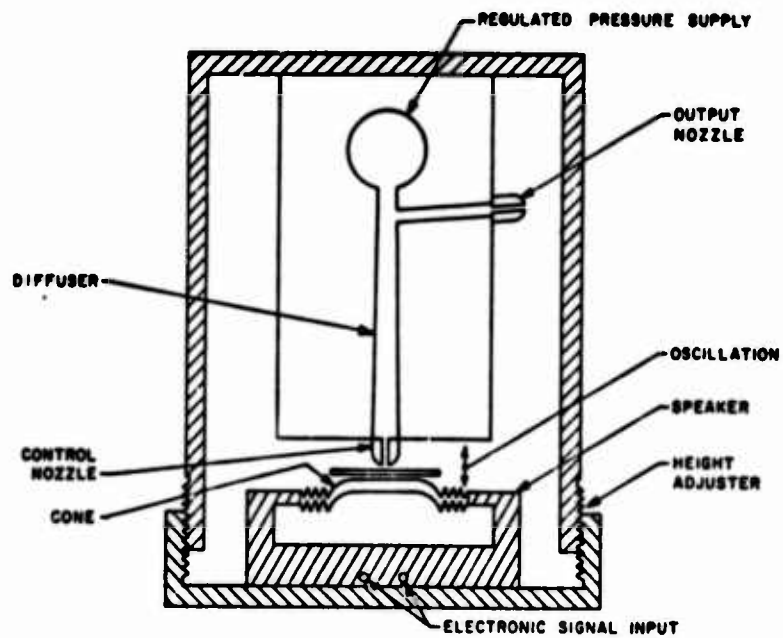


Figure 22. Speaker cone signal generator

mechanical and electromagnetic components have a low signal-to-noise ratio, so that the dynamic range is limited.

The speaker cone signal generator operates in approximately the same frequency range as the shaker table signal generator. Reduced noise in the speaker system, however, allows it to have a wider dynamic range. Adjustments can be made in the speaker cone signal generator to minimize the net throughflow.

The speaker cone, positioned as a flapper valve, loads a nozzle and controls the back pressure. The main flow is either diverted into the output nozzle or entrains flow from the output nozzle. In this manner the generated signal is a function of (1) the spacing between the speaker cone and the control nozzle (2) the regulated supply pressure, and (3) the electronic signal driving the speaker.

Neither signal generator has been developed to such a degree that a monochromatic, undistorted signal over the bandwidth of interest (1 to 200 Hz) can be obtained. This is because at low frequencies the fluidic signal generators do not operate at zero impedance; thus energy-conversion processes tend to distort the signals. Improved amplitude regulation at low frequencies can probably be attained by including a leveling circuit that uses a feedback signal to maintain the generated signal at a constant level. At higher frequencies, the available energy is not sufficient to produce pressure amplitudes as large as for lower frequencies. Also, resonances in the generator can occur within the bandwidth of interest. For, example in the test midrange, the resonant frequency of a mechanical flexure in one of the shaker tables was 65 Hz.

5.2.2 AC-Pressure Transducer System

The a-c pressure signals at the nodes were measured over wide pressure amplitude and wide frequency ranges. These measurements must be true, undistorted, and undelayed. In addition, measuring instrumentation cannot change the circuit performance by adding losses or dynamic effects.

Keeping this in mind, the frequency range, amplitude sensitivity, and installation configuration of pressure transducers become most important factors. The pressure transducers chosen respond from approximately 1 Hz to above 10^5 Hz, and are sensitive to signals as low as 90 dB (relative to $0.0002 \text{ dynes/cm}^2$ ($2 \times 10^{-5} \text{ Pa}$)). The system has flat response above about 20 Hz. Below 20 Hz, gain drops off at approximately 20 dB per decade. Phase shift is approximately zero throughout the frequency range of interest. Pressure signals less than 0.003 psi (20 Pa) rms may be sensed.

A condenser microphone (with a grill cover) is approximately an end section of a right circular cylinder and adds no fluid volume when it is flush-mounted in a flat wall of an enclosed volume. Microphone probe holders, therefore, were designed to fit flush into the walls of

enclosed volumes. A microphone was placed from the rear into a brass probe holder (fig. 23) with 3/8-24 pipe threads.

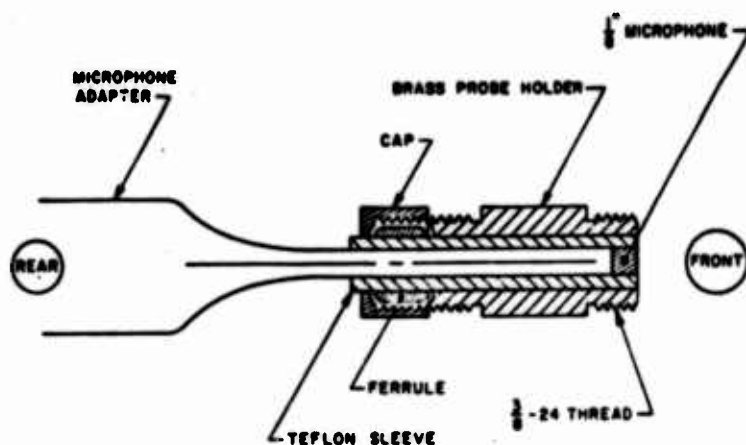


Figure 23. Straight microphone probe holder

At the rear, a cap through which the microphone adapter passes, forces a teflon ferrule to seal a teflon sleeve around the microphone.

Pressure measurements may also be made by placing a condenser microphone probe in an interconnecting passage between two components. These (1/8 in) diameter microphones fit relatively flush in the cylindrical walls of lines which are greater than twice the microphone diameter. In a similar configuration (fig. 24) to a flat wall probe, described above, a probe was mounted into one leg of a threaded brass tee. The tee was joined to two components with 3/8-24 threads.

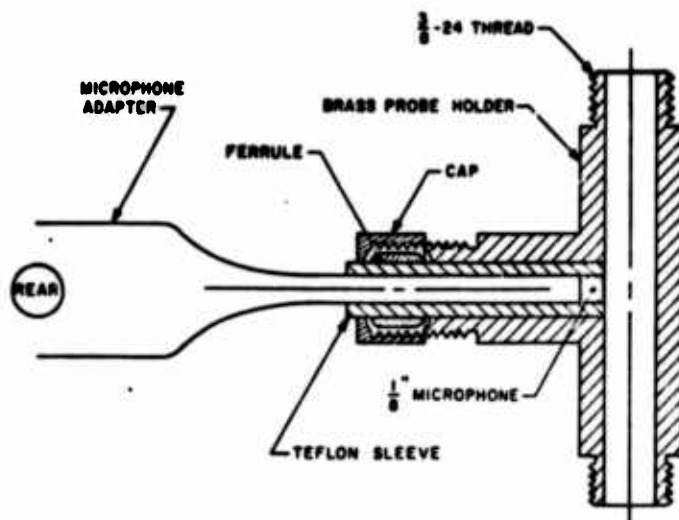


Figure 24. Tee microphone probe holder

To minimize additional contributions to response, length and volumes of air passages in the microphone probes are minimized. Expansions and contractions are used only when absolutely necessary. Teflon sleeves, seals, and tape make the entire test configuration leak proof.

Alternate pressure transducers that have been investigated include (1) variable reluctance diaphragm transducers with carrier demodulators, and (2) piezoelectric crystal transducers with charge amplifiers. The variable reluctance transducers cannot readily be flush-mounted; hence, they add dynamics. The piezoelectric transducers are a-c devices and fail to respond below about 10 Hz.

5.2.3 Computation and Output System

The computation and output system portion of the instrumentation processes input and output pressure signals from the pressure transducers. It computes the phase difference and the magnitude ratio between the output and input pressure signals and the frequency of the input pressure signal. These data are displayed as oscilloscope traces and as plots on an x-y-y plotter. The instrumentation computes the small signal, a-c response of the fluidic system. The ratio of an output-node pressure to an input-node pressure is the pressure transfer function between the input and the output of the system. These sinusoidal pressure response data apply for linear and almost linear studies, restricted to small signals. A Bode plot is one of the most meaningful representations of such sinusoidal input/output pressure data. In this study, both an automated method and a semi-automated method of producing Bode plots are used.

In the automated method, used in the latter part of the study, a commercially available frequency response analyzer or a commercially available gain/phase meter analyze the output and input waveforms. A magnitude ratio and a phase difference are displayed versus frequency.

Several semi-automated approaches were used. In the first approach, a phasemeter and a low-frequency a-c voltmeter were used. Phase difference was read directly from the phasemeter and ratios of the rms voltage output signal to the rms voltage input signal were computed.

Less automated Bode plots may be taken from oscilloscope traces. One method, used extensively before the automated equipment was obtained, analyzes photographs of output and input waveform traces from the oscilloscope. In this method magnitude ratios were calculated from photographs of oscilloscope waveforms. Assuming pure sine waves, peak-to-peak heights of both the inputs and outputs were measured, multiplied by appropriate scale factors, and adjusted with respect to calibration factors. Then the magnitude ratio or gain, G , was calculated and converted to dB gain, G_{dB} , between the input pressure, p_i , and the output pressure, p_o , as

$$G_{dB} = 20 \log_{10} \frac{p_o}{p_i} \quad (43)$$

Phase difference, ϕ , was measured in degrees from photographs of oscilloscope traces. The ratio of the distance between adjacent zero crossings for the pair of pressures, p_o and p_i , and the distance between consecutive zero crossings of the input pressure, p_i , was multiplied by 360 deg. Thus, pairs of input and output waveforms covering from 1.5 to 2.5 cycles were monitored simultaneously on an oscilloscope, photographed and the spacing measured by hand.

An alternate approach that was not used in reducing magnitude ratio, G , and phase difference, ϕ , analyzes Lissajous patterns photographed from oscilloscope traces. Output and input signals are applied to the vertical and horizontal amplifiers of an oscilloscope. Standard measurements on the Lissajous patterns give the magnitude ratio and phase difference between the two signals. However, when the signals are non-monochromatic, Lissajous patterns from oscilloscope traces are difficult to read.

5.2.4 Microphone Calibration

The input and output microphones were calibrated to ascertain what, if any, correction factors must be applied to the experimental voltage data. Bode plots were always made on relative a-c measurements. For this reason the microphones could be calibrated in a relative sense rather than in an absolute sense. Two microphones were placed in a tee at the output of the fluidic signal generator so that they sensed the same pressure. Magnitude ratio and phase difference for the pair of microphones were measured over the bandwidth and dynamic range of interest. For identical microphone systems, no differences are expected in amplitude ratio or in phase difference.

At a particular frequency, the fluidic signal generator was set to produce the required amplitude. Steady-state, a-c readings were made at each frequency. The peak-to-peak output amplitude of the microphones was read on the oscilloscope. From the amplitude data, magnitude ratios were calculated both as absolute numbers and as dB ratios; phase difference was read on a phase meter.

In this study there are differences in magnitude ratio between the two microphones. Thus, calibration factors are applied to all magnitude ratio data. However, phase-difference measurements between the two microphones is negligible.

5.2.5 Experimental Measurements

Sections 6 and 7 describe small signal, a-c tests that were performed on fluidic configurations (junctions and compensation networks), typically used in control applications. These configurations were constructed from the basic fluidic components discussed in section 3. For each of the test configurations, fluidic components and microphone probes were connected in airtight breadboard models.

Input signals at particular pressure amplitudes were applied at various frequencies. If the level of the input-pressure amplitude did not change (was flat) with respect to frequency, the frequency band was swept slowly enough to allow both the fluidic system and the electronic instrumentation to come to quasi-steady state at each frequency. Magnitude ratio and phase difference were recorded.

For that part of the frequency band, where the input signal is not flat, response data were taken point by point at each specified input pressure amplitude for several desired frequencies. Magnitude ratios and phase differences were then plotted point by point as a Bode plot.

6. SUMMING AND DISTRIBUTION JUNCTIONS

Small signal a-c tests are performed on both summing and distribution junctions. In each case, tests are defined in terms of desired test ranges as well as limitations of fluidic hardware and electronic instrumentation.

Experimental data are discussed and evaluated in terms of how well the response of several circuit models of the same fluidic component agrees with the nodal response of the physical fluidic configurations. Conclusions are developed to relate the performance of various circuit models to the performance of actual fluidic components.

6.1 Passive Summing Junction

An ideal passive fluidic summing junction is shown in section 3.4.1 to produce an output pressure that is proportional to the weighted sum of two or more input-pressure signals. As long as the input resistors are much smaller than the load resistors, the output pressure is independent of the resistance values. However, to minimize pressure attenuation through the junction, it becomes necessary to limit the resistance between the input and the output. Therefore, inequality relationships on load resistance are not followed in this section. The desired equivalent circuit for a passive summing junction with two input resistors and one load resistor is given in figure 25.

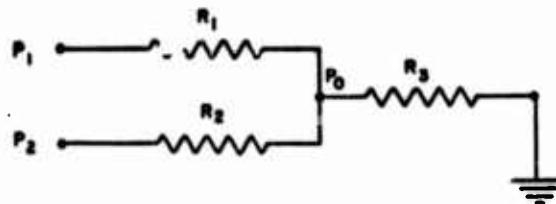


Figure 25. Simple equivalent circuit of passive summing junction

In the simplest one-to-one substitutions between the equivalent circuit (fig. 25) and actual physical hardware, each resistor is replaced by a capillary, so that

- $R_1 \rightarrow$ capillary 1,
- $R_2 \rightarrow$ capillary 2, and
- $R_3 \rightarrow$ capillary 3.

The junction is replaced by an enclosed volume, an air cylinder, in this case so that

Node $p_0 \rightarrow$ volume 1.

Hardware for the enclosed volume was first made by simply modifying a pneumatic cylinder. Modifications permit four fluidic components or pressure probes to be connected to the cylinder as shown in figure 26.

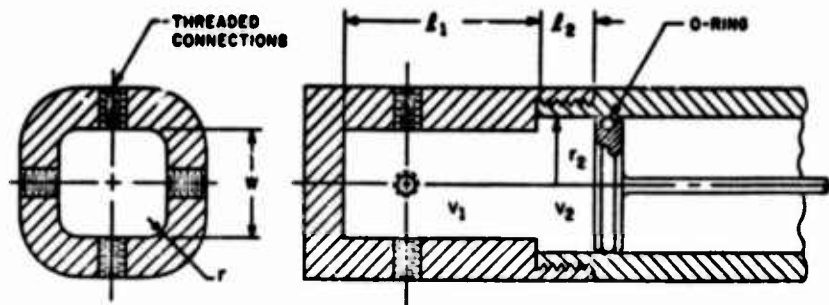


Figure 26. Modified air cylinder as an enclosed volume

In this model, the dimensions are

$$\begin{aligned}
 r_1 &= 2.38 \times 10^{-3} \text{m}, \\
 l_1 &= 2.286 \times 10^{-2} \text{m}, \\
 w &= 1.270 \times 10^{-2} \text{m}, \\
 r_2 &= 1.270 \times 10^{-2} \text{m}, \text{ and} \\
 l_2 &= 1.5 \times 10^{-1} \text{m}
 \end{aligned}$$

The small (though finite) minimum volume V_1 is calculated to be

$$V_1 = (w^2 - (4 - \pi)r_1^2)\ell_1 = 3.58 \times 10^{-6} \text{ m}^3. \quad (44a)$$

The total volume, V , is continuously adjustable from V_1 to a maximum allowable volume.

The total volume including the minimum volume is

$$V = (w^2 - (4 - \pi)r_1^2) + \pi r_2^2 \ell_2, \quad (44b)$$

$$= [3.58 \times 10^{-6} + 1.61 \times 10^{-4} \ell_2] \text{ m}^3. \quad (44c)$$

The range of volume is $3.58 \times 10^{-6} \text{ m}^3$ to approximately $80 \times 10^{-6} \text{ m}^3$. Unfortunately, slight leaks around the O-ring did not permit measurements at low frequencies. At higher frequencies, the impedance of a leak becomes high with respect to the system impedance, and hence becomes a negligible factor.

An improved enclosed cylindrical volume (fig. 27) with $r = 2.54 \times 10^{-2} \text{ m}$ accepts as many as five components or probes. This improved configuration proved not only to be airtight but also to be continuously adjustable in height, h , from 0 m to $2.54 \times 10^{-2} \text{ m}$. The volume, V , varies from virtually 0 m^3 to $50 \times 10^{-6} \text{ m}^3$. However, the minimum useable height is approximately about 1mm, which is equivalent to a volume of $6.45 \times 10^{-7} \text{ m}^3$.

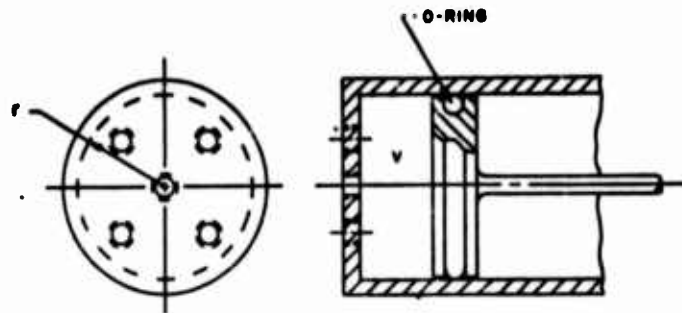


Figure 27. Improved enclosed volume

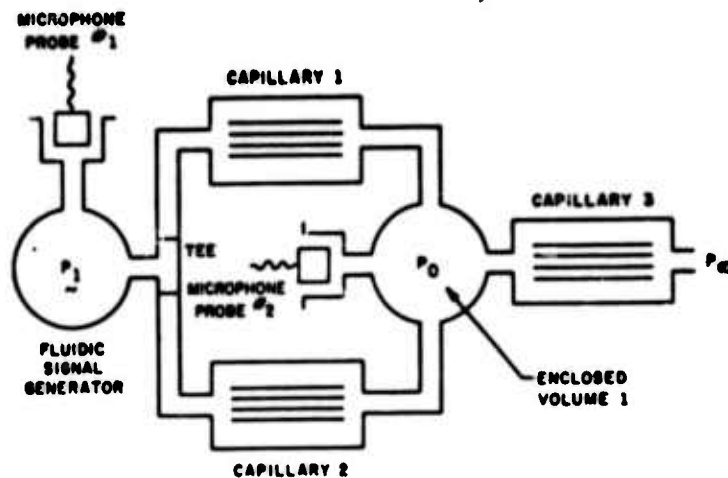


Figure 28. Test configuration for passive summing junction

The fluidic signal generator (fig. 28) is connected with a tee connection to both capillary 1 and capillary 2. In a true systems application, pressures from separate signal sources would be introduced into the summing junction. The loading capillary 3 exhausts to ambient pressure, p_{∞} .

Each of the three bundled parallel capillaries contains 25 capillary passages, 0.1525 mm (0.012 in.) in diameter and about 6.5 cm (2.5 in.) in length. The junction is the volume of figure 27 within the large air cylinder, 5.1 cm (2.0 in.) in diameter with a depth of 1.0 mm (0.04 in.). Capillary modules and microphone probes are sealed into the junction with teflon sleeves.

This junction is tested over a 2.5- to 200-Hz range with input-pressure amplitudes between about 25 and 62 Pa. The microphones are calibrated over the same bandwidth and pressure ranges. In the 20 mV rms and 50 mV rms output ranges for the microphones, corresponding to approximately 25 and 62 Pa rms, the calibration curves for the two microphones are slightly different.

Magnitude ratios and phase differences are measured (ref 24) for the summing junction (fig. 28) with the following dimensions:

$$\begin{aligned} \text{Capillary 1: } N &= 25, r = 1.525 \times 10^{-4} \text{m}, \ell = .0635 \text{m}, R = 1.07 \times 10^8 \frac{\text{kg}}{\text{m}^4 \text{sec}} \\ \text{Capillary 2: } N &= 25, r = 1.525 \times 10^{-4} \text{m}, \ell = .0635 \text{m}, R = 1.39 \times 10^8 \frac{\text{kg}}{\text{m}^4 \text{sec}} \end{aligned}$$

Canillary 3: $H = 25$, $r = 1.525 \times 10^{-4} \text{ m}$, $\ell = .0635 \text{ m}$, $R = 1.36 \times 10^8 \frac{\text{kg}}{\text{m}^4 \text{ sec}}$

Volume 1: $r = 2.54 \times 10^{-2} \text{ m}$, $h = 1.02 \times 10^{-2} \text{ m}$

Microphone 1:

Sensitivity - .81 mV/Pa,
Capacitance - 3.21 pF (picofarads).
Calibration - 20 mV/25 Pa, 50 mV/62 Pa @ 100 Hz.

Microphone 2:

Sensitivity - .82 mV/Pa,
Capacitance - 3.21 pf (picofarads),
Calibration - 16 mV/25 Pa, 42 mV/62Pa @ 100 Hz.

Correction factors from both the 25- and 62-Pa calibration data were applied to the measured magnitude ratios. Corrected Bode plots for magnitude ratio, G_{dB} , are shown with 25- and 62-Pa calibration data in figure 29a. It is felt that these correction factors fairly well bracket the experimental data range. The measured phase difference, ϕ , is plotted with 25- and 62-Pa calibration data in figure 29b.

To get a view of the validity of circuit models of components in the summing junction, a few simple linear circuit models were selected. The least expensive linear circuit analysis program in HDL is ECAP (sect 4 and ref 25), run on the IBM 1130 computer.

Values of resistance for the capillaries were taken from their static-calibration curves (fig. 19). Capacitance and inductance values were calculated for linear models for capillaries (sect 5.1) in equation (45) and (46),

$$C = \frac{\pi r^2 \ell}{n p_s} , \quad (45)$$

where (see sect 3.2) $n = 1$ at lower frequencies and $n = 1.4$ at higher frequencies; and

$$L = \lambda \frac{\rho \ell}{\pi r^2} , \quad (46)$$

where $\lambda = 4/3$ at lower frequencies (eq 13e) and $\lambda = 1$ at higher frequencies (eq 13d). The simple model of the junction itself includes only capacitance (sect 3.2). A frequency range from 2.5 to 200 Hz is swept in the ECAP programs. In Bode plots (fig. 29 a, b), theoretical curves A through G are plotted (1) for capillaries modeled as R and RLC, (2) for the polytropic coefficient, $n = 1$ and $n = 1.4$ and (3) for the inertance coefficient, $\lambda = 1$ and $\lambda = 4/3$.

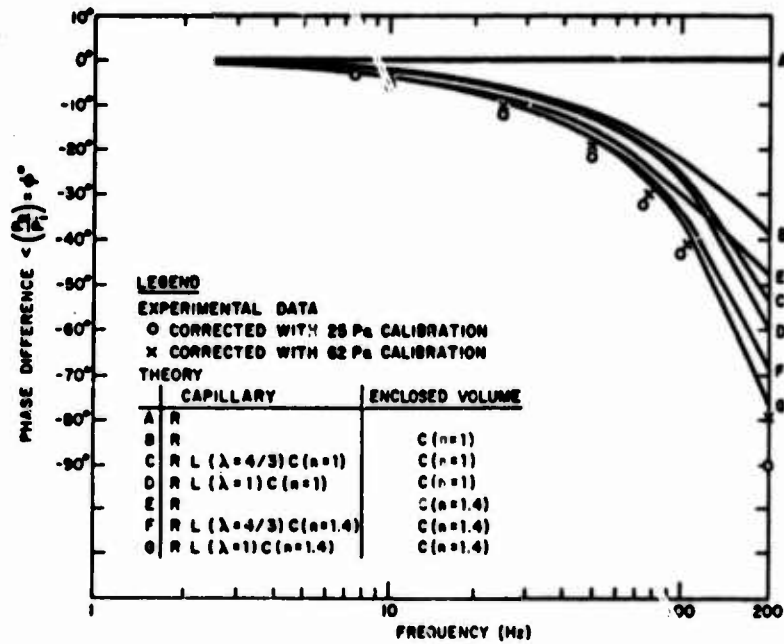
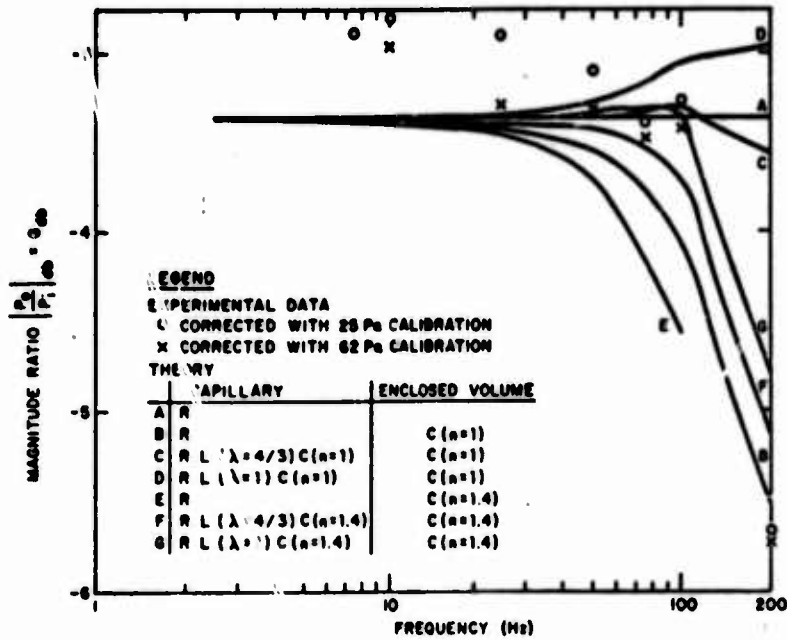


Figure 29. Bode plot for summing junction

In examining the experimental results, it is noted that the simplest model (curve A) in figures 29a, b is based on the assumptions that

- (1) capillaries are simply resistors, and
- (2) the node has zero impedance,

giving

$$G = -3.52 \text{ dB}, \quad (47a)$$

$$\phi = 0 \text{ deg.} \quad (47b)$$

These values are quite close to the low frequency experimental response in figures 29a, b. The corrected experimental values for low-frequency magnitude ratio, G , are within at worst .75 dB or 9 percent off from the predicted low-frequency value.

The response of the summing junction drifts away from the desired constant value at higher frequencies. The constant resistive models of the capillaries along with the zero-dynamics model of the junction are the only models that fail to predict a change from a constant value. The best linear models of those calculated include the following:

For the capillary, the measured value of resistance along with the low-frequency inductance gives the best fit to the magnitude ratio data.

The measured resistance value along with the high-frequency inductance for the capillary gives the best fit to the phase-difference data.

The low-frequency model of the capacitor is best, both in the capillary and in the junction.

All of these models of the summing junction with the exception of the constant valued one agree fairly well with experimental data up to about 25 Hz.

6.2 Passive Distribution Junction

The approach to the passive fluidic distribution junction is identical with the passive summing junction approach in section 6.1. An equivalent circuit for the passive distribution junction (fig. 30) has one input resistor R_1 to the junction and two output resistors R_2 and R_3 from the junction.

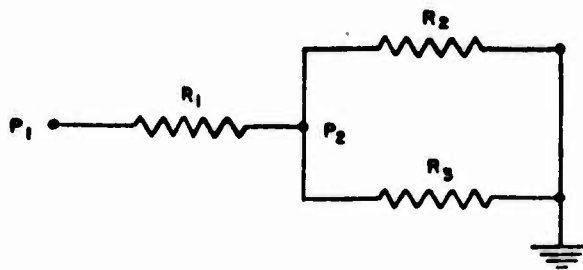


Figure 30. Simple equivalent circuit of passive distribution junction

Again in the design of physical hardware, there is a one-to-one replacement of the resistors by capillaries and the node by an enclosed volume

- $R_1 \rightarrow$ Capillary 1,
- $R_2 \rightarrow$ Capillary 2,
- $R_3 \rightarrow$ Capillary 3, and
- Node $p_2 \rightarrow$ Volume 1.

The test configuration (fig. 31) includes a fluidic signal generator at the input and two load capillaries exhausting to ambient pressure, p_∞ .

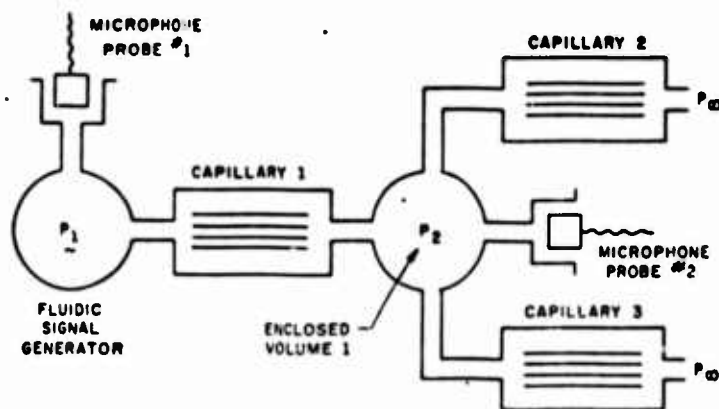


Figure 31. Test configuration for passive distribution junction

The same capillaries and the same enclosed volume from section 6.1 were used in these tests. The 25- and 62-Pa calibration curves were applied to the measured magnitude ratio data. Corrected Bode plots are presented

in figures 32a and 32b. ECAP programs were written for the distribution junction and the resulting theoretical Bode plots for linear models are presented as curves A through G in figures 32a, b. The three features of the models that were varied to prepare these plots were (1) the capillary was an R or an RLC, (2) the polytropic coefficient, n , was 1.0 or 1.4, and (3) the inertance coefficient, was 1 or $4/3$. To check the accuracy of the test results, again the simplest models were considered:

- (1) capillaries are resistors,
- (2) node has zero impedance

Theoretical the low frequency or d-c results from these simple models are

$$G = -9.54 \text{ dB}, \quad (48a)$$

$$\phi = 0 \text{ deg.} \quad (48b)$$

These predicted values are quite close to the experimental low-frequency values as can be seen in fig. 32. The corrected low-frequency magnitude ratio, G_{dB} , is within at worst 0.70 dB or 8 percent of the predicted low-frequency value up to 50 Hz.

Again all data are flat to about 25 Hz. Each of the linear models agrees quite well up to approximately this point. The models found best for the distribution junction are also best for the summing junction. From the magnitude ratio plot the capillary appears to be best modeled with the measured resistance and a low-frequency inductance. The phase-difference plot indicates that the capillary is best modeled with the measured resistance and the high-frequency inductance. The junction is best modeled by a low-frequency capacitance.

7. COMPENSATION NETWORKS

There are many applications in fluidics as well as other technologies in which compensation networks are useful. It is possible to implement a few such compensation networks solely by passive circuitry. For completeness, brief reviews of general compensation networks and fluidic compensation networks are presented first. Similarities and differences between the fluidic networks and the general theory are discussed; finally, several examples of fluidic compensation networks are presented.

These studies are intended to demonstrate both the use of certain fluidic components in subsystems and the application of the fluidic circuit models (sect 3) in representing fluidic subsystems. For each of the compensation networks studied, a simple equivalent circuit is presented where a fluidic component replaces each element of the equivalent circuit on a one-to-one basis. Then a new overall equivalent circuit is drawn to include added dissipative and storage elements.

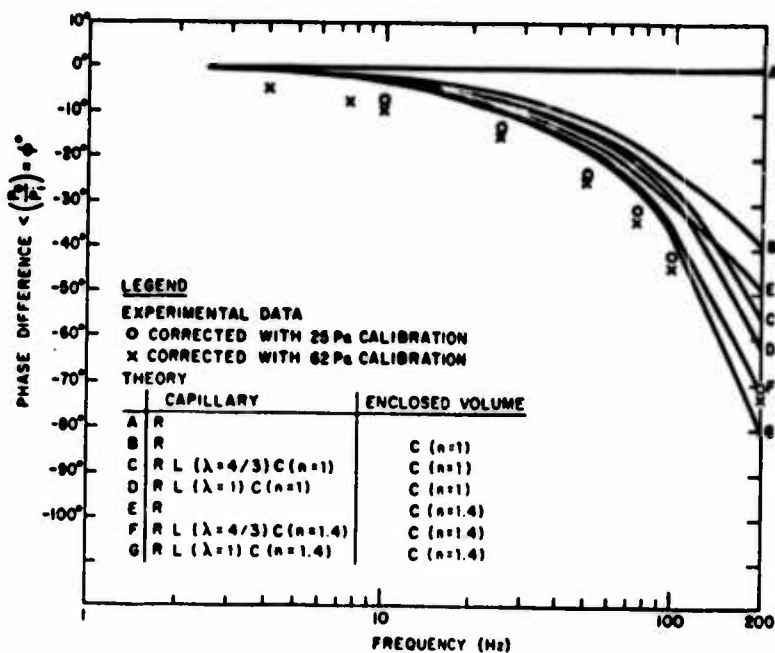
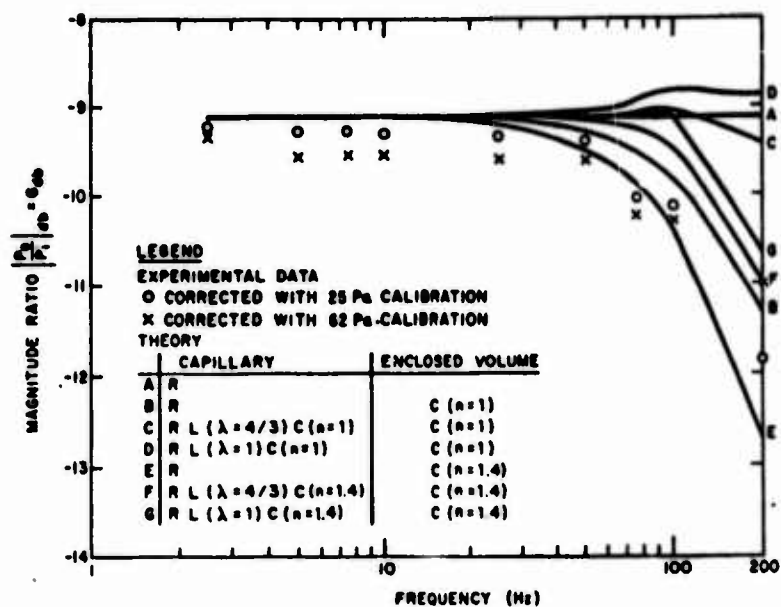


Figure 32. Bode Plot for distribution junction

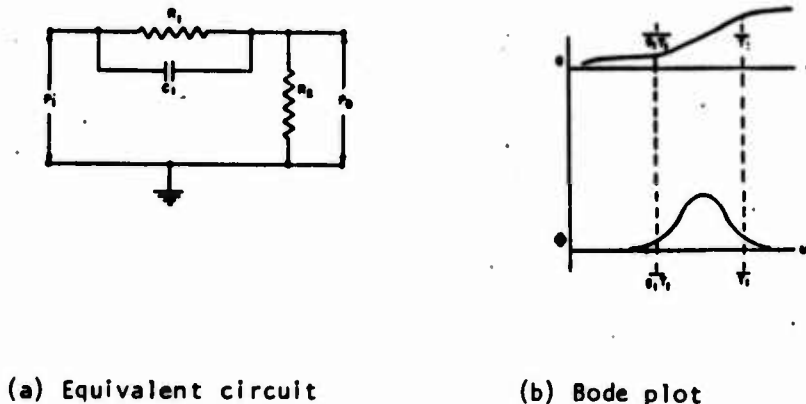
Experiments were conducted and the results are presented along with the theoretical predictions, calculated by computer, which are compared with the experimental results.

7.1 An Approach to Fluidic Compensation Networks

In terms of a-c signals, a compensation network is typically placed in a system to adjust both signal magnitude (attenuation) and signal phase to improve stability. The simplest compensation network is a passive series equalization network composed of resistors and capacitors. It may be placed in the forward loop, the feedback loop, or the load of a larger system. Overall system stability may be modified through careful selection of the configuration of the compensation network and of the values of its resistors and capacitors.

Compensation networks may be designed independently from the overall system in terms of constraints, both in the complex frequency domain and in the time domain. Constraints in the complex frequency domain may be specified for gain margin, phase margin, peak resonance, or bandwidth. Constraints in the time domain may be specified for rise time, delay time, settling time, or overshoot.

Basic compensation networks are phase lead, phase lag, and combinations of phase lead and phase lag. In a phase lead circuit, attenuation is found to be greater at low frequencies so that the amplitude ratio increases monotonically as a function of frequency. Phase angle difference increases to a peak and then decreases with frequency. A basic configuration and a typical Bode plot for phase-lead compensation are shown in figure 33.



(a) Equivalent circuit

(b) Bode plot

Figure 33. Phase lead compensation

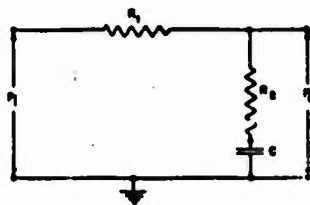
In this case, a parallel combination of resistors and capacitors

was placed between the input and output and a resistor was shunted to ground. The transfer function for the above phase lead network is

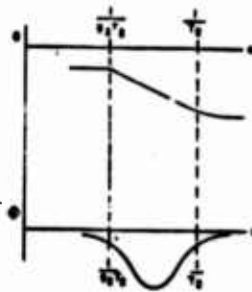
$$G = \frac{p_o(s)}{p_i(s)} = \frac{1}{g_1} \frac{1 + g_1 T_1 s}{1 + T_1 s}, \quad (49)$$

where the constant $g_1 > 1$, p_i and p_o are the input and output signals respectively, T_1 is the time constant, and s is the independent Laplace variable.

In phase-lag compensation, the amplitude ratio is found to decrease monotonically as a function of frequency. As the attenuation increases, the phase angle decreases and then increases. A basic configuration for a phase-lag compensation network and a typical Bode plot are shown in figure 34.



(a) Equivalent circuit



(b) Bode plot

Figure 34. Phase-lag compensation

In this case a resistor is placed between the input and output and a series combination of a resistor and capacitor is shunted to ground. The transfer function for a phase-lag network is

$$G = \frac{p_o(s)}{p_i(s)} = \frac{1 + g_2 T_2 s}{1 + T_2 s} \quad (50)$$

where $g_2 < 1$ and T_2 is the time constant.

To take advantage of both phase lead and phase-lag compensation while eliminating some of the disadvantages of either method used separately, lag-lead or lead-lag compensation networks are used. These more sophisticated circuits have additional free parameters that, in general, can be adjusted to meet more of the specifications. A basic configuration for a lag-lead or lead-lag compensation network in figure 35.

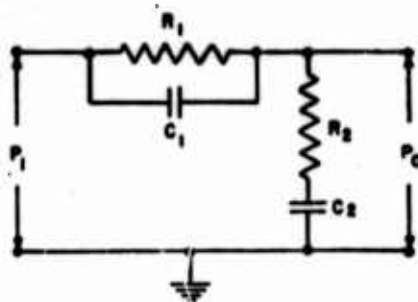


Figure 35. Lag-lead compensation network

In this network, a combination of parallel resistors and capacitors is placed in series between the input and output while a series combination of resistors and capacitors is placed in shunt to ground. For the configuration shown in figure 35, the transfer function is

$$G = \frac{p_o(s)}{p_i(s)} = \frac{(1 + g_3 T_3 s)(1 + g_4 T_4 s)}{(1 + T_3 s)(1 + T_4 s)}, \quad (51)$$

where the constant $g_3 > 1$ and the constant $g_4 < 1$, and T_3 and T_4 are two time constants.

Solving a compensation network involves determining values (where possible) of the parameters g_i and T_i that best satisfy the constraint specifications. Values of resistance and capacitance are calculated from these parameters. In some cases, however, values of resistance and capacitance cannot be determined to satisfy specified constraints for every circuit topology.

7.2 Passive Fluidic Compensation Networks

The approach to passive fluidic compensation networks is similar to the approach discussed in section 6 for passive summing and distribution junctions. Passive fluidic compensation networks were implemented to a first approximation by using available fluidic components on a one-to-one basis in replacing ideal circuit elements. Capillaries replaced resistors, enclosed volumes were used for grounded capacitors, bellows modules and diaphragm modules were used instead of point-to-point capacitors, and small enclosed volumes were used for nodes. However, it should be remembered that most fluidic components are not ideal; hence, there is a limit to the bandwidth and response if one-to-one replacement is used.

Input pressures to a typical compensation network may be the pressure signals from the outputs of proportional amplifiers and similarly

the output pressure of the compensation network may be the input pressure signal to the controls of another proportional amplifier.

However, as a first approximation, assume that the input is a zero-impedance (or ideal) source, and that the output looks into a constant linear load (a linear load (a linear capillary)).

Several passive pneumatic fluidic networks were experimentally investigated. In the following sections these experimental results are compared with computer predictions, using models presented in section 3.

7.3 Fluidic Lag Network

Several passive fluidic components including capillary modules, an enclosed volume, and a summing junction are connected as a lag network. A simple equivalent circuit (fig. 36) for a lag network is represented as a series resistor, R_1 , between the input and output and a capacitor, C_1 , shunted to ground at the output

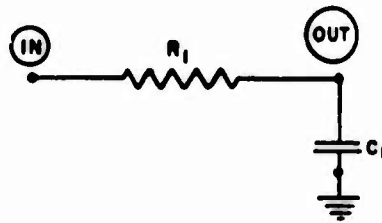


Figure 36. Schematic diagram of simple lag network

The simple equivalent circuit maybe implemented in fluidic hardware as shown schematically in figure 37.

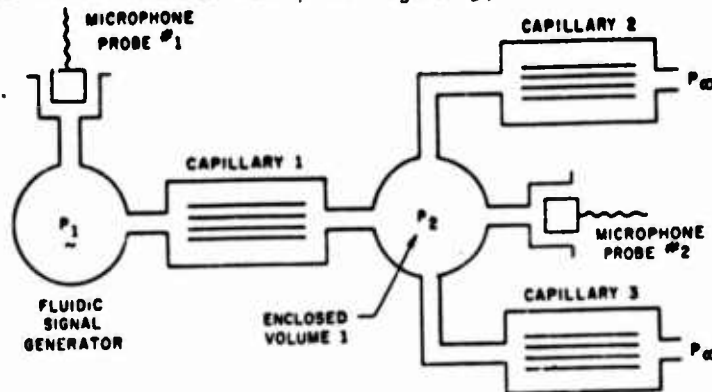


Figure 37. Test configuration for lag network

Resistor, R_1 , is replaced by capillary 1. Node OUT and the capacitor, C_1 , are replaced by volume 1.

The remaining fluidic hardware in figure 37 is a signal generator, a linear load, and microphones at nodes OUT and IN. The pressure generator in these tests is the Electrodyne piston generator. In producing a configuration that is somewhat typical of projected systems configurations, capillaries 2 and 3 are included as a pair of parallel finite output loads. Thus, node OUT is actually a passive distribution junction. In view of the added hardware, the equivalent circuit for the test configuration, using the simplest of models, i.e., a capillary as a resistor and a volume as a capacitor, is shown in figure 38. Note that for simplicity the resistance in capillaries 2 and 3 is combined and denoted as $R_2 = \frac{(R_{\text{capillary 2}}) \times (R_{\text{capillary 3}})}{(R_{\text{capillary 2}}) + (R_{\text{capillary 3}})}$.

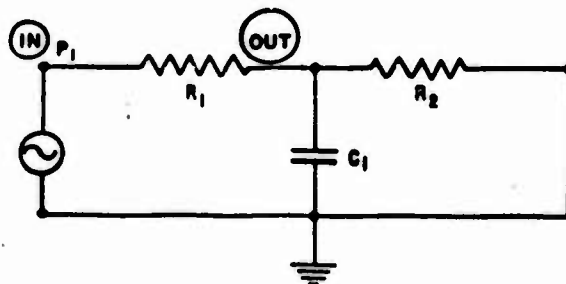


Figure 38. Resistive circuit model of experimental lag network

A transfer function for this circuit may be developed from the circuit equations. In the complex frequency domain, the transfer function between node IN and node OUT is given as equation (52).

$$\frac{P_2(s)}{P_1(s)} = \frac{R_2}{R_1 + R_2} \left[\frac{1}{1 + \frac{R_1 R_2 C_1}{R_1 + R_2} s} \right] \quad (52)$$

Values of resistors, R_1 and R_2 , and capacitor, C_1 , are calculated from the relationships (in terms of geometry and fluid properties) in section 3 for capillaries and enclosed volumes.

For the capillaries used in these test configurations, the capacitive reactance is insignificant when compared with the inductive reactance. Thus, only resistance and inductance of the capillaries are considered in the following discussion. When models of the capillary include both

resistance and inductance, the equivalent circuit for the physical implementation (fig. 37) may be drawn as figure 39. Here again inductance in capillaries 2 and 3 is combined and written as

$$L_2 = \frac{(L_{\text{capillary 2}}) \times (L_{\text{capillary 3}})}{(L_{\text{capillary 2}}) + (L_{\text{capillary 3}})}$$

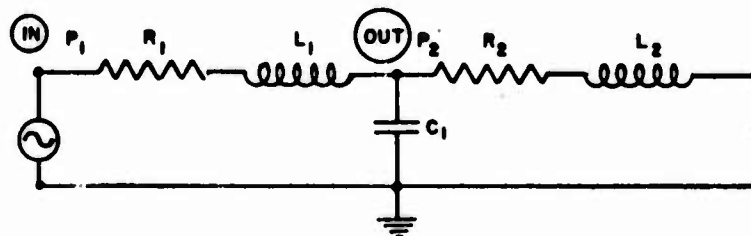


Figure 39. Resistive and inductive circuit model of experimental lag network

The transfer function between node OUT and node IN may be written as equation (53),

$$\frac{P_2(s)}{P_1(s)} = \frac{R_2 + L_2 s}{(R_1 + R_2) + (L_1 + L_2 + C_1 R_1 R_2) s + C_1 (R_1 L_2 + R_2 L_1) s^2 + C_1 L_1 L_2 s^3} \quad (53)$$

7.3.1 Sensitivity Analysis

Of interest to the engineer is the change in phase difference with respect to changes of the length of the capillaries and with respect to the volume of the enclosed volume. A sensitivity analysis is used for determining these results.

Within the framework of fluidic circuit analysis, it is possible to calculate the influence that one or more circuit parameters (or values) will have upon an overall performance of the equivalent circuit representation. These calculations are performed in terms of a sensitivity analysis. A sensitivity analysis computes the rate of change of response variables at a specified operating point as functions of specified circuit parameters.

7.3.2 Sensitivity Analysis for Added Dynamics in a Fluidic Lag Network

A sensitivity analysis was performed to determine the added phase

difference that is attributed to inductance accompanying resistance in the capillaries, and capacitance added at the output node in the enclosed volume. The change of response as a function of changes in lengths and volumes was calculated. Here, sensitivity analysis determines phase shift per unit length as a function of the inductance of each capillary, and phase shift per unit volume as a function of the capacitance of node OUT.

Gain for the resistive-inductive circuit model of the lag network is obtained from the transfer function (eq 53) as

$$G(j\omega) = \frac{R_2 + jL_2\omega}{[R_1 + R_2 - C_1(R_1L_2 + R_2L_1)\omega^2] + j[(L_2(L_1 + L_2) - R_2^2C_1L_1)\omega^2 - C_1L_1L_2^2\omega^4]} \quad (54a)$$

from which phase difference angle ϕ is

$$\phi(j\omega) = \arctan \left[\frac{(R_1L_2 - R_2L_1 - R_1R_2^2C_1)\omega - R_1C_1L_2^2\omega^3}{R_2(R_1 + R_2) + [L_2(L_1 + L_2) - R_2^2C_1L_1]\omega^2 - C_1L_1L_2^2\omega^4} \right] \quad (54b)$$

Capacitance and inductance, defined in equation (22) and (18b) respectively, may be rewritten as functions of node volume and capillary length,

$$C = (C_n + C_v) = \left(\frac{V_n}{K_1} + C_v \right) , \quad (55a)$$

$$L = K_2\ell , \quad (55b)$$

where

$$K_1 = n\rho_0,$$

$$K_2 = \lambda \frac{\rho}{N\pi r^2} ,$$

V_n = volume of the node,

C_n = capacitance of the node, and

ℓ = capillary length.

Then the phase difference angle, ϕ , may be rewritten from equations 54b and (39a, b) as

$$\phi(j\omega, V_n, \ell_1, \ell_2) = \arctan \left[\frac{(-R_2 K_2 \omega) \ell_1 + (R_1 K_2 \omega) \ell_2 - (R_1 K_2^2 \omega^3 + R_1 R_2 \omega) \left(\frac{V_n}{K_1} + C_V \right)}{R_2 (R_1 + R_2) - R_2^2 C_V K_2 \omega^2 \ell_1 + K_2^2 \omega^2 \ell_1 \ell_2 - K_2^3 \omega^2 \left(\frac{V_n}{K_1} + C_V \right) \ell_1 \ell_2^2 - R_1 K_1 - R_2^2 K_2 \omega \ell_1 \frac{V_n}{K_1} + K_2^2 \omega^2 \ell_2^2} \right] \quad (56)$$

Partial derivatives of the phase-difference angle, ϕ , may be taken with respect to the three variables ℓ_1 , ℓ_2 , and V_n :

$$\frac{\partial \phi}{\partial \ell_1} = \frac{1}{\left[1 + \left(\frac{1}{\ell_2} - \frac{K_2}{K_1} V_n \omega^2 \right) \ell_1 \right]^2 + \left[-\frac{K_1}{K_2} V_n \omega \ell_1 \right]^2} \quad (57a)$$

$$\frac{\partial \phi}{\partial \ell_2} = \frac{1}{\left[1 + \left(\frac{1}{\ell_1} - \frac{K_2}{K_1} V_n \omega^2 \right) \ell_2 \right]^2 + \left[-\frac{K_1}{K_2} V_n \omega \ell_1 \right]^2} \quad (57b)$$

and

$$\frac{\partial \phi}{\partial V_n} = \frac{1 + \frac{\ell_2}{\ell_1}}{\left[1 + \left(\frac{1}{\ell_2} - \frac{K_2}{K_1} V_n \omega^2 \right) \ell_2 \right]^2 + \left[-\frac{K_1}{K_2} V_n \omega \ell_2 \right]^2} \quad (57c)$$

The critical dimensions of the fluidic components shown in figure 39 and studied in this sensitivity analysis are

- Capillary 1: $N = 25$, $r = 1.525 \times 10^{-4} \text{m}$, $\ell = 0.07 \text{m}$,
- Capillary 2: $N = 25$, $r = 1.525 \times 10^{-4} \text{m}$, $\ell = 0.08 \text{m}$, and
- Volume 1: $V = 3.58 \times 10^{-6} \text{m}^3$.

From the expressions for sensitivity in equation (57), the linearized phase shift from the total lengths of the capillaries and from the total volume of the junction may be calculated. Linearized phase shifts are approximated in equation (58) as the products of total length or total volume and the sensitivities about the midpoints of length and volume.

$$\Delta\phi(l_1) = \left. \frac{\partial\phi}{\partial l_1} \right|_{\left(\frac{l_1}{2}, l_2, V_n\right)} l_1, \quad (58a)$$

$$\Delta\phi(l_2) = \left. \frac{\partial\phi}{\partial l_2} \right|_{\left(l_1, \frac{l_2}{2}, V_n\right)} l_2, \quad (58b)$$

$$\Delta\phi(V_n) = \left. \frac{\partial\phi}{\partial V_n} \right|_{\left(l_1, l_2, \frac{V_n}{2}\right)} V_n \quad (58c)$$

The added linearized phase shift is plotted as a function of frequency for each parameter: l_1 , l_2 , and V_n in figure 40.

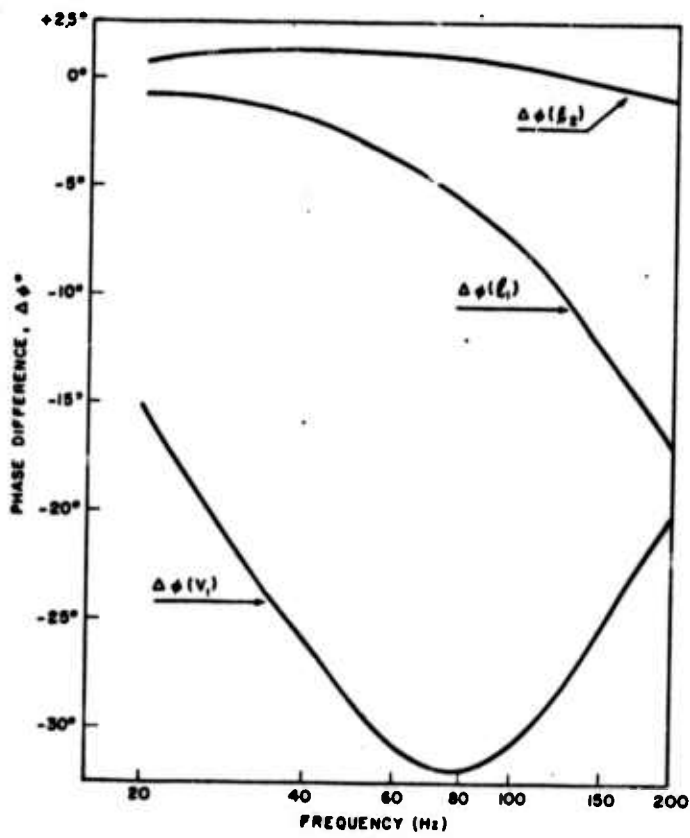
For this specific lag network configuration up to 100 Hz, the maximum lengths, $(l_1)_{\max}$ and $(l_2)_{\max}$, and the maximum volume, $(V_n)_{\max}$, were allowed to produce at most 18 deg phase shift (1/20 of a wavelength).

For a maximum phase lag of 6 deg per fluidic component, the linearized approximations give maximum values of

$$(l_1)_{\max} = 6^\circ / \left. \frac{\partial\phi}{\partial l_1} \right|_{100 \text{ Hz}} = 5.40 \text{ cm} \quad (59a)$$

$$(l_2)_{\max} = 6^\circ / \left. \frac{\partial\phi}{\partial l_2} \right|_{100 \text{ Hz}} = \text{unlimited} \quad (59b)$$

$$(V_n)_{\max} = 6^\circ / \left. \frac{\partial\phi}{\partial V_n} \right|_{100 \text{ Hz}} = 0.67 \text{ cm}^3 \quad (59c)$$



7.8

Figure 40. Added linearized phase shift in lag network

7.3.3 Models of Lag Network

Tests on the fluidic lag network (fig. 37) were performed from 10 to 200 Hz at each of three input pressures: 20, 200, and 1000 Pa rms. Because of limitations in the experimental equipment (discussed in sect 5), some measurements over this bandwidth and pressure range could not be obtained.

Critical information pertaining to the experimental lag circuit in figure 37 is as follows:

- Capillary 1: $N = 25$, $r = 1.525 \times 10^{-4} \text{m}$, $\ell = .07 \text{m}$, $R = 2.38 \times 10^8 \frac{\text{kg}}{\text{m}^4 \text{sec}}$
- Capillary 2: $N = 25$, $r = 1.525 \times 10^{-4} \text{m}$, $\ell = .08 \text{m}$, $R = 2.73 \times 10^8 \frac{\text{kg}}{\text{m}^4 \text{sec}}$
- Capillary 3: $N = 25$, $r = 1.525 \times 10^{-4} \text{m}$, $\ell = .09 \text{m}$, $R = 3.07 \times 10^8 \frac{\text{kg}}{\text{m}^4 \text{sec}}$
- Volume 1: $V = 3.58 \times 10^{-6} \text{m}^3$
- Microphone 1: B & K $\frac{1}{8}$ in., Type 4138 - S/N 292038
Sensitivity - 37.2 $\mu\text{V}/\mu\text{bar}$
Calibration - (.12 V peak to peak)/(124 dB, ref $2 \times 10^{-4} \mu\text{bar}$)@ 250 Hz
- Microphone 2: B & K $\frac{1}{8}$ in., Type 4138 S/N 228411
Sensitivity - 32.0 $\mu\text{V}/\mu\text{bar}$
Calibration - (.08 V peak-to-peak)/(124 dB, ref $2 \times 10^{-4} \mu\text{bar}$) @ 250 Hz

Experimental results are shown in a Bode plot (fig. 41). When compared with figure 34b, this plot is a low-frequency segment of a typical lag network. As the magnitude ratio decreases, the phase difference becomes more negative.

In the computational models for the capillaries and the volume from section 3, several simplifying assumptions were made:

- (1) The enclosed volume is a linear, frequency independent capacitor.
- (2) The enclosed volume is approximately a rectangular box with dimensions $(1.28 \times 10^{-2} \text{cm}) \times (1.28 \times 10^{-2} \text{cm}) \times (2.30 \times 10^{-2} \text{cm})$.
- (3) The polytropic coefficient, $n = 1.0$.
- (4) Linear values of resistance, R , in the capillaries were computed.
- (5a) Contributions to the response from L's and C's in the capillaries are negligible.
- (5b) Linear values for the L's and C's in the capillaries were computed.

Small signal analyses of cases A (capillary as R) and B (capillary as RLC) were computed using NET-2 between 1 and 200 Hz. Bode plots for these two cases are also presented in figures 41a, b.

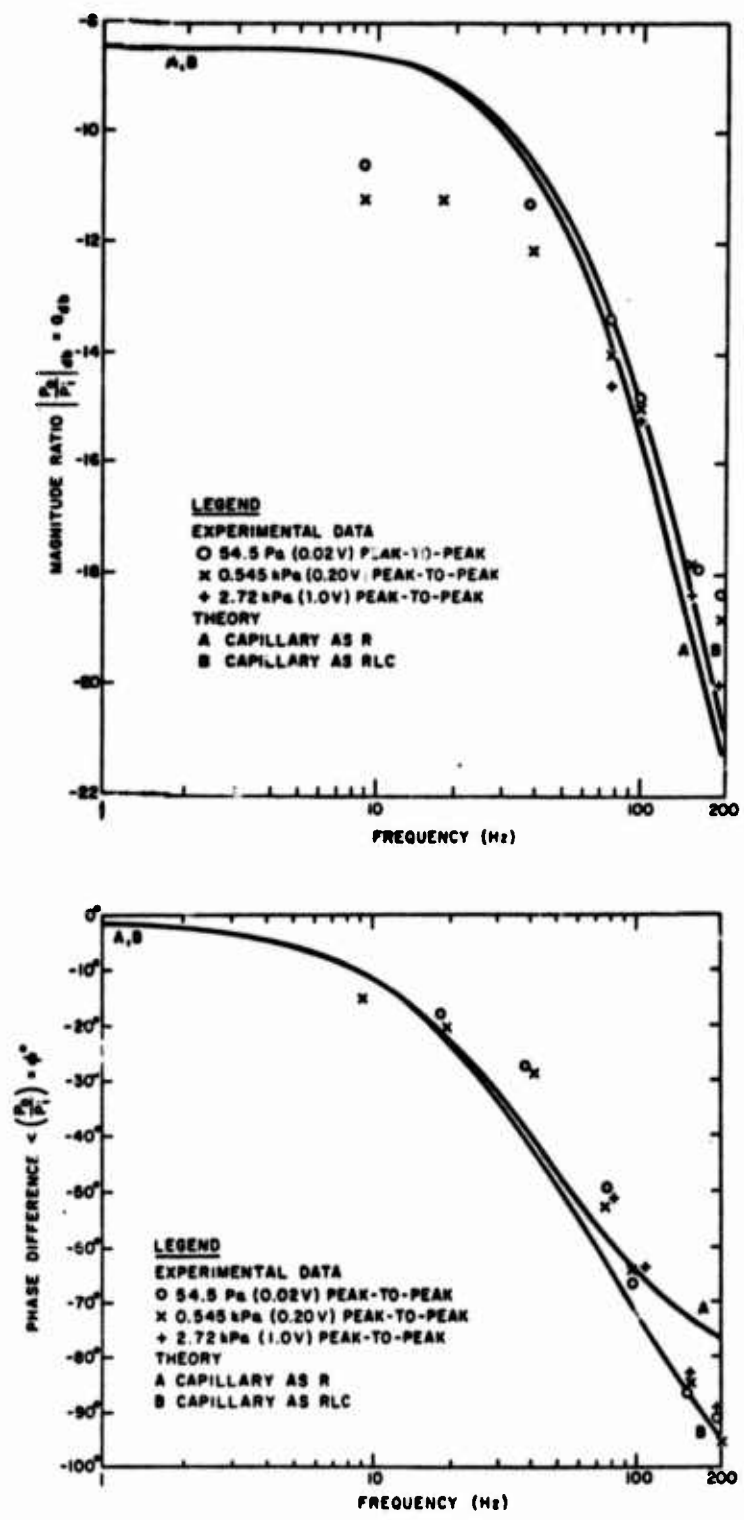


Figure 41. Bode plot for lag network

In the magnitude ratio plot (fig. 41a), there is essentially no difference for small signal analysis between cases A and B. Agreement between experimental results and theory in the phase-difference plot was improved slightly at the higher frequencies (fig. 41a, b) by considering the contribution of L's and C's in the circuit models of capillaries.

7.4 Fluidic Lead Network

Several fluidic components, including capillaries, junctions, and two different mechanical capacitors--a bellows module and a diaphragm module were also connected and tested as a lead network. The simplest equivalent circuit (fig. 42) for the lead network is a point-to-point capacitor, C_1 , between the input and the output with a resistor, R_1 , shunted the output to ground.

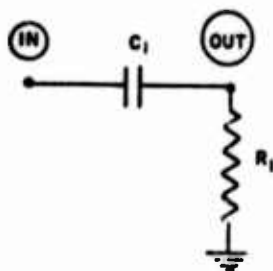


Figure 42. Schematic diagram of simple lead network

This network may be implemented with fluidic hardware, including a bellows module as shown in figure 43.

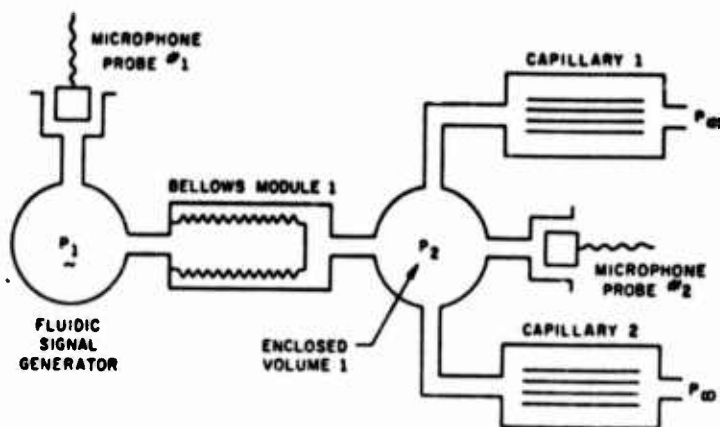


Figure 43. Fluidic lead network with bellows module

The components were again substituted one-to-one for the ideal circuit elements. Capillaries replaced resistors and small fluidic volumes replaced nodes. The point-to-point capacitor, C_1 , between the input and output nodes was replaced by a fluidic bellows module. This hardware was made compatible with the test hardware by including a signal generator, load capillary 2 and pressure transducers at both node IN and node OUT. During the tests, two sinusoidal pressure generators were used, a piston generator and the speaker cone generator. An equivalent circuit for the overall test configuration (fig. 43) is shown in figure 44. The resistive portions of capillaries 1 and 2 are combined so that

$$R_1 = \frac{(R_{\text{capillary 1}}) \times (R_{\text{capillary 2}})}{(R_{\text{capillary 1}}) + (R_{\text{capillary 2}})}$$

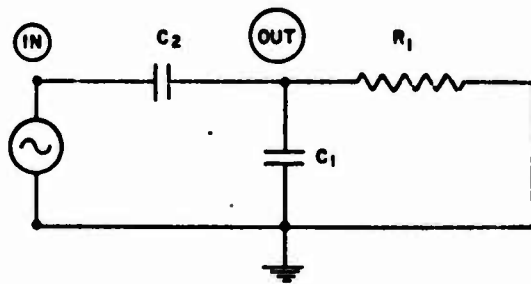


Figure 44. Circuit of experimental lead network

The bellows module was built from a pneumatic bellows having an undeflected length, ℓ_1 , and inner and outer radii, r_1 and r_2 , respectively as shown in figure 45.

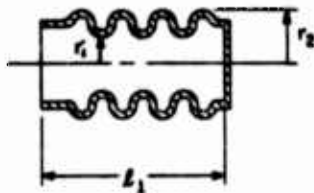


Figure 45. Bellows schematic diagram

The spring constant is $1.09 \times 10^4 \frac{\text{kg}}{\text{sec}^2}$. The permissible maximum deflection (within the elastic limit) was 0.686 mm. The dimensions are

$$\begin{aligned} r_1 &= .635 \text{ cm,} \\ r_2 &= .854 \text{ cm,} \\ \ell_1 &= 1.450 \text{ cm.} \end{aligned}$$

A fluidic bellows module (point-to-point capacitor) is made by soldering a bellows into a cylindrical container of length ℓ_2 with an inner radius r_3 . The entire package is of the form shown in figure 46,

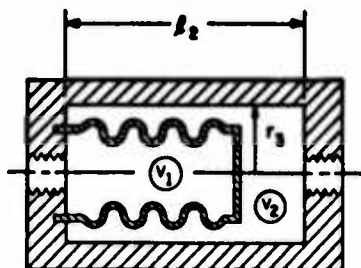


Figure 46. Bellows module

where

$$\begin{aligned} r_3 &= 0.927 \text{ cm} & \text{and} \\ \ell_2 &= 1.777 \text{ cm} \end{aligned}$$

The volumes, V_1 and V_2 , of the two chambers are approximated as

$$V_2 = \pi [r_3^2 \ell_2 - \left(\frac{r_1 + r_2}{2} \right)^2 \ell_1] = 2.96 \text{ cm}^3 \quad (60a)$$

$$V_1 = \pi \left(\frac{r_1 + r_2}{2} \right)^2 \ell_1 = 1.84 \text{ cm}^3 \quad (60b)$$

The added resistances and capacitances due to inlet and outlet and added volume cause dissipation and parasitics. Hopefully, it is possible to design a purer point-to-point capacitor, with a bellows module that

minimizes these effects (by making passages short and chambers small). The critical information for the lead network including the bellows module is as follows

Capillary 1: $N = 25$, $r = 1.525 \times 10^{-4} \text{m}$, $\ell = .08 \text{m}$, $R = 2.73 \times 10^8 \frac{\text{kg}}{\text{m}^4 \text{sec}}$

Capillary 2: $N = 25$, $r = 1.525 \times 10^{-4} \text{m}$, $\ell = .09 \text{m}$, $R = 3.07 \times 10^8 \frac{\text{kg}}{\text{m}^4 \text{sec}}$

Node 1: $V = 3.58 \text{ cm}^3$

Bellows 1: $V = 1.84 \text{ cm}^3$, $V_2 = 2.96 \text{ cm}^3$

$A = 1.27 \times 10^{-4} \text{ m}^2$, $k = 1.09 \times 10^4 \frac{\text{kg}}{\text{sec}^2}$

Microphone 1: Same as in section 7.3.3.

Microphone 2: Same as in section 7.3.3.

Frequency is swept from 2.5 to 135 Hz at input pressures of 1.0 kPa and 2.0 kPa rms. Experimental results are given as a Bode plot (fig. 47a, b). When these results are compared with figure 33b, they are seen to be only the high-frequency segment of a lead network. While the magnitude ratio increases, the phase difference becomes less positive, approaching zero.

Eleven different computational models from section 3 were considered, using the following assumptions:

- (1) The bellows module is a Pi of linear capacitors. The horizontal bar of the Pi is a point-to-point capacitor. Its vertical legs are grounded capacitors. When the bellows module is placed at the output of the signal generator, the grounded input capacitor is considered as part of the signal generator. This capacitor is neglected in an overall circuit representation of the network.
- (2) The capillary models are
 - A, C, H) calculated linear R's,
 - B, D, I) calculated linear R's, linear L's and grounded linear C's;
 - E). measured linear R's, linear L's and grounded linear C's;
 - F, J) calculated nonlinear R's;
 - G, K) calculated nonlinear R's, linear L's and grounded linear C's.
- (3) Grounded C's in the node, the bellows module and the capillary modules are
 - A, B) frequency independent with $n = 1.0$;
 - C, D, E, F, G) frequency independent with $n = 1.4$;
 - H, I, J, K) frequency dependent.

Small signal a-c analyses of cases A, B, C, D and E calculated using NET-2, between 2.5 and 100 Hz are also plotted in figure 47. These plots handle five linear, frequency-independent circuit models.

Both the magnitude ratio plot and the phase-difference plot are improved when the polytropic coefficient is changed from 1.0 (cases A and B) to 1.4 (cases C, D, and E).

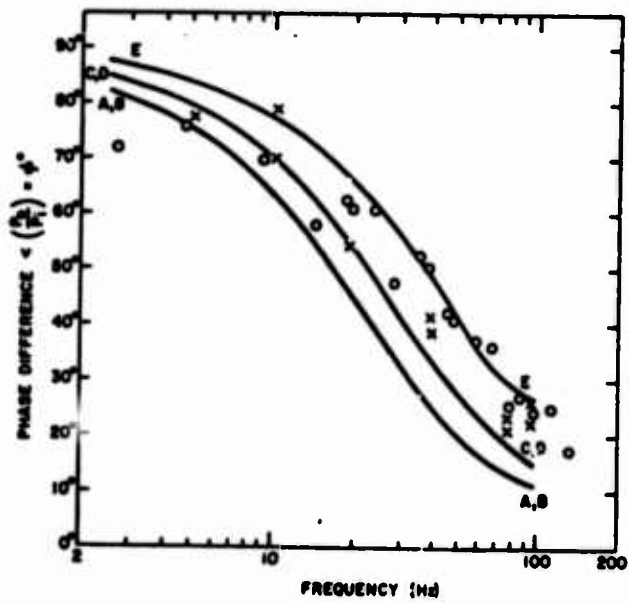
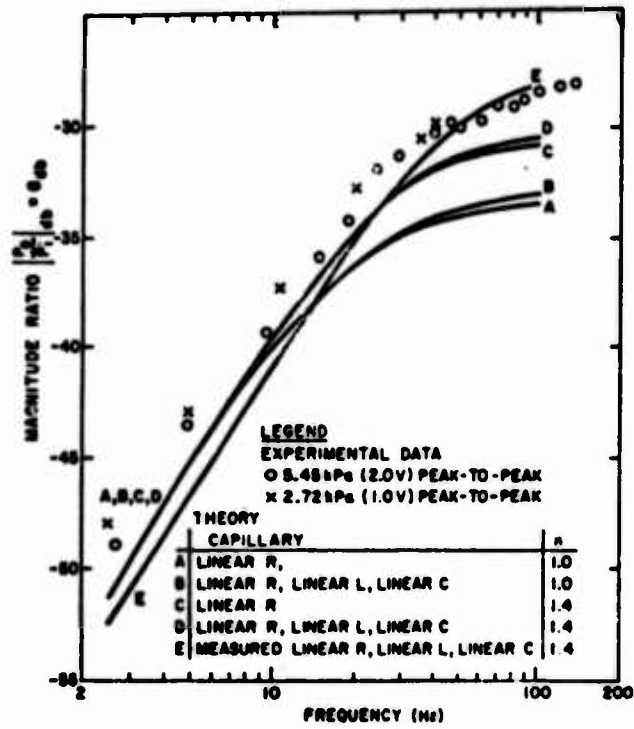


Figure 47. Bode plot for lead networks with bellows

A virtually insignificant improvement is seen in the magnitude ratio curves by adding L and C (cases B and D) to the purely resistive model (cases A and C) of capillary models. No change in ϕ is noted.

A measured capillary resistance, R, (case E) improves the magnitude ratio curve over the case when the calculated value of R is used (case D).

To compare the merits of choosing nonlinear R's and frequency-dependent enclosed volumes, a set of eight cases (C, D and F through K) were computed between 2.5 and 100 Hz using SLIC. These are small signal a-c analyses in which the nonlinear resistances are set at d-c operating points. Bode plot data for the lead network are tabulated in table I. Compared to the experimental data, the magnitude ratio is improved at the higher frequencies when L's and C's are added (cases F, G, J and K). Phase difference is slightly improved at the higher frequencies for added L's and added frequency dependent C's (cases J and K).

Table II summarizes comparisons of the theory in table I at 2.5, 40, and 100 Hz, between the more sophisticated circuit models (cases D, F, and H) and the simplest model (case C). The most significant changes are produced at higher frequencies by adding L's and C's.

In general the more sophisticated models seem to produce slightly improved agreement with the experimental data. The best agreement occurs for (1) the measured values of R, (2) the RLC circuit models simulating capillary modules, and (3) the polytropic coefficient $n = 1.4$.

7.5 Fluidic Lag-Lead Network with Bellows Module

The desired lag-lead network is identical with the ideal lead network presented in figure 42 with the exception that a resistor was placed in shunt across the point-to-point capacitor between node IN and node OUT as shown in figure 48.

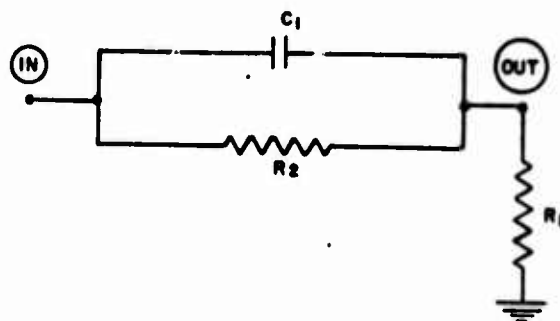


Figure 48. Schematic of simple lag-lead network.

TABLE I LEAD NETWORK RESPONSE

Case →	Exp't	C		F		D		G		H		I		J		K	
		Capillary		Capillary		Capillary		Capillary		Capillary		Capillary		Capillary		Capillary	
Freq (Hz)		R = lin	R = ni	R = lin	R = ni	R = lin	R = ni	R = lin	R = ni	R = lin	R = ni	R = lin	R = ni	R = lin	R = ni	R = lin	R = ni
		C = 0	C = 0	C ≠ 0	C ≠ 0	C = 0	C = 0	C = 0	C = 0	C = 0	C = 0	C = 0	C = 0	C = 0	C = 0	C = 0	C = 0
		L = 0	L = 0	L ≠ 0	L ≠ 0	L = 0	L = 0	L = 0	L = 0	L = 0	L = 0	L = 0	L = 0	L = 0	L = 0	L = 0	L = 0
		Volume		Volume		Volume		Volume		Volume		Volume		Volume		Volume	
		C ≠ C(f)	C ≠ C(f)	C ≠ C(f)	C ≠ C(f)	C ≠ C(f)	C ≠ C(f)	C ≠ C(f)	C ≠ C(f)	C ≠ C(f)	C ≠ C(f)	C ≠ C(f)	C ≠ C(f)	C ≠ C(f)	C ≠ C(f)	C ≠ C(f)	C ≠ C(f)
		R ≠ R(f)	R ≠ R(f)	R ≠ R(f)	R ≠ R(f)	R ≠ R(f)	R ≠ R(f)	R ≠ R(f)	R ≠ R(f)	R ≠ R(f)	R ≠ R(f)	R ≠ R(f)	R ≠ R(f)	R ≠ R(f)	R ≠ R(f)	R ≠ R(f)	R ≠ R(f)
		Magnitude ratio		Magnitude ratio		Magnitude ratio		Magnitude ratio		Magnitude ratio		Magnitude ratio		Magnitude ratio		Magnitude ratio	
		X10 ⁻²	X10 ⁻²	X10 ⁻²	X10 ⁻²	X10 ⁻²	X10 ⁻²	X10 ⁻²	X10 ⁻²	X10 ⁻²	X10 ⁻²	X10 ⁻²	X10 ⁻²	X10 ⁻²	X10 ⁻²	X10 ⁻²	X10 ⁻²
2.5		.24	.24	.24	.24	.24	.24	.24	.24	.24	.24	.24	.24	.24	.24	.24	.24
5		.47	.47	.47	.47	.47	.47	.47	.47	.47	.47	.47	.47	.47	.47	.47	.47
10		.91	.91	.91	.91	.91	.91	.91	.91	.91	.91	.91	.91	.91	.91	.91	.91
20		1.62	1.62	1.64	1.64	1.64	1.64	1.58	1.58	1.58	1.58	1.58	1.58	1.61	1.61	1.61	1.61
40		2.39	2.39	2.49	2.49	2.49	2.49	2.34	2.34	2.34	2.34	2.34	2.34	2.43	2.43	2.43	2.43
80		2.86	2.86	3.02	3.02	3.02	3.02	2.81	2.81	2.81	2.81	2.81	2.81	2.96	2.96	2.96	2.96
100		2.94	2.94	3.11	3.11	3.11	3.11	2.89	2.89	2.89	2.89	2.89	2.89	3.06	3.06	3.06	3.06
		Phase Difference		Phase Difference		Phase Difference		Phase Difference		Phase Difference		Phase Difference		Phase Difference		Phase Difference	
		-85.59	-85.59	-85.85	-85.85	-85.85	-85.85	-85.22	-85.22	-85.22	-85.22	-85.22	-85.22	-85.48	-85.48	-85.48	-85.48
		-81.24	-81.24	-81.77	-81.77	-81.77	-81.77	-80.78	-80.78	-80.78	-80.78	-80.78	-80.78	-81.29	-81.29	-81.29	-81.29
		-72.92	-72.92	-73.89	-73.89	-73.89	-73.89	-72.41	-72.41	-72.41	-72.41	-72.41	-72.41	-73.37	-73.37	-73.37	-73.37
		-58.49	-58.49	-60.02	-60.02	-60.02	-60.02	-58.16	-58.16	-58.16	-58.16	-58.16	-58.16	-59.65	-59.65	-59.65	-59.65
		-39.26	-39.26	-40.86	-40.86	-40.86	-40.86	-39.38	-39.38	-39.38	-39.38	-39.38	-39.38	-40.94	-40.94	-40.94	-40.94
		-22.28	-22.28	-23.08	-23.08	-23.08	-23.08	-22.72	-22.72	-22.72	-22.72	-22.72	-22.72	-23.53	-23.53	-23.53	-23.53
		-18.03	-18.03	-18.47	-18.47	-18.47	-18.47	-18.50	-18.50	-18.50	-18.50	-18.50	-18.50	-18.97	-18.97	-18.97	-18.97

Table II: Percentage Changes from Simple Linear,
Frequency-Independent Lead Network

Parameters measured	Frequency		
	2.5 Hz	40 Hz	100 Hz
Magnitude Ratio, G			
Model			
Nonlinear R in capillaries	0	0	0
Added LC in capillaries	0	+4%	+6%
Frequency dependent C in volumes	-4%	-2%	-1%
Phase Difference, ϕ			
Model			
Nonlinear R in capillaries	0	0	0
Added LC in capillaries	-0.3%	-4%	-2%
Frequency dependent C in volumes	+0.4%	-0.3%	-3%

Each ideal circuit element was replaced on a one-to-one basis by the same equivalent fluidic component as in section 4. Also capillary 3 replaced shunting resistor, R_2 . The overall fluidic test network is shown in figure 49.

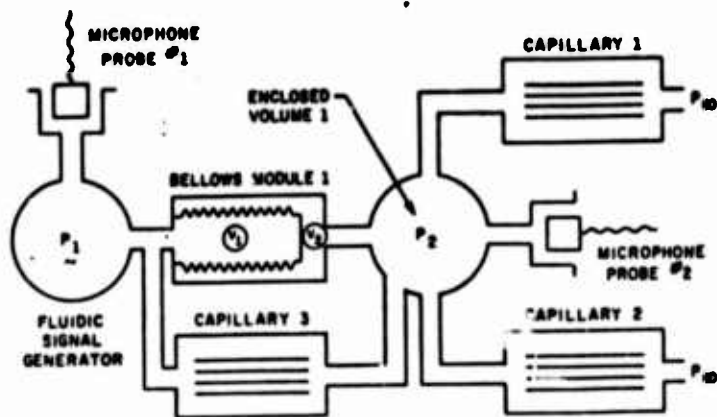


Figure 49. Fluidic lag-lead network with bellows module

A circuit representing the overall fluidic hardware is shown in figure 50.

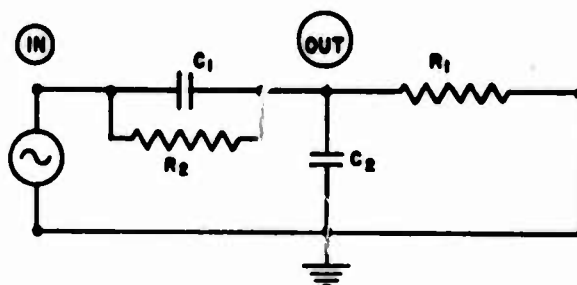


Figure 50. Circuit of experimental lag-lead network with bellows module

The same fluidic components and microphones are used as in section 7.4 with the addition of a capillary. Introduction of a tee fitting at node IN is ignored in the calculations.

Capillary 3: $N = 8$, $r = 1.525 \times 10^{-4} \text{m}$, $\ell = .03 \text{m}$, $R = 4.41 \times 10^8 \frac{\text{kg}}{\text{m}^4 \text{sec}}$

Experimental results are presented as a Bode plot (fig. 51) between 2.5 and 100 Hz at an input pressure of 1000 Pa rms. These results are similar to those of the low-frequency segment of a lag network in figure 34.

Again the circuit models from section 3 were selected. Identical assumptions were made in developing the eleven sets of models (cases A through K) for the lag-lead network. Bode plots of cases A through E were calculated between 2.5 and 100 Hz with small signal a-c analyses using NET-2.

The computed magnitude ratio plot for cases A and B and the computed phase difference for case C compare most favorably with the experimental data. The best models for both the magnitude ratio and the phase difference are different from those found in section 7.4 for the lead network.

By adding L's and C's to models of the capillary module, there is considerable improvement in the predicted values of phase difference at higher frequencies.

Again small signal a-c analyses for eight cases (C, D and F through K) were computed using SLIC between 2.5 and 100 Hz. Bode plots are tabulated in table III. Predicted magnitude ratio is in best agreement with experimental results at the lower frequencies for the linear resistance models (cases C, F, H, and J). The best agreement between the predicted and experimental phase difference was found when the capillaries were purely resistive (cases C, D, H and I).

Table IV summarizes comparisons at 2.5, 40, and 100 Hz between the sophisticated models (cases D, F and H) and the simplest model (case C). The most drastic differences occur (1) for added L's and C's at high frequencies, and (2) for frequency-dependent volumes at low frequencies.

Overall the best model seems to include pure linear resistances, and a polytropic coefficient $n = 1.0$.

7.6 Fluidic Lead Network with Diaphragm Module

In sections 7.4 and 7.5, a bellows module has been studied as a point-to-point capacitor. A diaphragm module replaces the bellows module in the version. Similar tests were performed. Only the differences in configuration and results are noted in this section. For the lag-lead network (sect 7.5), the point-to-point capacitor C_1 between nodes IN and OUT (fig. 48) may be implemented with a diaphragm module instead of with a bellows module. The configuration with the diaphragm module is shown in figure 52.

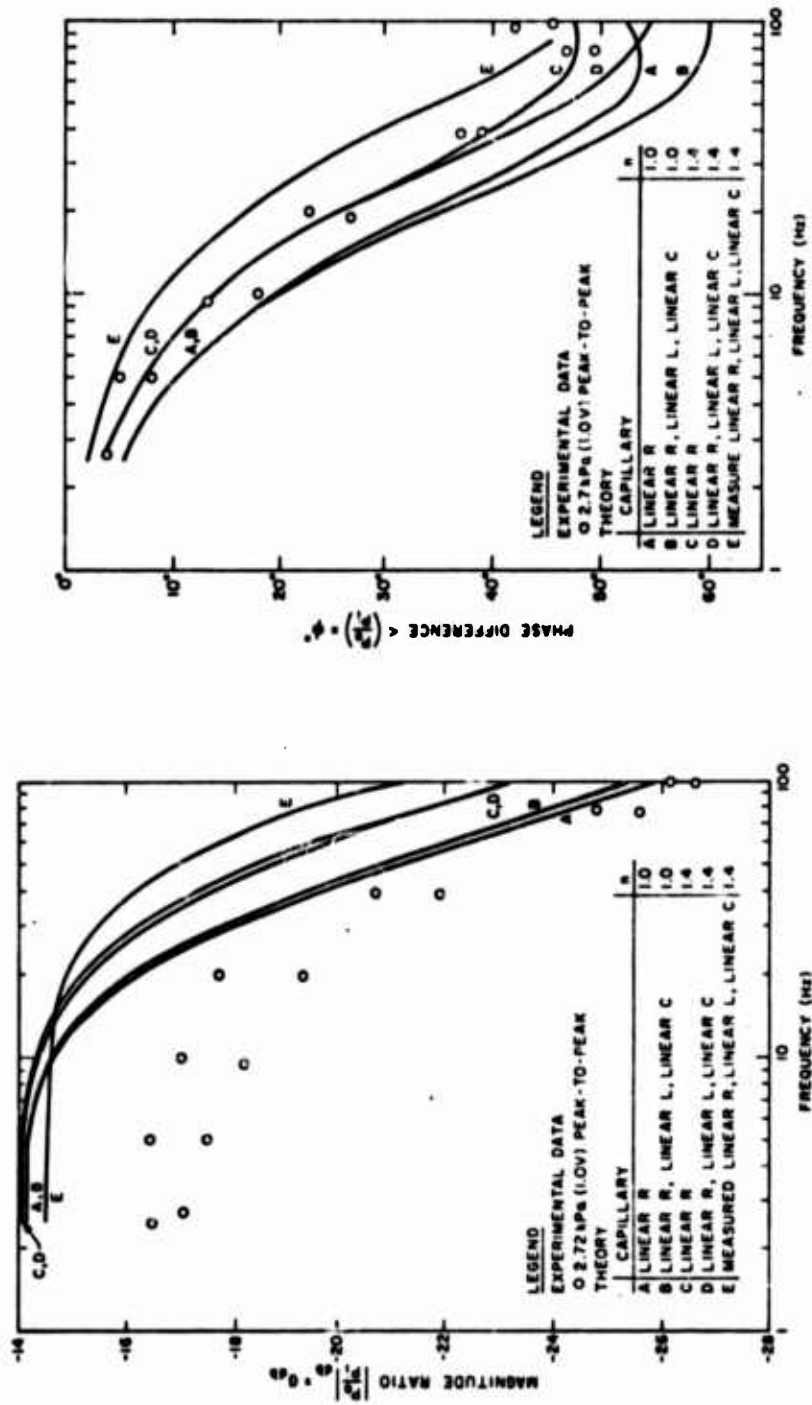


Figure 51. Bode plot for lag-lead network with bellows

Table IV Percentage Changes from Simple Linear,
Frequency-Independent Lag-Lead Network

Magnitude Ratio, G	Frequency		
	2.5 Hz	40 Hz	100 Hz
Nonlinear R in capillaries	-2%	-2%	-2%
Added LC in capillaries	0	+3%	+1%
Frequency Dependent C in Volume	-0.5%	-1.5%	-1%

Phase Difference, ϕ	Frequency		
	2.5 Hz	40 Hz	100 Hz
Nonlinear R in capillaries	+0.3%	-0.1%	-1.2%
Added LC in capillaries	0	+5.1%	+16.6%
Frequency Dependent C in Volume	+10.0%	0	-0.9%

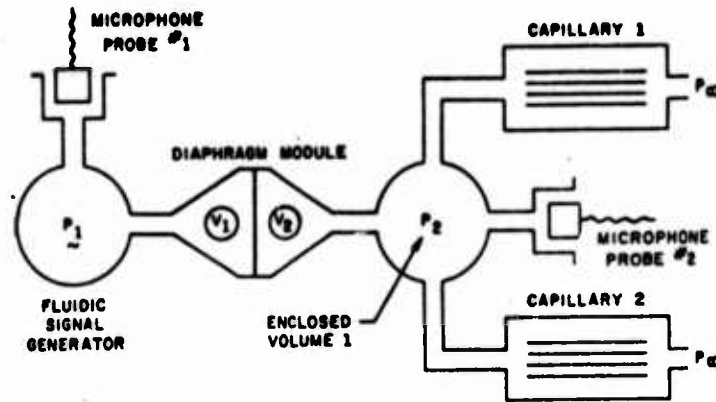


Figure 52. Fluidic lead network with diaphragm module

The same fluidic elements and microphones were used with the exception that bellows module has replaced by the diaphragm module.

The diaphragm was constructed from a thin sheet of either unstressed natural rubber or unstressed polyurethane. The diaphragm in these tests has the following specification

$$h = .33 \text{ mm}$$

$$E = 1.25 \times 10^6 \frac{\text{Kg}}{\text{m} \cdot \text{sec}^2}$$

In forming the diaphragm module, the thin diaphragm was positioned in an unstressed state between two tapered chambers, in which cross-sectional area was smoothly varied from the passage size to the diaphragm size. A cross-sectional drawing is shown in figure 53.

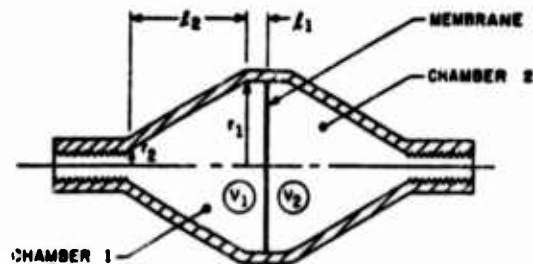


Figure 53. Diaphragm Module

The diaphragm module is symmetrical about the membrane. Each of the chambers in figure 53 is made up of a cylinder and frustrum of a cone. Dimensions are

$$\begin{aligned}r_1 &= 1.27 \times 10^{-2} \text{ cm} \\r_2 &= 6.35 \times 10^{-3} \text{ cm} \\l_1 &= 6.35 \times 10^{-3} \\l_2 &= 1.016 \times 10^{-2} \text{ cm}\end{aligned}$$

Volume of the two identical chambers was computed as

$$V_1 = V_2 = 5.54 \times 10^{-6} \text{ m}^3$$

An equivalent circuit for the overall test configuration is shown in figure 54.

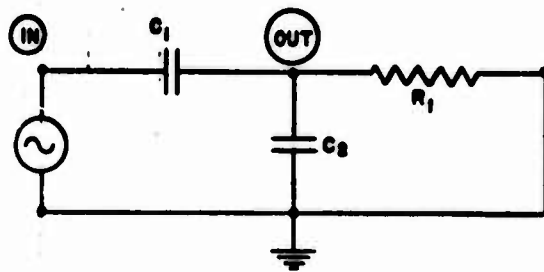


Figure 54. Circuit of experimental lead with diaphragm module

This configuration was tested in the range between 2.5 and 100 Hz. Experimental results are presented as a Bode plot (figure 55). When compared with typical Bode plots in section 7.1, this plot has approximately the form of the high-frequency segment of a lead network.

Computational models were again selected from section 3; however,

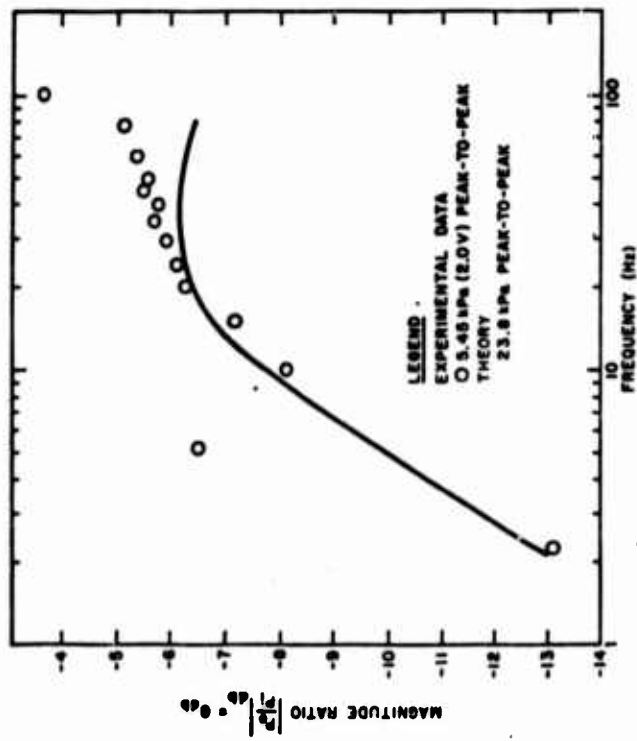
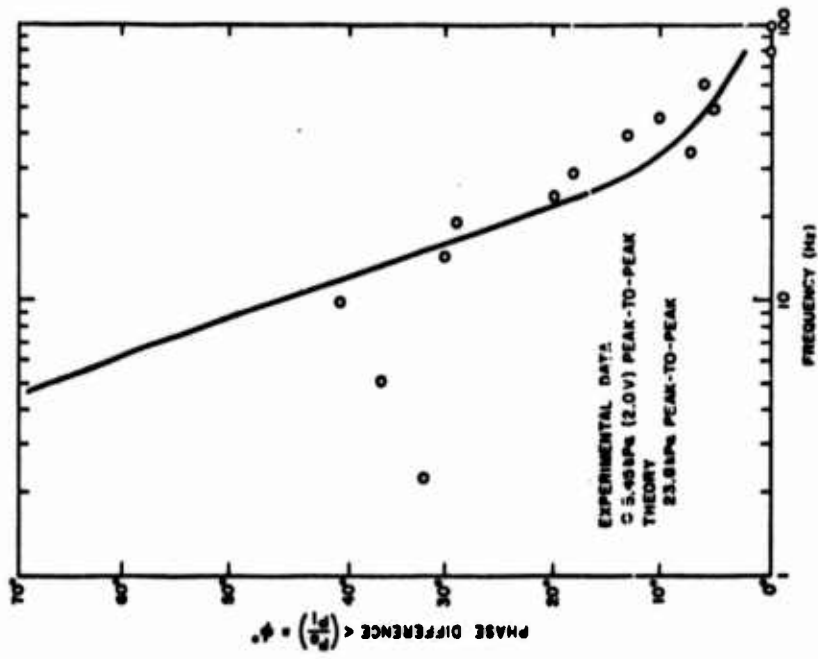


Figure 55. Bode plot for lead network with diaphragm

only one set of models was calculated. The following assumptions are included:

- (1) The enclosed volume of the junction is a linear, frequency-independent capacitor with volume equal to $3.59 \times 10^{-6} \text{ m}^3$.
- (2) The polytropic coefficient, $n = 1.0$.
- (3) Capillary modules are modeled as pure, linear resistors.
- (4) The load is considered to be two capillaries, each with $\ell = 0.07 \text{ m}$.
- (5) The diaphragm module is a Pi of capacitors. The horizontal bar of the Pi is a nonlinear point-to-point capacitor. Its vertical legs are grounded, linear capacitors. When the diaphragm module is placed at the output of the signal generator, the grounded input capacitor is considered as part of the signal generator. This capacitor is neglected in an overall circuit representation of the network.
- (6) The input pressure is approximately 10 kPa rms.

A transient response was calculated using DSL/90 for frequencies between 2.5 and 80 Hz. Magnitude ratio and phase difference were measured from these time plots and are presented as Bode plots in figure 55. Theoretical results for the magnitude ratio at low frequency and for the phase difference at high frequency agree best with the experimental results.

8. DESIGN APPROACH TO FLUIDIC CONFIGURATIONS

Modeling and experimental efforts expended designing individual components and subsystems are directed toward a specific goal: to develop accurate circuit models for designing fluidic systems. The studies in this paper and continuing studies will eventually allow various fluidic components to be modeled as one or more fluidic circuits, each predicting fluidic signal response over a specific operating range within a specified error.

Circuit models of fluidic components are defined in terms of four items:

- (1) Network topologies are given as arrays of source, dissipation, and storage elements.
- (2) Values of circuit elements are given as constants or as variables (dependent on pressure, flow, time or frequency). Element values are defined in either open or closed form in terms of parameters which are bounded or unbounded and discrete or continuous.
- (3) Operating ranges are given for bandwidth and pressure amplitude.
- (4) Mean or maximum response errors are specified over the operating ranges.

Fluidic component models are being organized in the form of a catalog. However, it must be kept in mind that these models are not all

inclusive. Only selected cases have been studied in the current development of circuit models. In fact, individual components and small subsystems have even been tested by partially isolating their terminal nodes. Because of the valuable data in every circuit simulation, the design approach therefore must necessarily include procedures for improving component models.

It is possible to envision a fluidic design approach over ranges in which the fluidic models have been cataloged. This approach (fig. 56) consists of both basic design (within the dashed lines) and peripheral circuit model improvements. The envisioned design approach is to:

- (1) Specify the network problem,
- (2) Construct an equivalent circuit,
- (3) Select fluidic models that simulate equivalent circuits,
- (4) Construct new equivalent circuits in terms of fluidic-component models,
- (5) Adjust parameters of the models in fulfilling specifications to determine a physically realizable configuration,
- (6) Determine experimental response of an implemented physical configuration, and
- (7) Compare test results and required response in defining response error.

8.1 Specification of the Network Problem

Specification of the network problem is made (fig. 56) in terms of either the required output nodal response of the physical configurations or an equivalent circuit. The input signals and loads are given and possible fluidic components are suggested.

One or more required aspects of the nodal response are specified as a value plus or minus an error. Standard forms of nodal response should be discussed such as steady-state d-c response, steady-state a-c response, and transient response. Steady-state d-c response is defined by attenuation ratios between nodes. Critical aspects in defining steady-state a-c nodal response should be given through performance criteria in the complex frequency domain based on values of gain margin, phase margin, bandwidth, peak resonance, and break frequencies. Transient nodal response, observed through performance criteria in the time domain, is based on values of rise time, delay time, settling time, and overshoot.

The set of passive fluidic components that can be used in these designs will include orifices, area changes, and transmission lines, as well as those discussed in section 3 (capillaries, enclosed volumes, bellows modules, and diaphragm modules).

8.2 Construction of an equivalent circuit

Section 8.1 specifies either the output nodal response or the

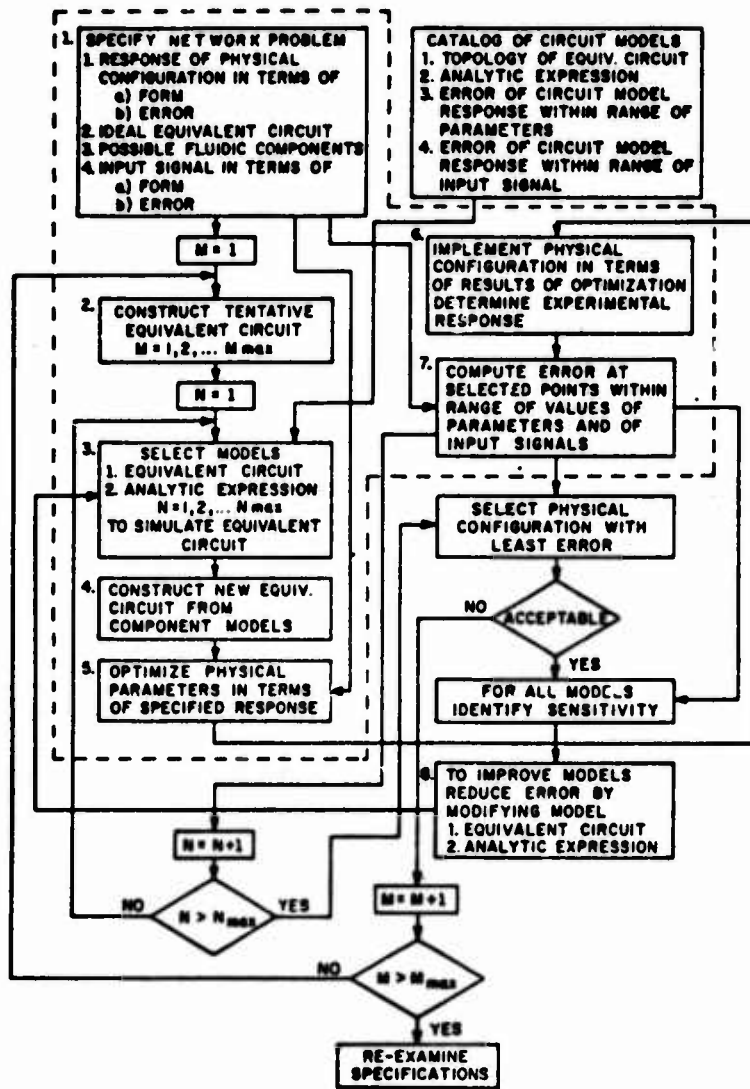


Figure 56. Flow chart of design approach

equivalent circuit. If only the response is specified, one or more simple circuits can be synthesized. The lowest order circuits that satisfy the form of the response will be selected. Many texts and references such as Chesnut and Mayer (ref 26) present lengthy tables of low-order circuit topologies, their ranges of element values, and their output nodal response forms.

For fluidics, element values are to be defined parametrically along with the circuit configuration in the model catalog. Section 8.5 outlines techniques for selecting and adjusting values of circuit elements to satisfy the design specifications.

8.3 Selection of Fluidic Models that Simulate Equivalent Circuit

Based on the circuit topology and the allowable ranges of element values, a realizable fluidic simulation model can be developed. The existing model catalog is checked for components that, over the specified operating ranges, can possibly simulate the specified forms of pure resistance, of pure inductance, and of pure capacitance. For example, a linear resistor can be replaced by a capillary; a point-to-point capacitor by a bellows module or a diaphragm module; and a grounded capacitor and a node, by an enclosed volume.

One or more models that seem to best match the equivalent circuit over the specified operating ranges are selected from this catalog. It is important, however, to realize that the selected circuit is not unique.

8.4 Construction of New Equivalent Circuits Representing Fluidic Components

The basic equivalent circuit can now be developed into a new circuit with more complete models of fluidic components from the catalog. For example, for some operating ranges, a linear resistor that is simulated by a fluidic capillary is replaced by a RLC circuit (sect 3.1).

8.5 Adjustment of Parameters to Fulfill Specifications

Where possible in the specified operating ranges, satisfactory agreement (within the allowed error) is sought between the specified response and the simulated response of fluidic circuits developed in section 8.4. There are two possible approaches for obtaining satisfactory agreement. First, the element values or the parameters within expressions defining the element values, may be adjusted. Second, the circuit topology may be changed. In this paper, however, only element values and element parameters are adjusted.

Since optimization can be a lengthy iterative procedure, the NET-2 circuit analysis program, which has self-contained optimization procedures, is used. A computerized optimization procedure automatically minimizes the error between the simulated and specified responses as a function of the design parameters. One form of error (or performance criterion) is the integrated least squares difference between the simulated and specified results on a Bode plot.

Computed design parameters can now be used directly in specifying fluidic components.

It is impossible in many cases to adjust parameters in a given simulation to produce the specified response. Difficulties arise because compatibility can not be achieved among the specified response, the allowable fluidic components, and the selected circuit topology. Two aspects of the problem that introduce a lack of compatibility are non-realizability of certain values of the circuit components and non-realizability of certain circuit functions with passive components.

8.6 Determination of Experimental Response of an Implemented Fluidic Configuration

A breadboarded fluidic model can now be implemented on the basis of a circuit topology and of selected parameter values. Specified input signals and loads are connected to the fluidic components and pressure measurements are taken simultaneously at a pair of nodes. Results are plotted in convenient forms.

8.7 Comparison of Measured and Specified Fluidic Response in Defining Error

Performance criteria are numerical values that define the error between measured and specified responses. For example, in the static case, a performance criterion might be an integrated least squares difference between the measured and specified values of instantaneous resistance. In the dynamic case it might be an integrated least squares difference, either between measured and specified curves or between measured and specified points on response curves. More meaningful performance criteria are being investigated.

If the specified error criteria can be met, then the component models lead to satisfactory designs.

8.8 Improvement of Circuit Models

In these initial phases of fluidic model development and fluidic circuit design, the model catalog may also be improved by examining errors between experimental and specified response. In fact to validate and, where possible, to extend their operating ranges, many circuit models should be used to simulate equivalent circuits (sect 8.3).

In general, the discrepancies between the experimental and specified response (sect 8.7) can be attributed to the use of non-ideal physical fluidic components to predict the nodal response of an idealized circuit. Improved agreement in the simulated and experimental nodal response data can be obtained by relating circuit topology and element values to additional experimental response data.

A useful approach for improving models is sensitivity analysis.

Using sensitivity analysis, the change in nodal response, produced by changing a parameter about the given operating point, can be calculated. Sensitivity analysis gives relative errors caused by changing various parameters. Also, the sensitivity of key parametric relationships (sect 8.3) that define the nodal response can be calculated.

By adding engineering insight to the results of engineering analyses, improved model topologies and improved expressions for element values can be suggested. Improved circuit models lead to an improved design approach.

9. CONCLUSIONS

One of the most important conclusions of this paper is that useable circuit models of fluidic components can be synthesized. It remains only to develop a design approach that selects the best component model from a catalog.

Various circuit topologies and forms of analytic expressions were investigated in this study. Models are linear or nonlinear and frequency independent or frequency dependent. The magnitude of the nonideal effects on network response is seen to depend on the overall configuration, the operating frequency, and the operating pressure of the component.

Circuit models have not as yet been evaluated against ideal response specifications. Some of the effects of nonideal resistance, capacitance, and inductance will definitely be felt in attempting to produce ideal responses in fluidic networks.

As a start toward a fluidic design guide, Bode response results developed in sections 6 and 7 are summarized in table V. In each configuration the bandwidth is tabulated for experimental magnitude ratios within ± 10 percent of the computer models and experimental phase differences within ± 10 deg of the computer models.

It is of interest to note in table V that the simple, pure, linear models of components are entirely adequate (within the ± 10 percent and ± 10 deg error limits) for some portions of the frequency range. It appears that error and frequency range can be traded off against each other, so that in many cases simple models readily estimate the performance of components in many circuits.

By minimizing the complexity of circuit models that still predict response, the cost of computer-aided circuit analysis and design is also minimized.

Table V. Error Ranges for Models of Subsystems - 10 percent, 10 deg

1. Passive Summing Junction (Figure 29 a & b) 25-62 Pa, 7.5-200 Hz

<u>Capillary</u>			<u>Volume</u>		$.9 < \frac{ G(\text{Model}) }{ G(\text{Exp't}) } < 1.1$	$ \phi(\text{Model}) - \phi(\text{Exp't}) < 10^\circ$
R	L	C		C		
linear	-	-	-	-	up to 140 Hz	up to 25 Hz
linear	-	-	n = 1.0	n = 1.0	→	up to 60 Hz
linear	$\lambda = \frac{4}{3}$	n = 1.0	n = 1.0	n = 1.0	up to 145 Hz	up to 65 Hz
linear	$\lambda = 1$	n = 1.0	n = 1.0	n = 1.0	up to 130 Hz	up to 70 Hz
linear	-	-	n = 1.4	n = 1.4	up to 90 Hz	up to 90 Hz
linear	$\lambda = \frac{4}{3}$	n = 1.4	n = 1.4	n = 1.4	entire range	entire range
linear	$\lambda = 1$	n = 1.4	n = 1.4	n = 1.4	entire range	entire range

Table V: Error Ranges for Models of Subsystems - 10 percent, 10 deg (cont'd)

2. Passive Distribution Junction (Figure 32 a & b) 25-62 Pa, 2.5-200 Hz

Capillary	Volume		$.9 \leq \left \frac{G(\text{Model})}{G(\text{Exp't})} \right < 1.1$	$ \phi(\text{Model}) - \phi(\text{Exp't}) < 10^\circ$
	L	C		
linear	-	-	up to 80 Hz	up to 15 Hz
linear	-	-	entire range	up to 40 Hz
linear	$\frac{4}{3}$	n = 1.0	up to 85 Hz	up to 60 Hz
linear	1	n = 1.0	up to 75 Hz	up to 75 Hz
linear	-	-	entire range	up to 90 Hz
linear	$\frac{4}{3}$	n = 1.4	entire range	entire range
linear	1	n = 1.4	up to 90 Hz	entire range

3. Lag Network (Figure 41 a & b) 0.02-1.0 kPa, 9-200 Hz

Capillary	Volume		$.9 \leq \left \frac{G(\text{Model})}{G(\text{Exp't})} \right < 1.1$	$ \phi(\text{Model}) - \phi(\text{Exp't}) < 10^\circ$
	L	C		
linear	-	-	35 → 180 Hz	entire range
linear	$\frac{4}{3}$	n = 1.0	35 → 185 Hz	up to 35 Hz, 50 Hz and up

Table V: Error Ranges for Models of Subsystems - 10 percent, 10 deg (cont'd)
 4. Lead Network with Bellows (Figure 47 a & b, Table I) 1. - 2. kPa, 2.5-100 Hz

Capillary		Volume		Bellows		$.9 \leq \frac{G(\text{Model})}{G(\text{Exp't})} < 1.1$	$ \phi(\text{Model}) - \phi(\text{Exp't}) < 10^\circ$
R	L	C	C	Point to Point C	grounded C		
linear	-	-	n = 1	linear	linear	up to 15 Hz	up to 15 Hz
linear	$\lambda = \frac{4}{3}$	n = 1	n = 1	linear	linear	up to 15 Hz	up to 15 Hz
linear	-	-	n = 1.4	linear	linear	up to 15 Hz	entire range
linear	$\lambda = \frac{4}{3}$	n = 1.4	n = 1.4	linear	linear	up to 15 Hz, 30 Hz and up	entire range
measured linear	$\lambda = \frac{4}{3}$	n = 1.4	n = 1.4	linear	linear	50 Hz and up	entire range
nonlinear	-	-	n = 1.4	linear	linear	invalid	entire range
nonlinear	$\lambda = \frac{4}{3}$	n = 1.4	n = 1.4	linear	linear	invalid	entire range
linear	-	-	n = f(ω)	linear	linear	invalid	entire range
nonlinear	-	-	n = f(ω)	linear	linear	invalid	entire range
linear	$\lambda = \frac{4}{3}$	n = f(ω)	n = f(ω)	linear	linear	invalid	entire range
nonlinear	$\lambda = \frac{4}{3}$	n = f(ω)	n = f(ω)	linear	linear	invalid	entire range

Table V: Error Ranges for Models of Subsystems - 10 percent, 17 deg (cont'd)

5. Lag-Lead Network (Figure 51 a & b, Table III) 1. kPa, 2.5-100 Hz

Capillary		Volume		Bellows		$.9 \leq \frac{G(\text{Model})}{G(\text{Exp't})} < 1.1$	$ \phi(\text{Model}) - \phi(\text{Exp't}) < 10^\circ$
R	L C	C	Point to Point C	Point to grounded C			
linear	-	-	n = 1	linear	linear	50 Hz and up	entire range
linear	$\lambda = \frac{4}{3}$	n = 1	n = 1	linear	linear	50 Hz and up	up to 30 Hz
linear	-	-	n = 1.4	linear	linear	up to 30 Hz	entire range
linear	$\lambda = \frac{4}{3}$	n = 1.4	n = 1.4	linear	linear	entire range	up to 80 Hz
measured linear	$\lambda = \frac{4}{3}$	n = 1.4	n = 1.4	linear	linear	entire range	entire range
nonlinear	-	-	n = 1.4	linear	linear	entire range	entire range
nonlinear	$\lambda = \frac{4}{3}$	n = 1.4	n = 1.4	linear	linear	entire range	up to 80 Hz
linear	-	-	n = f(ω)	linear	linear	entire range	up to 80 Hz
nonlinear	-	-	n = f(ω)	linear	linear	entire range	entire range
linear	$\lambda = \frac{4}{3}$	n = f(ω)	n = f(ω)	linear	linear	entire range	up to 80 Hz
nonlinear	$\lambda = \frac{4}{3}$	n = f(ω)	n = f(ω)	linear	linear	entire range	up to 80 Hz

6. Lead Network with Diaphragm (Figure 55 a & b) 2 kPa, 10-80 Hz

Capillary		Volume		Diaphragm		$.9 \leq \frac{G(\text{Model})}{G(\text{Exp't})} < 1.1$	$ \phi(\text{Model}) - \phi(\text{Exp't}) < 10^\circ$
R	L C	C	Point to Point C	Point to grounded C			
linear	-	-	n = 1.4	nonlinear	n = 1.4	up to 60 Hz	entire range

10. LITERATURE CITED

- (1) Kirshner, Joseph M., Fluid Amplifiers, McGraw-Hill Co., New York, 1966.
- (2) Blackburn, John F., Gerhard Reethof, J. Lowen Shearer, Fluid Power Control, MIT Press, Cambridge, Mass, 1960.
- (3) White, Harry N., "Analysis of the Steady-Flow Pneumatic Resistance of Parallel Capillaries," Proceedings of the Fluid Amplification Symposium, Volume I, HDL, Washington, DC, October 1965.
- (4) Merritt, Herbert E., Hydraulic Control Systems, Wiley, New York, 1967.
- (5) Rohmann, C. P. and E. C. Grogan, "On the Dynamics of Pneumatic Transmission Lines," Transaction of the ASME, pp. 853-874, May 1957.
- (6) Turnquist, Ralph O., "Fluerics (Fluid Amplification), 18. A Fluid-State Digital Control System," HDL, Washington, DC, February 1966.
- (7) Katz, Silas and Edgar Hastie, "Fluerics 31. The Transition from Isothermal to Adiabatic Capacitance in Cylindrical Enclosures," HDL-TM-71-35, HDL, Wash, DC, 1971.
- (8) Katz, Silas and Edgar Hastie, "Pneumatic Passive Lead Networks for Fluidic Systems," Joint Automatic Control Conference, St. Louis, 1971.
- (9) Belsterling, Charles A., Fluidic Systems Design, Wiley-Interscience, New York, 1971.
- (10) Manion, F. M., "Dynamic Analysis of Flueric Proportional Amplifier," ASME Paper no. 68-FE-49, 1968.
- (11) HDL Staff, "Fluerics 23. A Bibliography," HDL-TR-1495 (R A), Washington, DC, October 1971.
- (12) Shearer, Jesse L., Arthur T. Murphy and Herbert H. Richardson, Introduction to System Dynamics, Addison-Wesley, Reading, Mass, 1967.
- (13) Chua, Leon O., Introduction to Nonlinear Network Theory, McGraw-Hill Book Co., New York, 1969.
- (14) Iseman, Joseph M., "Computer-Aided Fluidic Circuit Analysis and Design," Proceedings of the HDL State-of-the-Art Symposium, 30 Sept - 3 Oct 1974.
- (15) Del Toro, Vincent, Electrical Engineering Fundamentals, Prentice-Hall, Edgewood Cliffs, New Jersey, 1972.

- (16) Reid, Karl N., "Fluid Transmission Lines," School of Mechanical and Aerospace Engineering, Oklahoma State University, Stillwater, Oklahoma, July-August 1968.
- (17) Kirshner, J. M. and S. Katz, Design Theory of Fluidic Components, Chapter 2, In Publication by Academic Press, New York, 1974.
- (18) Iseman, Joseph M., "Computerized Equivalent Circuit Models of Fluidic Capillaries," 1974 Army Numerical Analysis Conference, Philadelphia, PA, 13-14 February 1974. In publication.
- (19) Alexander, J. Eugene and J. Milton Bailey, Systems Engineering Mathematics, Prentice-Hall, Englewood Cliffs, New Jersey, 1962.
- (20) Daniels, F. B., "Acoustical Impedance of Enclosures," Journal of the Acoustical Society of America, Vol. 19, No. 4, p. 569, July 1947.
- (21) Kop, Harold M., "An Improved Version of SLIC," Memorandum No. ERL-M364 Electronics Research Laboratory, College of Engineering, University of California, Berkeley, 3 August 1972.
- (22) Malmberg, Allan F., "Preliminary User's Manual, NET-2 Network Analysis Program," Harry Diamond Laboratories, September 1972.
- (23) Bloom, H. M., "DSL/90 Programming Manual," HDL-TM-7113, HDL, Wash., DC, October 1971.
- (24) White, Dyrull V., "Pneumatic Fluidic Summing and Distribution Junctions," Proc. Student Trainee Technical Symposium, HDL, 1973.
- (25) Anon. "ECAP, 1620 Electronic Circuit Analysis Program," International Business Machines Corp., Report no. H20-0170-1, White Plains, NY, 1965.
- (26) Chestnut, Harold and Robert W. Mayer, Servomechanisms and Regulating System Design, Vol. II, Wiley, New York, 1955.

A LAMINAR FLUIDIC MULTIPLIER AND A
REVIEW OF THE STATE-OF-THE-ART

by

ROBERT L. WOODS*

ABSTRACT

The state-of-the-art of fluidic multiplication is reviewed, and a new approach to fluidic multiplication is introduced. This approach uses a laminar proportional amplifier as the basic multiplying element. As shown in this paper, the gain of a proportional amplifier is proportional to the power jet pressure when operated in the laminar regime, thereby allowing gain change or multiplication. A preconditioning and buffering circuit is used to linearize and isolate the multiplier from other circuitry.

Prepared for the Harry Diamond Laboratories
Fluidics State-of-the-Art Symposium
30 Sept - 04 Oct 74

*Fluidic Systems Research Branch
Harry Diamond Laboratories

1. INTRODUCTION

Multiplication or gain-change is a function often needed in fluidic computation and control circuits. Some of the applications are (1) straight multiplication of two signals for computation purposes, (2) division of one signal by another, accomplished by putting a multiplier in the feedback loop of a high-gain amplifier, (3) function generation, such as squaring, and (4) gain change, i.e., variation of the system gain for control purposes.

In spite of the need for multipliers, the ones that exist today are lacking in performance, simplicity, and availability. In Section 2 we review the state-of-the-art, and discuss methods that have been used to achieve multiplication. These include the use of (1) amplifier bias sensitivity, (2) mechanical moving parts, (3) the quarter-square principle, (4) digital computation, and (5) three-dimensional effects with unconfined jets. In Sections 3 and 4 we present a new approach to fluidic-multiplication that offers the possibility of substantially improved performance.

2. STATE-OF-THE-ART IN FLUIDIC MULTIPLIERS

In the early days of fluidics, there was more concern for the performance characteristics of individual components than for systems; consequently, little work was done toward multiplication. As components were developed, more systems were being built and the need for multiplication became more apparent. The approaches taken toward fluidic multipliers have been to utilize inherent device characteristics or to build circuits to accomplish the effect as discussed below. Actually, most concepts discussed below fall into the category of gain changers since the second input decreases gain with increasing input. A true multiplier, however, increases gain with both inputs and has zero gain at zero input. Thus, a nonlinear inversion of the second input is usually required to convert gain changers into true multipliers. Some gain changers might be useful as dividers over a limited range.

2.1 Planar Amplifier Gain Sensitivity

A generally undesirable characteristic of a planar proportional amplifier is its sensitivity to mean input level (or bias) [1,2]. However, if the amplifier is sufficiently sensitive to mean input level, the effect can be used to accomplish gain change or, with linearizing circuitry, multiplication. For most amplifiers, a gain change of 2- or 3-to-one is the maximum to be expected. The gain change is in inverse proportion to mean input level (above 15%) as shown in figure 1.

Beduhn [3] reports a three-stage amplifier arrangement in which the gain can be varied by adjusting the interaction vent pressure of the driving amplifier to increase the mean input level to the third stage (Figure 2). There are some unresolved questions of operation; however, a gain change of 3.7-to-1 was reported. Again, the gain decreases with signal input, which is generally unsuited for multiplication.

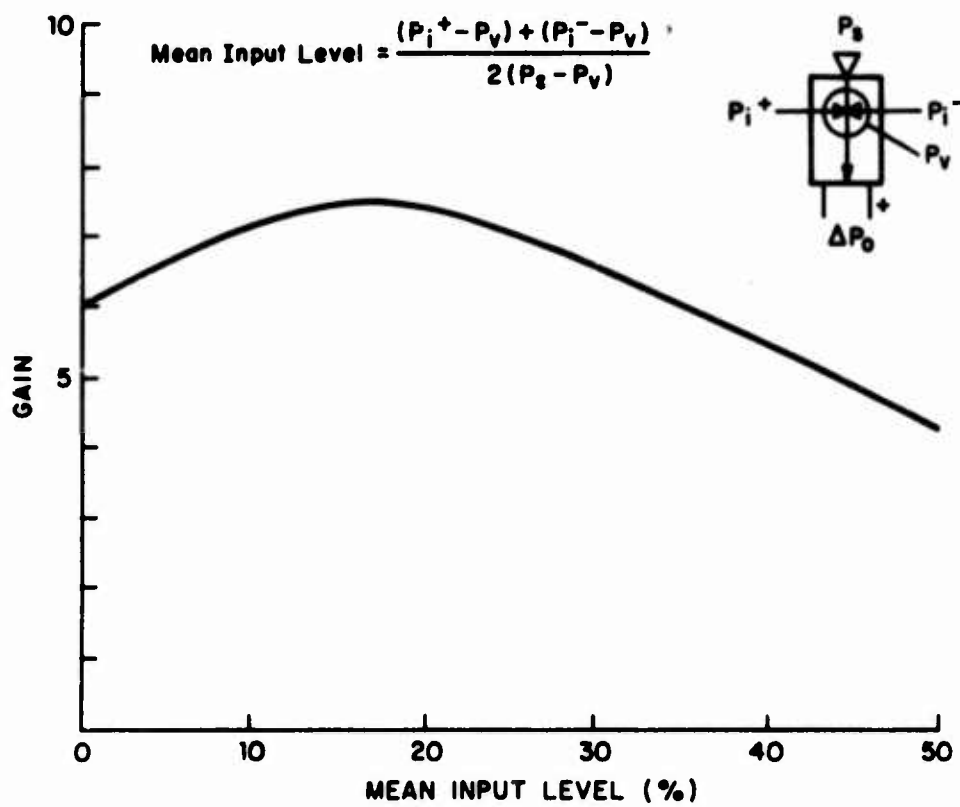


Figure 1. Gain Sensitivity to Mean Input Level (Typical Characteristics)

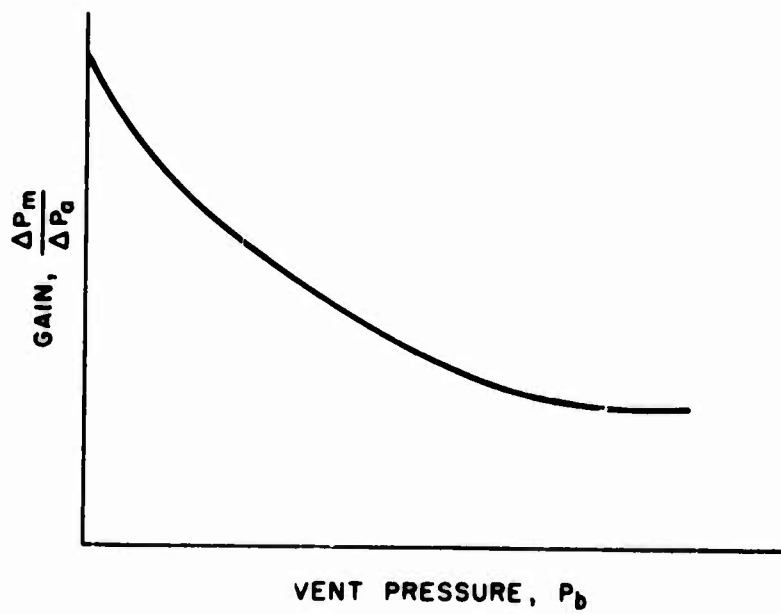
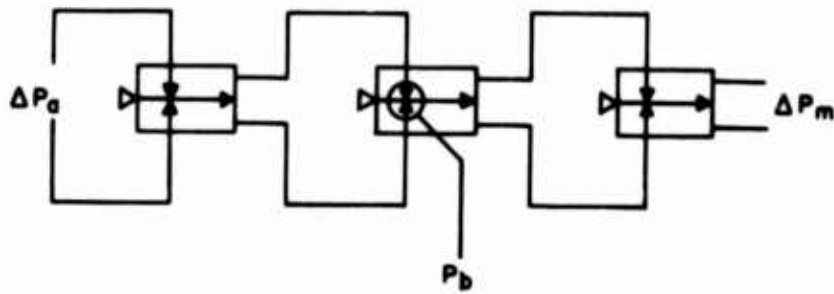


Figure 2. Mean Input Level Sensitive Gain Changing Circuit [3]

Multiplication is easier in devices using moving parts. One approach to accurate multiplication is the pin amplifier [4]. In this device, the differential output pressure is a function of the supply pressure and the position of a pin located in the interaction region as shown in figure 3. Bellows can be used to convert pressure to position as shown. Another approach is a flapper-nozzle or similar variable attenuation arrangement. Both of the above mentioned methods are useful as multipliers as well as gain changers.

2.2 Circuitry to Perform Multiplication

The quarter-square multiplier is one of the most commonly used multipliers in electrical circuits and can be used in fluidics. The principle is based on the identity $AB = \frac{1}{4} [(A+B)^2 - (A-B)^2]$. As shown in figure 4, the steps involved in evaluating the right side of the equation, summing, differencing, squaring, and scaling functions, are within the realm of present fluidics [5]. Hence, the multiplier is workable, but complex and lacking in linear range.

By providing flow sources to the inputs of a planar fluid amplifier whose input resistance is a function of the supply pressure, one can make the gain sensitive to the ratio of the amplifier supply pressure and the mean input level (fig. 5). In this circuit arrangement, a gain change of 2.5-to-1 is reported [6]. This would appear to be one of the most straightforward approaches to gain change using conventional devices.

A dual-differencing amplifier circuit is described in which the offset on nonlinear transfer curves determines the circuit gain (fig. 6) [7,8,9]. This circuit can reduce gain to zero in an inverse manner; it is suspected, however, that the linearity and range are lacking.

A digital multiplier can be implemented using a bistable amplifier with pulse-width, pulse-height modulation. A triangular waveform is fed into one control and a variable bias level is fed into the other. The width of each output pulse is thereby proportional to the control bias signal and the amplitude is proportional to the supply-pressure signal as seen in figure 7. The output pulse is filtered to give a constant output signal that is proportional to the product of pulse width and pulse height. Frequency-response problems, nonlinearities introduced by amplifier hysteresis, and small linear operating range in both channels limit its applicability.

Another method has been disclosed in a US Patent [10]; however, we were unable to get the circuit to perform.

2.3 Three-Dimensional Devices

After trying planar devices and computation circuitry, the next step is to try three-dimensional effects. One approach is a two-axis, four-receiver amplifier [6] as shown in figure 8. This device can operate as a gain changer as well as a four-quadrant multiplier. As depicted [6],

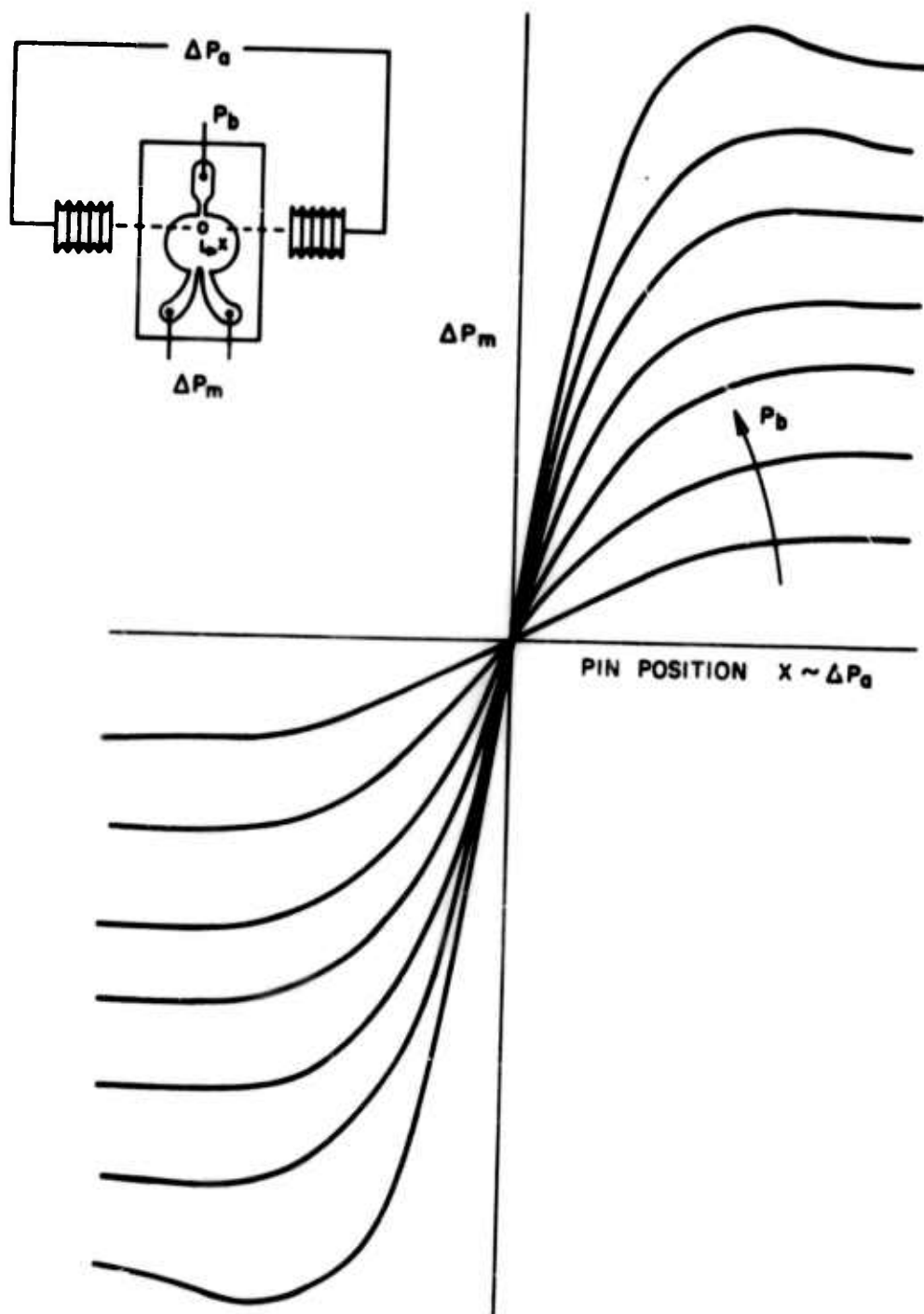


Figure 3. Mechanical Input Pin Amplifier Multiplier (Typical Characteristics)

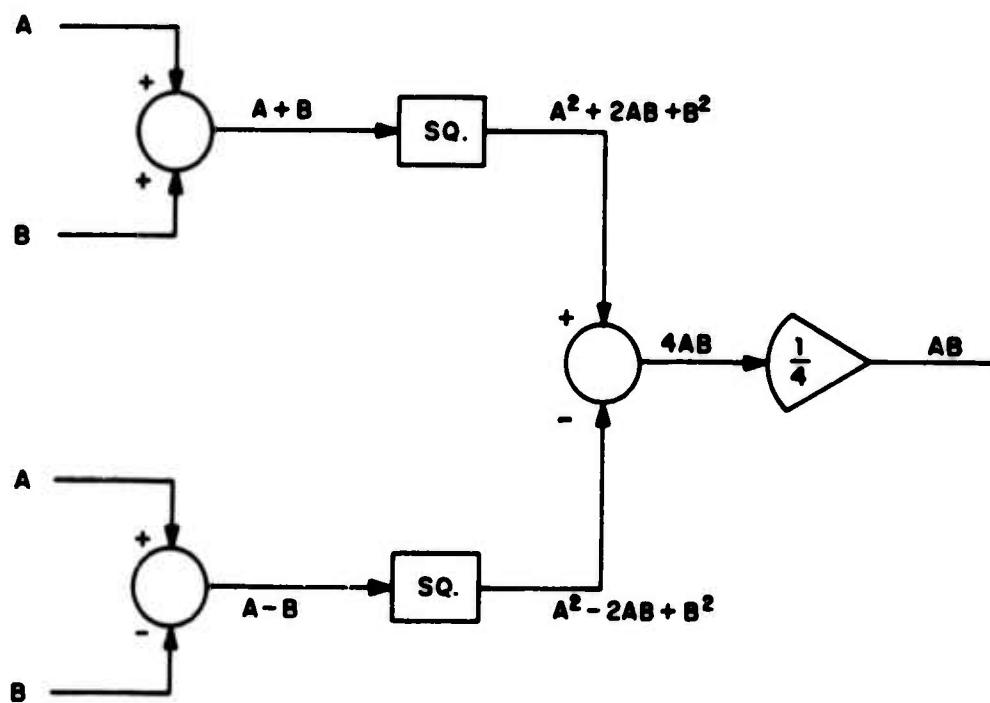


Figure 4. Quarter-Square Multiplier Circuit

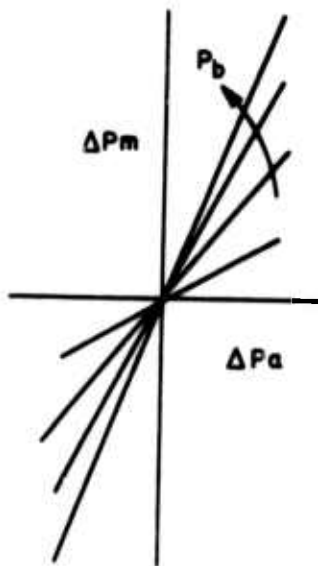
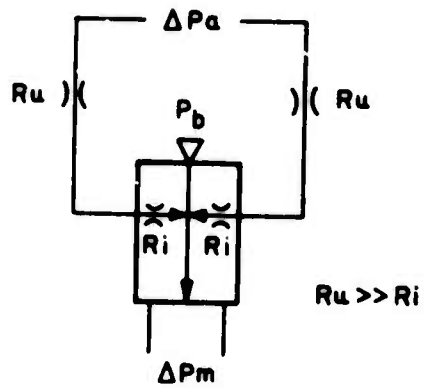


Figure 5. Flow-Driven Amplifier Gain Changer [6]

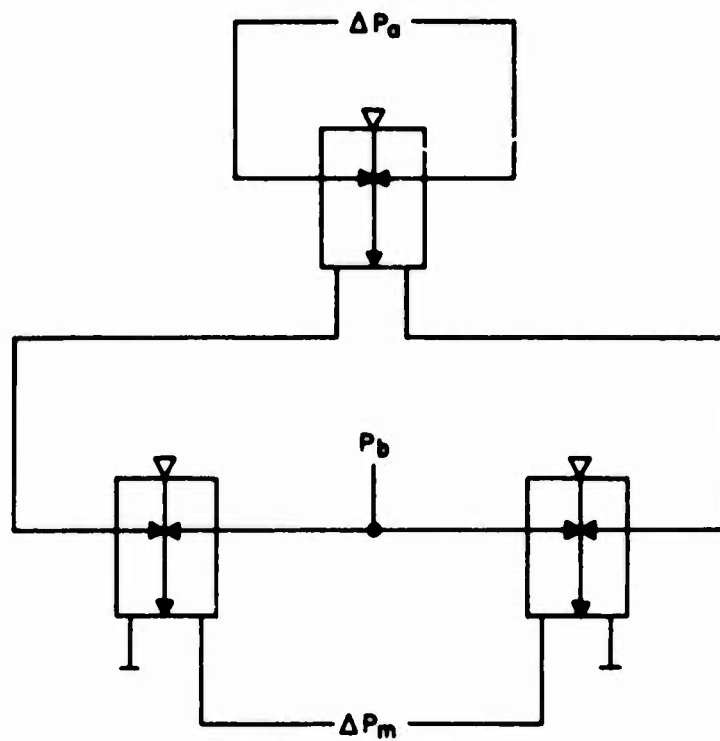


Figure 6. Dual-Differencing Multiplier Circuit [9]

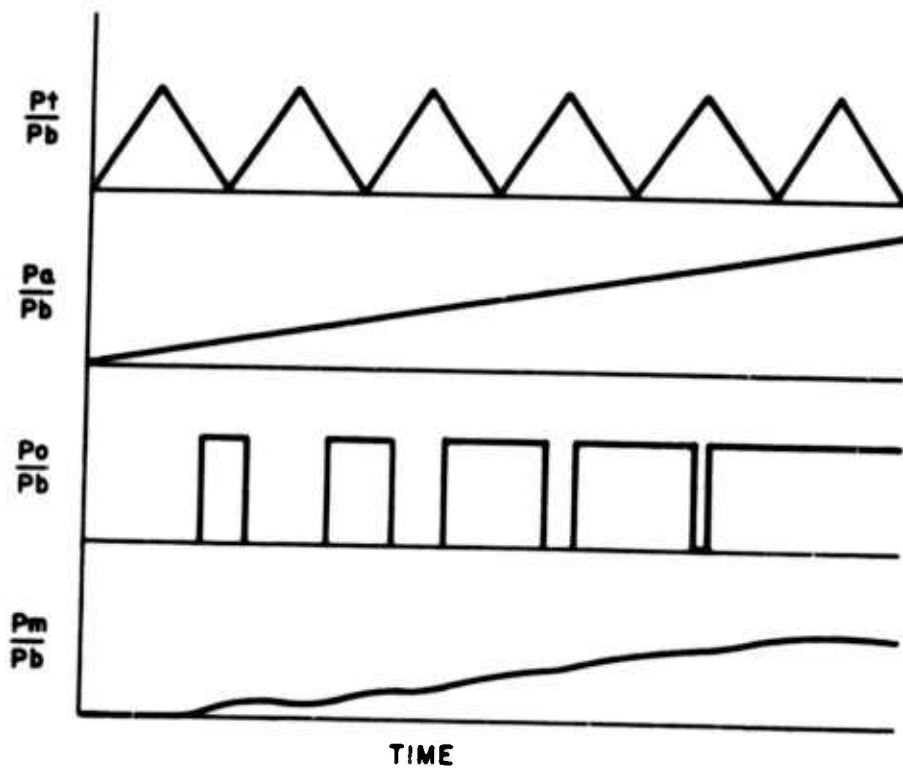
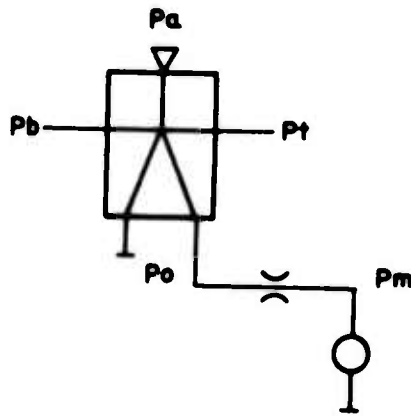


Figure 7. Digital Multiplier (Typical Responses)

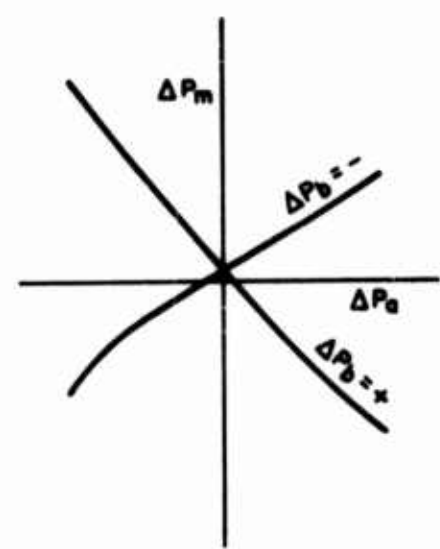
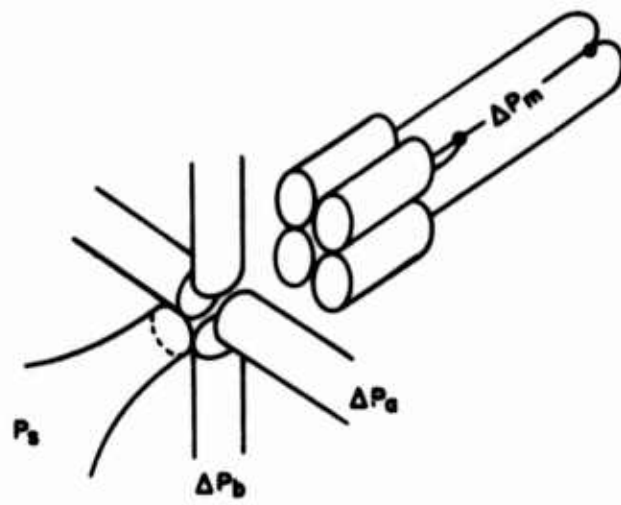


Figure 3. Two-Axis, Four-Receiver Multiplier [6]

the device uses round jets in an unconfined interaction region; this arrangement was found to have difficulties in the early days of fluidics.

Another three-dimensional device uses a control input in the third axis to deflect the power jet out of the plane of the device through a vent [11]. Still another three-dimensional device has an input normal to the amplifier geometry to alter the power jet profile in the confined interaction region and thereby change gain [11]. Gain changes of about 10-to-1 are possible; however, again the gain change is nonlinear and is in inverse proportion to the second input. All of the details were not worked out, but the device shows promise.

3. LAMINAR MULTIPLIER CONCEPT

Up to this point we have discussed some of the previous work on fluidic multiplication using turbulent flow amplifiers. We now introduce a new multiplication concept based on the Reynolds-number dependency of laminar flow amplifiers.

3.1 Amplifier Characteristics

A generally undesirable characteristic of an amplifier when operated in the laminar regime is its gain dependence upon supply pressure as shown by figure 9; however, it is this dependence that allows a laminar amplifier to be used as a gain changer or multiplier. It can be seen in figure 9 that from the transfer characteristic

$$\Delta P_o = G \Delta P_i, \quad (1)$$

and the gain-supply pressure characteristic

$$G = K P_s, \quad (2)$$

the output signal is the product of the input signal, ΔP_i , and the supply pressure, i.e.,

$$\Delta P_o = K P_s \Delta P_i. \quad (3)$$

The primary input, signal A, is the input signal to the amplifier; and the secondary input, signal B, is the amplifier supply pressure. The transfer gain can be changed almost linearly from zero to a maximum value with increasing supply pressure; thus, the device is useful as a multiplier as well as a gain changer.

3.2 Isolated Multiplier Performance

Several amplifiers were tested for linearity and range of gain change with supply pressure. The overall best configuration was a centered commercial amplifier with a power nozzle width of 0.5 mm (0.020 in.) and an aspect ratio of 0.5. The transfer characteristics for various supply pressures are given in figure 10. The linearity, low noise, and consistency of the data should be noted.

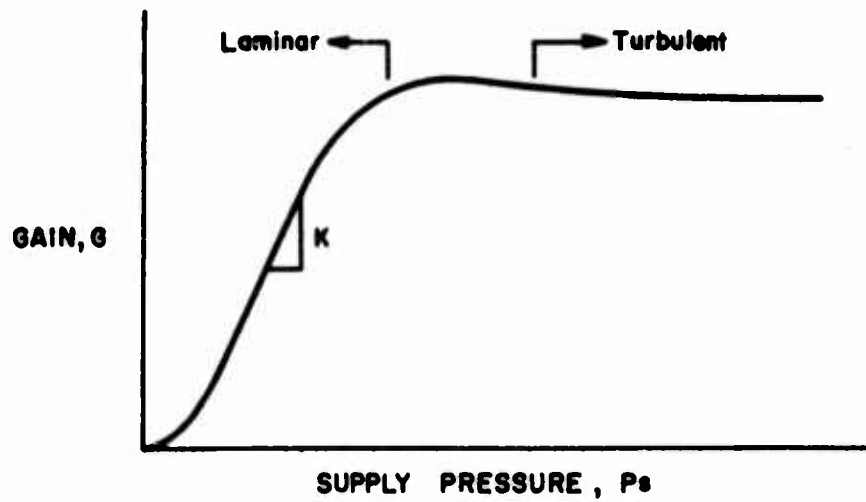
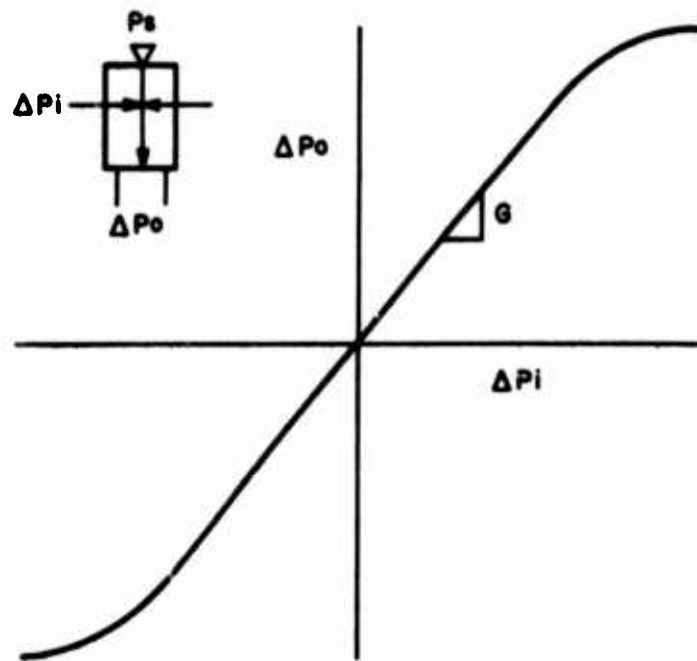


Figure 9. Gain versus Supply Pressure for a Proportional Amplifier (Typical).

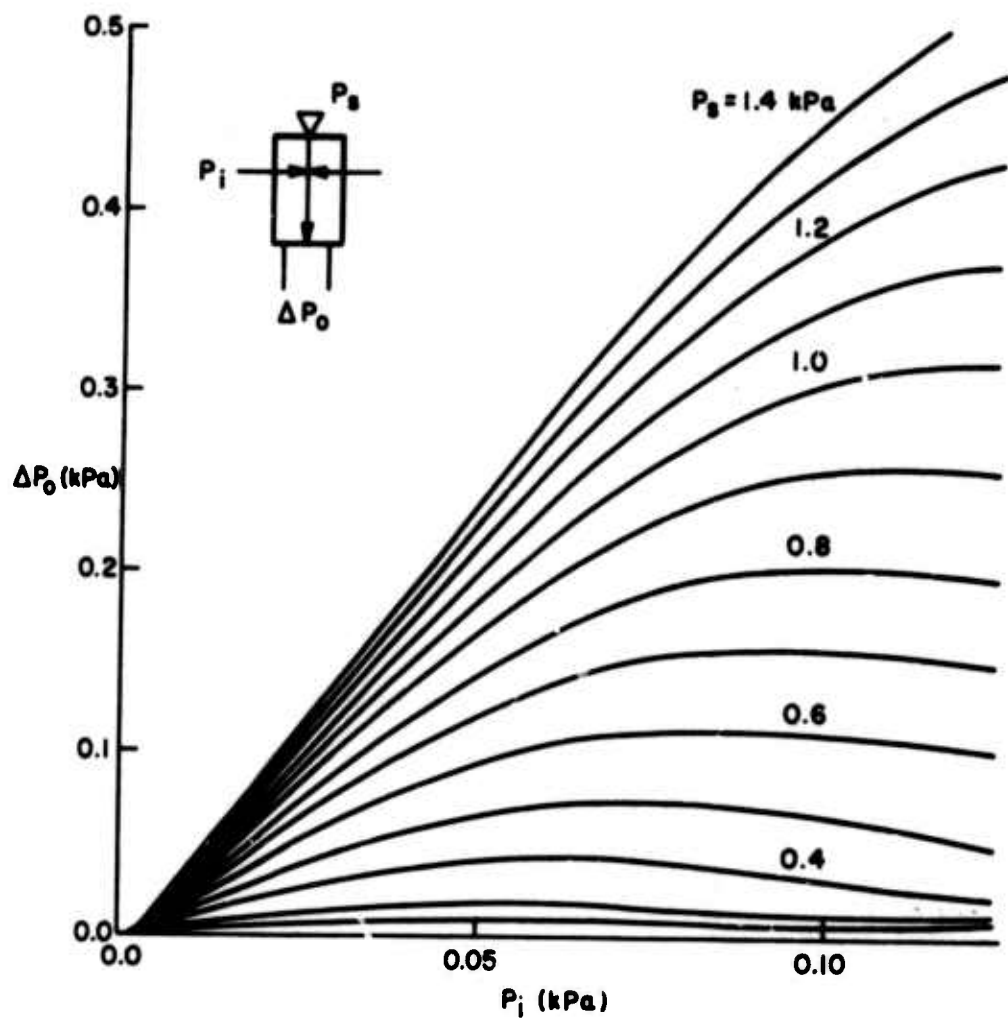


Figure 10. Isolated Multiplier Characteristics (Experimental)

The small-signal gain of this device is plotted against supply pressure in figure 11. This curve can best be characterized by a straight line with a slight offset. The points at which the curve deviates more than ± 10 percent from a straight line with offset are designated P_{smin} and P_{smax} .

If precise computation is not required, the device serves well as a multiplier or as an excellent gain changer with no further modifications. It is possible, however, to enhance this linearity and performance as discussed in the following sections.

4. UTILIZATION CIRCUITRY

There are three conditions that must be matched for optimum operation of this multiplier: (1) the gain-versus- P_s curve should be offset to allow the gain curve to pass through zero; (2) the mean input level to the multiplier should be carefully staged to avoid unexpected gain degradation of the multiplier; and similarly, (3) the mean output level of the multiplier (which would vary with supply pressure) should be held constant to avoid level sensitivity problems in the next stage. In addition, the input and output signal levels should be consistent with the fluidic circuitry in which the multiplier will be used. The circuit discussed below accomplishes these goals.

4.1 Preconditioning and Buffering

The primary problem to be solved is the offsetting of the supply pressure to the multiplier. This can be accomplished by using a biased fluid amplifier with single-sided transfer characteristics as that shown in figure 12. The amplifier supply pressure is selected so that P_{ob} at saturation is slightly greater than P_{smax} ; and the input bias is selected so that P_{ob} equals P_{smin} at null input signal, P_b . In this manner, the supply pressure to the multiplier ranges from P_{smin} to P_{smax} as the input signal P_b varies from zero, thereby allowing the gain to be linearized with respect to P_b .

A second preconditioning amplifier is required to provide a predictable, low mean input level to the multiplier in order to isolate the multiplier from an arbitrary driving signal. This is accomplished with an amplifier operating with the same supply pressure as the B-channel pre-driver and with a large attenuation of the output signal to match signal levels to the multiplier (A-channel pre-driver capable of almost saturating the multiplier with maximum B-channel signal).

Finally, the multiplier output is buffered from any other circuitry as shown in figure 13. Since the supply pressure to the multiplier varies, the mean output level of the multiplier varies. This variation in mean output level could affect the gain of a succeeding stage if proper attention is not paid to staging. The buffer-amplifier supply pressure and power nozzle should be selected so that the maximum output signal from the multiplier is below saturation of the buffer amplifier to

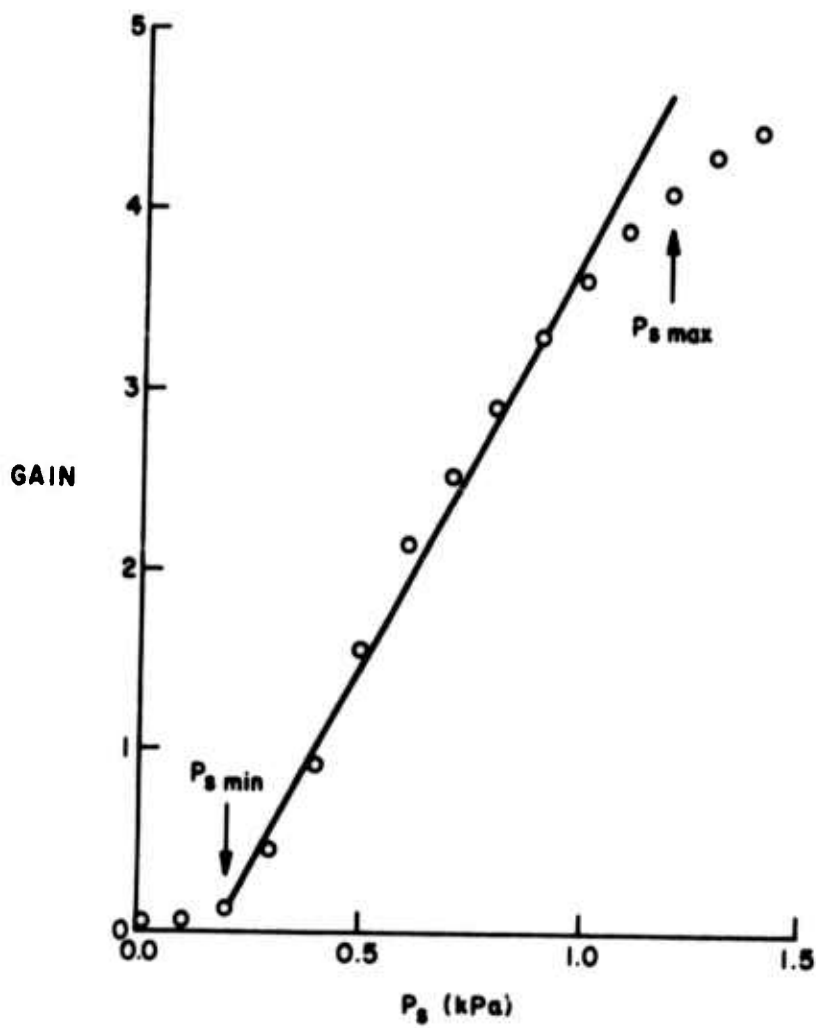


Figure 11. Gain versus Supply Pressure for Isolated Multiplier (Experimental)

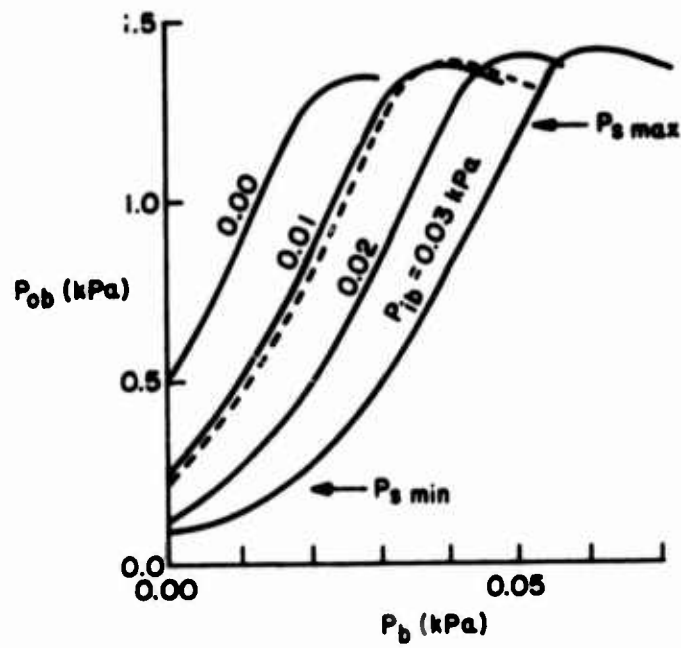
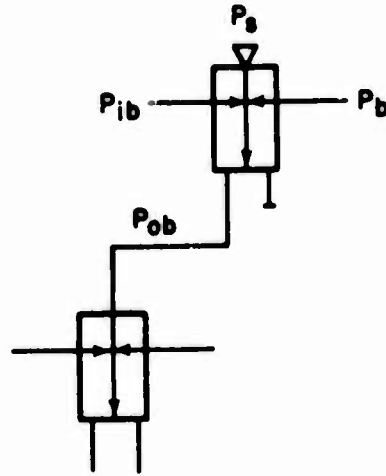


Figure 12. Pressure Offset Using Preconditioning Amplifier (Experimental)

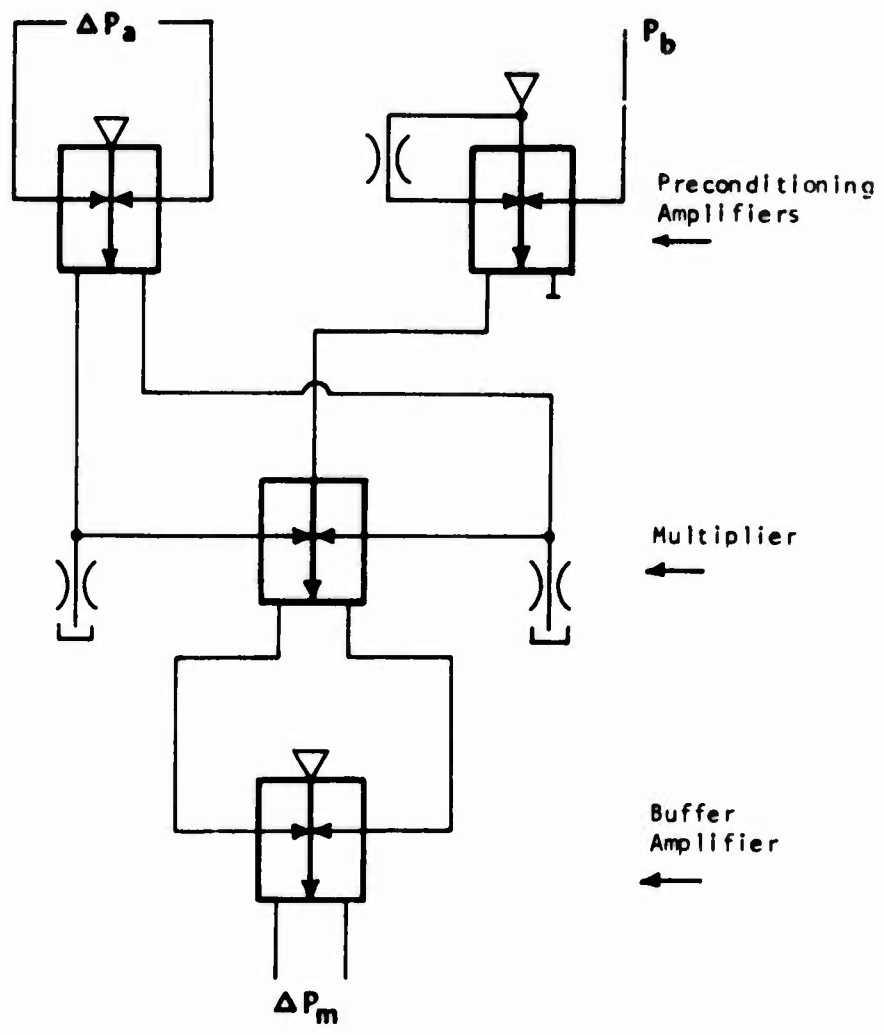


Figure 13. Laminar Multiplier Circuit with Pre-Conditioning and Output Buffering

provide a low mean input level. The mean output level of the buffer will thus be constant, and normal staging techniques can be used to other circuitry.

4.2 Circuit Performance

The circuit of figure 13 has been connected in the laboratory using amplifiers of 0.5-mm (0.020 in.) power nozzle width with an aspect ratio of 0.5. The supply pressures, bias offset, and attenuation were selected as discussed above.

The transfer characteristics of the circuit for both input channels are shown in figure 14. This circuit can be used as a true multiplier, since the circuit has zero gain with zero input in both channels, and gain increases linearly with both inputs as shown by figure 15.

Figure 15 shows the performance of the device. The input range* of the A-channel (amplifier inputs) is greater than 50:1 and the B-channel (power supply) range is 20:1. All amplifiers are operated with laminar flow, so that signal noise is several hundred below the maximum signals. There are no "jumps" that commonly occur in similar circuits.

There are some possible drawbacks to this circuit in that (1) the signals are of low pressure in order to operate in the laminar-flow regime (smaller devices could use higher pressures); (2) being laminar, the circuit is sensitive to temperature; and (3) tuning of the bias offset may be required to maintain the high performance stated above in the B-channel.

5. SUMMARY

Previously used methods of fluidic multiplication have been reviewed. These methods have drawbacks which include component nonlinearities, input signal inversion and limited functional range. A new method, based on laminar-flow amplifiers, has been presented. It shows promise in that a true multiplication with a functional range of 20 to 1 is accomplished without signal inversions.

However, the operating signal pressures are low to operate in laminar-flow regime, and this operating regime is temperature sensitive. These areas can be improved with more research. An additional refinement needed in the circuit is in the method of maintaining exact offset bias during system flow changes.

6. ACKNOWLEDGEMENTS

The author wishes to thank Mr. Halbert D. Baden, formerly with Fluidics Systems Research Branch, Harry Diamond Labs, for his critical role in the experimental development of this circuit.

*Range is defined as the ratio of maximum signal to minimum signal in which there is less than 10 percent deviation from the linear approximation.

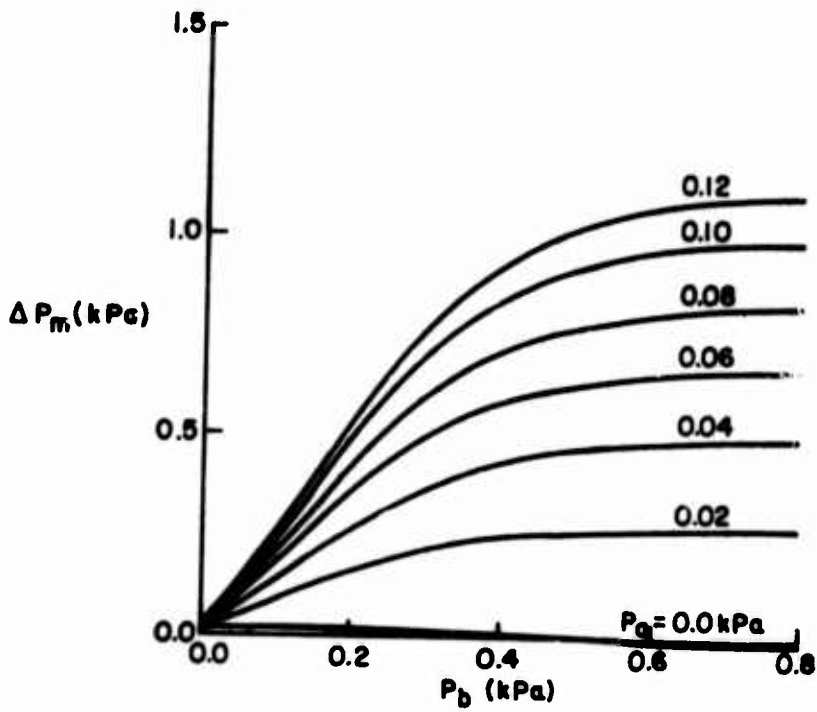
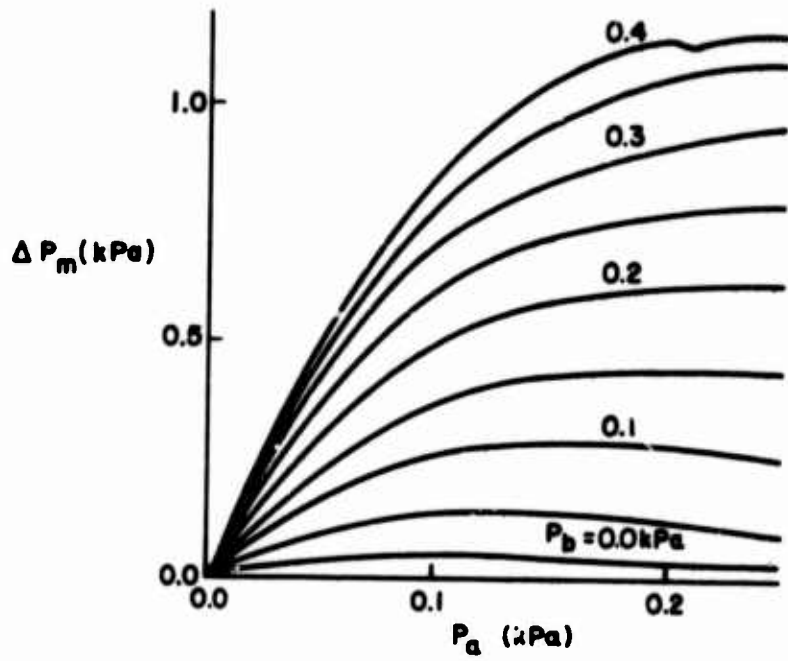


Figure 14. Laminar Multiplier Circuit Transfer Characteristics (Experimental)

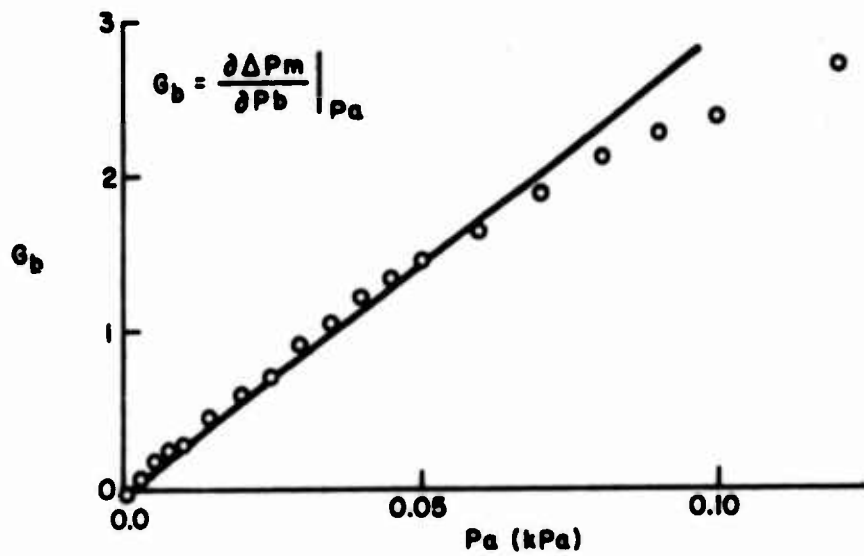
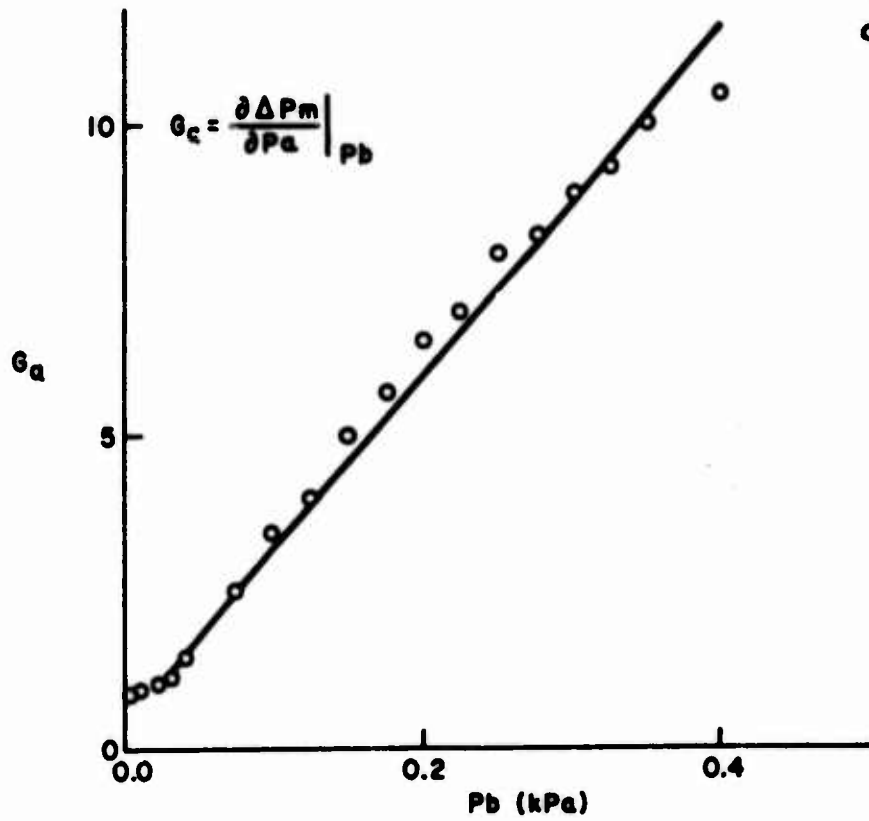


Figure 15. Gain Characteristics of Multiplier Circuit

7. LITERATURE CITED

1. Van Tilburg, R. W. and Cochran, W. L., "Development of a Proportional Fluid Amplifier For Multistage Operation," Proc. of the Fluid Amplification Symposium, Vol. II, pp 313, Harry Diamond Labs, May 1964.
2. Van Tilburg, R. W. et al, "Fluerics 21. Optical Fabrication of Fluid Amplifiers and Circuits," Harry Diamond Labs, May 1966.
3. Beduhn, W. G., "An Automatic Flueric Gain Changer Circuit for Flight Control Systems," Advances In Fluidics, pp 415-425, ASME, New York, 1967.
4. Harvey, W. T. and Merritt, J. W., "Electro-fluidic Transducer," US Patent No. 3,638,671, 1 Feb 72.
5. Haspert, J. K., "Flueric Squaring Circuit," US Patent No. 3,495,774, 17 Feb 70.
6. Ringwall, C. G., "Fluidic Processing of Alternating Pressure Signals," ASME Paper No. 67-WA/FE-43, November 1967.
7. Rainer, C. W., "Fluid Circuit," US Patent No. 3,499,460, 10 Mar 70.
8. Hoglund, M. J., "Fluid Circuit," US Patent No. 3,530,870, 29 Sep 70.
9. Hoglund, M. J., "Proportional Fluidic Gain Changer," US Patent No. 3,687,150, 29 Aug 72.
10. Urbanosky, J. F., "Flueric Multiplier," US Patent No. 3,556,121, 19 Jan 71.
11. Neradka, V. F. and Turek, R. F., "Flueric Variable Gain Component Feasibility Study," Final Report to NAVAIR under contract No. N00019-68-C-0317, by Bowles Engr. Co., January 1969.
12. Chapin, Donald W., "Fluidic Multiplier," US Patent No. 3,537,466, 03 Nov 70.

**FLUIDIC IMPEDANCE MEASUREMENT
WITH A
HALF-BRIDGE CIRCUIT**

by

**Kenji Toda
and
Silas Katz**

Submitted for Presentation at:
The Harry Diamond Laboratories
Fluidic State-of-the-Art Symposium
30 Sep - 4 Oct 1974
Adelphi, Maryland

ABSTRACT

The measurement of fluidic impedance by the half-bridge comparison method is developed theoretically and demonstrated experimentally.

The method is tested on a fluid transmission line and on a cylindrical tank whose impedances are known. The measured impedances generally agree within 10 percent of the expected values over the frequency range. However, there are some frequencies on the transmission line where discrepancies of up to 35 percent are observed.

Measurements of the input impedance of a typical laminar proportional amplifier show that it is predominantly resistive up to 100 Hz.

NOMENCLATURE

- A - cross-sectional area, m^2
- C_1 - capacitance of volume between known and unknown impedances, m^5/kN
- C_2 - capacitance of transducer holes, m^5/kN
- d - diameter, m
- f - frequency, Hz
- f_v - viscous characteristic frequency, Hz
- j - complex operator, $\sqrt{-1}$
- J_0 - Bessel function of zero order
- J_1 - Bessel function of first order
- ℓ - length, m
- L_2 - inertance of transducer hole, $kN - s^2/m^5$
- n - number of tubes in parallel
- N_p - Prandtl number
- p - pressure at input measuring station, kN/m^2
- p_i - input pressure in line, kN/m^2
- p_x - pressure at output measuring station, kN/m^2
- p_o - output pressure in line, kN/m^2
- Δp - pressure drop, kN/m^2
- q - volume flow, m^3/s
- R - real part of known series impedance, $kN \cdot s/m^5$
- R_x - real part of unknown impedance, $kN \cdot s/m^5$
- R_2 - resistance of transducer hole, $kN \cdot s/m^5$
- S - sensitivity
- T_1, T_2 - transducer scale factors, $kN/m^2 \cdot V$
- V_1, V_2 - transducer readings (forward), V
- V_3, V_4 - transducer readings (reverse), V
- X - imaginary part of known series impedance, $kN \cdot s/m^5$
- X_x - imaginary part of unknown impedance, $kN \cdot s/m^5$
- Y - shunt admittance, $m^5/kN \cdot s$
- Z - known series impedance, $kN \cdot s/m^5$
- Z_c - correction impedance, $kN \cdot s/m^5$
- Z_g - general impedance, $kN \cdot s/m^5$
- Z_n - magnitude of impedance, $kN \cdot s/m^5$
- Z_{oo} - input impedance of open line, $kN \cdot s/m^5$
- Z_{oc} - input impedance of blocked line, $kN \cdot s/m^5$
- Z_x - unknown impedance (uncorrected), $kN \cdot s/m^5$
- Z_{xc} - unknown impedance (corrected), $kN \cdot s/m^5$

- Z_T - impedance of tank, $\text{kN}\cdot\text{s}/\text{m}^5$
- β - compressibility, kN/m^2
- γ - ratio of specific heats
- ϵ - fractional error,
- ν - kinematic viscosity, m^2/s
- ρ - density, kg/m^3
- ϕ_F - phase reading (forward), radians
- ϕ_R - phase reading (reverse), radians
- ϕ - average phase, radians

1. INTRODUCTION

A knowledge of the impedances of passive and active fluidic components is essential to the rational design of fluidic circuits. For the small amplitude pressure and flow signals that often occur in fluidic circuits, we define fluidic impedance here, in accordance with the MIL-STD-1306A [1], as the ratio of the pressure drop, Δp , across a component to the volume flow, q , through the component. Thus, the general impedance, Z_g , may be expressed as

$$Z_g = \Delta p/q$$

This definition agrees also with the ASA standard acoustic impedance [2].

Now, despite their importance, fluidic impedance measurements are made infrequently. There are two reasons for this:

- 1) The impedance can frequently be calculated quite accurately, and
- 2) The impedance is difficult to measure directly because of the need for dynamic flow measurements.

However, impedance measurements have been made for fluidic amplifiers, where the theoretical impedance formulation is somewhat uncertain. Brown [3] measured the input and output impedances of a proportional fluid amplifier. A hot wire was employed for the dynamic flow measurement. Madsen [4] described the application of the hot wire in fluidic components. Both of these investigations show that the use of the hot wire technique is inconvenient. Another method, the half-bridge circuit, was employed by Brown, Boparai, and Sheikh [5] to determine the input impedance of a proportional, fluid amplifier. The half-bridge circuit, which we consider in greater detail in this paper, is basically a known and unknown impedance in series. Brown, et al. [5] selected very small bore tubing for the known impedance. In this way, they were assured of an essentially resistive component throughout the frequency range of interest.

While information and examples of the measurements of fluidic impedance is rather sparse, many different methods have been devised for the measurement of acoustic impedance. Actually, the acoustic methods may be separated into three types:

1. Direct Method

In this method pressure and flow are measured directly. One way to measure flow, the hot wire, has already been mentioned. In another embodiment of the direct method, the signal driver to the impedance is a piston in a cylinder. The flow is determined by controlling the displacement of the piston.

2. Transmission Line Method

In this method a transmission line is placed between the signal

source and the impedance to be measured. In one arrangement a probe is moved along the transmission line to locate the maximum and minimum pressures. The ratio of the pressures and the location of the minimum relative to the unknown impedance determine its magnitude.

3. Comparison Method

This method requires a known standard impedance to compare with the unknown impedance. Bridge circuits of various types employ the comparison method.

In this paper we consider fluidic impedance measurement by the half-bridge comparison method. Although the half-bridge arrangement is not new, recent advances in fluid-line theory now make it more convenient for impedance measurement, than it was in the past.

2. HALF-BRIDGE CIRCUIT

2.1 Basic Circuit

Figure 1 shows a schematic drawing of the half-bridge circuit. The circuit consists of a known impedance and an unknown impedance in series. For the known impedance, we have selected a bundle of three capillary tubes in parallel. The reason for this choice is that the impedance of tubes can be computed quite accurately using the Nichols [6] and Brown [7] fluid line models. The capillaries are essentially resistive at frequencies far below the viscous characteristic frequency, f_v (NOTE: $f_v = 4\nu/A$ where ν is the kinematic viscosity and A is the cross-sectional area). However, for the range of frequencies of interest here (up to 1000 Hz), capillaries smaller than 0.070 mm would be required to provide a predominantly resistive component. Tubes of this size are difficult to work with and are subject to clogging. In our circuit we use 0.450 mm capillary tubes and treat them as complex impedances with resistive and reactive parts.

Now to measure the magnitude of the unknown impedance, Z_x , with this circuit we require two pressure transducers and a signal generator. The input transducer, at pressure p , is upstream of the known impedance and the output transducer at pressure p_x , is between the two impedances. If the known impedance is treated as a transmission line the half-bridge circuit pressure ratio may be expressed as

$$\frac{p_x}{p} = \frac{Z_x}{Z_x \cosh \sqrt{ZY} + \sqrt{Z/Y} \sinh \sqrt{ZY}} \quad (1)$$

where Z is the series impedance and Y is the shunt admittance of the capillaries. Quite often the shunt admittance is negligible. This would be the case for liquids at all frequencies or for gases at low

frequencies. When Y is small enough to make the propagation factor (\sqrt{ZY}) small also, equation 1 reduces to the familiar relation

$$\frac{p_x}{p} = \frac{Z_x}{Z_x + Z} \quad (2)$$

The determination of the unknown impedance requires measurements of the amplitude and phase of the pressure (p and p_x) and the calculations with either equations 1 or 2. As we shall show in section 3, the accuracy of the impedance measured by the half-bridge method depends on the relative values of the known and unknown impedances.

The main purpose of our half-bridge circuit is to find the input impedance of fluidic amplifiers that have passages of approximately 1.0 mm by 0.5 mm. We have, therefore, chosen the capillary bundle to be compatible with these dimensions. The capillary bundle consists of three tubes with an inside diameter of 0.45 mm and a length of 25.4 mm. From the theory of Nichols [6] and Brown [7], the series impedance, Z , and shunt admittance, Y , of lines in parallel is

$$Z = \frac{j[2\pi f \rho \ell / (nA)]}{2J_1[j^{3/2}(8f/f_v)^{1/2}]} \quad (3a)$$

$$1 - \frac{j^{3/2}(8f/f_v)^{1/2} J_0[j^{3/2}(8f/f_v)^{1/2}]}{2J_1[j^{3/2}(8f/f_v)^{1/2}]}$$

$$Y = j \left[\frac{2\pi f n A \ell}{\gamma B} \right] \left[1 + \frac{2(\gamma-1)J_1[j^{3/2}(8N_p f/f_v)^{1/2}]}{j^{3/2}(8N_p f/f_v)^{1/2} J_0[j^{3/2}(8N_p f/f_v)^{1/2}]} \right] \quad (3b)$$

where

- $j = \sqrt{-1}$,
- $f =$ frequency, Hz
- $\rho =$ density, kg/m^3
- $\ell =$ length of tubes, m
- $n =$ number of tubes in parallel
- $\gamma =$ ratio of specific heats
- $B =$ compressibility, kN/m^2
- $N_p =$ Prandtl number
- $J_0 =$ Bessel function of zero order
- $J_1 =$ Bessel function of first order

The capillary bundle (3 tubes, $d = 0.00045$ m, $\ell = 0.0254$ m) has a shunt admittance that has a negligible effect on the half-bridge circuit up to about 1000 Hz. The dominant part of the known component is its series impedance, Z . For convenience we may write Z and Z_x in complex form as

$$Z = R + j X \quad (4a)$$

$$Z_x = R_x + jX_x \quad (4b)$$

where R and R_x are the real parts, and X and X_x are the reactive parts of the impedances. Figures 2 and 3 show the X-R plots of the capillary bundle that were calculated from equation 3a for air and hydraulic fluid (MIL-STD 5606-B). Frequency and temperature are parameters on the plots. The solid lines represent constant temperature, and the dashed lines represent constant frequency. For example, air at 20°C and 200 Hz has $Z = (.1535 + j .1040) (10)^6 \text{ kN} \cdot \text{sec}/\text{m}^5$. Under the same conditions of temperature and frequency the hydraulic oil series impedance is $Z = (.190 + j .077) (10)^9 \text{ kN} \cdot \text{sec}/\text{m}^5$.

2.2 Actual Circuit

Figure 4 shows a lumped equivalent circuit for the actual half-bridge circuit. The difference between the actual circuit and the basic circuit is the inclusion of the effects of the transducer mounting holes and the volume between the known and unknown impedance. In the actual circuit the impedance previously designated as Z_x is the parallel combination of the corrected unknown impedance, Z_{xc} , and the correction impedance, Z_c . Thus, after Z_x is computed from equation 1 or 2 we may find the corrected unknown impedance by

$$Z_{xc} = \frac{Z_x}{1 - Z_x/Z_c} \quad (5)$$

The correction impedance, Z_c , is the parallel combination of the volume capacitance, C_1 , and the transducer well impedance. Thus,

$$Z_c = \frac{(1 - 4\pi^2 f^2 L_2 C_2) + j(2\pi f R_2 C_2)}{(-4\pi^2 f^2 R_2 C_1 C_2) + j(2\pi f [C_1 + C_2] - 8\pi^3 f^3 L_2 C_1 C_2)} \quad (6)$$

where R , L and C refer to the transducer well and are estimated from its dimensions. In general, and especially at the lower frequencies, Z_c is a very large impedance compared to Z_x .

The ratio of the actual pressures measured in the transducer wells, p_x/p , is the same as the ratio of chamber pressures, p_o/p_i . Thus, no other correction factors are required.

3. SENSITIVITY OF THE HALF-BRIDGE CIRCUIT

As previously mentioned, the unknown impedance is calculated from equations 1 or 2 and from measurements of the magnitude and phase of the pressures p and p_x . Errors in these measurements cause errors in

the calculated impedance value. The magnitude of the impedance error, however, may be more or less than the instrumentation errors and depends on the parameters of the half-bridge circuit. The purpose of this discussion is to indicate quantitatively the effects that the circuit parameters have on the impedance error. Let us begin by defining the sensitivity, S , of the half-bridge circuit as

$$S = \frac{(dZ_x)/Z_x}{d(p_x/p)/(P_x/p)} \quad (7)$$

The sensitivity defined in equation 7 represents the relation between pressure measurement changes and impedance changes. To formulate equation 7 in terms of circuit parameters, we use the simplified relation of equation 2 in conjunction with equation 4 to obtain

$$\frac{p_x}{p} = \frac{R_x + jX_x}{(R + R_x) + j(X + X_x)} \quad (8)$$

Differentiation of equation 8 by the rules of complex algebra, and using equation 4 yields the sensitivity function as

$$S = 1 + \left[\frac{RR_x + XX_x}{R^2 + X^2} \right] + j \left[\frac{RX_x - XR_x}{R^2 + X^2} \right] \quad (9)$$

In this case, the sensitivity function by itself is not easily interpreted. As a result, let us consider only the differential $dZ_x/d(p_x/p)$ which from equations 7 and 9 which we may express as

$$\frac{dZ_x}{d(p_x/p)} = S(Z_x + Z) \quad (10)$$

For purposes of this analysis, we consider only those cases in which the real and imaginary portion of the measurement error are equal in magnitude and are in phase.

Now, we designate the fractional error, ϵ , as a real number that applies equally to both the real and imaginary parts of the pressure ratio measurements. That is

$$d(p_x/p) = \epsilon(1 + j) \quad (11)$$

The substitution of equation 11 into equation 10 and subsequent normalization by $Z_n = (R_x^2 + X_x^2)^{1/2}$ leads to

$$\frac{\Delta R_x}{\epsilon Z_n} = \frac{[R + X][(R + R_x)^2 - (X + X_x)^2] - 2[R - X][R + R_x][X + X_x]}{[R^2 + X^2][R_x^2 + X_x^2]^{\frac{1}{2}}} \quad (12a)$$

$$\frac{\Delta X_x}{\epsilon Z_n} = \frac{[R - X][(R + R_x)^2 - (X + X_x)^2] + 2[R + X][R + R_x][X + X_x]}{[R^2 + X^2][R_x^2 + X_x^2]^{\frac{1}{2}}} \quad (12b)$$

Equation 12 a and b represents the fractional error in the real and imaginary parts of the unknown impedance per unit fractional error, ϵ , in the pressure ratio measurements. The fractional error ratios, $\Delta R_x/\epsilon Z_n$ and $\Delta X_x/\epsilon Z_n$, from equation 12 a and b are shown plotted versus R_x/R in figures 5 and 6 for $X/R = 0$ (low frequency) and in figures 7 and 8 for $X/R = 1$ (viscous characteristic frequency of capillaries). In all cases the reactive portion of the unknown impedance X_x/R appears as a parameter on the curves.

For the low frequencies ($X/R = 0$, figures 5 and 6), only the results for the positive values of X_x/R are given on the curves. The reason for this is that when the unknown reactive portion is negative, the real and imaginary fractional error ratios are interchanged. Thus at $X/R = 0$

$$\left[\frac{\Delta R_x}{\epsilon Z_n} \right] \frac{X_x}{R} = \left[\frac{\Delta X_x}{\epsilon Z_n} \right] \frac{-X_x}{R}$$

The fractional error ratios in both real and imaginary parts of the unknown impedance increase monotonically when R_x/R is greater than one and increasing. When R_x/R decreases from one the error ratios depend significantly on the X_x/R ratio. For $X_x/R \leq 0.20$ the error ratios increase, and for $X_x/R \geq 0.50$ the error ratios decrease. If, for example, R_x/R is always between 0.20 and 5.00, the low-frequency error ratios do not exceed 9. Under these conditions a one percent fractional error results in, at most, a 9 percent error in the real and imaginary components of the normalized unknown impedance ($\Delta R_x/Z_n$ and $\Delta X_x/Z_n$).

At the intermediate frequencies ($X/R = 1$) the fractional resistance error ratio, ($\Delta R_x/\epsilon Z_n$, Figure 7) is approximately the same as the low frequency case for R_x/R greater than one. However, for low values of

R_x/R the resistance error ratio is considerably lower than in the low-frequency regime. The fractional-reactance error ($\Delta X_x/\epsilon Z_n$, Figure 8) decreases when R_x/R is greater than two. For the lower values of R_x/R_1 the fractional error depends on the X_x/R ratio, and gets very high when X_x/R is also low. In all cases the fractional-error ratio is less than 12 if R_x/R falls in the range of 0.20 and 10.00.

4. EXPERIMENTAL PROCEDURE TO DETERMINE IMPEDANCE

4.1 Instrumentation Set-Up

Figure 9 shows a block drawing of the test arrangement. A fluidic signal generator (developed at HDL by K. Toda) has a dynamic range of approximately 60db and a frequency range up to 1000 Hz. The signal generator supplies low-level, fluid signals to the half-bridge circuit (the known impedance and test specimen in series). The pressure at each end of the known impedance is sensed by a microphone-pressure transducer and preamplifier combination. The amplitude of the output of the microphones is measured by a distortion insensitive rms voltmeter with accuracy ± 0.04 percent of reading plus 0.02 percent of full scale. The phase of the microphone outputs is measured on a gain-phase meter with an accuracy of ± 0.1 degrees. An electronic-function generator drives the fluidic signal generator and the driving frequency is measured by a frequency counter.

4.2 Test Procedure

The component, whose impedance is to be determined, is placed downstream of the known impedance. The data are then taken one frequency at a time. Thus, to begin a test, the frequency is set at the function generator and measured by the frequency counter. With the frequency fixed, the waveform of the input-pressure signal is observed on an oscilloscope. The amplitude signal from the function generator is adjusted until the waveform is reasonably sinusoidal. At this point, the voltage (V_1 and V_2) from the microphone transducers and their phase relation (ϕ_F) are recorded. The pressures at the measuring stations are

$$p = V_1 T_1 \quad (13a)$$

$$p_x = V_2 T_2 \quad (13b)$$

where T_1 and T_2 are the scale factors for the microphone transducers.

Since the scale factors of the microphones are not the same, the ratio of voltages, V_2/V_1 , is not equal to the pressure ratio, p_x/p . To

eliminate consideration of the transducer scale factors, we now reverse the position of the microphones and record voltages V_3 and V_4 and phase

ϕ_R . In this case the pressures at the measuring stations are

$$p = V_3 T_2 \quad (14a)$$

$$p_x = V_4 T_1 \quad (14b)$$

From equations 13 and 14 we may express the pressure ratio, p_x/p , in terms of the voltage readings only as

$$\frac{p_x}{p} = \left[\frac{V_4 V_2}{V_3 V_1} \right]^{1/2} \quad (15)$$

The phase value, ϕ , is taken as the average of the forward and reverse phase readings, so that

$$\phi = \frac{\phi_F + \phi_R}{2} \quad (16)$$

The process described above is repeated for each frequency desired.

4.3 Calculation Procedure

The forward and reverse test data from the microphones are used to determine p_x/p and ϕ from equations 15 and 16. The pressure ratio magnitude and phase angle are then transformed into the complex representation ($R_e [p_x/p] + jI_m [p_x/p]$) and the computation proceeds with complex variables. Equations 1 and 3 are now applied and a solution is obtained for Z_x , the uncorrected impedance of the test specimen. Finally the use of equations 5 and 6 determines the corrected values of the real and imaginary parts of the unknown impedance.

The FORTRAN listing of a program to perform the calculations described above is given in appendix A. In addition the FORTRAN program was adapted, by Arthur Hausner of HDL, to the WANG 520 language [9] so that the calculations could be performed on the WANG programmable desk calculator.

5. EXPERIMENTAL RESULTS

To check the half-bridge impedance measuring setup, experiments were performed on two configurations which had impedances that were theoretically calculable. Additional experiments were made to determine the input impedance of a laminar proportional amplifier.

Figure 10 shows the calculable configurations. The cylindrical brass test line 0.00164 m in diameter and 0.762 m long was tested open (as shown in figure 10a) and with one end blocked by a flat plate. The open

and closed input impedance of the test line, Z_{oo} and Z_{oc} are:

$$Z_{oo} = \sqrt{Z/Y} \tanh \sqrt{ZY} \quad (17a)$$

$$Z_{oc} = \sqrt{Z/Y} \coth \sqrt{ZY} \quad (17b)$$

where Z and Y are obtained from equations 3a and b using the appropriate dimensions for the test line (the diameter of the test line was confirmed by static measurements and the Hagen-Poiseuille equation).

Figure 10b shows the other calculable impedance, a cylindrical tank (0.0367 m long and 0.0238 m diameter) and entrance section (0.020 m long and 0.0032 m diameter). The impedance of the tank is calculated by inverting the admittance formulation given in equation 3b. The resistance of the short entrance section is estimated from Shapiro, Siegel and Kline [8] as $607 \text{ kN} \cdot \text{sec}^2/\text{m}^5$. Thus the impedance of the tank and entrance length combination is:

$$Z_T = 607 + \frac{1}{Y} + j[2.98](2\pi f) \quad (18)$$

where the tank dimensions must be used in equation 3b to find Y .

Figures 11 and 12 present the data taken on the test line and the theory given in equations 17a and b. In each figure the solid line is the theoretical real part and the dashed line is the theoretical imaginary part of the test line impedance. When the test line is open (Figure 11), resonances occur at about 200 and 400 Hz where the impedance is a minimum and has no imaginary part. The impedance also has no imaginary part at frequencies of about 95 Hz, 300 Hz and 500 Hz. In these cases, the impedance has a local maximum. For the closed test line (fig. 12) the pattern is reversed. Resonances occur at about 90 Hz, 300 Hz and 500 Hz, the frequencies of minimum impedance. The local maximum impedance values occur at approximately 200 and 410 Hz. The data superimposed on figures 11 and 12 show good agreement with the theoretical predictions near the resonant conditions. However, discrepancies of up to 35 percent of impedance magnitude (R_x/Z_n and X_x/Z_n) may be observed in the real part maxima and the imaginary part minima. These discrepancies exceed the expected errors developed in the sensitivity analysis. As an additional check, the data was retaken with two of the known impedance tubes blocked. This increased the upstream impedance by a factor of 3 and should have lessened the disagreement in the vicinity of the maxima and minima. Nevertheless, the results obtained with one tube in the known impedance bundle produced results that were within a few percent of those shown in figures 11 and 12. The possibility that the discrepancies might be caused by a lack of rigidity in the brass test line was eliminated when steel and tygon test lines of the same dimensions also yielded approximately the same results. Thus the reason for the discrepancies in those selective frequency regions is not clear.

Figure 13 compares the data taken on the tank-entrance length combination with the theory expressed in equation 18. In this case the agreement between data and theory is good throughout the test range. The discrepancies are always less than 10 percent.

Tests were also performed to measure the input impedance of a laminar proportional amplifier with a power nozzle width of 0.51 mm, a control nozzle width of 2.03 mm and a depth that consisted of 6 parallel 0.1 mm thick laminates. The power jet pressure was 1.0 kN/m². Throughout the tests, the steady flow in the opposite side control was adjusted to maintain equal blocked output pressures. Figure 14 shows the input impedance of the amplifier. As might be anticipated, the impedance is primarily resistive at the low frequencies. At 100 Hz the inductive reactance is only 10 percent of the resistance. This percentage increases with frequency and at 500 Hz the reactance is 88 percent of the resistance.

6. SUMMARY

Impedance measurement by the half-bridge circuit is considered in detail. The half-bridge method is a comparison method and, therefore, requires a reference impedance. A parallel array of capillary tubes was selected for the reference impedance because the Nichols Brown model for fluid transmission lines provides an accurate representation of the impedance.

A sensitivity analysis of the half-bridge circuit showed that the relative sizes of the unknown and reference impedances affects the overall accuracy of the method. For example, at low frequencies if the unknown impedance is much larger or much smaller than the reference impedance, experimental errors are magnified.

The experimental setup and measurement procedure is indicated. In addition a very general computer program is listed so that impedances can be computed from measurements on components for any size and number of tubes in the capillary-bundle reference impedance.

To test the half-bridge method, the impedance was measured on several passive components for which the impedance could also be analytically determined. These components included an open-and-closed, long-fluid line and a tank-entrance combination. The agreement between measurement and theory was within 10 percent for the tank-entrance combination and was equally good for the lines near the resonant frequencies. However, there was up to 35 percent discrepancy at intermediate frequencies where the impedance magnitudes were largest. We are unable to explain these large discrepancies.

As an example of the utility of the half-bridge method, the results of measurements of the input impedance of a laminar-proportional amplifier are given.

REFERENCES

1. ("Military Standard) Fluidics, Terminology and Symbols," MIL-STD-1306A, 08 December 1972.
2. Beranek, L. L., "Acoustic Measurements," John Wiley & Sons, 1949, pp 302-361.
3. Brown, F. T., "Stability and Response of Fluid Amplifiers and Fluidic Systems," NASA CR 72192, DSR 5169-3, (Contract NAS 3-5203) 1 Oct 67.
4. Madsen, B. B., "Hot-Wire Anemometry as a Means of Measuring Dynamic Flow Characteristics of Fluidic Components and Systems," Third Cranfield Fluidics Conference, Turin, May 1968.
5. Brown, F. T., Boparai, J. S., and Sheikh, T. M., "Design of a Near-Optimal Fluidic Operational Amplifier," Lehigh University, Technical Report Number 16, June 1973.
6. Nichols, N. B., "The Linear Properties of Pneumatic Transmission Lines," Transactions of the Instrument Society of America, Vol. 1, 1962, pp 5 - 14.
7. Brown, F. T., "The Transient Response of Fluid Lines," Journal of Basic Engineering, Transactions ASME Series D, Vol. 84, No. 4, December 1962, pp 547-553.
8. Shapiro, A. H., Siegel, R., and Kline, S. J., "Friction Factors in the Laminar Entry Region of a Smooth Tube," Proceedings of the Second US National Congress of Applied Mechanics, 1954, p 733-741.
9. Hausner, A. and H. Bloom, "Fortran IV Compiler for Wang 520 Calculator," HDL-TM-73-15, July 1973.

```

C PROGRAM TO COMPUTE IMPEDANCE FROM DATA TAKEN ON HALF-BRIDGE
C
  COMPLEX Z,Y,ZC,G,CS,CC,CT,CI,PX,ZM,ZMC,ZN,ZD,ZCO
C TRANSDUCER HOLE CORRECTION PARAMETERS
  CD=8.7881E-08
  CF=6.4351E-08
  ED=3.41
  RD=3.284E+08
C
C FOR KNOWN UPSTREAM IMPEDANCE ENTER DIAMETER OF TUBES ,D , LENGTH
C OF TUBES, EL , IN METERS , AND NUMBER OF TUBES , EN
C
  D=.00045
  EL=.0254
  EN=3.
C
C ENTER KINEMATIC VISCOSITY, V, IN SQ. M. PER SEC., DENSITY, DEN., IN KG.
C PER CUBIC M, BULK MODULUS, COMP, IN KN. PER SQ. M. AND RATIO OF
C SPECIFIC HEATS, GL
C
  V=14.86E-06
  DEN=1.2
  COMP=101.35
  GL=1.4
C
C ENTER NUMBER OF DATA POINTS, N
C
  N=74
  DO 7 I=1,N
  READ (5,4) F,PI1,PI2,PO1,PO2,PH1,PH2
C
C DATA IS READ HERE . DATA CARDS FOLLOW $DATA CARD
C AT END OF PROGRAM AND MUST HAVE FORMAT 4 .
C FREQUENCY IN CCL. 1-10 , INPUT VOLTS IN COL. 11-20 ,21-30
C OUTPUT VOLTS IN COL. 31-40 , 41-50 , PHASE DEGREES
C IN COL. 51-60 , 61-70
C
  4 FORMAT (7F10.1)
  PM=SQRT(PO1*PO2/(PI1*PI2))
  R=(PH1+PH2)/(2.*57.2958)
  PR=PM*COS(R)
  PAI=PM*SIN(R)
  PX=CMPLX(PR,PAI)
  CALL CHAMP (D,EL,V,DEN,COMP,GL,EN,F,Z,Y,ZC,G)
  CALL COHY ( G,CS,CC,CT,CI)
  ZM=PX*ZC*CS/(1.-PX*CC)
  EB=ED*DEN
  CB=CF/(COMP*GL)
  CA=CD/(COMP*GL)
  RB=RD*V
  WNR=1.-39.478*F*F*EB*CB
  WNI=6.283*F*RB*CB
  ZN=CMPLX(WNR,WNI)
  WDR=-39.478*F*F*RB*CA*CB
  WDI=6.283*F*(CA+CB)-248.05*F*F*F*EB*CA*CB
  ZD=CMPLX(WDR,WDI)
  ZCO=ZN/ZD
  ZMC=ZM/(1.-ZM/ZCO)
  WRITE (6,10) F,ZMC
10 FORMAT ( F10.1,2E15.4)

```

7 CONTINUE

STOP

END

\$IBFTC SK1

SUBROUTINE CHAMP (DIA,EL,VIS,DEN,COMP,GL,EN,FREQ,Z,Y,ZC,GAM)

COMPLEX Z,Y,ZC,GAM,C,CJ0Z,CJ1Z,CJOY,CJ1Y,DNZ,DNY

C=CMPLX(0.0,1.0)

OM=6.283185*FREQ

OMV=32.*VIS/(DIA*DIA)

AZ=SQRT(2.*OM/OMV)

AY=.84*AZ

WLA=OM*DEN*EL/(EN*785.4*DIA*DIA)

WCA=OM*EN*.7854*1/DIA*DIA*FL/(GL*COMP)

CALL BERI (AZ,0,ZR0,ZI0,1.E-10)

CALL BERI (AZ,1,ZR1,ZI1,1.E-10)

CALL BERI (AY,0,YR0,YI0,1.E-10)

CALL BERI (AY,1,YR1,YI1,1.E-10)

CJ0Z=CMPLX(ZR0,ZI0)

CJ1Z=CMPLX(ZR1,ZI1)

CJOY=CMPLX(YR0,YI0)

CJ1Y=CMPLX(YR1,YI1)

DNZ=2.*CJ1Z/(C*CSQRT(C)*AZ*CJ0Z)

Z=C*WLA/(1.-DNZ)

DNY=2.*(GL-1.)*CJ1Y/(C*CSQRT(C)*AY*CJOY)

Y=C*WCA*(1.+DNY)

ZC=CSQRT(Z/Y)

GAM=CSQRT(Z*Y)

RETURN

END

\$IBFTC SK2

SUBROUTINE COHY (GM,CSNH,CCSH,CTNH,CCTH)

COMPLEX GM,CSNH,CCSH,CTNH,CCTH

AL=REAL(GM)

BL=AIMAG(GM)

SH=SINH(AL)

CH=COSH(AL)

SN=SIN(BL)

CS=COS(BL)

XP=SH*CS

XQ=CH*SN

CSNH=CMPLX(XP,XQ)

XV=CH*CS

XW=SH*SN

CCSH=CMPLX(XV,XW)

CTNH=CSNH/CCSH

CCTH=1./CTNH

RETURN

END

\$IBFTC SK3

SUBROUTINE HERI(ARG,NU,BER,BEI,ERROR)

DOUBLE PRECISION SR,SI,S(4),C(4),X4,T,FN,FK

SI = 2.3561944901923449 * FLOAT(NU)

X4 = ARG*ARG*.25

C(1) = DCOS(SI)

S(1) = DSIN(SI)

DO 5 I = 2,4

K = I-1

C(I) = -S(K)

5 S(I) = C(K)

T = 1./GAMMA(FLOAT(NU) + 1.)

```

SR = T*C(1)
SI = T*S(1)
I = 2
DO 30 K = 1,1000
FN = K + NU
FK = K
T = ((T/FK)/FN)*X4
SR = SR + T*C(I)
SI = SI + T*S(I)
IF(T.LE.ERROR*DMIN1(DABS(SR),DABS(SI))) GO TO 35
I = I + 1
IF (I.EQ.5) I = 1
30 CONTINUE
35 IF((ARG.NE.0.). OR.(NU.NE.0)) GO TO 40
X4 = 1.
GO TO 45
40 X4 = (ARG*.5)**NU
45 BER = SR*X4
REI = SI*X4
RETURN
END

```

\$DATA

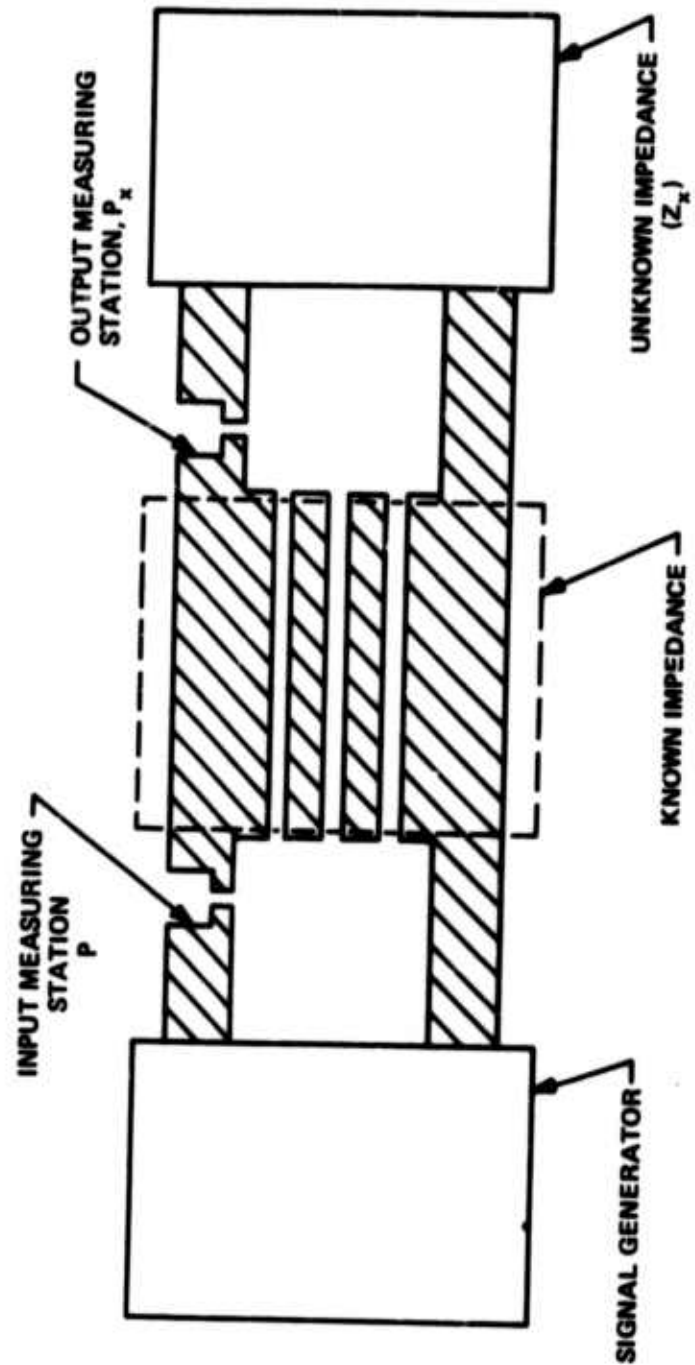


Figure 1. Schematic of Half-Bridge Circuit

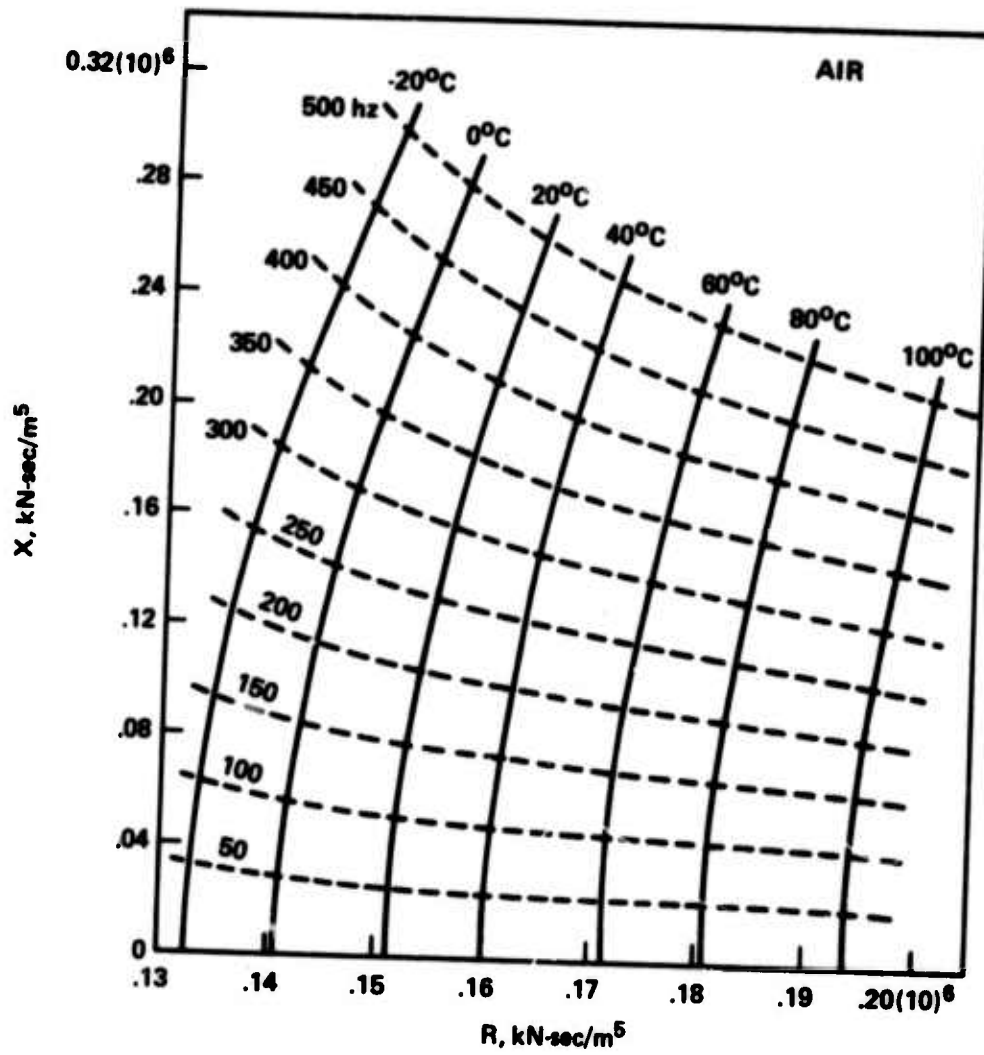


Figure 2. Capillary Impedance (Air)
 3 tubes, $d = 0.45 \text{ mm}$, $l = 25.4 \text{ mm}$

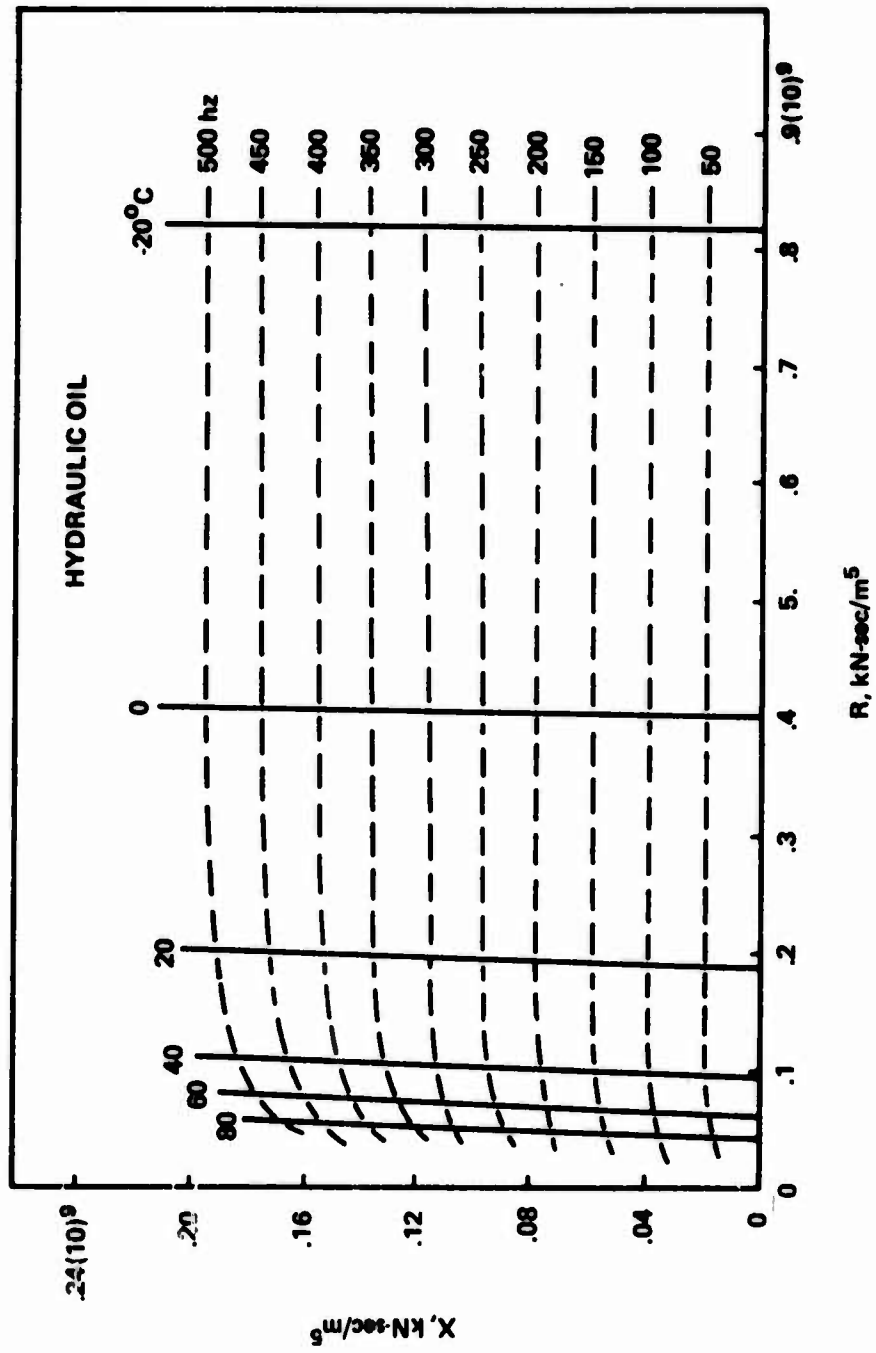


Figure 3. Capillary Impedance (Hydraulic Oil)
3 tubes, $d = 0.45$ mm, $L = 25.4$ mm

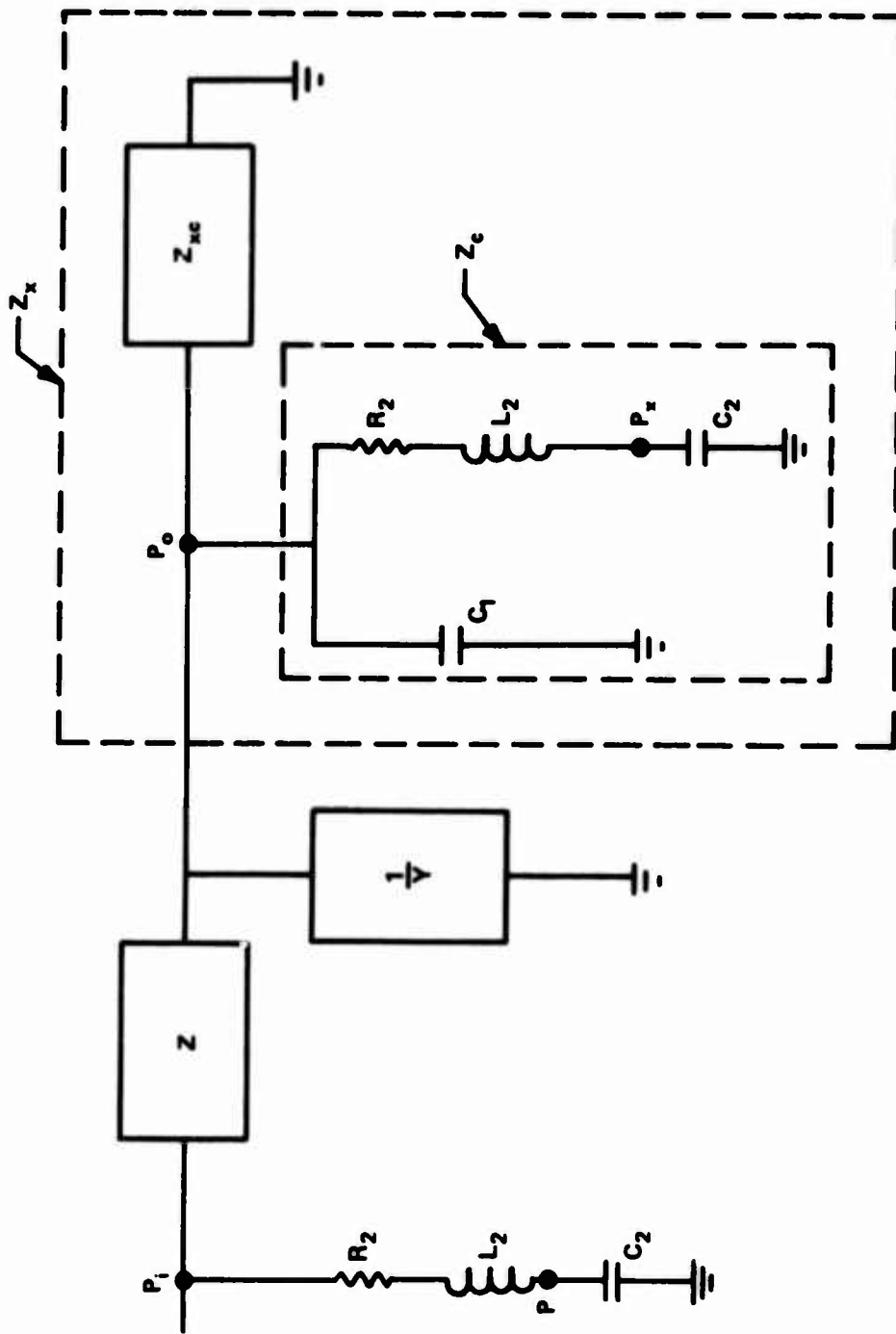


Figure 4. Lumped Equivalent Circuit for Half-Bridge

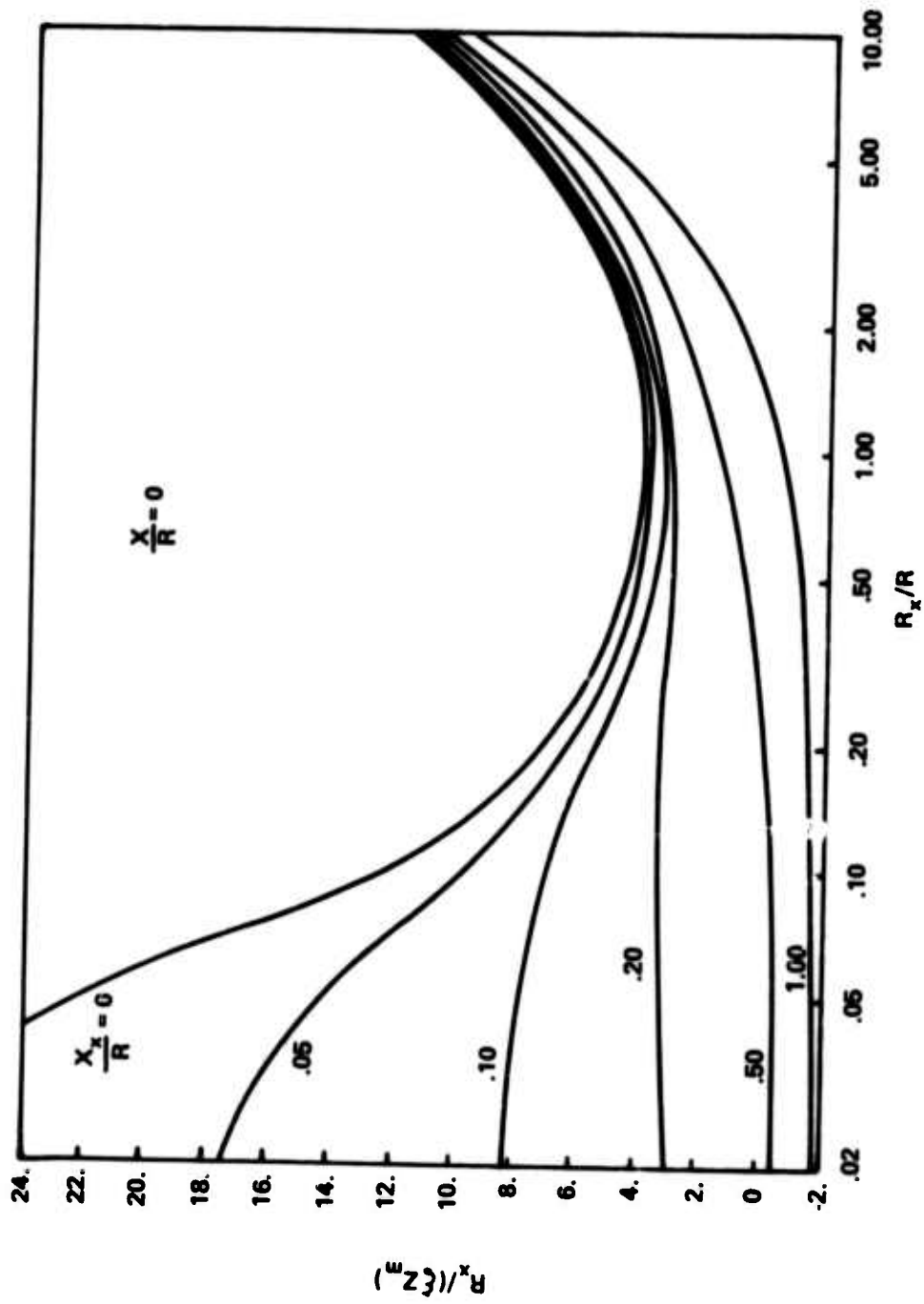


Figure 5. Fractional Error in Real Part of Unknown Impedance ($x/R = 0$)

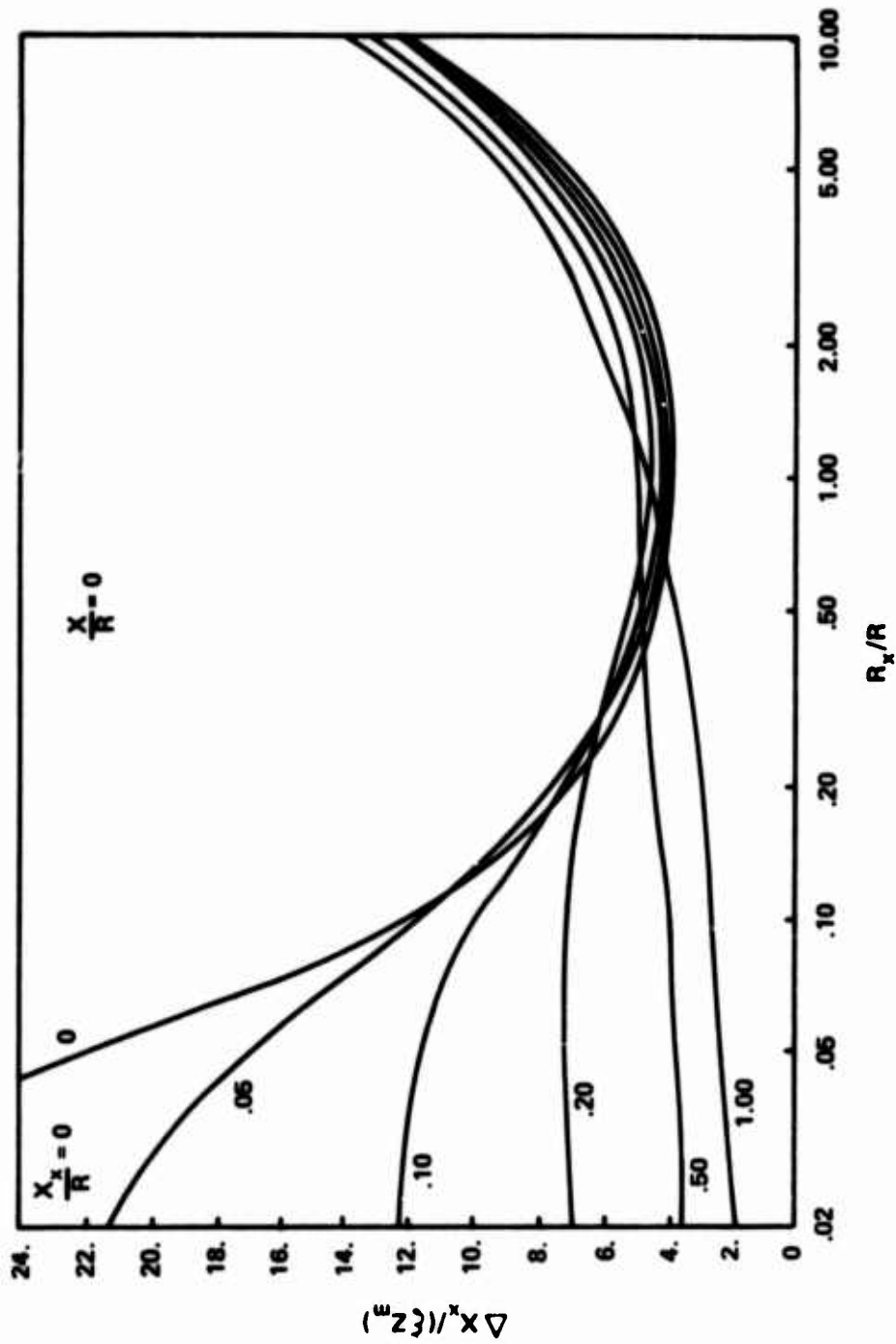


Figure 6. Fractional Error in Imaginary Part of Unknown Impedance ($x/R = 0$)

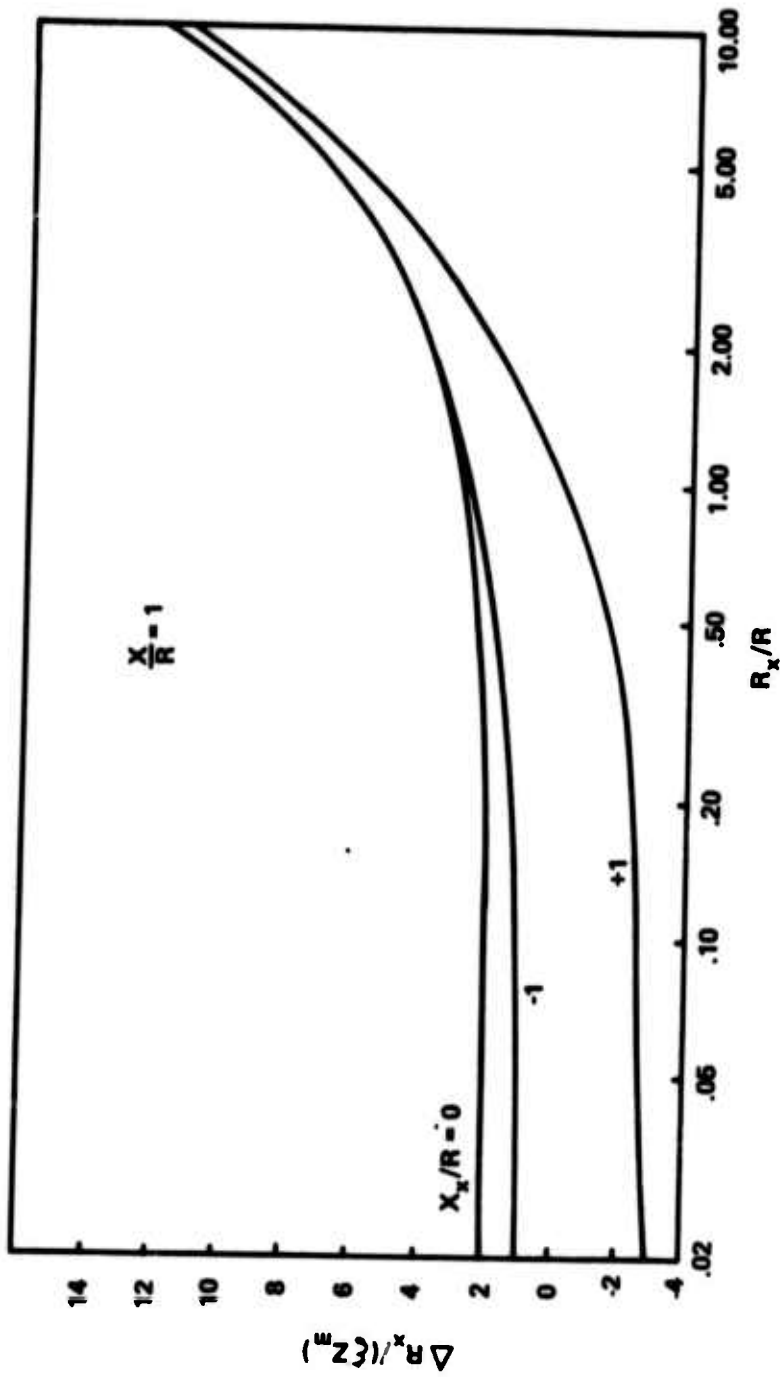


Figure 7. Fractional Error in Real Part of Unknown Impedance ($X/R = 1$)

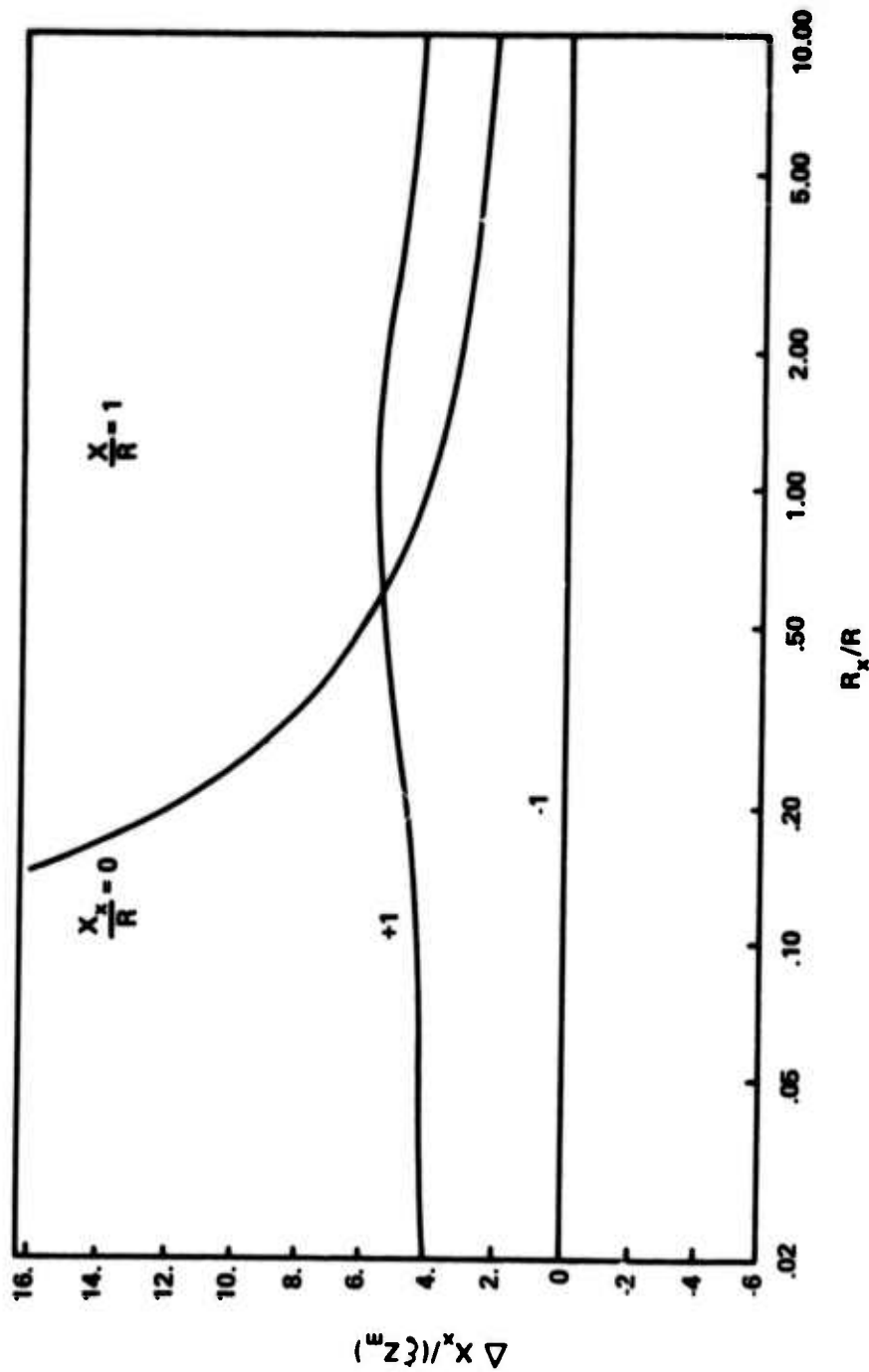


Figure 8. Fractional Error in Imaginary Part of Unknown Impedance ($x/R = 1$)

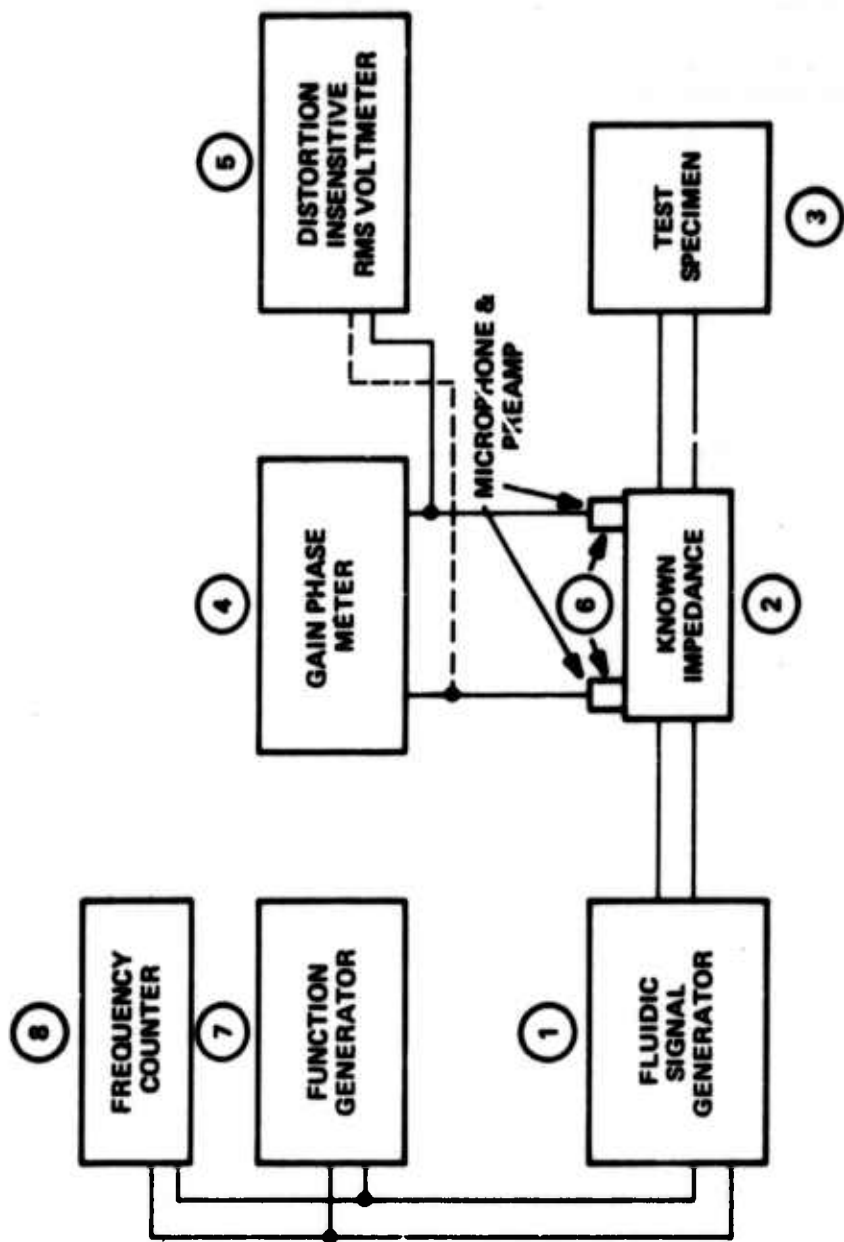


Figure 9. Test Instrumentation Setup

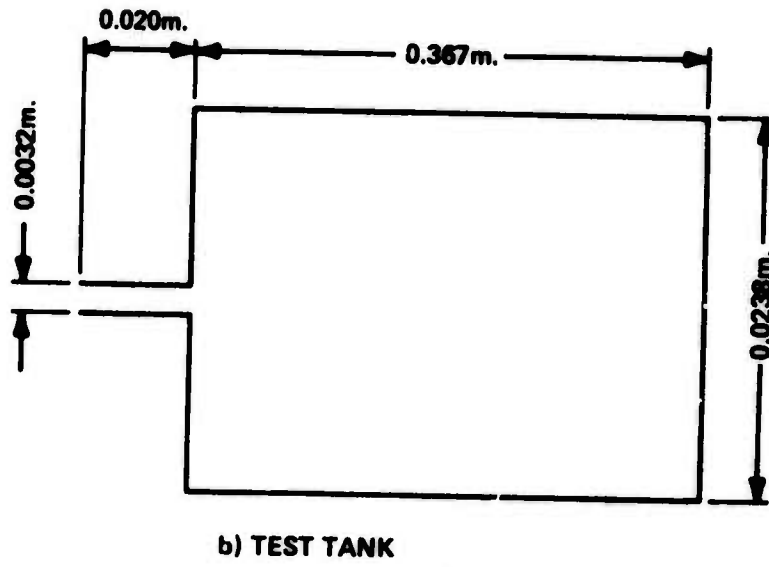
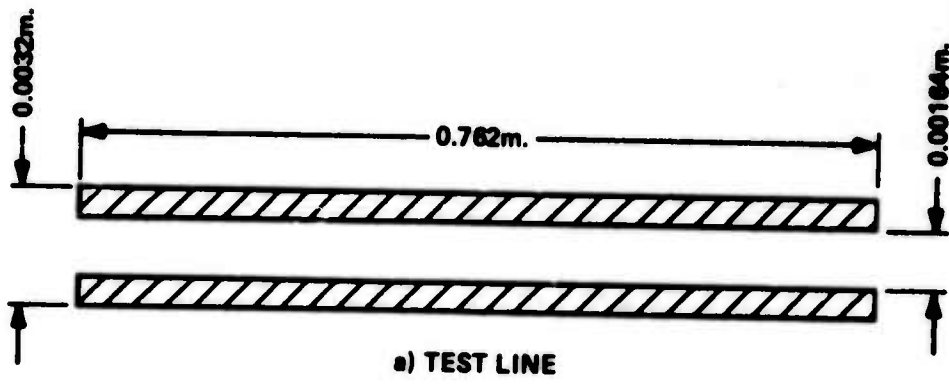


Figure 10. Calculable Impedances

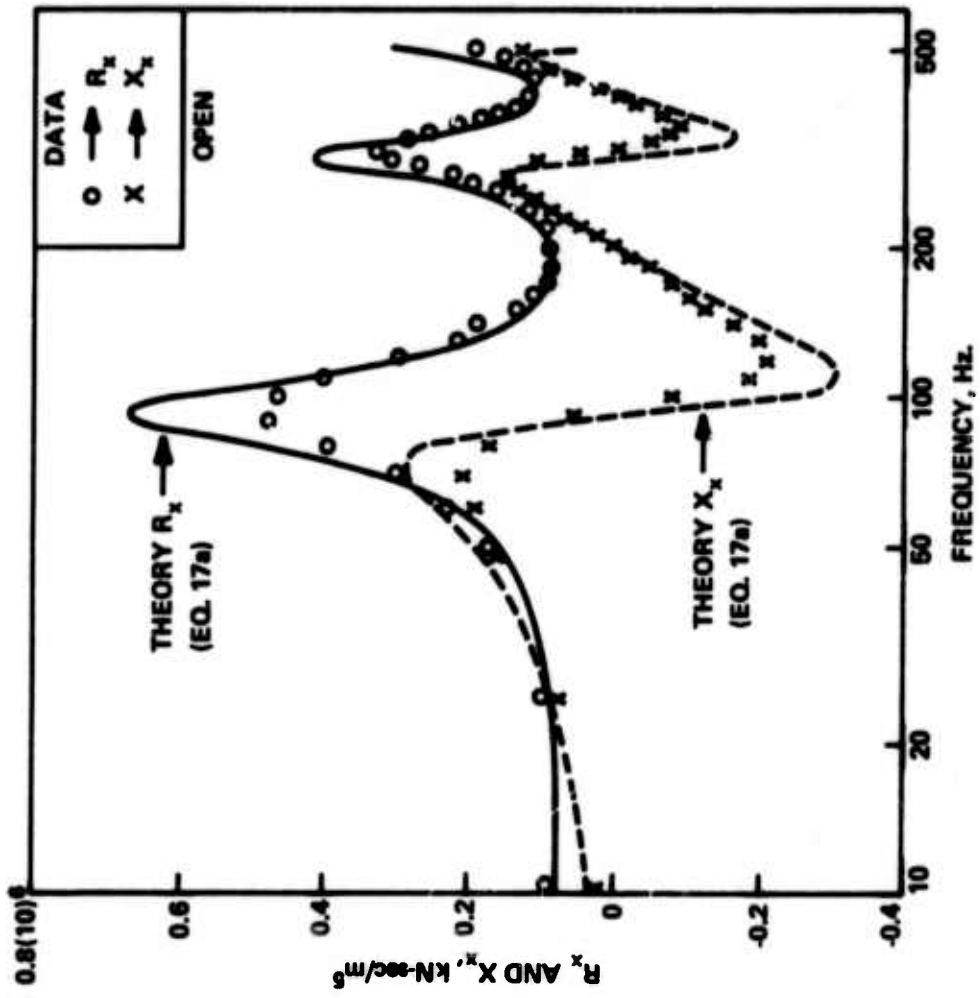


Figure 11. Impedance of Open Test Line

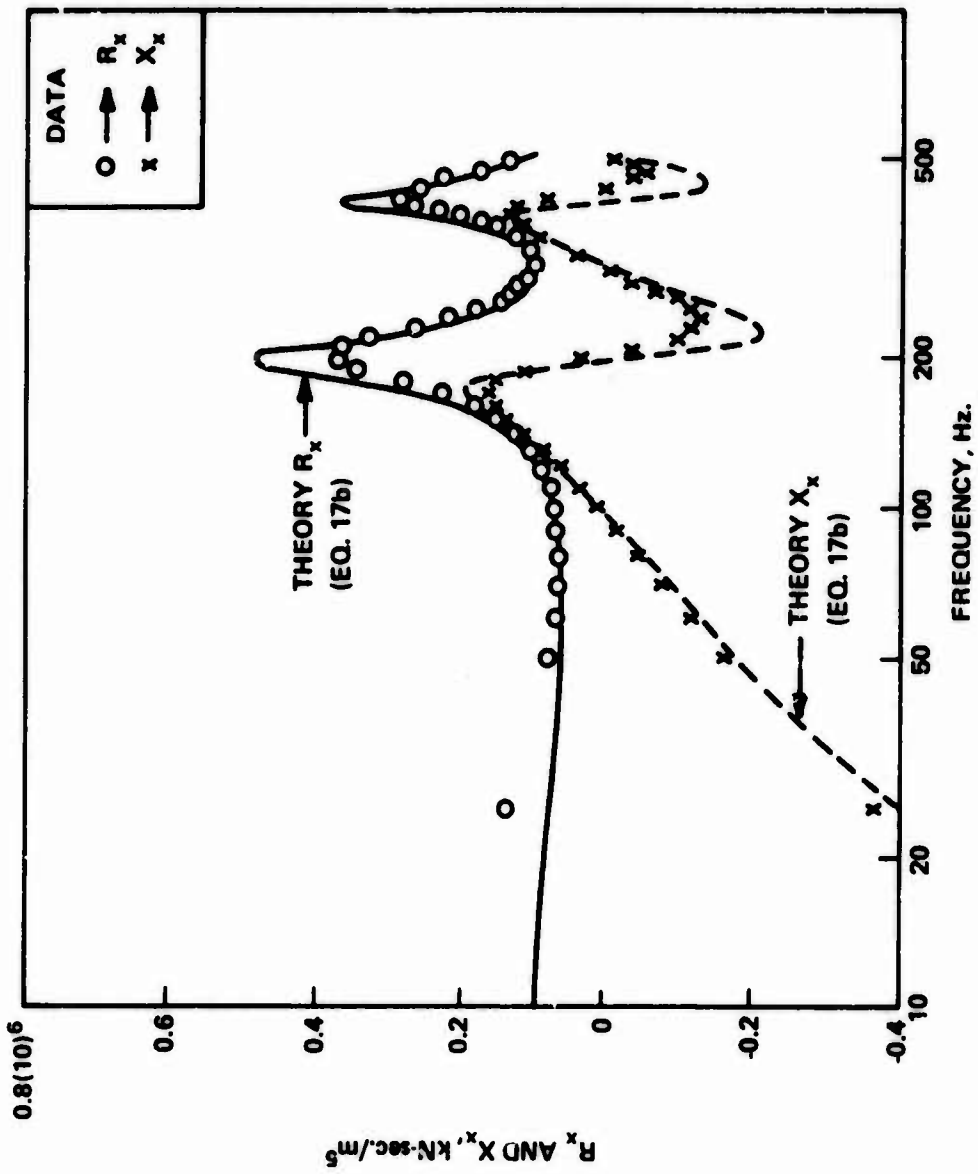


Figure 12. Impedance of Closed Test Line

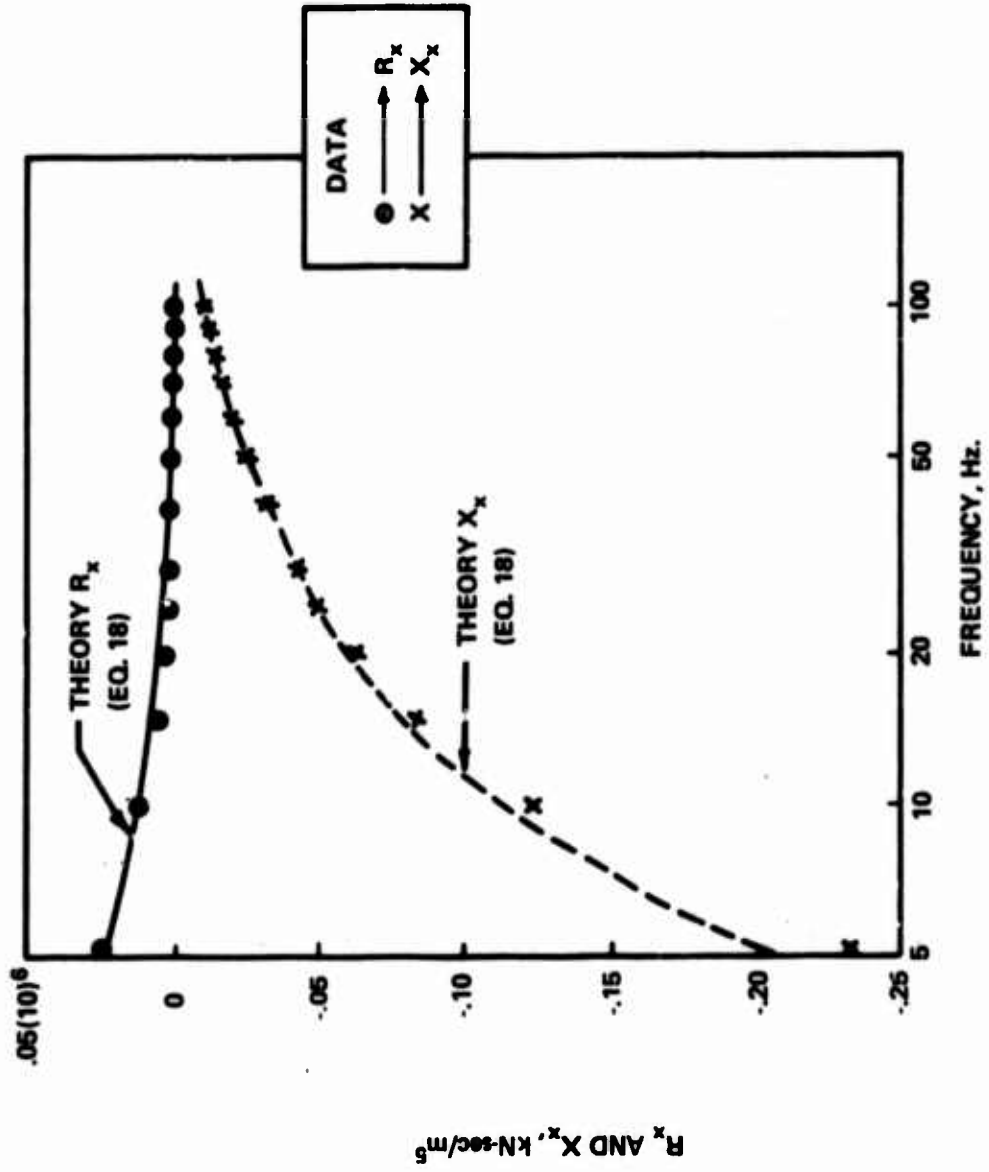


Figure 13. Impedance of Tank-Entrance Length Combination

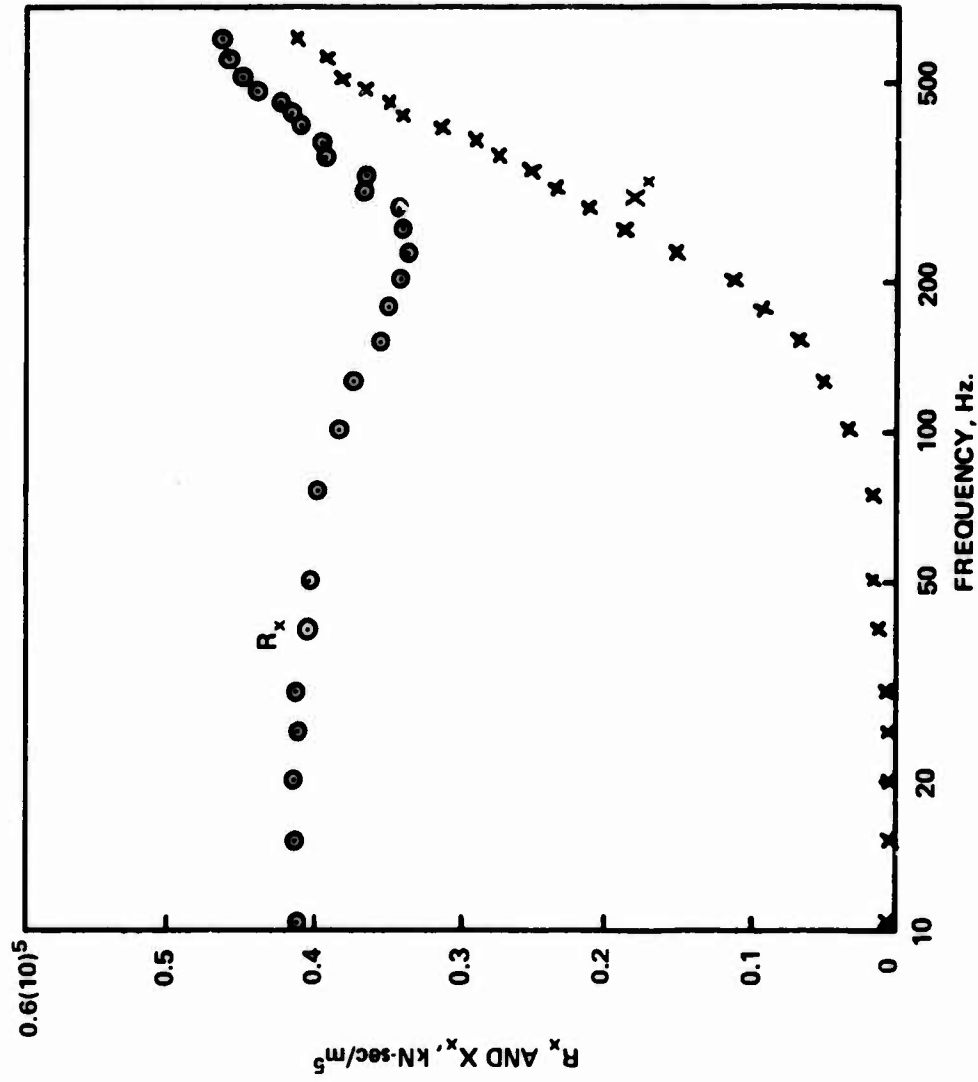


Figure 14. Impedance of Laminar Proportional Amplifier

ENGINEERING APPROXIMATIONS FOR
FLUIDIC INTERCONNECTIONS

H. L. Moses
Department of Mechanical Engineering
Virginia Polytechnic Institute & State University

R. A. Comparin
Department of Mechanical Engineering
Newark College of Engineering

ABSTRACT

An experimental study of signal transmission in fluidic interconnections is described. Both rectangular channels and flexible tubing typically used in fluidic circuits are considered. Steady flow pressure losses for various line configurations are correlated in terms of friction factors and minor loss coefficients. Circuit design based on these results and gate characteristics is discussed. Experimental results for the transient response to the output of a typical digital gate are presented. An approximate correlation for estimating the total delay time in the switching of the downstream gate is suggested.

SYMBOLS

a	Channel Height
b	Channel Width
c	Sonic Speed
d_h	Hydraulic Diameter
f	Friction Factor
g_c	Gravitational Constant
K	Minor Loss Factor
N_R	Reynolds Number
L	Channel Length
p	Pressure
t	Time
Δt	Total Delay Time
V	Velocity
ρ	Fluid Density
τ	Time Constant
ν	Fluid Kinematic Viscosity

Subscripts

1	Upstream End of Channel
2	Downstream End of Channel
c	Control
i	Initial
f	Final
t	Total

INTRODUCTION

The successful design of fluidic circuits often depends primarily upon careful consideration of the physical layout of the gates and the design of the interconnections.

Once the required logic has been determined, the implementation of fluidic hardware to accomplish a desired control function presents the designer with some unique problems. The interconnections in a fluidic circuit are made either with tubing or with channels in an integrated circuit block. In both cases the fluid must follow a complex path through channels with change of direction, change of area, branches, and many restrictions. Figure 1 illustrates the typical interconnections used.

Figure 2 shows a schematic of a complex interconnection between digital gates with typical curves for the pressure as a function of time at the upstream and downstream ends of the line, where p_c is the control pressure required to switch.

The circuit designer must be able to design the interconnections to carry signals for a wide range of operating conditions. Typical design situations can be categorized according to the relative importance of the steady state and transient behaviors. The simplest case, which is also a common and important one, is low frequency applications where the predominate concern is to limit the steady flow losses in the interconnecting passages. In other situations only the transient behavior is of concern, while a third, and more complex situation, occurs when both the steady state losses and the transient behavior must be considered simultaneously.

A considerable amount of work has been done on the propagation of signals in fluid lines, and there is a large body of literature devoted to the subject. A survey of techniques for modeling fluid transmission lines was recently given by Goodson and Leonard (1). For steady state losses in fluid lines, there is also a great deal of information available, much of it in typical elementary textbooks on fluid mechanics.

Although the general concepts associated with both transient and steady flow apply to fluidic circuits, there is a need for specific design information and simple procedures or techniques. For steady flow analysis there is not enough information available on loss coefficients for typical fluidic connections. In the case of transient behavior a typical fluidic circuit involves short, complex lines where the application of sophisticated mathematical analysis does not present a viable design technique.

This paper is intended to be an aid for designers by providing a reasonably simple and reliable design technique for fluidic interconnections. The steady state approach is sufficiently accurate for most

applications but more information on loss coefficients would be helpful. The prediction of transient behavior is presented as a workable approximation and is in no way intended as a substitute for more rigorous approaches where the transient behavior is critical.

EXPERIMENT

Experiments were conducted with rectangular channels and flexible tubing typical of those used in fluidic circuits. The ceramic channels were constructed with various lengths, sizes, and geometric configurations. Figure 3 is a photograph of typical channels. A total of 23 different line geometries were tested as listed in Table 1. (The layer step refers to rectangular channels in different horizontal planes connected by a vertical, cylindrical hole.) Two channels of each geometry were tested at various flow rates, or nozzle loads. Additional experiments were conducted on rectangular channels in actual integrated circuits, especially constructed so that pressures could be measured at various points in the circuit. Flexible tubing with inside diameters of 0.075 and 0.125 inch were tested along with typical fittings.

Steady flow pressure losses were measured with static taps, located a known distance apart, and a water manometer. Minor loss factors were determined by subtracting the pressure drop for a straight channel from that for a channel of the same length and size but different geometric configuration. The flow rate was measured with calibrated laminar flow channels.

For the transient experiments, the static taps were replaced with pressure transducers connected to an oscilloscope. (The vertical, pressure, scale was not calibrated in all cases, so the traces show the pressure relative to the steady flow value.) The transient signal at the upstream end of the channel was the output of a commercially available flip-flop, which was controlled by an OR/NOR gate. Similar gates were used as loads at the downstream end of the line. All of the gates had a nominal nozzle size of 0.010 x 0.020 inches. The tests were conducted at supply pressures to the flip-flop of 5 and 10 psig. The experimental apparatus and procedure are described more fully in references 2 and 3.

Steady Flow Pressure Loss

The steady flow total pressure loss for a rectangular channel or a tube can be expressed as a function of the fully developed friction factor, f , and minor loss coefficients, K ,

$$\Delta p_t = \left(f \frac{L}{d_h} + \sum K \right) \frac{\rho V^2}{2g_c} \quad (1)$$

When the velocity is constant, the total pressure loss is the same as the drop in static pressure. For incompressible flow,

$$\Delta p_t = \left(p_1 + \frac{\rho v_1^2}{2g_c} \right) - \left(p_2 + \frac{\rho v_2^2}{2g_c} \right). \quad (2)$$

The hydraulic diameter is defined as

$$d_h = 4 \frac{\text{area}}{\text{perimeter}} = \frac{2ab}{a+b} \quad (\text{for rectangular channel}) \quad (3)$$

= diameter (for tube).

The Reynolds number is

$$N_R = \frac{v d_h}{\nu} \quad (4)$$

The friction factor for fully developed laminar flow can be calculated from the equation of motion, which agrees well with experiments (see references 4 and 5) for example).

$$f = \frac{C}{N_R} \quad (5)$$

The constant, C, is equal to 64 for tubing and depends on the aspect ratio for channels--56 for a square channel and 96 for a two-dimensional channel (very low aspect ratio). The aspect ratio is the channel height to width ratio a/b, defined such that it is equal to or less than 1.0.

Figure 4 shows the theoretical and experimental values of the friction factor for rectangular channels and tubes as a function of the Reynolds number and aspect ratio. Although there is some experimental scatter, the data follow the theory reasonably well. The experimental values have been reduced from the measured data by one dynamic head to account for entrance losses, which should be included as a minor loss. This approximation probably introduces some error, but was suggested from a more detailed analysis (reference 6).

In the above analysis for the friction factor, equation 5, it is assumed that the flow is essentially laminar, although equation 1 is valid for laminar or turbulent flow. The agreement between theory and experiment indicates that this assumption is reasonable for the cases tested, which were considered to be those most often encountered in actual fluidic circuits. (Turbulent flow was treated in reference 7).

Minor losses are, in general, difficult to treat analytically. There are, however, some standard approximations, such as those for

sudden area changes, and some analyses for specific cases (see reference 8, for example). The approach taken here is strictly empirical and it is expected that in most cases an uncertainty of one dynamic head will not be critical. (The minor loss approach is used instead of an equivalent length because the loss coefficient is more nearly constant with flow rate for laminar channel flow). Table 2 gives the minor loss coefficients determined from the experiments. For area changes, the upstream velocity is generally used, but here the minor loss factor must be based on the velocity used in equation 1. Thus, K for the tubing adaptor is based on the velocity in the downstream tube and is much higher than normal for this geometry.

To use the above results for circuit design, one must know the gate characteristics. For safe design, one should use minimum characteristics such as those specified by the manufacturer or determined from a statistical study. Figure 5 shows minimum characteristics for a typical, commercially available OR/NOR gate. (Based on a statistical study, these characteristics are somewhat conservative). For example, the intersections of the minimum control nozzle impedance curve (for the load considered) and the maximum switch pressure curve determines the minimum flow required. The difference between the minimum output pressure at this flow and the maximum switch pressure is the maximum pressure loss that can be tolerated in the interconnecting line.

Transient Behavior

Although the oscilloscope traces (Figure 6) represent the actual transient pressure in the lines in response to the output signal of a flip-flop, they depend on the particular geometry tested. Thus the results are included here primarily for qualitative use in design, or, at best, a very rough quantitative approximation. The results should be used with caution for geometries other than those tested. The signal depends on the driving gate and load as well as the interconnecting line. For all of the experiments reported here, the gates had a nozzle size of 0.010 x 0.020 inch, and the line size should be considered in relation to this area.

Figure 6 shows typical results taken from approximately 200 oscilloscope traces. They are intended to show, at least qualitatively, the effect of line size, length, load, supply pressure, and geometry on the transient signal. Results are included for the signal rise, when the gate is switched into the line, and signal decay, when the gate is switched out.

To interpret these results, it is helpful to define a time constant, τ , based on the initial slope of the non-dimensional pressure curve.

$$\frac{1}{\tau} \equiv \frac{d}{dt} \left. \frac{p - p_i}{p_f - p_i} \right|_{p = p_i} \quad (6)$$

For the rectangular channels, the time constant at the upstream end of the line depends primarily on the gate characteristics. In all cases tested

$$\tau_1 \approx 0.2 \times 10^{-3} \text{ sec (rectangular channels)} \quad (7)$$

for rise and decay of the signal. The shape of the curve depends on the channel size and load. For medium channels (0.035 x 0.060 inch) with one nozzle load and large channels (0.055 x 0.060 inch) with two or three nozzle loads, the signal is roughly linear to its final steady value, but some wave reflections are apparent. For large channels with one nozzle load, the pressure increases to its final value with the first wave reflection. For the small channels, the initial pressure exceeds and then decays to its final value.

At the downstream end of the rectangular channels, the time constant is approximately

$$\tau_2 \approx 0.4 - 0.5 \times 10^{-3} \text{ sec (rectangular channels)} \quad (8)$$

for all but the smallest channels tested. (There is a slight increase with length and size, but most of the channels are within the above approximation). Again, for medium channels with one nozzle load and large channels with two or three nozzle loads, the signal is roughly linear to its final value. For large channels with one nozzle load, there is an initial overshoot in the pressure. For small channels, there is more delay in reaching the final pressure. With the linear approximation, the total delay time for a signal to reach a given value, p_c , can be estimated.

$$\Delta t \approx \frac{L}{c} + \tau_2 \frac{(p_c - p_i)}{(p_f - p_i)} \text{ (rectangular channels)} \quad (9)$$

Although equation 9 is empirical and very approximate it agrees within 0.1×10^{-3} sec for 90 per cent of the channels tested and within 0.2×10^{-3} sec for all of the channels.

For the flexible tubing, the transient behavior is more exponential as would be expected for a resistance-capacitance circuit. This behavior is due to the relatively large volume of the tubes and the large resistance of the tubing adapter. The pronounced effect of increased load is because the loads were added by parallel tubes from the upstream end, rather than adding them at the downstream end as was done with the rectangular channels. For the tubing tested, the time constant varies from $1.0 - 2.0 \times 10^{-3}$ sec for one nozzle load to $4.0 - 5.0 \times 10^{-3}$ sec for three nozzle loads.

CONCLUSIONS

The steady flow pressure losses in typical fluidic interconnections can be calculated reasonably well using a fully developed friction factor and minor loss coefficients. Except for long lines with large minor losses, a line cross-section of approximately 10 times the load nozzle area should be a safe design rule. In this case, one dynamic head in the line is approximately 1.0 per cent of the control pressure and 0.1 per cent of the supply pressure.

For the transient response, a line area of approximately 10 times the load area also gives a reasonably well matched condition. For the gates and lines tested, the total time delay is approximately the sonic delay plus $0.4 - 0.5 \times 10^{-3}$ sec.

REFERENCES

1. Goodson, R. E. and Leonard, R. G., "A Survey of Modeling Techniques For Fluid Line Transients", Journal of Basic Engineering, Trans. ASME, Vol. 94, Series D, No. 2, June 1972, pp. 474-482.
2. Senger, D. E., "An Experimental Study of Fluid Transmission Lines", M. S. Thesis, Virginia Polytechnic Institute and State University, Mechanical Engineering Department, August 1971.
3. Miller, C. W., Jr., "Prediction of the Operational Characteristics of Fluidic Transmission Lines", M. S. Thesis, Virginia Polytechnic Institute and State University, Mechanical Engineering Department, May 1972.
4. Allen, J. and Grunberg, N. D., "The Resistance to the Flow of Water Along Smooth Rectangular Passages and the Effect of a Slight Convergence or Divergence of the Boundaries", Phil. Mag., Series 7, Vol. 23, No. 154, March 1973, p. 491.
5. Rothfus, R. R., Kermode, R. I., and Hackworth, J. H., "Pressure Drop in Rectangular Ducts", Chemical Engineering, Vol. 71, December 7, 1964, pp. 175-176.
6. Sparrow, E. M., Hixon, C. W., and Shavit, G., "Experiments on Laminar Flow Development in Rectangular Ducts", Journal of Basic Engineering, Trans. ASME, Vol. 89, Series D, No. 1, March 1967, pp. 116-124.
7. Davies, G. E., "An Empirical Expression for the Resistance of Small Bore Tubes to Turbulent Flow", Paper D2, 2nd Cranfield Fluidics Conference, Cambridge, England, January 1967.
8. Katz, S., "Mechanical Potential Drops at a Fluid Branch", ASME Paper No. 67 - WA/FE - 13, November 1967.

TABLE 1 RECTANGULAR CHANNELS

<u>Geometry</u>	<u>Cross-Sections (in.)</u>	<u>Lengths (in.)</u>
Straight	.020 x .060	3
Straight	.020 x .060	6
Straight	.020 x .060	9
Straight	.020 x .030	6
Straight	.020 x .120	6
Straight	.035 x .060	6
Straight	.055 x .060	3
Straight	.055 x .060	6
90 Deg. Bend (sharp)	.020 x .060	6
90 Deg. Bend (sharp)	.055 x .060	6
90 Deg. Bend (0.6 in. rad.)	.020 x .060	6
90 Deg. Bend (1.2 in. rad.)	.020 x .060	6
45 Deg. Bend	.020 x .060	6
135 Deg. Bend	.020 x .060	6
1-layer step	.020 x .060	6
1-layer step	.055 x .060	6
3-layer step	.020 x .060	6
5-layer step	.020 x .060	6
5-layer step	.055 x .060	6
"T"	.020 x .060	3
"T"	.055 x .060	3
"Y"	.020 x .060	3
"Y"	.055 x .060	3

TABLE 2 MINOR LOSS COEFFICIENTS

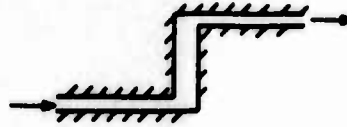
GEOMETRY

ENTRANCE LOSS

1

LAYER CHANGE

3-5



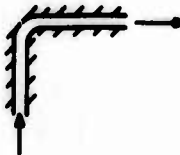
BENDS

90° - sharp

2-3

90° - long radius ($r \geq 10b$)

0-1



45° - sharp

0-1



135° - sharp

2-3



T-CHANNEL

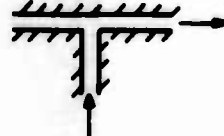
IN-LINE

0



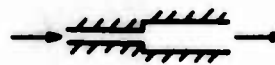
NORMAL

0-1



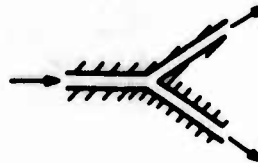
AREA CHANGE

0-1



Y-CHANNEL

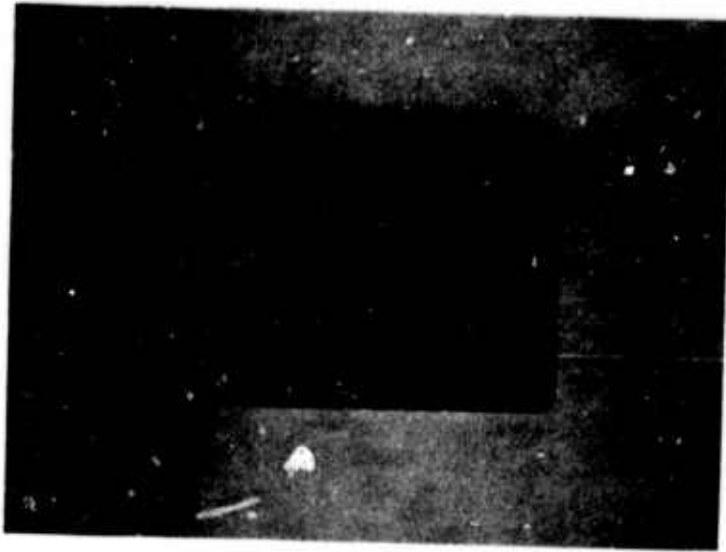
0-1



TUBING ADAPTER

8-10





(a) tubing connections



(b) channels in an integrated block

Fig. 1 Typical Interconnections

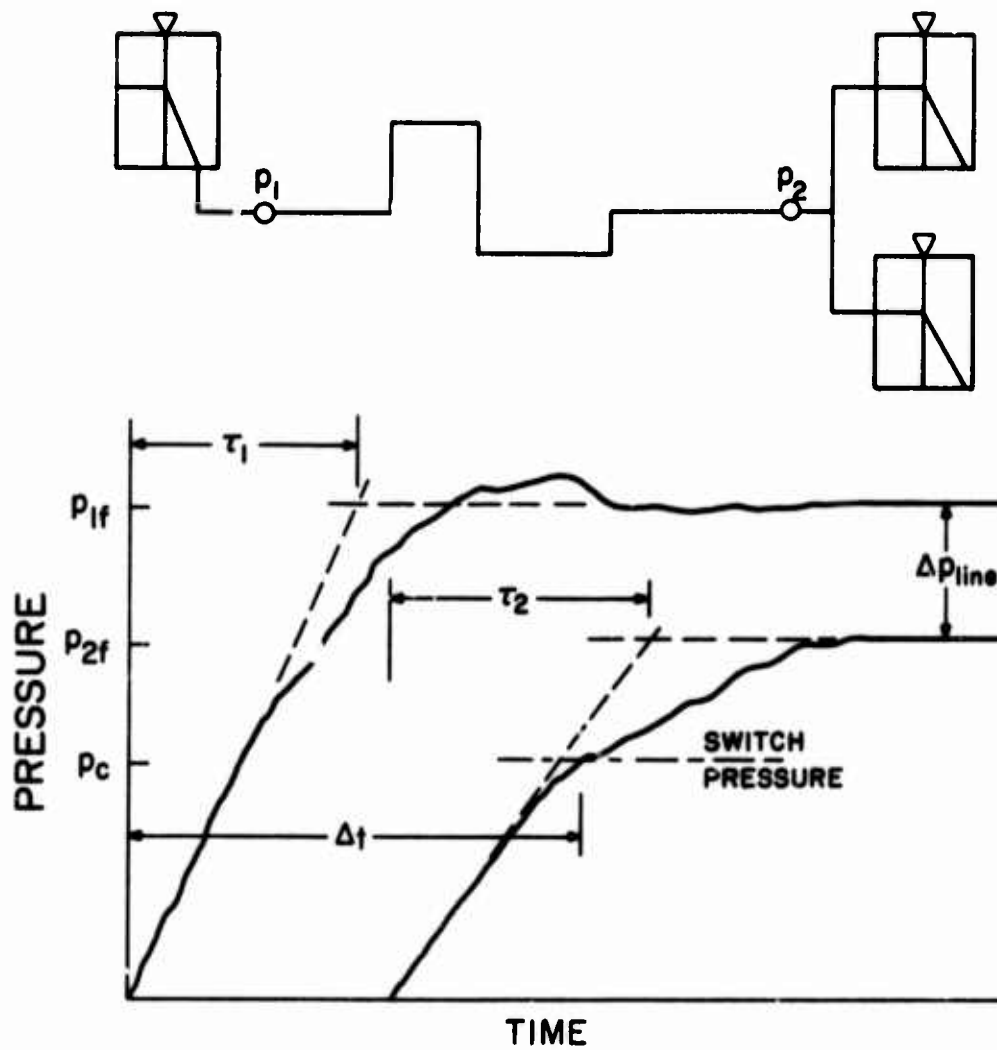


FIG. 2 SKETCH OF INTERCONNECTIONS AND DIGITAL SIGNAL

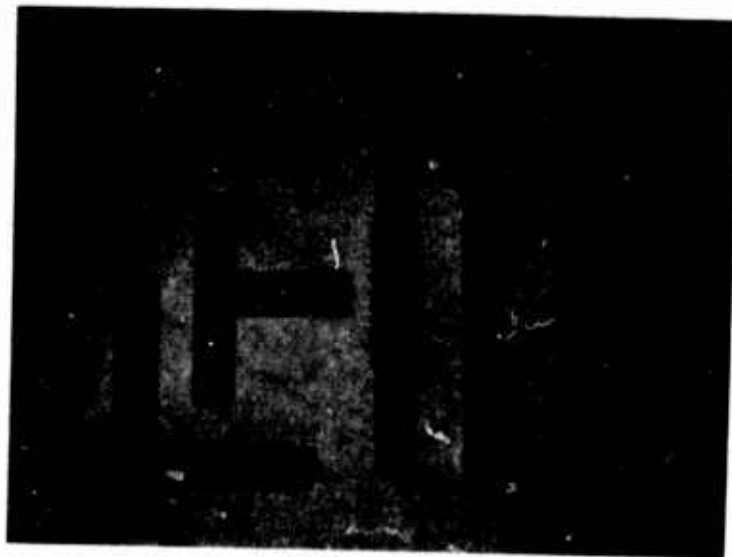


Fig. 3 Typical Channels

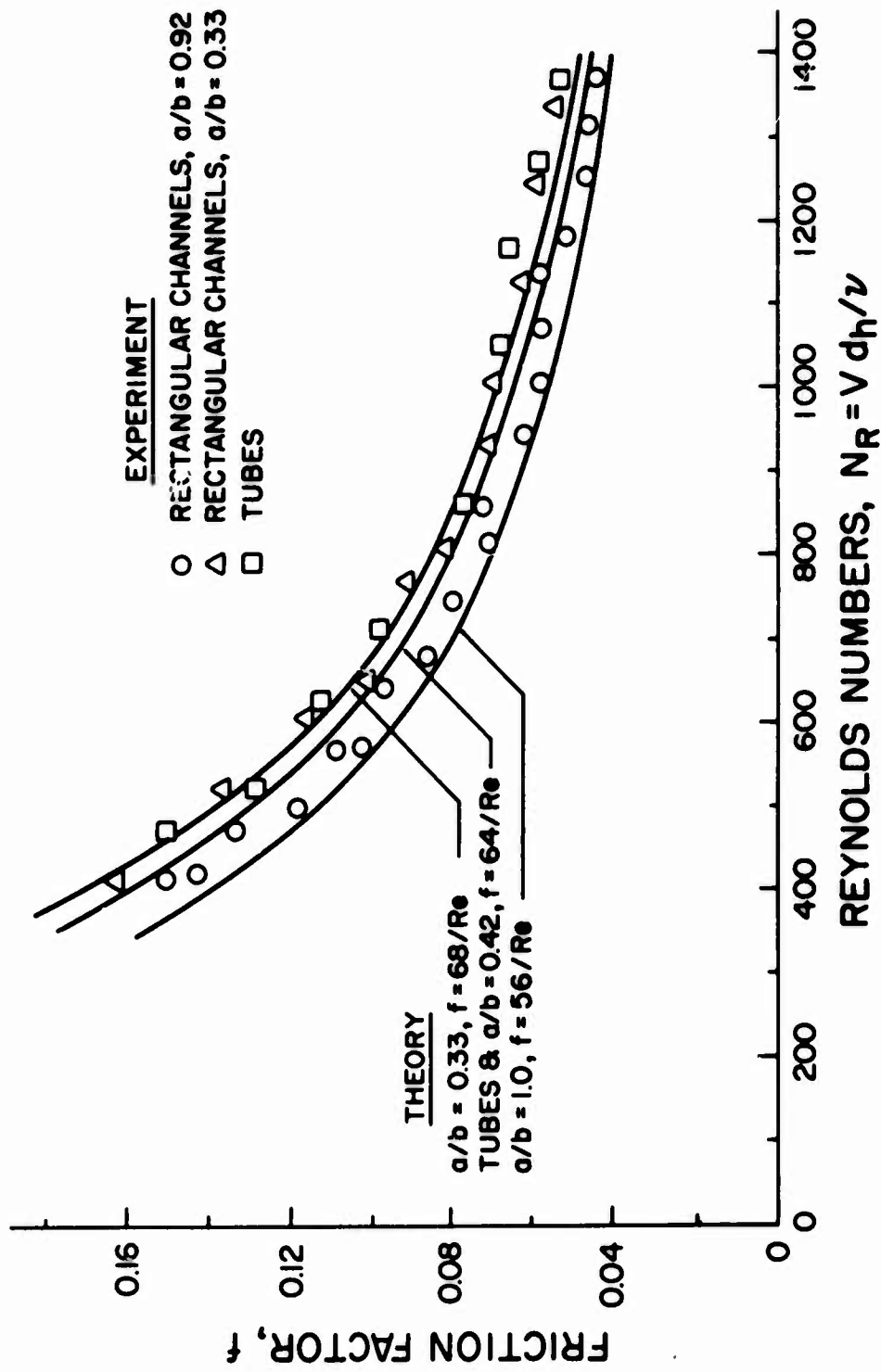


FIG. 4 FRICTION FACTOR FOR RECTANGULAR CHANNELS AND TUBES

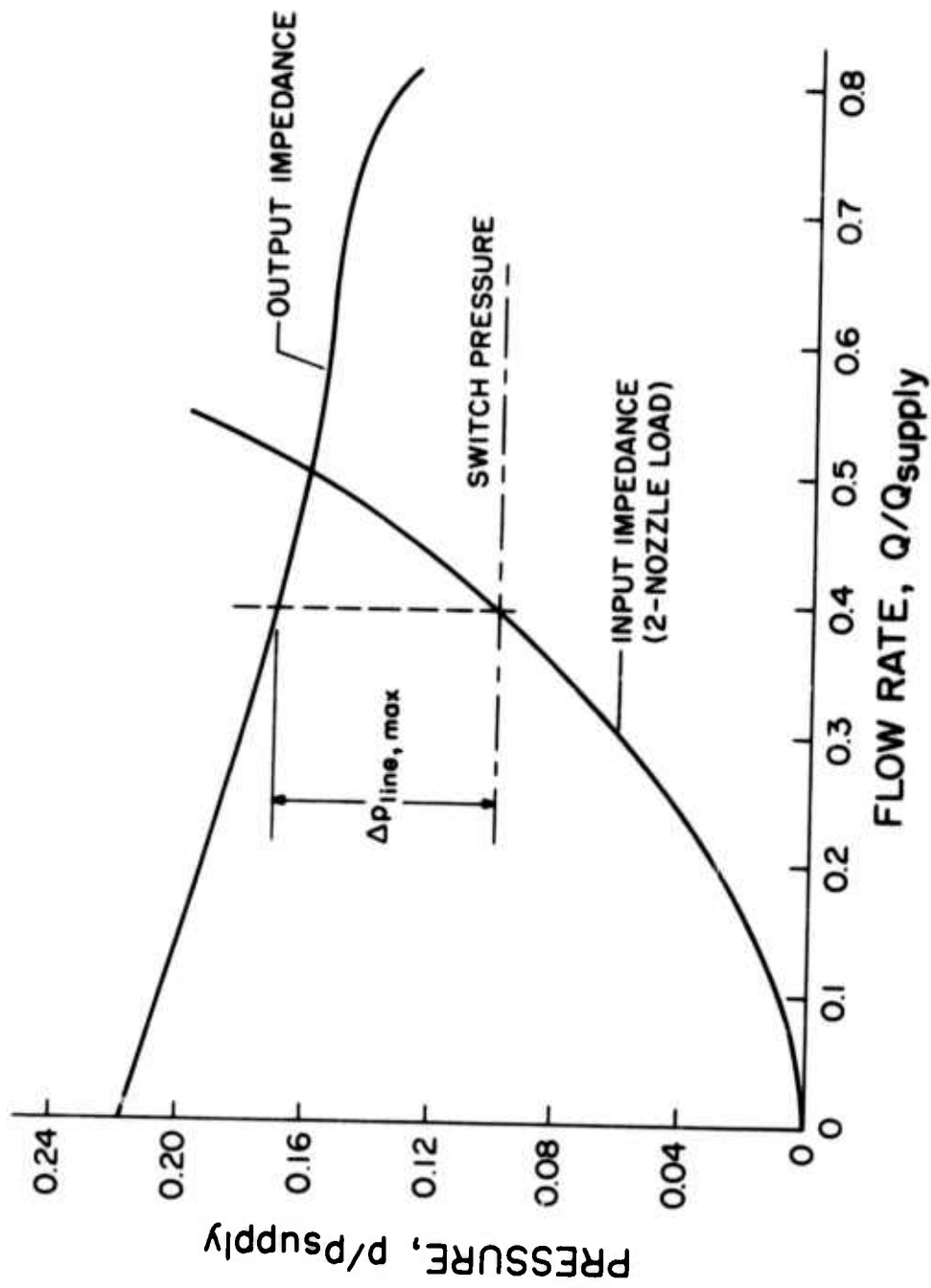
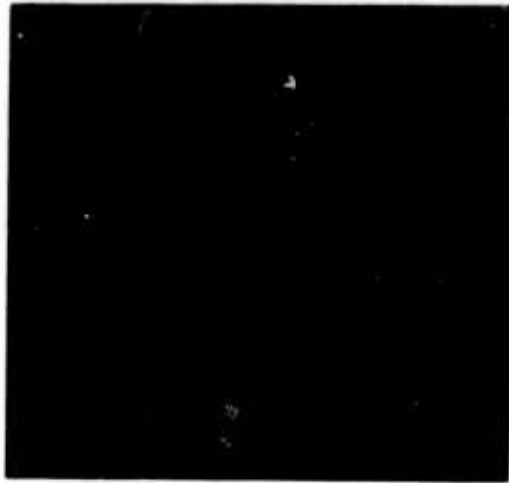
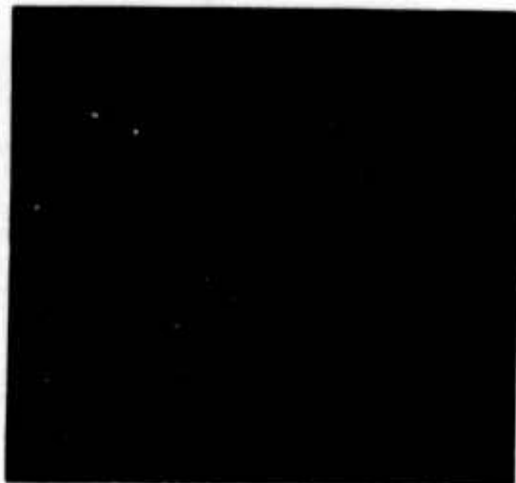


FIG. 5 STEADY STATE GATE CHARACTERISTICS



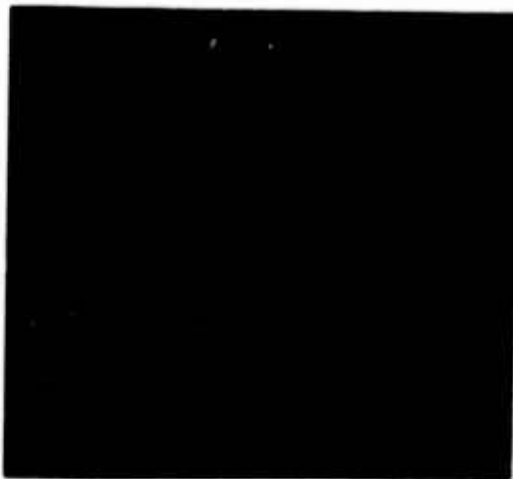
3-Inch Channel
Three-Nozzle Load

$P_s = 5$ psig



6-Inch Channel
Three-Nozzle Load

$P_s = 5$ psig



6-Inch Channel
Three-Nozzle Load

$P_s = 10$ psig

Channel Size = 0.055 x 0.06 inches

Sweep Rate = 0.5 msec/div



6-Inch Channel
One-Nozzle Load

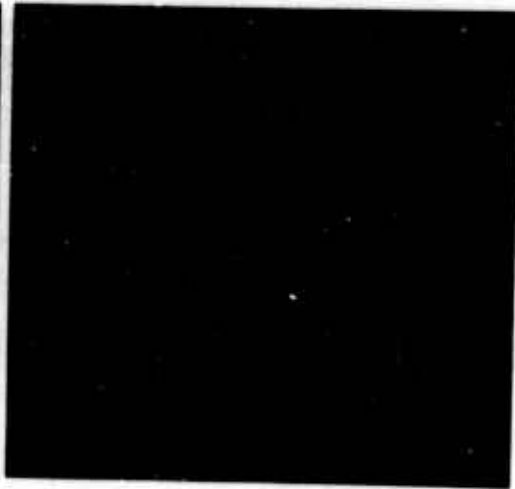
$P_s = 5$ psig

Pressure Scale Not Calibrated

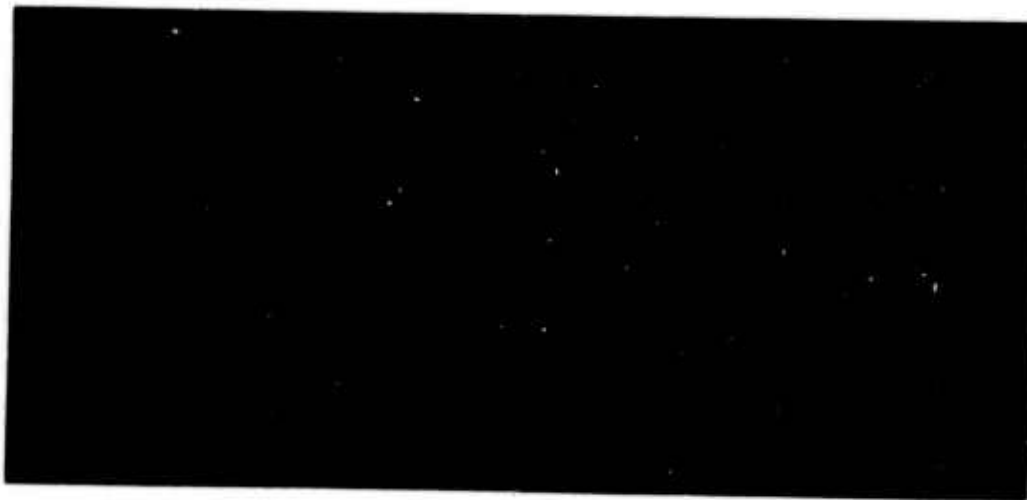
Fig. 6(a) Representative Oscilloscope Traces



0.020 x 0.60-inch 90° Long Radius
Length = 6 inches



0.020 x 0.060-inch Channel
Length = 9 inches



0.020 x 0.060-inch Channel
Length = 6 inches

0.020 x 0.030-inch Channel
Length = 6 inches

One-Nozzle Load

Sweep Rate = 0.50 msec/div

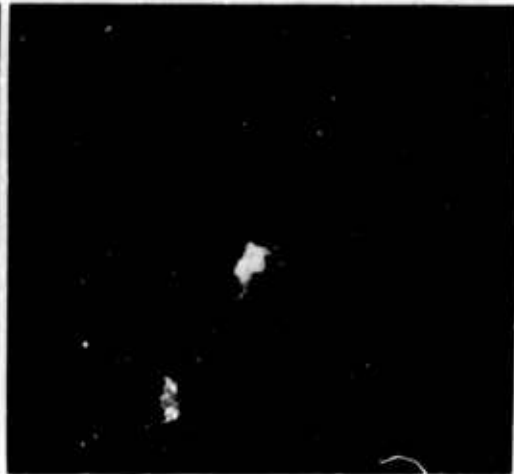
Pressure Scale Not Calibrated

$P_s = 5$ Psig

Fig. 6(b) Representative Oscilloscope Traces



One-Layer Step



T-Channel



90° - Sharp Bend



Y-Channel

Two - Nozzle Load

Channel Size = 0.055 x 0.06 inches

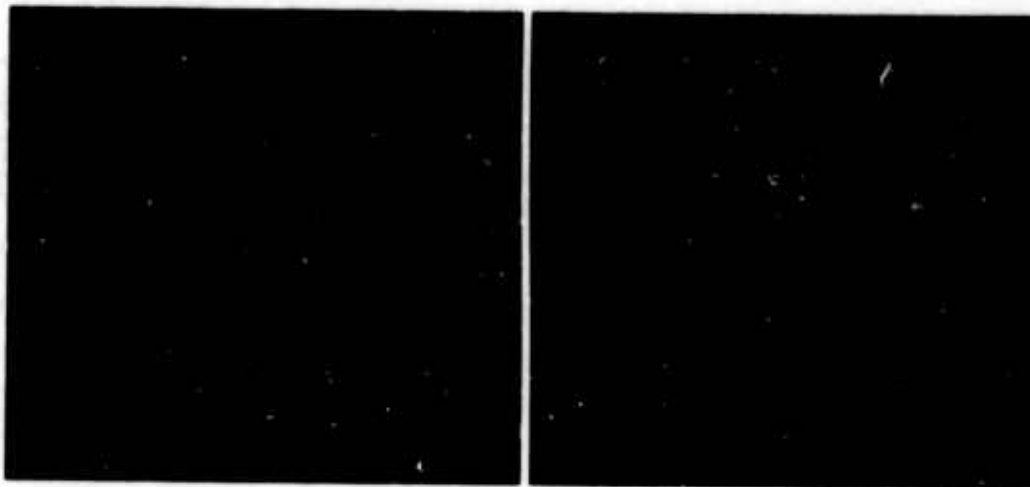
$P_s = 5$ psig

Length = 6 inches

Sweep Rate = 0.5 msec.div

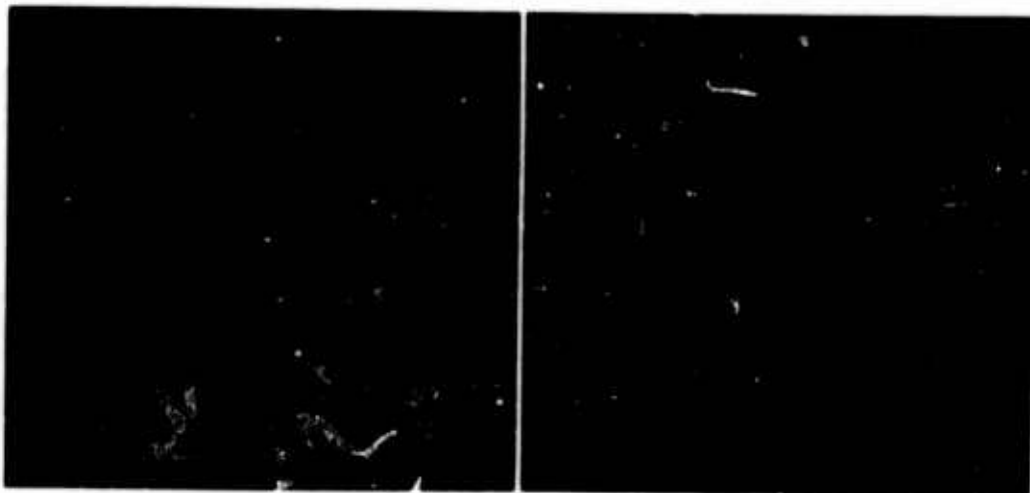
Pressure Scale Not Calibrated

Fig. 6(c) Representative Oscilloscope Traces



One-Layer Step
One-Nozzle Load

3-Inch Channel
Three-Nozzle Load



One-Layer Step
Three-Nozzle Load

6-Inch Channel
Three-Nozzle Load

Channel Size = 0.055 x 0.06 inches

$P_g = 5$ Psig

Length = 6 inches

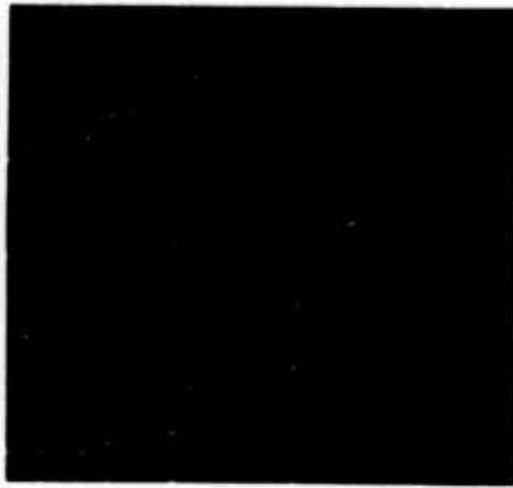
Sweep Rate = 0.5 msec/div

Pressure Scale Not Calibrated

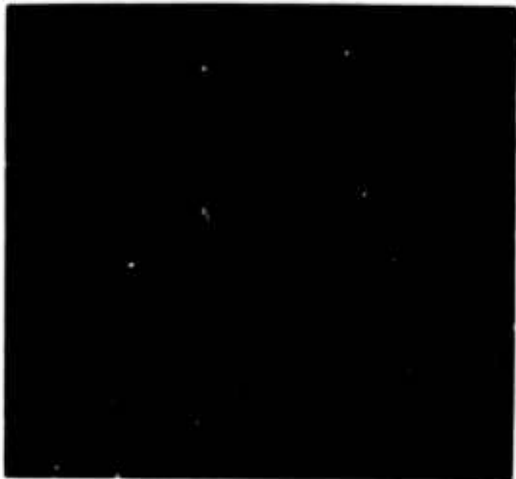
Fig. 6(d) Representative Oscilloscope Traces



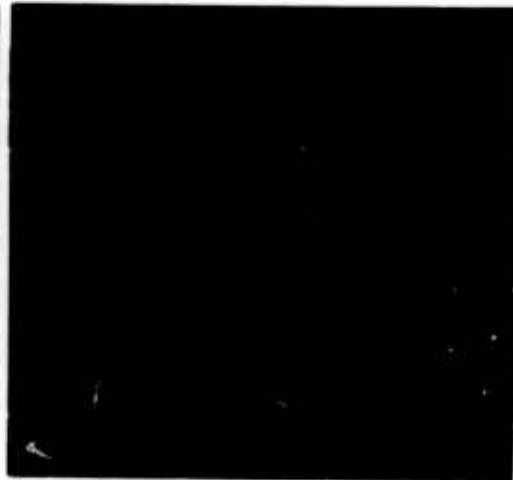
6-Inch Tube
Two-Nozzle Load



9-Inch Tube
Two-Nozzle Load



12-Inch Tube
Two-Nozzle Load



9-Inch Tube
One-Nozzle Load

Tube Size = 0.075-Inch I.D.
 $P_s = 5$ Psig

Sweep Rate = 2 msec/div
Pressure Scale Not Calibrated

Fig. 6(e) Representative Tube Oscilloscope Traces

**COMPARISON OF THE LINEAR RESPONSE OF CIRCULAR,
RECTANGULAR AND ANNULAR PNEUMATIC TRANSMISSION LINES**

**M.E. Franke
Professor of Mechanical Engineering
Air Force Institute of Technology
Wright-Patterson Air Force Base, Ohio 45433**

**E.F. Moore
Major, United States Air Force
Air Force Flight Dynamics Laboratory
Wright-Patterson Air Force Base, Ohio 45433**

ABSTRACT

A dimensionless frequency is defined which leads to a generalized presentation of the frequency dependent attenuation of lines of circular and noncircular cross section. Methods for determining the dimensionless frequency are presented.

NOMENCLATURE

A	=	area, in. ²
a	=	aspect ratio, b/h
b	=	width of rectangular cross section, in.
c	=	phase velocity, in./sec.
c _a	=	adiabatic free sonic velocity, in./sec.
D _c	=	diameter of circular line, in.
D _h	=	hydraulic diameter, 4A/P _w , in.
f	=	friction factor (Darcy-Weisbach), $4\tau_0 \frac{\rho \bar{u}^2}{2}$
h	=	height of rectangular cross section, in.
K _G	=	geometric parameter defined by equation (15)
K _L	=	inertance parameter defined by equation (7)
K _R	=	resistance parameter defined by equation (9)
L _a	=	adiabatic inertance per unit length, ρ^*/A , psi-sec/cis-in.
L _v	=	viscous inertance per unit length, psi-sec/cis-in.
P _w	=	wetted perimeter of line cross section, in.
Q	=	volumetric flow rate, A \bar{u} , cis
R _v	=	DC viscous resistance per unit length, psi/cis-in.
r	=	radius, in.
r _i	=	inside radius of annulus, in.
r _o	=	outside radius of annulus, in.
r*	=	radius ratio of annulus, r _i /r _o
Re	=	Reynolds number, $\rho \bar{u} D_h / \mu$
SN	=	Stokes number, $4\omega r^2 / \nu$
u	=	steady laminar flow velocity, in./sec
\bar{u}	=	average velocity, $\frac{1}{A} \int u dA$, in./sec
z	=	axial coordinate, in.
λ	=	line wavelength, in.
λ_a	=	adiabatic wavelength, in.
μ	=	dynamic viscosity, psi-sec
ν	=	kinematic viscosity, μ/ρ , in. ² /sec
ρ^*	=	reference density, psi-sec ² /in. ²
τ_0	=	shear stress at the wall, psi
Ω	=	dimensionless frequency
ω	=	signal frequency, rad/sec
ω_c	=	radian frequency, R _v /L _v , rad/sec
ω_v	=	characteristic frequency, R _v /L _a , rad/sec

Subscripts and Superscripts

c	=	radian frequency or circular line
n	=	concentric annular line
r	=	rectangular line
a	=	adiabatic conditions

INTRODUCTION

The small signal frequency response of pneumatic transmission lines of circular, rectangular, and concentric annular cross sections has been obtained [1-5]. For circular lines, Nichols [3] treated the problem as an equivalent circuit and expressed the results in terms of a series impedance and shunt admittance per unit length of line. Schaedel [4] and Moore and Franks [5] followed closely the approach of Nichols in obtaining the small signal response of rectangular and annular lines, respectively. The rectangular line results were shown to depend on the aspect ratio of the rectangular cross section, and, similarly, the annular results to depend on radius ratio of the annulus.

In steady flow it has been particularly useful to correlate the resistances of lines of noncircular cross sections with the resistance of circular lines through the classical hydraulic diameter. Similarly, in oscillatory flow, it would appear useful to be able to correlate the frequency response of noncircular lines to the response of circular lines. Besides the comparisons made between rectangular and circular lines [4] and between annular and circular lines [5], other attempts have been made to predict the response of rectangular lines using the concept of the hydraulic diameter [6,7].

The purpose of this paper is to present a dimensionless frequency for correlating the responses of circular, rectangular, and annular lines and to present methods for determining this dimensionless frequency.

FREQUENCY RESPONSE SOLUTIONS

Several dimensionless frequencies (or frequency ratios) have been defined in order to present generalized frequency response solutions for circular lines. Nichols [3] showed that the frequency response of a circular line is a function of the dimensionless frequency ratio ω/ω_v , where ω is the angular excitation frequency and ω_v is a viscous characteristic frequency defined as

$$\omega_v = \frac{R_v}{L_a} \quad (1)$$

R_v is the laminar DC viscous resistance per unit line length and L_a is the adiabatic inertance per unit line length. For any line, R_v and L_a are defined as

$$R_v = \frac{1}{Q} \left[- \frac{dp}{dx} \right] \quad (2)$$

and

$$L_a = \frac{\rho a^2}{A} \quad (3)$$

For a circular line, R_v and ω_v become

$$R_{vc} = \frac{8\pi\mu}{A_c^2} \quad (4)$$

and

$$\omega_{vc} = \frac{8\pi v}{A_c} \quad (5)$$

Other formulations of the dimensionless frequency have also been defined for the circular line; for example, Brown et al [8] used $\Omega = \omega r^2/v = 8\omega/\omega_{vc}$, while Goldschmied [9] used $SN = 4\omega r^2/v = 32\omega/\omega_{vc}$. In all of these cases, however, the dimensionless frequencies are proportional to $\omega A/v$.

Schaedel [4] showed that the response of rectangular lines of the same aspect ratio is a function of $\omega A/4v$, while Moore and Franke [5] showed that the response of concentric annular lines of the same radius ratio is a function of $\frac{\omega A}{8\pi v}$. Typical results for the attenuation per line wavelength of rectangular and annular lines are plotted in Figs. 1 and 2, respectively. Circular line results are included in Fig. 2 as a special case of the annular line with the inside radius $r_1 = 0$. The dependence on aspect ratio and radius ratio as well as signal frequency is clearly shown.

GENERALIZED RESPONSE OF NONCIRCULAR LINES

The αl curves shown in Figs. 1 and 2 for different aspect ratios and radius ratios all have the same general shape. Thus, it would seem possible that the results for different aspect or radius ratios could be generalized and related to a single curve. This can be accomplished approximately by using the dimensionless frequency defined by equation (1) with R_v taken as the resistance of the particular cross section being considered.

A better approach is to include the inertance effects in the dimensionless frequency as well as the resistance effects and to present the results as a function of the dimensionless frequency ω/ω_c , where ω_c is the radian frequency defined by Nichols [3] as

$$\omega_c = \frac{R_v}{L_v} \quad (6)$$

Here R_v is defined by equation (2), and L_v , the low-frequency or viscous inertance, is defined by

$$L_v = \left[\frac{1}{A} \int \left(\frac{u}{v} \right)^2 dA \right] \cdot L_a = K_L \cdot L_a \quad (7)$$

where K_L depends on the laminar fully-developed velocity distribution.

The $\alpha\lambda$ results shown in Figs. 1 and 2 are replotted in Fig. 3 as a function of ω/ω_c . The families of curves for different aspect and radius ratios are now reduced approximately to a single curve. By incorporating the geometric dependence of aspect and radius ratio in ω_c , lines of different sizes and cross sections are shown to have approximately the same generalized frequency behavior. The circular line attenuation is also included in Fig. 3, where ω_c for the circular line is the same as that given by Nichols [3]; i.e.,

$$\omega_{cc} = \frac{R_{vc}}{L_{vc}} = \frac{\frac{8\pi\mu}{A_c^2}}{\frac{4}{3}L_{ac}} = \frac{6\pi\nu}{A_c} = \frac{3}{4}\omega_{vc} \quad (8)$$

Fig. 3 shows $\alpha\lambda$, the attenuation per line wavelength. In order to obtain α , the attenuation per unit length, it is necessary to know λ , the wavelength in the line for each ratio ω/ω_c . Curves of λ/λ_a vs. $\omega A/4\nu$ for rectangular lines and vs. $\omega A/8\pi\nu$ for annular lines are given in [4] and [5] respectively. These curves are not reproduced herein; however, they show relative aspect and radius ratio effects similar to the $\alpha\lambda$ curves, Figs. 1 and 2. The families of curves depicting λ/λ_a reduce approximately to one curve representing circular, rectangular and annular lines when plotted against ω/ω_c as shown in Fig. 4. The ratio λ/λ_a is also the ratio of the propagation or phase velocity in the line to the free sonic (adiabatic) velocity; i.e., $\lambda/\lambda_a = c/c_a$ [3,4,5].

The results in Figs. 1 to 4 were computed assuming standard properties of air at 80°F. The numerical differences in $\alpha\lambda$ in Fig. 3 for the range of aspect or radius ratios shown in Figs. 1 and 2 were small and cannot be seen in Fig. 3. The maximum difference in $\alpha\lambda$ between circular and rectangular lines was 1.05 db at $\omega/\omega_c = 6.0$ for $a = 10$. The maximum difference between annular and circular lines was 1.40 db at $\omega/\omega_c = 6.0$ for $r^* = 0.8$. For $\omega/\omega_c \leq 0.1$ the difference was less than 0.09 db, and for $\omega/\omega_c \geq 10$ the difference was less than 1.25 db.

The maximum difference in λ/λ_a between circular and rectangular lines was 0.035 at $\omega/\omega_c = 2.0$ and $a = 10$. The maximum difference between circular and annular lines was 0.046 at $\omega/\omega_c = 3.0$ and $r^* = 0.8$. For $\omega/\omega_c \leq 0.1$ the maximum difference for both rectangular and annular lines was less than 0.017 and for $\omega/\omega_c \geq 10$ the maximum difference was less than 0.025. The maximum departure of λ/λ_a from that predicted for the circular line for the range of aspect and radius ratios considered occurred for the annular line of radius ratio $r^* = 0.8$, as shown on

Fig. 4. All other configurations are nearer to the circular line results.

It is noted that whereas $\alpha\lambda$ vs. ω/ω_c gives the tightest grouping of the $\alpha\lambda$ curves, λ/λ_g vs. ω/ω_v gives a slightly better grouping of the λ/λ_g curves, where ω_v is defined by equation (1).

DETERMINATION OF ω_c

The determination of values of ω_c for noncircular lines reduces essentially to obtaining values of R_v and L_v . A convenient method for obtaining R_v is to relate the R_v of the line with the noncircular cross section to that of a circular cross section; i.e.,

$$\frac{R_v}{R_{v_c}} = K_R \frac{A_c^2}{A^2} \quad (9)$$

where K_R for rectangular lines and annular lines depends on aspect ratio and radius ratio, respectively. Values of K_R have been calculated [4,5] and a few are given in Table I. The viscous inertance L_v is obtained from values of K_L , equation (7), for each geometric configuration. Values of K_L have also been calculated [4,5,10] and a few are given in Table I.

Starting with equation (6), a convenient equation for computing ω_c is easily derived as

$$\omega_c = \frac{K_R}{K_L} \frac{8\pi\nu}{A} \quad (10)$$

For circular lines: $K_{R_c} = 1$ and $K_{L_c} = 4/3$; thus $\omega_{c_c} = 6\pi\nu/A_c$. Values of ω_c for noncircular lines can easily be obtained using values from Table I or using the equations or data from the references [4,5,10].

The steady flow laminar resistance R_v does not depend on frequency; consequently, R_v may be expressed in terms of the classical steady-flow parameters:

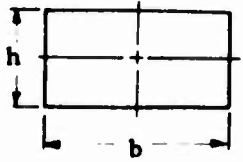
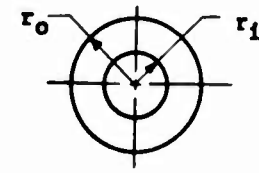
$$R_v = fRe \frac{\mu}{2D_h^2 A} \quad (11)$$

where D_h is the conventional hydraulic diameter, f is the friction factor and Re is the Reynolds number. For a circular line, $D_h = D_c$ and $fRe = 64$; therefore,

$$R_{v_c} = 64 \frac{\mu}{2D_c^2 A_c} \quad (12)$$

TABLE I

Fully Developed Laminar Flow Parameters for Rectangular and Annular Lines

									
b/h	K_{Rr}	K_{Lr}	$f_r Re_r$	K_{Gr}	r_i/r_o	K_{Rn}	K_{Ln}	$f_n Re_n$	K_{Gn}
1	1.1322	1.3785	56.91	1.2733	0	1.0000	1.3333	64.00	1.0000
2	1.3920	1.3475	62.19	1.4324	0.1	1.7068	1.2298	89.37	1.2222
3	1.8133	1.3120	68.36	1.6977	0.2	2.1645	1.2168	92.35	1.5000
4	2.2671	1.2876	72.93	1.9895	0.3	2.7232	1.2101	93.85	1.8571
5	2.7317	1.2714	76.28	2.2918	0.5	4.4649	1.2035	95.25	3.0000
10	5.0959	1.2365	84.68	3.8515	0.8	13.4890	1.2004	95.92	9.0000
∞	∞	1.2000	96.00	∞	1.0	∞	1.2000	96.00	∞

Dividing equation (11) by equation (12)

$$\frac{R_v}{R_{vc}} = \frac{fRe}{64} \frac{D_c^2}{D_h^2} \frac{A_c}{A} \quad (13)$$

where fRe , D_h , and A are determined for the noncircular cross section being considered. Selected values of fRe are given in Table I for rectangular and annular cross sections. The relationship between K_R and fRe is obtained from equations (9) and (13)

$$K_R = \frac{fRe}{64} \frac{D_c^2}{D_h^2} \frac{A}{A_c} = \frac{fRe}{64} K_G \quad (14)$$

where K_G is a geometric shape factor defined as

$$K_G = \frac{D_c^2}{D_h^2} \frac{A}{A_c} = \frac{4A}{\pi D_h^2} = \frac{P^2}{4\pi A} \quad (15)$$

K_G is a constant for each geometric cross section. It is important to note that when $D_h = D_c$ the areas of the noncircular cross section A and

equivalent diameter circle A_c are not equal and $K_G = A/A_c$. Likewise, when $A = A_c$ the hydraulic diameters are not equal and $K_G = D_c^2/D_{hr}^2$. Expressions for K_G are given in Table II for circular, rectangular and annular cross sections.

TABLE II

Geometric Cross Section Factor

<u>cross section</u>	<u>K_G</u>
circular	1
rectangular	$(a + 1)^2/\pi a$
concentric annular	$\frac{1 + r^*}{1 - r^*}$

Selected values of K_G are included in Table I for rectangular and annular cross sections.

USE OF HYDRAULIC DIAMETER

Results based on hydraulic diameter can be used to predict line performance for small signal oscillatory flow. At a given signal frequency, Fig. 3 shows that for the same attenuation on lines of different cross section, the ω_c 's must be the same. The use of equivalent hydraulic diameter for a noncircular line, however, leads to an ω_c that is, in general, not equal to ω_{c_c} . This will now be illustrated for a rectangular line.

From equation (10), the ratio $\omega_{c_r}/\omega_{c_c}$ is

$$\frac{\omega_{c_r}}{\omega_{c_c}} = \frac{4}{3} \frac{K_{R_r}}{K_{L_r}} \frac{A_c}{A_r} \quad (16)$$

By substituting for K_{R_r} from equation (14), the ratio becomes

$$\frac{\omega_{c_r}}{\omega_{c_c}} = \frac{4}{3} \frac{f_r Re_r}{64} \frac{1}{K_{L_r}} \frac{D_c^2}{D_{hr}^2} \quad (17)$$

For $D_{hr} = D_c$, equation (17) reduces to

$$\frac{\omega_{c_r}}{\omega_{c_c}} = \frac{4}{3} \frac{f_r Re_r}{K_{L_r} 64} \quad (18)$$

Typical values of ω_{cR}/ω_{cC} and $\sqrt{\omega_{cR}/\omega_{cC}}$ as a function of aspect ratio are shown in Table III using the values of $f_R Re_R$ and K_{LR} from Table I.

TABLE III

Frequency Ratio Parameters for Rectangular Lines for $D_{hR} = D_C$

b/h	ω_{cR}/ω_{cC}	$\sqrt{\omega_{cR}/\omega_{cC}}$
1	0.86	0.93
2	0.96	0.98
3	1.09	1.04
4	1.18	1.09
5	1.25	1.12
10	1.43	1.19

The ratio $\sqrt{\omega_{cR}/\omega_{cC}}$ can be interpreted approximately as the ratio of the viscous attenuation of rectangular to circular lines of the same hydraulic diameter at a given frequency. The values of $\sqrt{\omega_{cR}/\omega_{cC}}$ given in Table III confirm the attenuation results of Healey and Carlson [6] and explain the differences they found between the rectangular line solutions and circular line solutions of the same hydraulic diameter. When using circular line equations to predict rectangular line results, the differences can be avoided if the rectangular line friction factor ($f_R Re_R$) and inertance L_{VR} are included in the calculations.

SUMMARY

A method has been presented which leads to a generalized presentation of the frequency response of lines of circular and noncircular cross section. As a result parameters of interest, such as $\alpha\lambda$ and λ/λ_a , for lines of different sizes and cross section configurations can be represented approximately by a single curve when plotted against the dimensionless frequency $\omega/\omega_c = \omega L_V/R_V$. Values of R_V and L_V depend on the particular cross section being considered and are determined from fully-developed laminar viscous flow distributions. The frequency dependent attenuation of noncircular lines can also be closely predicted using equivalent hydraulic diameter, provided the steady-flow parameters of resistance and inertance for each cross-sectional configuration are used.

REFERENCES

1. Iberall, A.S. "Attenuation of Oscillatory Pressures in Instrument Lines," Journal of Research, National Bureau of Standards, Vol. 45, 1950, pp 85-108.
2. Brown, F.T., "The Transient Response of Fluid Lines," Journal of Basic Engineering, Trans. ASME, Series D, Vol. 84, No. 3, Sep 1962, pp 547-553.
3. Nichols, N.B., "The Linear Properties of Pneumatic Transmission Lines," Transactions of the Instrument Society of America, Vol 1, 1962, pp 5-14.
4. Schaedel, H., "A Theoretical Investigation of Fluidic Transmission Lines with Rectangular Cross-Section," Third Cranfield Fluidics Conference, May 1968, Turin, Paper K-3, The British Hydromechanics Research Association, Cranfield, Bedford, England.
5. Moore, E.F., and Franke, M.E., "The Small Signal Response of Annular Pneumatic Transmission Lines," to be presented at the Joint Fluids Engineering - CSME Conference, May 1974, Montreal, Canada.
6. Healey, A.J. and Carlson, R.J., "Frequency Response of Rectangular Pneumatic Transmission Lines," ASME Paper No. 69-WA/FLCS-5, 1969.
7. Franke, M.E., Lymburner, F.C., and Karam, J.T., Jr., "Experimental Frequency Response of Fluidic Transmission Lines," Proceedings of the Fourth Cranfield Fluidics Conference, Paper E1, March 1970, Coventry, England, The British Hydromechanics Research Association, Cranfield, Bedford, England.
8. Brown, F.T., Margolis, D.L. and Shah, R.P., "Small-Amplitude Frequency Behavior of Fluid Lines with Turbulent Flow," Journal of Basic Engineering, Trans. ASME, Series D, Vol. 91, No. 4, 1969, pp 678-693.
9. Goldschmied, R.R., "On the Frequency Response of Viscous Compressible Fluids as a Function of Stokes Number," NASA TM X-53785, Sep 1968, NASA Marshall Space Flight Center.
10. Lundgren, T.S., Sparrow, E.M., and Starr, J.R., "Pressure Drop Due to the Entrance Region in Ducts of Arbitrary Cross Section," Journal of Basic Engineering, Trans. ASME, Vol. 86, Series D, No. 3, 1964, pp 620-626.

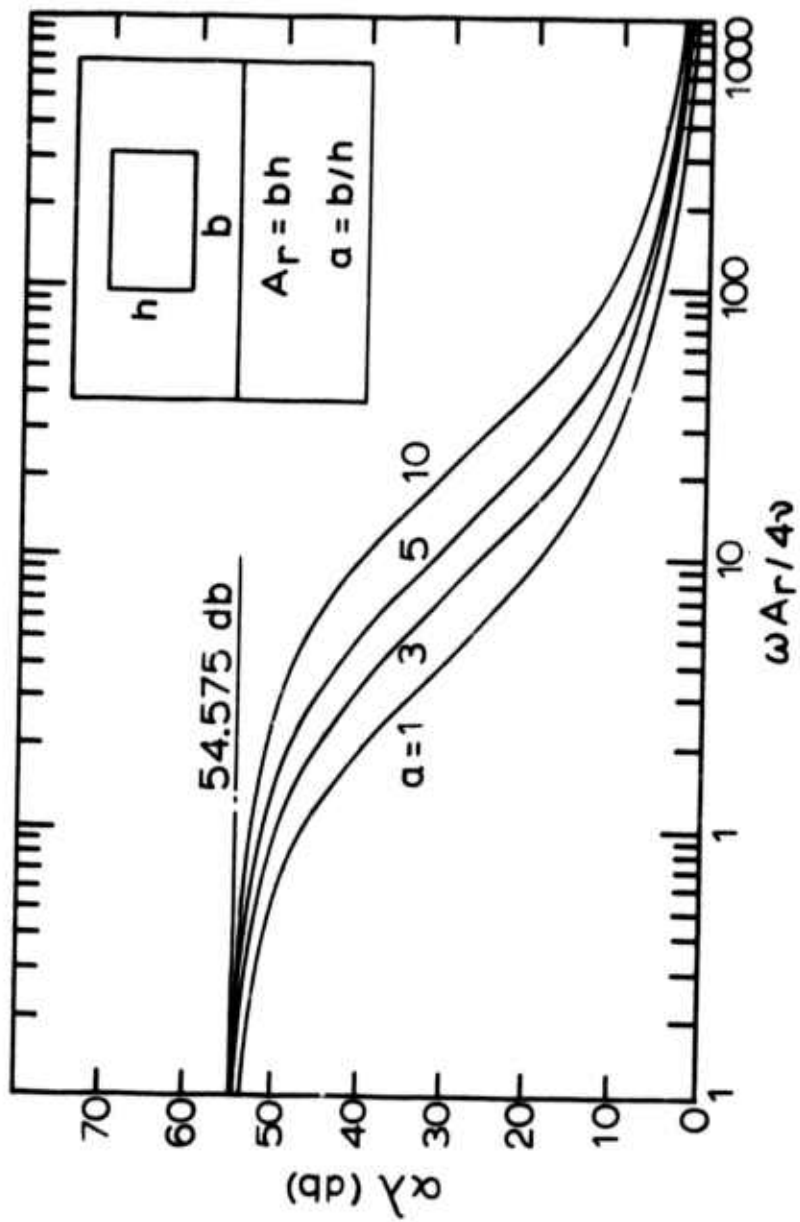


Fig. 1 Attenuation per line wavelength for rectangular lines

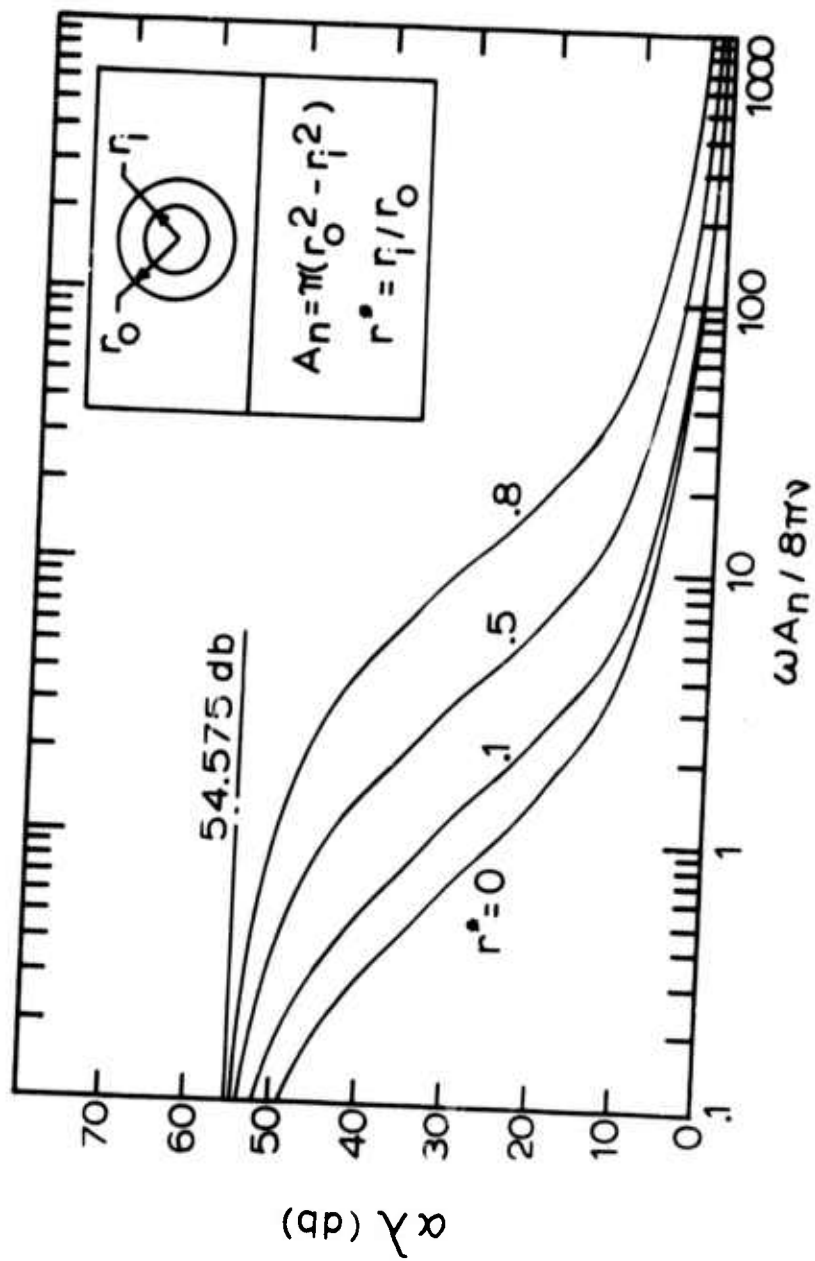


Fig. 2 Attenuation per line wavelength for annular lines

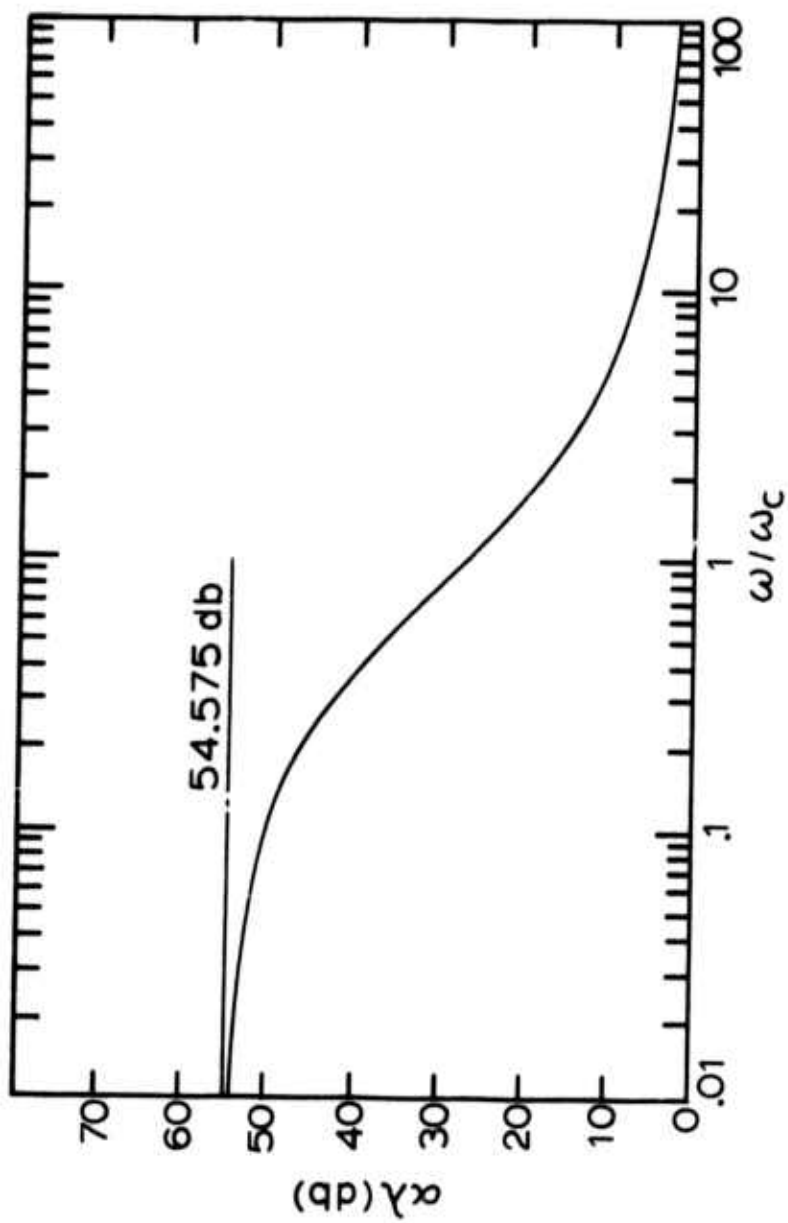


Fig. 3 Attenuation per line wavelength for circular, rectangular, and annular lines

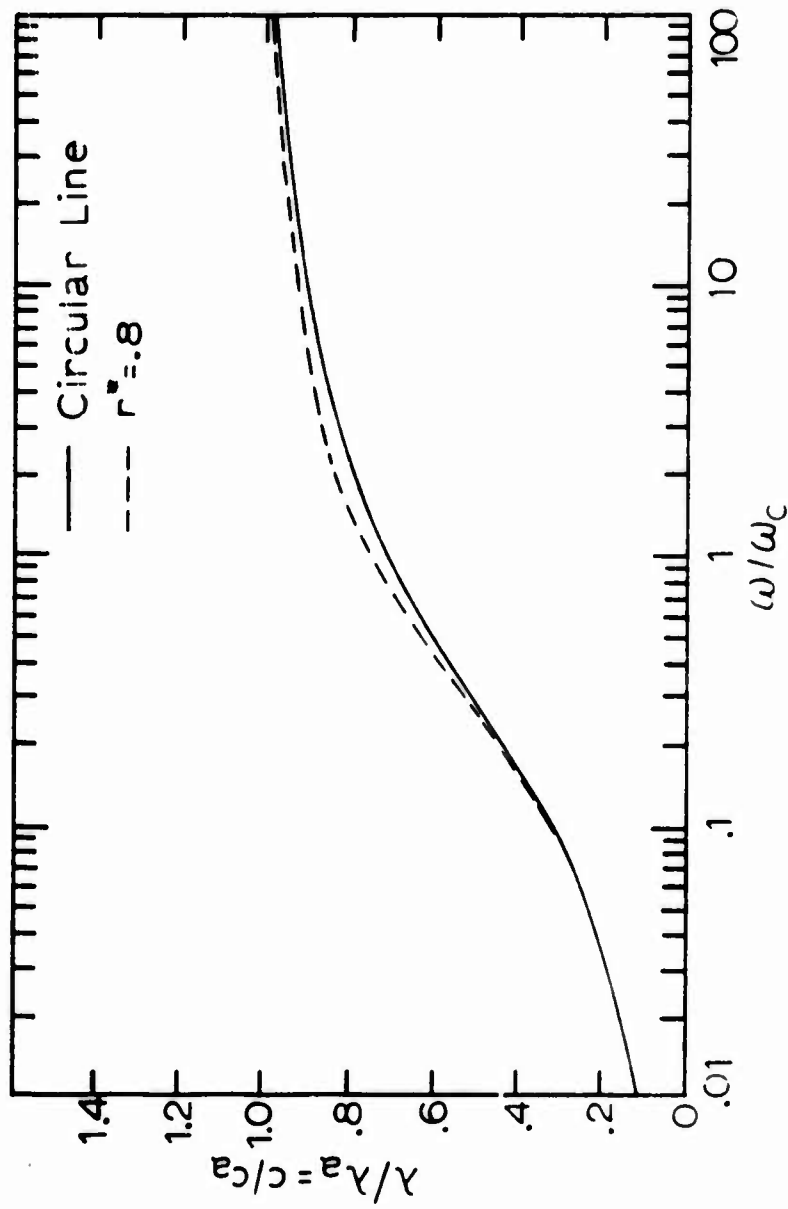


Fig. 4 Wavelength ratio for circular, rectangular, and annular lines

THE EFFECT OF THROUGHFLOW ON SIGNAL PROPAGATION IN
FLUID LINES

by

S. KATZ
A. HAUSNER
N. A. EISENBERG

To be presented at:
Harry Diamond Laboratories
Fluidic State-of-the-Art Symposium
30 Sep - 4 Oct 1974
Adelphi, Maryland

NOMENCLATURE

a	- speed of sound, m/sec
A	- cross sectional area, m ²
b	- $Mrg/[2(1-M^2)]$, m ⁻¹
B ₁	- arbitrary constant, kN-sec/m ²
B ₂	- arbitrary constant, kN-sec/m ²
C _a	- adiabatic capacitance per unit length, m ⁴ /kN
F	- $[8\omega/\omega_v]^{1/2}$ or $[(\pi P_n)/(2Dn)]^{1/2}$
g	- $(Z_{ca}/Z_c) + (Z_c/Z_{ca})$
h	- propagation constant
j	- $\sqrt{-1}$, complex operator
L _a	- adiabatic inertance per unit length, kN-sec ² /m ⁶
m	- $0.5 M [(Z_{ca}/Z_c) - (Z_c/Z_{ca})]$
N _d	- dissipation number, $\omega_v x/(8a)$
N _M	- Mach Number, U/a
N _p	- propagation number, $[2 \omega x/(\pi a)]$
N _{PR}	- Prandtl number
p	- absolute pressure, kN/m ²
P	- pressure signal in Laplace or frequency domain, kN-sec/m ²
P ₀	- entrance pressure in Laplace or frequency domain, kN-sec/m ²
r	- radial dimension, m
Q	- volume flow in Laplace or frequency domain, m ³
R	- tube radius, m
Q ₀	- entrance volume flow in Laplace or frequency domain, m ³
T	- absolute temperature, °K
\hat{u}	- Laplace transform of perturbation velocity, m
U	- steady throughflow velocity, m/sec
x	- axial distance along line, m
Y	- shunt admittance per unit length, m ⁴ /kN-sec
Y _c	- characteristic admittance, $[y/z]^{1/2}$, m ⁵ /kN-sec
Y _v	- variable shunt admittance per unit length, m ⁴ /kN-sec
Z	- series impedance per unit length, kN-sec/m ⁶
Z _c	- characteristic impedance, kN-sec/m ⁵
Z _{ca}	- adiabatic characteristic impedance, $[L_a/C_a]^{1/2}$, kN-sec/m ⁵
Z _{CT}	- characteristic impedance with throughflow, kN-sec/m ⁵
Z _{oo}	- input impedance of open line, kN-sec/m ⁵
Z _{oT}	- input impedance of line with throughflow, kN-sec/m ⁵
Z _L	- load impedance, kN-sec/m ⁵
Z _v	- variable series impedance per unit length, kN-sec/m ⁶

- γ - ratio of specific heats,
- Γ - complex propagation factor per unit length, m^{-1}
- Γ_a - adiabatic propagation factor per unit length, m^{-1}
- Γ_T - $\Gamma (1 + m^2)^{1/2} / (1 - M^2)$, m^{-1}
- Γ_v - variable complex propagation factor per unit length, m^{-1}
- ν - kinematic viscosity, m^2/sec
- ρ - density, kg/m^3
- ω - radial frequency, rad/sec
- ω_v - characteristic viscous frequency, rad/sec
- θ - Laplace transform of temperature, $^{\circ}K - sec$
- α - thermal diffusivity, m^2/sec

ABSTRACT

The propagation of small amplitude fluid signals superimposed on a steady throughflow is investigated analytically. A fixed component model and a variable component model are presented. In the fixed component model convective terms are added to the transmission line equations. In the variable component model the fluid equations are solved for a throughflow with a uniform velocity profile and the solution is then placed in the transmission line form.

Both models show that the characteristic impedance of the line changes with throughflow. The throughflow has more effect in the variable component model than in the fixed component model. In both models the real part of the characteristic impedance is almost independent of the direction of throughflow. At low frequencies the real part decreases with throughflow. When the frequency exceeds the viscous characteristic frequency, throughflow has virtually no effect on the characteristic impedance. The imaginary part of the characteristic impedance depends on the direction of throughflow. For large reverse throughflows the characteristic impedance is predominantly resistive.

1. INTRODUCTION

In fluidic circuits pressure and flow signals must be transported through fluid lines. The change in signal waveform during the passage of the signals has been the subject of numerous publications. This problem is not limited to the field of fluidics. Similar problems with different formulations and objectives have received widespread attention in closely allied fields. Examples of this are:

- 1) The propagation of sound in ducts is considered extensively in acoustics
- 2) The reduction of noise in ducts is investigated in aero-engineering, air conditioning and vibrations
- 3) Oscillating flow in pipes is studied in fluid mechanics and hydraulics

To organize the tremendous amount of technical information available on fluid signal propagation we will first attempt to sort out some of the important developments in the fluidics literature. This will also serve to place the current paper in some perspective.

A complete description of the behavior of fluid lines depends on circuit models and component models. In dealing with circuit models a primary consideration is whether the circuit must be considered as a distributive system or may be approximated in some convenient manner with lumps. When the length of the fluid line is much smaller than a wave length the line can be adequately modeled with a single lump. The single lump representation will be quite acceptable in fluidic applications where the signal frequencies are low or where the signals travel only a short distance. The single lumped circuit model probably covers a majority of the applications. As the line length increases relative to a wave length an accurate circuit model requires an increasing number of lumps. A point is reached where it is more accurate to treat the line with a distributed circuit model.

The distributive circuit model for fluid lines with small amplitude signals is the same as the circuit model for electrical transmission lines. The models are fully described in electrical engineering text books such as Ware and Reed [1] and King [2] and come from solutions of the telegraphers' equation. The transfer matrix of a two port model based on these solutions has found widespread use in the study of fluid line circuit models and appears in papers by Raizada [3], Oldenburger [4], [5], Reid [6], Goodson and Leonard [7], Brown [8], Sidell and Wormley [9] and many others. Various approximations to the distributed circuit models have been considered by Oldenburger and Goodson [10], Ansari and Oldenburger [11], Oldenburger [4], [5], Johnson and Wandling [12], Raizada [3], Kirshner and Katz [13], and others.

All of the above references [1 - 13] pertain to circuit models without through-flow. In fluidic applications the small amplitude pres-

sure and flow signals are often superimposed on a steady flow. The signal propagation with through-flow is usually treated numerically by the method of characteristics as shown in Streeter and Wylie [14] for hydraulic fluids and in Brown [15] for gases. However, an analytic formulation of the distributed circuit transfer matrix with through-flow has been approximated by Cooley [16] and Orner and Cooley [17].

The distributed circuit models describe the performance of the fluid line in terms of two components: a) the series impedance per unit length, Z and b) the shunt admittance per unit length, Y . Rather complete models of these components, including distributed friction and heat transfer effects, have been developed by Nichols [18] and Brown [19] for circular lines and by Schaedel [20] for rectangular lines. These component models involve Bessel functions and other infinite series. As a result the component models are often simplified or approximated. High and low frequency approximations to the component models are given by Nichols [18], Brown [19], Rohmann and Grogan [21]. Krishnaiyer and Lechner [22] and Karam and Franke [23]. Simplified component models are discussed by Goodson and Leonard [7], Kirshner and Katz [13] and others.

In the component models also, the effects of through-flow have received less attention. Brown, Margolis, and Shah [24] have adjusted the component models to include a turbulent through-flow. Small through-flows have been shown experimentally to have negligible effect on the transfer function of terminated fluid lines by Franke, Karam, and Lymburner [25], and Franke, Malanowski, and Martin [26].

Orner [27] has used the basic fluid equations to show that throughflow alters both the transfer matrix and the component model. He assumed a fully developed parabolic throughflow.

In this paper we present and compare two approaches to the through-flowing line. One approach, the fixed component model, is an extension of the work done by Cooley [16] and Orner and Cooley [17]. In this approach we develop the exact transfer matrix with the assumption that the component models are not functions of throughflow and are known in advance. The matrix is then used in conjunction with the Nichols-Brown (no throughflow) component model to approximate the effect of throughflow on signal propagation. The other approach, the variable component model, is similar to that of Orner [27] except that the steady throughflow is assumed to have a uniform velocity profile. This approach produces a change in transfer matrix as well as a change in the series and shunt component models.

2. THE FIXED COMPONENT MODEL

2.1 Basic Equations

Figure 1 shows a schematic drawing of the entrance section of a fluid transmission line with uniform through-flow. The velocity of the

steady through-flow is designated as U . The small amplitude signal variables, pressure (P) and volume flow (Q) are in the Laplace or frequency domain and refer to conditions at some axial distance, x , along the line from the entrance. The initial conditions at the entrance to the line ($x = 0$) are called P_0 and Q_0 .

The basic equations that apply to this case come from the momentum and continuity equations of fluid mechanics. Orner and Cooley [17] and Brown [15] express these equations in the form:

$$L_a U \frac{\partial Q}{\partial x} + \frac{\partial P}{\partial x} + ZQ = 0 \quad (1a)$$

$$C_a U \frac{\partial P}{\partial x} + \frac{\partial Q}{\partial x} + Y P = 0 \quad (1b)$$

with the bounding values,

$$\text{at } x = 0, P = P_0, Q = Q_0$$

where L_a is the adiabatic inertance per unit length ($L_a = \rho/A$), C_a is the adiabatic capacitance per unit length ($C_a = A/\gamma p$), Z is the series impedance per unit length, and Y is the shunt admittance per unit length.

Equations 1a and 1b are in the usual transmission line form except for the convective first terms in each equation ($L_a U \partial Q/\partial x$ and $C_a U \partial P/\partial x$). As stated by Orner and Cooley [17] these convective terms represent the effect of through-flow by a Doppler shift. Thus in this formulation the series impedance and shunt admittance (Z and Y) are assumed to be independent of the through-flow. This assumption allows us to proceed directly with the solutions of equations 1a and 1b, after which we may use one of the line models (that was determined without through-flow) for Z and Y .

Let us first separate the signal variables in the basic equations. If equation 1(b) is multiplied by $L_a U$ and subtracted from equation 1(a) we obtain:

$$Q = \frac{U Y L_a P - (1 - N_M^2) \partial P / \partial x}{Z} \quad (2)$$

where $N_M^2 = L_a C_a U^2 = \text{Mach number squared}$

Differentiation of equation 2 and combination with equation 1(b) leads to:

$$(1 - N_M^2) \frac{\partial^2 P}{\partial x^2} - N_M \Gamma g \frac{\partial P}{\partial x} - \Gamma^2 P = 0 \quad (3)$$

where the propagation factor without through-flow $\Gamma = \sqrt{ZY}$, $g = \frac{Z_{Ca}}{Z_c} + \frac{Z_c}{Z_{Ca}}$
 Z_c is the characteristic impedance without through-flow ($Z_c = \sqrt{Z/Y}$) and Z_{Ca}
is the adiabatic characteristic impedance ($Z_{Ca} = \sqrt{L_a/C_a}$).

Now when P is found from a solution of equation 3, Q may be determined from equation 2.

2.2 Transfer Matrix with Throughflow

From elementary differential equation theory the solution of equation 3 is:

$$P = e^{bx} [B_1 e^{\Gamma_T x} + B_2 e^{-\Gamma_T x}] \quad (4)$$

where

$$b = \frac{N_M \Gamma g}{2(1 - N_M^2)}$$

$$\Gamma_T = \frac{\Gamma (1 + m^2)^{\frac{1}{2}}}{1 - N_M^2}$$

$$m = \frac{N_M}{2} \left[\frac{Z_{ca}}{Z_c} - \frac{Z_c}{Z_{ca}} \right]$$

and B_1 and B_2 are arbitrary constants. An expression for Q in terms of the arbitrary constants can be obtained by applying equation 4 in equation 2. After some algebraic manipulation the results for P and Q in matrix notation are:

$$\begin{pmatrix} P \\ Q \end{pmatrix} = e^{bx} \begin{pmatrix} e^{\Gamma_T x} & e^{-\Gamma_T x} \\ e^{\Gamma_T x} Y_c (m - \sqrt{1 + m^2}) & e^{-\Gamma_T x} Y_c (m + \sqrt{1 + m^2}) \end{pmatrix} \begin{pmatrix} B_1 \\ B_2 \end{pmatrix} \quad (5)$$

$$\text{where } Y_c = \frac{1}{Z_c} = \sqrt{Y/Z}$$

If we now use the boundary conditions that at $x = 0$, $P = P_0$ and $Q = Q_0$, matrix 5 becomes

$$\begin{vmatrix} P_0 \\ Q_0 \end{vmatrix} = \begin{vmatrix} 1 & 1 \\ Y_c (m - \sqrt{1+m^2}) & Y_c (m + \sqrt{1+m^2}) \end{vmatrix} \begin{vmatrix} B_1 \\ B_2 \end{vmatrix} \quad (6)$$

To obtain the transfer matrix we note that the inverse of matrix 5 may be expressed as

$$\begin{vmatrix} B_1 \\ B_2 \end{vmatrix} = \frac{e^{-bx}}{2\sqrt{1+m^2}} \begin{vmatrix} e^{-\Gamma_T x} (m + \sqrt{1+m^2}) & -Z_c e^{-\Gamma_T x} \\ -e^{\Gamma_T x} (m - \sqrt{1+m^2}) & Z_c e^{\Gamma_T x} \end{vmatrix} \begin{vmatrix} P \\ Q \end{vmatrix} \quad (7)$$

The multiplication of matrices 6 and 7 now leads to:

$$\begin{vmatrix} P_0 \\ Q_0 \end{vmatrix} = \frac{e^{-bx}}{\sqrt{1+m^2}} \begin{vmatrix} (\sqrt{1+m^2} \cosh \Gamma_T x & Z_c \sinh \Gamma_T x \\ -m \sinh \Gamma_T x & \sqrt{1+m^2} \cosh \Gamma_T x \\ Y_c \sinh \Gamma_T x & + m \sinh \Gamma_T x \end{vmatrix} \begin{vmatrix} P \\ Q \end{vmatrix} \quad (8)$$

Matrix 8 is the transfer matrix of the fluid line with through-flow. Cooley [16] and Orner and Cooley [17] obtain a similar formulation by approximating the roots of equation 3.

When there is no through-flow, $N_M = m = b = 0$, and matrix 8 reduces to the familiar form:

$$\begin{pmatrix} P_o \\ Q_o \end{pmatrix} = \begin{pmatrix} \cosh \Gamma x & Z_c \sinh \Gamma x \\ Y_c \sinh \Gamma x & \cosh \Gamma x \end{pmatrix} \begin{pmatrix} P \\ Q \end{pmatrix} \quad (9)$$

2.3 Characteristic Impedance With Through-Flow

The determination of characteristic impedance may be approached in several different ways. First, from the basic definition of characteristic impedance as the input impedance of an infinite length of line open at the end. Second, from the fact that a finite length of line loaded with its characteristic impedance is a matched line (no reflections) and therefore has the same input impedance as an infinite line. Still another way of looking at characteristic impedance is as the load impedance which makes the input impedance independent of line length. All of these approaches lead to the same result. To demonstrate this let us begin by writing the input impedance, Z_{oT} , of a throughflowing line loaded with an impedance, Z_L (where $P = Z_L Q$). From matrix 8 we obtain:

$$\frac{P_o}{Q_o} = Z_{oT} = \frac{Z_L \sqrt{1 + m^2} + (Z_c - m Z_L) \tanh \Gamma_T x}{\sqrt{1 + m^2} + (m + Y_c Z_L) \tanh \Gamma_T x} \quad (10)$$

From the first definition, the characteristic impedance of a line with through-flow is:

$$Z_{CT} = \lim_{x \rightarrow \infty} Z_{oT} \quad \text{when } Z_L = 0 \quad (11)$$

If we apply the definition given in equation 11 in conjunction with equation 10 the result is:

$$Z_{CT} = \frac{Z_c}{\sqrt{1 + m^2} + m} = Z_c [\sqrt{1 + m^2} - m] \quad (12)$$

When $m = 0$, the characteristic impedance is the same as for the line without through-flow. Now $m = 0$ if either the Mach number is zero or $Z_c = Z_{Ca}$. This latter conditions occurs at high frequencies. Thus we will just state here and show more clearly in Section 2.7 that the characteristic impedance becomes independent of throughflow for high frequency signals.

Another way to obtain the result given in equation 12 is to use the second method; thus, write equation 10 with $Z_{cT} = Z_{oT} = Z_L$. This leads to the quadratic equation:

$$Y_c Z_{cT}^2 + 2m Z_{cT} - Z_c = 0 \quad (13)$$

and the positive root of equation 13 is:

$$Z_{cT} = \frac{\sqrt{1 + m^2} - m}{Y_c} = Z_c [\sqrt{1 + m^2} - m] \quad (14)$$

2.4 The Input Impedance of Open Lines with Throughflow

Equation 10 represents the general expression for the input impedance of a line terminated with load impedance, Z_L . As a specific example let us now formulate the input impedance for the case of the open tube.

For the open tube of finite length there is zero ambient pressure at the output and thus $Z_L = 0$. In this case the input impedance, Z_{oo} , from equation 10 reduces to:

$$Z_{oo} = \frac{Z_c \tanh \Gamma_T x}{\sqrt{1 + m^2} + m \tanh \Gamma_T x} \quad (15)$$

If in addition to the tube being open at the end, the Mach number equals 1, then Γ_T approaches infinity and $\tanh \Gamma_T x$ approaches unity. As a result equation 15 becomes:

$$(Z_{oo})_{N_M = 1} = \frac{Z_c}{\sqrt{1 + m^2} + m} = Z_{cT} \quad (16)$$

and we obtain the result that an open tube with a throughflow Mach number equal to unity has an input impedance equal to the characteristic impedance. Therefore, the line is matched. We could have anticipated

this result since at $N_M = 1$ there can be no signal propagation upstream and no reflections.

2.5 Transfer Function of Terminated Line with Throughflow

The pressure transfer function of the terminated line with throughflow can be obtained from matrix 8 with $P = Z_L Q$. The result is:

$$\begin{bmatrix} P \\ P_0 \end{bmatrix} = \frac{e^{bx} \sqrt{1+m^2}}{\sqrt{1+m^2} \cosh \Gamma_T x + \left(\frac{Z_C}{Z_L} - m\right) \sinh \Gamma_T x} \quad (17)$$

2.5.1 Matched Line

When the line is loaded with its characteristic impedance (equation 12), the transfer function given in equation 17 becomes:

$$\begin{bmatrix} P \\ P_0 \end{bmatrix} = \frac{e^{bx}}{\cosh \Gamma_T x + \sinh \Gamma_T x} = e^{-(\Gamma_T - b)x} \quad (18)$$

$$Z_L = Z_{CT}$$

The quantity $(\Gamma_T - b)$ is the propagation operator with throughflow. From the definitions following equation 4, the propagation operator with throughflow may be expressed as:

$$(\Gamma_T - b) = \left[\frac{\Gamma}{1 - N_M^2} \right] \left[-\frac{N_M g}{2} + (1 + m^2)^{1/2} \right]. \quad (19)$$

At high frequencies, m approaches zero and g approaches 2. Thus, equation 19 may be approximated as:

$$(\Gamma_T - b) \approx \frac{\Gamma}{1 + N_M}. \quad (20)$$

The effect of the throughflow on high frequency signals is to reduce attenuation and increase propagation speed by a factor of $1 + N_M$.

2.6 Nichols-Brown Component Model

Thus far we have considered only the circuit formulation for various cases with throughflow. To demonstrate the effect of throughflow we must choose component models for the series impedance and shunt

admittance. The component models chosen come from the work of Nichols [18] and Brown [19], and we place them in the forms:

$$\frac{Z}{\omega L_a} = \frac{j}{\left[1 - \frac{2 J_1(j^{3/2} F)}{j^{3/2} F J_0(j^{3/2} F)}\right]} \quad (21a)$$

$$\frac{Y}{\omega C_a} = j \left[1 + \frac{2(\gamma - 1) J_1(j^{3/2} \sqrt{N_p} F)}{j^{3/2} \sqrt{N_p} F J_0(j^{3/2} \sqrt{N_p} F)}\right] \quad (21b)$$

where

$$F = [8 \omega / \omega_v]^{1/2} = [(\pi N_p) / (2 N_d)]^{1/2},$$

$$\omega_v = \frac{8\pi v}{A} = \text{characteristic viscous frequency,}$$

$$N_p = \frac{2}{\pi} \left(\frac{\omega X}{a}\right) = \text{propagation number,}$$

$$N_d = \frac{1}{8} \left(\frac{\omega_v X}{a}\right) = \text{dissipation number,}$$

$$v = \text{kinematic viscosity, and}$$

$$N_{pR} = \text{Prandtl number.}$$

Also, the following relations are useful in evaluating the circuit model.

$$\frac{Z_c}{Z_{Ca}} = \left[\left(\frac{Z}{\omega L_a}\right) / \left(\frac{Y}{\omega C_a}\right) \right]^{1/2} \quad (22a)$$

$$\Gamma_x = \frac{\pi N_p}{2} \left[\left(\frac{Z}{\omega L_a}\right) \left(\frac{Y}{\omega C_a}\right) \right]^{1/2} \quad (22b)$$

This completes the development of the fixed component model. The theoretical results obtained from this model are discussed in section 2.7.

2.7 Effects of Throughflow (Fixed Component Model)

The parameters of fluid lines that we have considered (i.e., characteristic impedance, propagation factor and the input impedance, and transfer function with various terminations) are all complex quantities. The derived expressions for these quantities are also rather involved in complex algebra. Thus, although we may observe and call attention to the

effects of the superimposed throughflow, we are unable in general to explain the result in physical terms.

Figures 2 and 3 show the effects of throughflow on the real and imaginary parts of the characteristic impedance. When the signal frequency exceeds the viscous characteristic frequency ($\omega/\omega_v \geq 1$), the characteristic impedance is predominantly resistive and is virtually independent of throughflow. Since throughflow acts to alter phase relations, the frequency region with negligible phase dependency is unaffected. At low frequencies ($\omega/\omega_v < 0.1$), there are two effects: (1) the real part of Z_{CT} decreases with throughflow but is independent of the throughflow direction, and (2) the imaginary part of Z_{CT} increases for reverse flow and decreases for forward flow. As a result, the characteristic impedance of a line with a large reverse flow is almost entirely resistive at all signal frequencies.

In contrast to the characteristic impedance, the input impedance of a line depends on the line length. This adds another parameter to the input impedance formulation. As a result we plot input impedance versus propagation number for a particular value of dissipation number. The effect of throughflow on line input impedance is shown in figures 4 and 5 for the open line. The dissipation number is fixed at 0.01. To accentuate the effect of throughflow, the Mach number used is 0.3. At lower Mach numbers, particularly those of 0.1 and less, the throughflow effect is so small that it is difficult to distinguish from the case without throughflow. The figures show that the input impedance curves are shifted leftward by the throughflow and that the difference in the amplitude of the peaks is small. Thus, the principal effect of throughflow is to make the line appear shorter.

3. VARIABLE COMPONENT MODEL

Let us begin by introducing the transmission line equations:

$$\frac{\partial P}{\partial x} = -Z_v Q \quad (23a)$$

$$\frac{\partial Q}{\partial x} = -Y_v P \quad (23b)$$

where in this case Z_v and Y_v are the series impedance and shunt admittance that are functions of throughflow. The corresponding propagation operator for throughflow, Γ_v , is then

$$\Gamma_v^2 = Z_v Y_v \quad (24)$$

If equation 24 is normalized with the adiabatic propagation factor ($\Gamma_a = j \omega \sqrt{L_a C_a}$), the result is:

$$\frac{a^2 \Gamma_v^2}{\omega^2} = \left(\frac{Z_v}{\omega L_a}\right) \left(\frac{Y_v}{\omega C_a}\right) \quad (25)$$

Now Γ_v may be expressed in terms of a propagation constant, h , so that $\Gamma_v = \omega h/a$. Thus, equation 25 becomes:

$$h^2 = \left(\frac{Z_v}{\omega L_a}\right) \left(\frac{Y_v}{\omega C_a}\right) \quad (26)$$

At this point we turn to the momentum, continuity, and energy equations. Our objective is to obtain a solution of these equations for the case of a small perturbation signal superimposed on a uniform throughflow. Following this, the solution will be placed in the form of the transmission line equations 23a and 23b.

3.1 Basic Equations

In terms of Laplace transform variables, the momentum, continuity, and energy equations may be written as:

$$U \frac{\partial \hat{u}}{\partial x} + \frac{1}{\rho} \frac{\partial P}{\partial x} + s \hat{u} - \frac{v}{r} \frac{\partial}{\partial r} \left(r \frac{\partial \hat{u}}{\partial r} \right) = 0 \quad (27a)$$

$$\frac{U}{\rho} \frac{\partial P}{\partial x} + \frac{\partial \hat{u}}{\partial x} + s \left[\frac{P}{\rho} - \frac{\theta}{T} \right] - \frac{U}{T} \frac{\partial \theta}{\partial x} = 0 \quad (27b)$$

$$U \frac{\partial \theta}{\partial x} + (\gamma - 1) T \frac{\partial \hat{u}}{\partial x} s \theta - \frac{\alpha}{r} \frac{\partial}{\partial r} \left(r \frac{\partial \theta}{\partial r} \right) = 0 \quad (27c)$$

where \hat{u} and θ are the Laplace transforms of the perturbation velocity, and temperature; T is the absolute temperature and α is the thermal diffusivity.

The method of separation of variables leads to the solutions of equations 27 in the form:

$$\hat{u} = \frac{P_o \Gamma_v e^{\Gamma_v x}}{\rho v B^2} \left[\frac{J_o(jBr)}{J_o(jBR)} - 1 \right] \quad (28a)$$

$$\theta = \frac{T(\gamma - 1) P_0 e^{\Gamma_V x}}{\Gamma_P} \left[1 - \frac{J_0(j B \sqrt{N_P} R)}{J_0(j B \sqrt{N_P} R)} \right] \quad (28b)$$

$$P = P_0 e^{\Gamma_V x} \quad (28c)$$

where $B = ([s + U \Gamma_V] / v)^{1/2}$,
 $R =$ tube radius.

The integration of equations 28 over the cross section leads to:

$$Q = \frac{A P_0 \Gamma_V e^{\Gamma_V x}}{2 v B^2} \left[\frac{2 J_1(j B R)}{j B R J_0(j B R)} - 1 \right] \quad (29a)$$

$$\frac{\bar{h}}{h} = \frac{T(\gamma - 1) P_0 e^{\Gamma_V x}}{\gamma P} \left[1 - \frac{2 J_1(j B \sqrt{N_P} R)}{j B \sqrt{N_P} R J_0(j B \sqrt{N_P} R)} \right] \quad (29b)$$

where we note that

$$B R = \left(8 \frac{\omega}{\omega_V} \right)^{1/2} (j + N_M h)^{1/2} \quad (29c)$$

If we use equations 28c and 29a to obtain a relation of the type indicated in equation 23a, we find that

$$Z_V = \frac{L_a v B^2}{\left[1 - \frac{2 J_1(j B R)}{j B R J_0(j B R)} \right]} \quad (30)$$

Since B is a function of Γ_V (or h), then Z_V is also a function of Γ_V (or h).

Now if we average the terms in the continuity equation 27b and apply equation 29b, the result may be placed in the form of equation 23b; thus, we obtain:

$$Y_V = C_a v \beta^2 \left[1 + \frac{2(\gamma - 1) J_1(j \beta \sqrt{N_p} R)}{j \beta \sqrt{N_p} R J_0(j \beta \sqrt{N_p} R)} \right] \quad (31)$$

Here again we should note that Y_V is a function of λ_V (or h).

The substitution of equations 30 and 31 into equation 26 leads to a transcendental equation in the propagation constant, h . From this, h can be determined numerically and the result used in equations 30 and 31 to show the effects of throughflow on the series impedance and shunt admittance.

In addition, the characteristic impedance with throughflow, Z_{CT} , is equal to $[Z_V/Y_V]^{1/2}$ for the variable component case.

3.2 Effects of Throughflow (Variable Component Model)

Figures 6 and 7 show the effects of throughflow on the imaginary parts of the series impedance (inertance) and the shunt admittance (capacitance). In figure 6, for zero Mach number the normalized inertance goes from 1.333 at low frequencies to 1.000 at high frequencies. For positive Mach numbers, the normalized inertance of the line decreases as Mach number increases; and for reverse throughflow, the inertance increases as the Mach number decreases. The effects of throughflow on capacitance (fig. 7) is very similar to that of the inertance (fig. 6). Throughflow has only a small effect on the real parts of the series impedance and shunt admittance.

The variable component model shows the effects of the throughflow on the series impedance and shunt admittance. However, these parameters do not provide a basis for comparing the variable and fixed component models. The reason for this is that the fixed component model takes throughflow into account by a convective term in the modified transmission-line equation 1, whereas the variable component model uses the transmission-line equations 23.

To compare the two models, we may examine the characteristic impedance of the line with throughflow. The real parts of the characteristic impedance determined from the fixed and variable component models are compared in figure 8 for $N_M = 0.3$. When ω/ω_v is less than 0.1, the variable model characteristic impedance is smaller than that of the fixed model. Since the fixed model values at low frequencies are already less than the case without throughflow (fig. 2), the variable component model tends to produce larger deviations from the case without throughflow. Thus, the effects of throughflow are enhanced by taking the component variation into account. In comparing the imaginary parts of the characteristic impedance (fig. 9), the same conclusions apply.

4. SUMMARY

The description of fluid transmission lines consists of a circuit representation and then an evaluation of the components in the circuit. We investigated the propagation of small amplitude fluid signals superimposed on a steady throughflow of uniform velocity. Two types of distributed circuits were assumed. In one type of distributed circuit, the components are fixed at their values without throughflow and the effects of throughflow are a direct consequence of the particular circuit formulation selected. The other distributed circuit is the conventional transmission line arrangement. In this case the effects of throughflow are taken into account by variations in the components.

The fixed component model and the variable component model provide distinct approximations of the influence of throughflow. Both models show that throughflow alters the characteristic impedance of the line. The variable component model produces larger changes than does the fixed component model. In general, the results demonstrate that the real part of the characteristic impedance is practically independent of the throughflow direction and at low frequencies it decreases as throughflow increases. When the frequency exceeds the viscous characteristic frequency throughflow does not affect the characteristic impedance. The reactance portion of the characteristic impedance, on the other hand, depends on the direction of throughflow. For large reverse flow, the characteristic impedance is predominantly resistive throughout the frequency range.

A major effect of throughflow on terminated lines is to make the lines appear shorter. This is a consequence of the increased speed of signal propagation.

5. LITERATURE CITED

- (1) Ware, L. A. and H. R. Reed, "Communications Circuits," John Wiley & Sons, 1949, pp 71-120.
- (2) King, R. W. P., "Transmission Line Theory," McGraw-Hill Company, 1955.
- (3) Raizada, R. S., "Linear Dynamic Properties of Fluid Transmission Lines," Fluid Control Systems, Engineering Proceedings P-45, The Pennsylvania State University, March 1967, pp 27-57.
- (4) Oldenburger, R., "Infinite-Product Analysis of Fluid Transmission Lines," Fluid Control Systems, Engineering Proceedings P-45, The Pennsylvania State University, March 1967, pp 58-69.
- (5) Oldenburger, R., "Theory of Distributed Systems," Journal of Basic Engineering, Transactions ASME Series D, Vol. 92, No. 1, March 1970, pp 1-10.
- (6) Reid, K. N., "Fluid Transmission Lines," Short Course In Fluid Control Systems, Oklahoma State University, 1968.
- (7) Goodson, R. E. and R. G. Leonard, "A Survey of Modeling Techniques for Fluid Line Transients," Journal of Basic Engineering, Transactions ASME Series D, Vol. 94, No. 2, June 1972, pp 474-482.
- (8) Brown, F. T., "A Unified Approach to the Analysis of Uniform One-Dimensional Distributed Systems," Journal of Basic Engineering Transactions ASME Series D, Vol. 89, No. 2, pp 423-432.
- (9) Sidell, R. S. and D. N. Wormley, "Transient and Frequency Modulated Signal Transmission In Fluid Lines and Networks," Massachusetts Institute of Technology Report EPL-72-70167-2.
- (10) Oldenburger, R. and R. E. Goodson, "Simplification of Hydraulic Line Dynamics By Use of Infinite Products," Journal of Basic Engineering Transactions ASME Series D, Vol. 86, 1964, pp 1-10.
- (11) Ansari, J. S. and R. Oldenburger, "Propagation of Disturbance in Fluid Lines," Journal of Basic Engineering Transactions ASME Series D, Vol. 89, No. 2, June 1967, pp 371-378.
- (12) Johnson, B. L. and D. E. Wandling, "Transfer Functions and Input Impedances of Pressurized Piping Systems," Journal of Basic Engineering Transactions ASME Series D, Vol. 89, No. 2, June 1967, pp 440-444.
- (13) Kirshner, J. M. and S. Katz, "Design Theory of Fluidic Components," Academic Press Publication in January 1975.

- (14) Streeter, V. L. and E. B. Wylie, "Hydraulic Transients," McGraw-Hill Book Company, 1967.
- (15) Brown, F. T., "A Quasi Method of Characteristics with Application to Fluid Lines with Frequency Dependent Wall Shear and Heat Transfer," Journal of Basic Engineering, Transaction ASME Series D, Vol. 91, No. 2, June 1969, pp 217-227.
- (16) Cooley, W. C., "Experimental Study of Through-Flowing Pneumatic Lines," MS Thesis, Case Institute of Technology, January 1969.
- (17) Orner, P. A. and W. C. Cooley, "Experimental Study of Through-Flowing Pneumatic Lines," Journal of Basic Engineering, Transactions ASME Series D, Vol. 92, No. 4, December 1970, pp 849-856.
- (18) Nichols, N. B., "The Linear Properties of Pneumatic Transmission Lines," Transactions of the Instrument Society of America, Vol. 1, 1962, pp 5-14.
- (19) Brown, F. T., "The Transient Response of Fluid Lines," Journal of Basic Engineering, Transactions ASME Series D, Vol. 84, No. 4, December 1962, pp 547-553.
- (20) Schaedel, H., "A Theoretical Investigation of Fluidic Transmission Lines with Rectangular Cross Section," Paper K3, Third Cranfield Conference, May 1968.
- (21) Rohmann, C. P. and E. C. Grogan, "On the Dynamics of Pneumatic Transmission Lines," Transactions ASME Vol. 79, 1957, p 853.
- (22) Krishnaiyer, R. and T. J. Lechner, "An Experimental Evaluation of Fluidic Transmission Line Theory," Advances In Fluidics ASME Publication, May 1967.
- (23) Karam, J. T. and M. E. Franke, "The Frequency Response of Pneumatic Lines," Journal of Basic Engineering Transactions, ASME Series D, Vol. 89, No. 2, June 1967, pp 371-378.
- (24) Brown, F. T., D. L. Margolis and R. P. Shah, "Small-Amplitude Frequency Behavior of Fluid Lines with Turbulent Flow," Journal of Basic Engineering Transactions ASME Series D, Vol. 91, No. 4, December 1969, pp 678-693.
- (25) Franke, M. E., J. T. Karam, Jr. and F. C. Lymburner, "Experimental Frequency Response of Fluidic Transmission Lines," Fourth Cranfield Conference, Sponsored by British Hydromechanics Research Association. March 1970, Paper E1.
- (26) Franke, M. E., A. J. Malanowski, and P. S. Martin, "Effects of Temperature, End Conditions, Flow, and Branching on the Frequency Response of Pneumatic Lines," Journal of Dynamic Systems, Measurement Control, Transactions ASME Series G, Vol. 94, No. 1, March 1972, pp 15-20.

- (27) Orner, P. A., "Linear Dynamic Modelling of Flowing Fluid Lines,"
Journal of Basic Engineering, Transactions ASME Series D, Vol. 91,
No. 4, December 1969, pp 740-749.

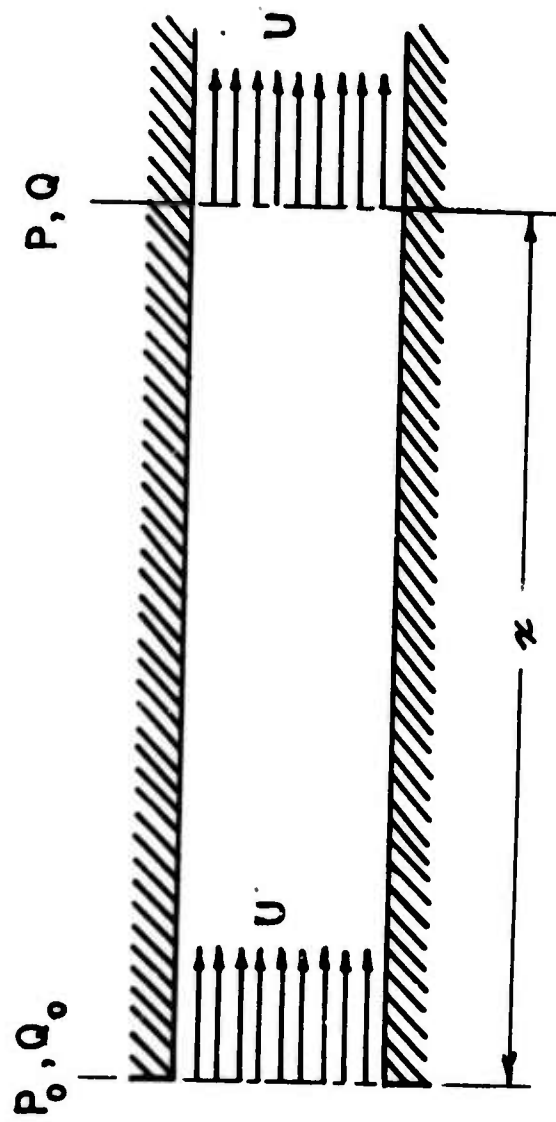


Figure 1. Fluid Transmission Line

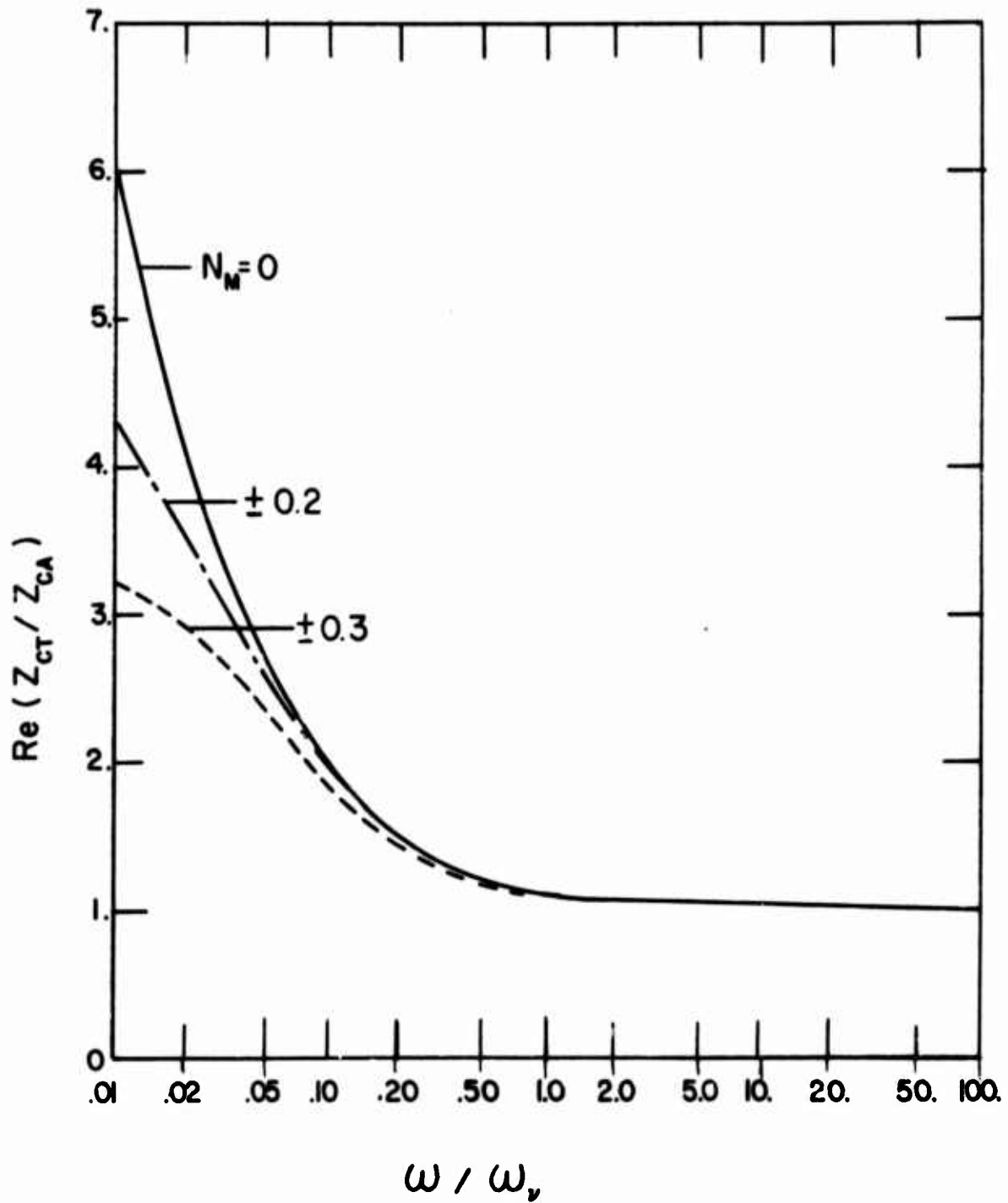


Figure 2. Real Part of Normalized Characteristic Impedance with Throughflow versus normalized angular frequency

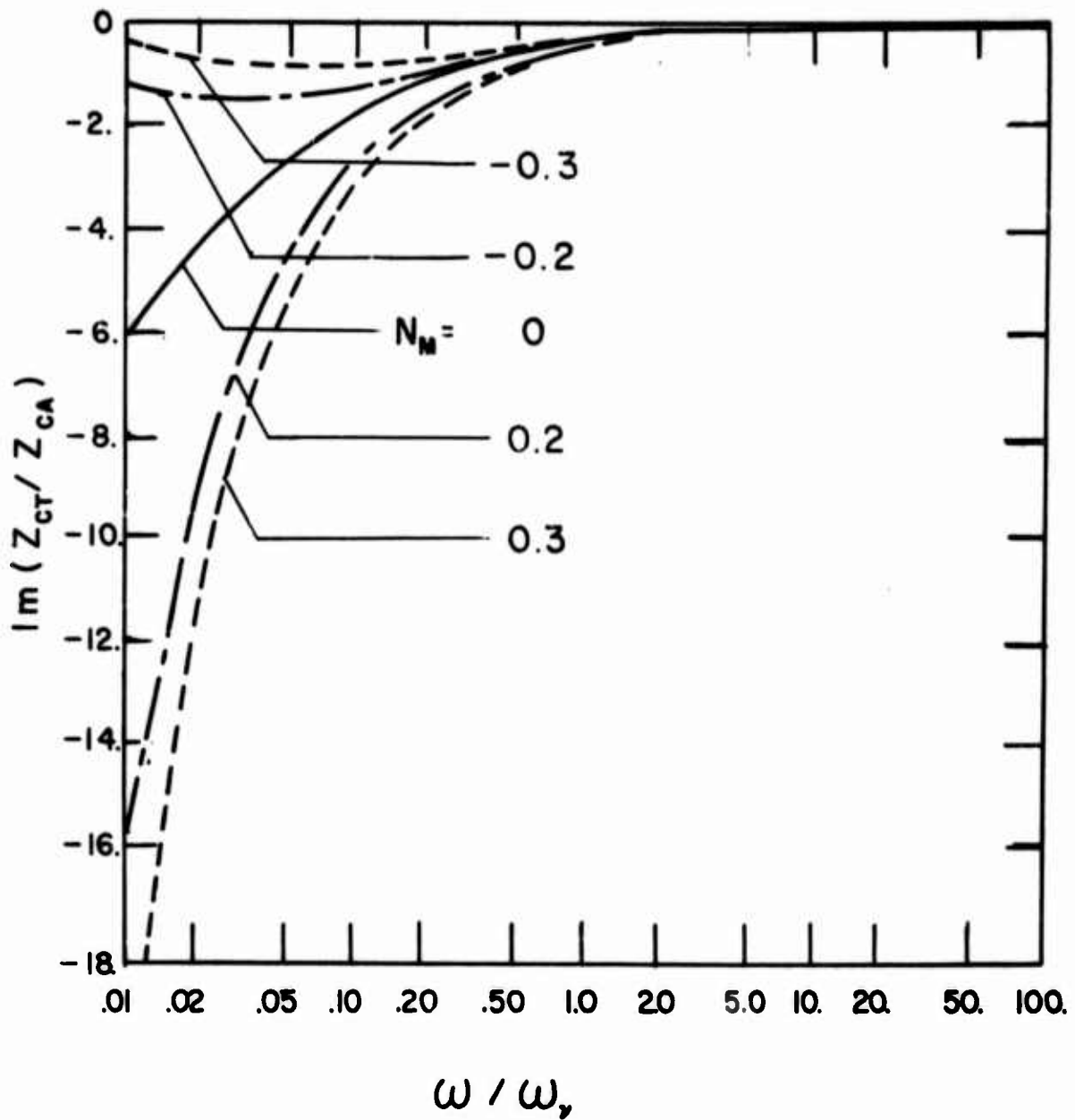


Figure 3. Imaginary Part of Normalized Characteristic Impedance with Throughflow versus Normalized angular Frequency

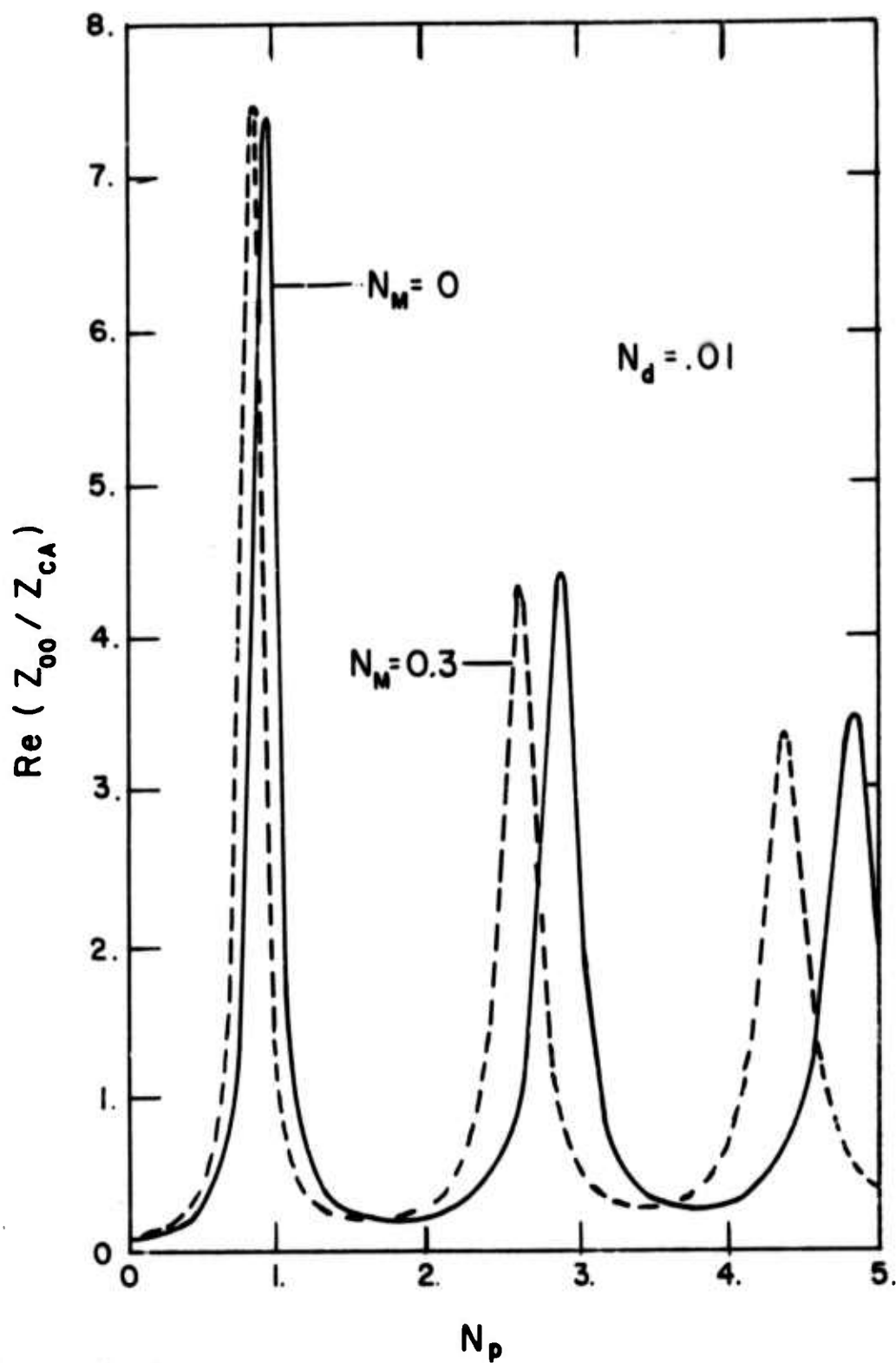


Figure 4. Real Part of Normalized Input Impedance of Open Line with Throughflow versus Propagation Number ($Z_L = 0$)

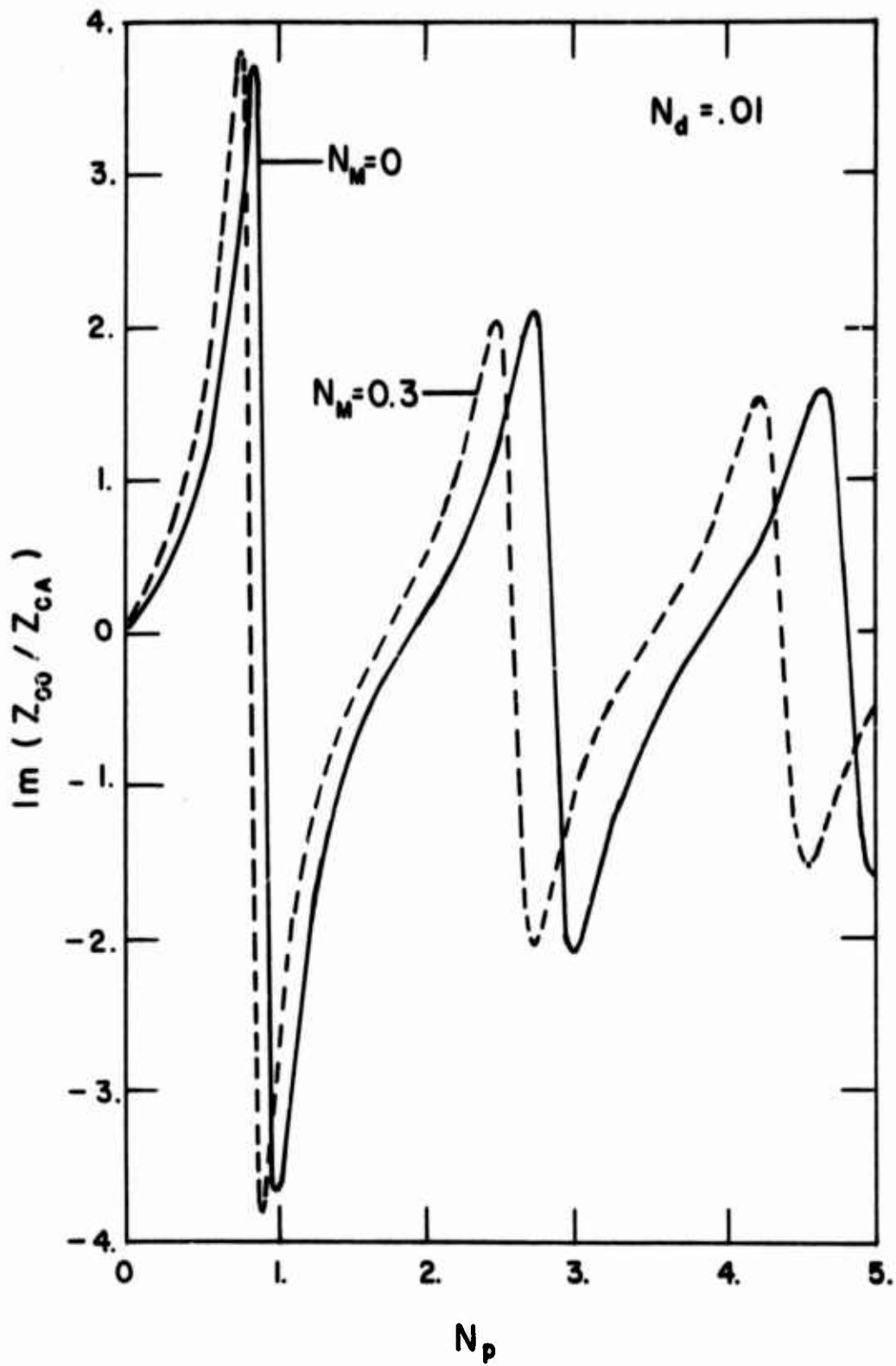


Figure 5. Imaginary Part of Normalized Input Impedance of Open Line with Throughflow versus Propagation Number ($Z_L = \infty$)

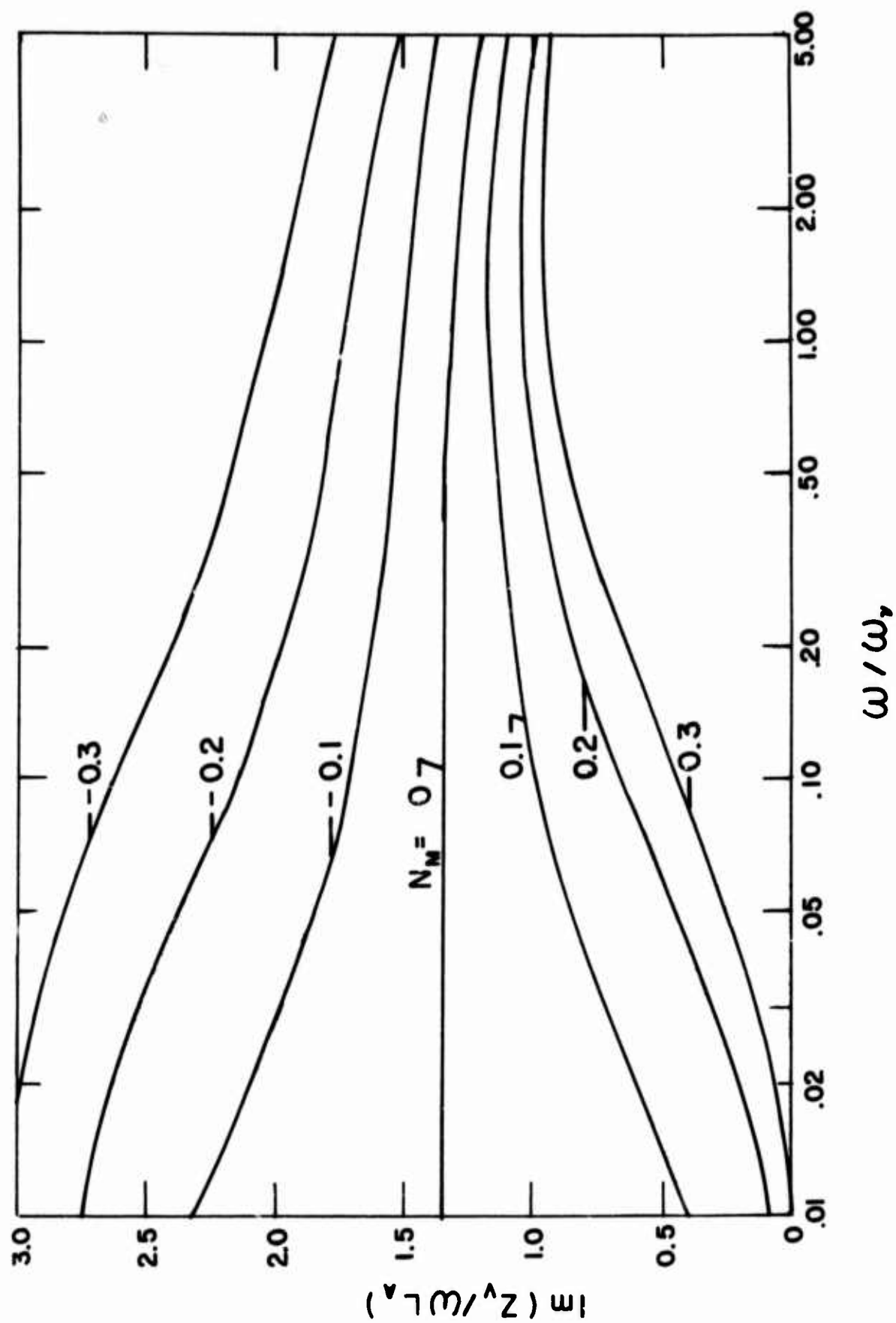


Figure 6. Variation in Imaginary Part of Series Impedance Due to Throughflow

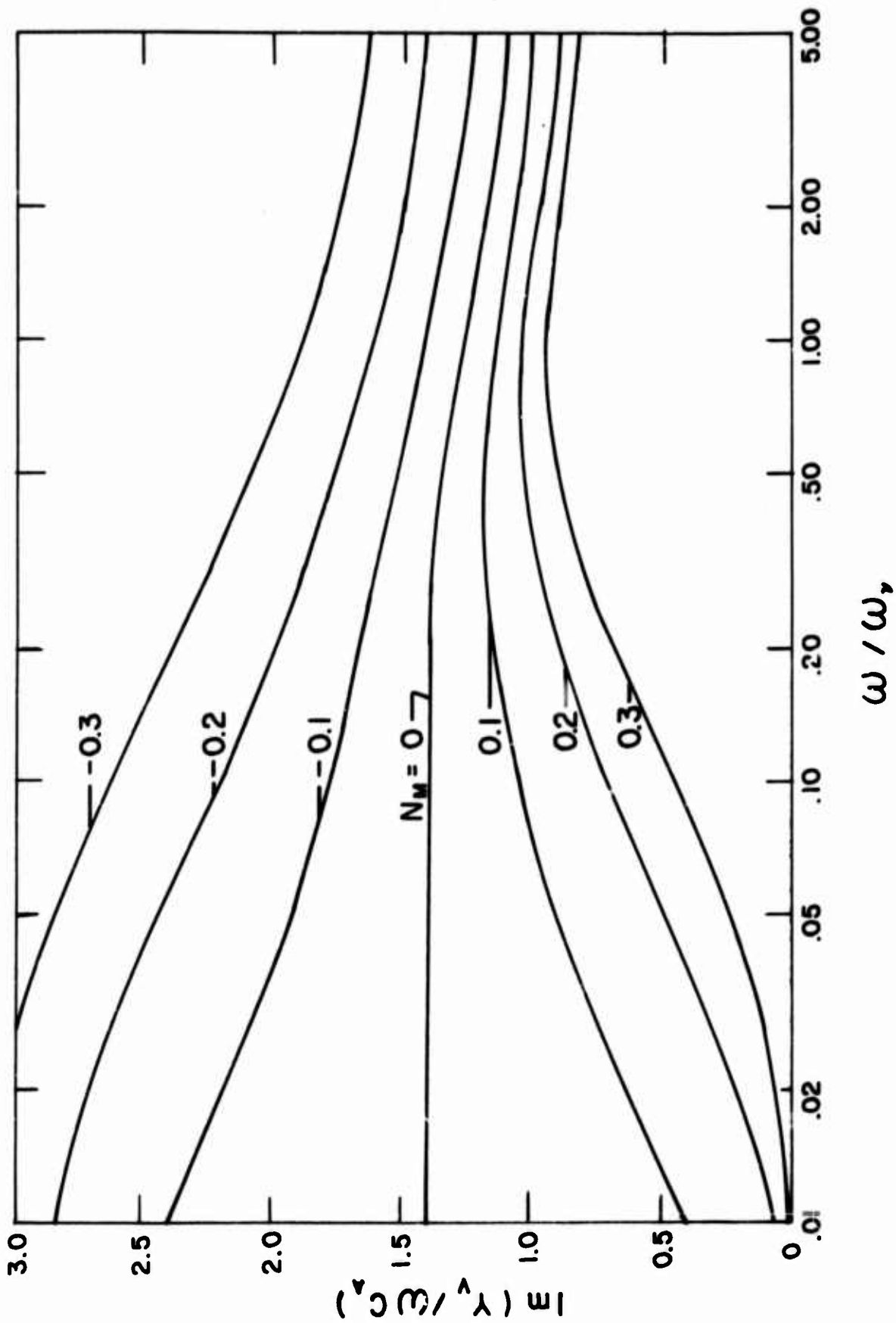


Figure 7. Variation in Imaginary Part of Shunt Admittance Due to Throughflow

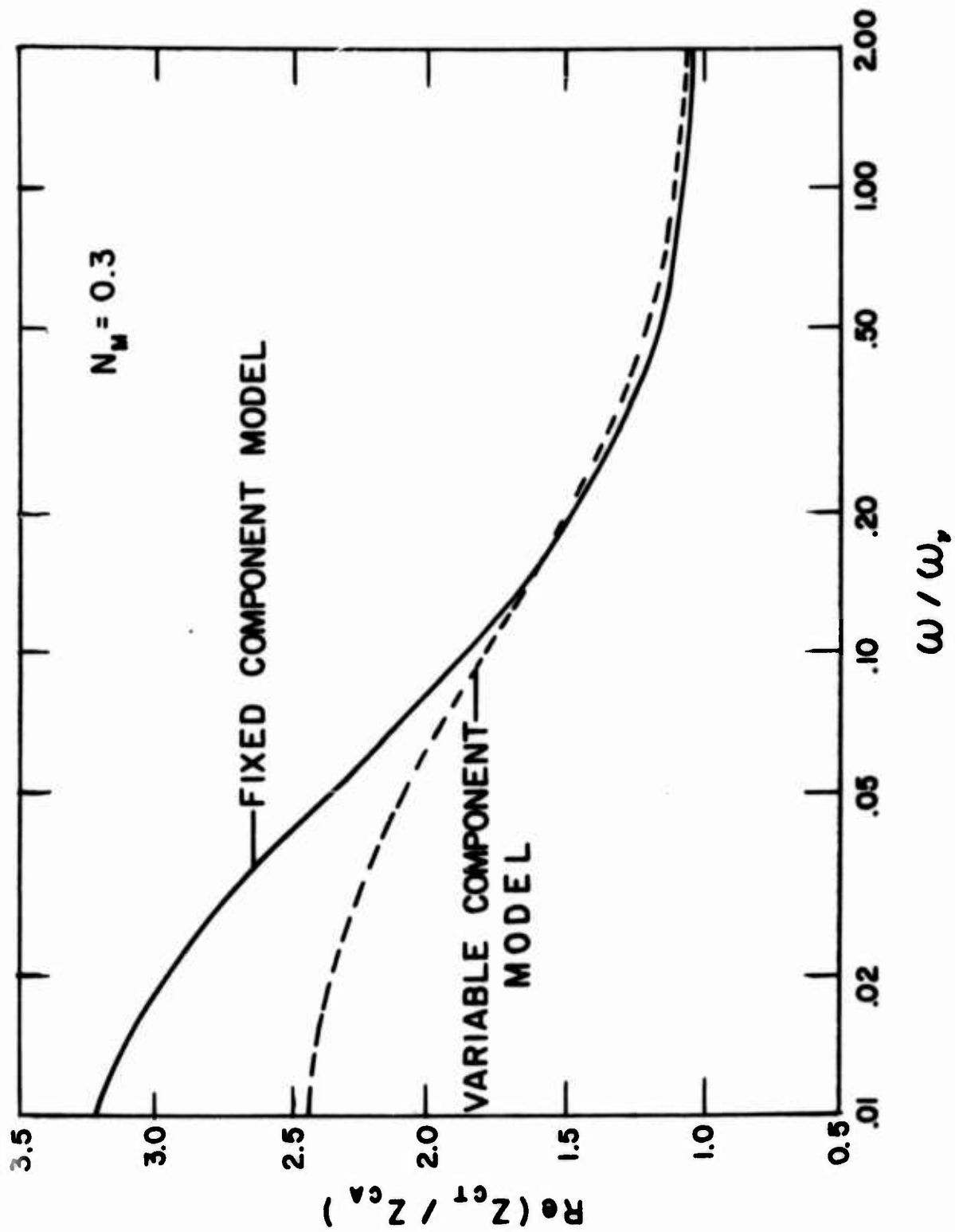


Figure 8. Comparison of Fixed and Variable Component Models for the Real Part of the Characteristic Impedance

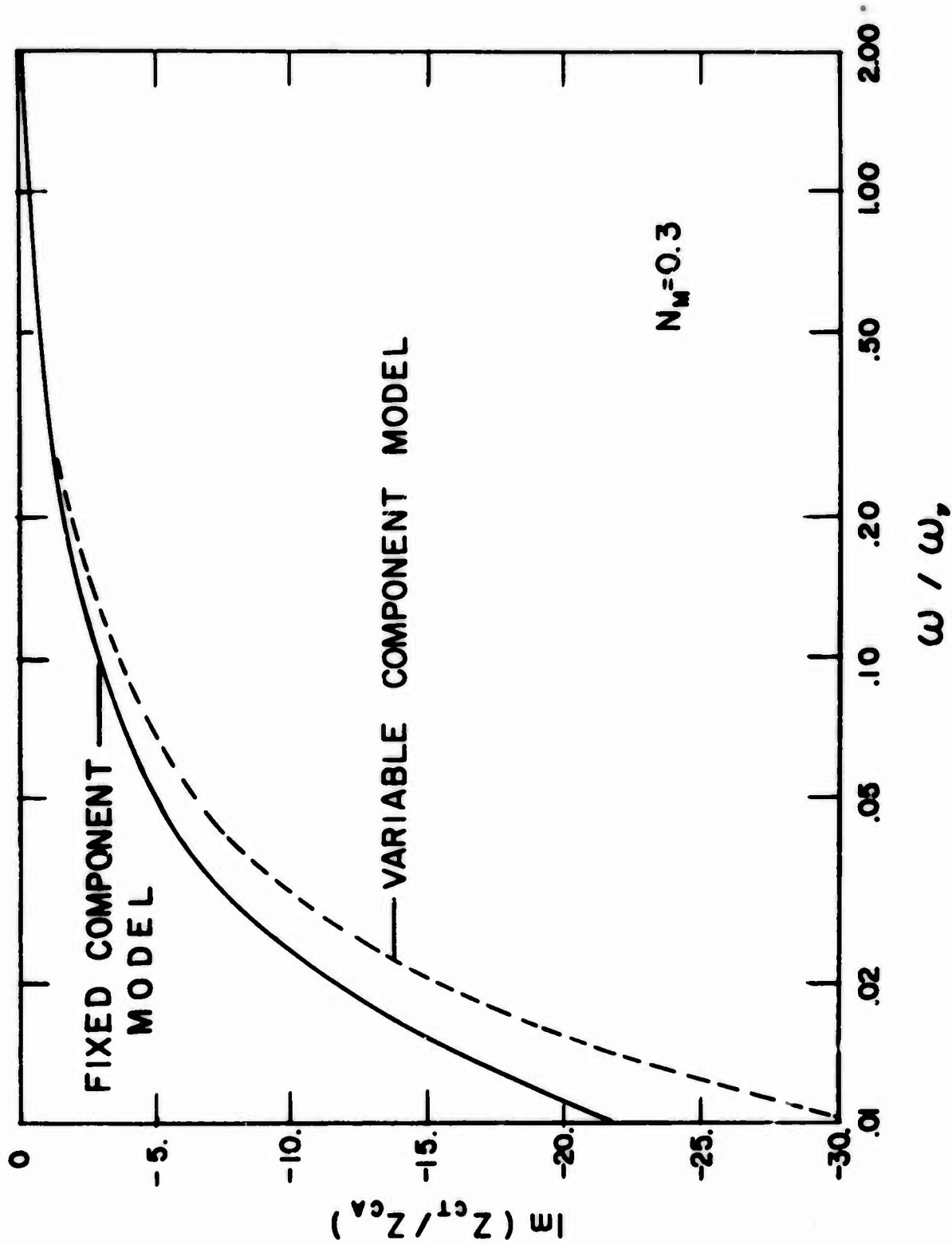


Figure 9. Comparison of Fixed and Variable Component Models for the Imaginary Part of the Characteristic Impedance

REPORT ON THE SIXTH CRANFIELD FLUIDICS CONFERENCE.

J.K. ROYLE, Ph.D., FIMechE, FRAeS, UNIVERSITY OF SHEFFIELD, U.K.

Introduction.

The sixth meeting was held in Churchill College, Cambridge, on 26 - 28 March 1974. After nearly a decade covering the span of the Cranfield Fluidics Conferences, 36 papers were presented from 78 which were offered, and 125 delegates attended from 18 countries.

The Organising Committee have had an introspective look over the past year or two at the format and title of the Fluidics Conference and the matter was discussed at an informal forum of the delegates during the conference. The forum was organised under the title "The Role of Fluidics in Fluid Power." The discussion was wide ranging: it was noted that several papers involved applications with mechanical moving parts which, a decade ago, and even now, could be equally well presented in a conference on fluid power, or pneumatics. If the "ic" were to be omitted from fluidic, would we lose momentum in a subject which is now finding its own areas of application over an ever increasing field? If future conferences were organised under a more general heading such as Fluid Control, with specific sessions covering the range of fluid power, pneumatics, hydraulic control, fluerics, and the like, would the topic of fluid control be stimulated or otherwise?

Opinions varied as to how wide the net should be cast in terms of control hardware, but there was general assent that the name fluidics and/or fluerics should at least be retained in specific sessions of a conference. To industrial users of fluidics, the name is immaterial and what is important is the grouping of relevant papers directed towards the same areas of application where one can visualise the alternative solutions of fluidics, pneumatics, hydraulics, and electronics.

Review.

In a short review of the sixth C.F.C., it is impossible to do justice to all the papers and contributions. Over nine sessions the papers were grouped under the varied headings :

1. Flow Measurement,
2. Sensing devices and techniques,
3. Fluid Mechanics,
4. Applications of heavy current devices,
5. Design of digital devices and circuits I,
6. Design of digital devices and circuits II,
7. Design of analogue devices and circuits,
8. Process control and material handling applications,
9. Specialised devices and applications.

Flow Measurement.

Four papers, (1,2,3,4,) included an interesting development(1) of a process sensor for on-line measurement of fluid flow rate or viscosity. The principle involved concerns the measurement of static

pressure drop with a radial inflow through a thin cylindrical chamber. The favourable pressure gradient maintains laminar conditions at high Reynolds number and the device has been tested with both liquids and gases. The paper suggests that the device can be developed to indicate continuously the effective viscosity of non-Newtonian fluids. Discussion centred on the effects of "heat-slip", i.e. on the possible effects on local viscosity of the increased shear rate and energy dissipation near the boundaries.

A further paper(2) was concerned with the development of a fluidic pneumotachograph for monitoring the respiratory flow rate of infants and neonates, and reflects the considerable interest, developing in the U.K., in the use of fluidics for monitoring respiratory and anaesthetic gas flows. In the paper an adaptation of the jet deflection anemometer is described (Fig.1), and an optimum value was sought for the angle between the power jets with a view to maximising the signal/noise ratio. A bandwidth of 6 Hz (for a drop of 3dB) is reported.

The edge-tone oscillator as a flowmeter(3) was studied experimentally and recommendations made for a flowmeter which can cover flow rates less than 10 l/min. It was found that nozzle exit width and shape and the sharpness of the pointed edge were highly sensitive terms which affect the range of stable oscillation and that the phenomenon of 'frequency jumping' can be prevented by the proper selection of nozzle-edge distance and sound absorbing material.

The fourth paper of this session(4) described a novel vortex flowmeter in which flow is introduced tangentially at the periphery of a thin chamber and exhausts axially from the central outlet. The tangential velocity is measured by a timing ball which is free to rotate along a track. Excellent linearity, though not proportionality, is reported for the relationship of frequency and volume flow rate.

Sensing Devices and Techniques.

Of the three papers presented verbally in this session, the first concerned an interesting study of a pneumatic neutron flux measurement device(5). Two systems are described and the paper is concerned with the computer simulation of the respective characteristics. In the first system a bimetallic strip is fabricated from an aluminium-uranium alloy on one side and unalloyed aluminium on the other. Exposure to a neutron flux heats up the alloyed side due to fissioning of uranium atoms. Deflection of the strip (Fig.2) is measured by a pneumatic position sensor. The second system relies on the increase in viscosity of a gas, with a temperature rise. A constant gas flow is passed through a small tube under laminar conditions and the pressure drop is therefore related to temperature. By using two tubes, made of the uranium-aluminium alloy, and the other of unalloyed aluminium, the differential heating due to neutron flux is converted to a differential pressure signal.

A statistical study on the accuracy of fluidic comparators(6) was concerned with the switching of a wall-attachment amplifier for rectangular pulse and ramp inputs after the stochastic parameters had been determined by experiment. Discussion on the paper highlighted the general need for comparative results for several types of element.

The dynamic response of an acoustically controlled turbulence amplifier(7) identified two characteristic frequency bandwidths over which the amplifier is sensitive to the control sound, the higher bandwidth being more significant and within the experimental range the fall and rise times are virtually equal and almost independent of control sound frequency and pressure level.

Fluid Mechanics.

A paper concerned with a fundamental approach for predicting and classifying the response time of fluid elements(8) was presented and a simple expression derived which relates response time with size, fluid, operating conditions (Reynolds number) and amplifier characteristics (pressure and flow rate gain). It is argued that a dimensionless figure of merit, i.e. a relative response time should be used to compare amplifiers of different size and gain. In some special cases, multistage amplifiers allow drastic reductions in response time compared with single stage amplifiers.

A paper concerning linearity of the co-flowing jet fluidic anemometer(9) explained and predicted that one might expect a linear variation of receiver signal with stream velocity for only a small range of velocity ratios and with a large axial separation between the nozzle and the receiver.

A paper which excited a great deal of attention and forms a noteworthy advance to the literature was concerned with the laminar proportional amplifier(10). In this new design depicted in Fig.3, the amplifier has a pressure gain of over 20 and a dynamic range greater than 2000 at bandwidth of 20 Hz. A typical amplifier can sense pressure signals of 0.5 n/m^2 with a bandwidth greater than 300 Hz. The flow field visualisation at operating Reynolds number is reproduced in Fig.4 and a single stage gain and noise level is shown in Fig.5.

Application of Heavy Current Devices.

This "heavy current" or "primary" fluidic session gave an interesting, though by no means an exhaustive, indication of the continuing and growing interests in large fluidic applications.

The paper "Flow control by use of digital and analogue switched vortex amplifiers(11) deals with the proposed use of large vortex units for control of water retained by a dam, as shown in Fig.6. Different types of control overflow were tested on models. With the overflow with a horizontal crest or overflow with a sloping crest, the vortex behaves as a digital unit and, with a vertical control slot, the output was a steady rating curve tending to oscillatory flow at lower pressure ranges.

A feasibility study of a supersonic fluidic amplifier capable of operation in a complete vacuum(12) was described in which the inactive output is deliberately allowed to leak in order that the interaction region can be kept pressurised (Fig.7). The application is to roll-control of a space launcher.

The same general topic in a completely different environment, i.e. thrust vector propulsion and steering of submersible vehicles(13), is illustrated in Figs. 8 and 9. This form of wake steering relies essentially on differential separation within the fixed shroud enclosing a

propeller and is strictly at the fringe of fluidics. Nevertheless, the results of preliminary tests are reported to be encouraging.

This session was completed by a paper on the high gain active diode(14). Essentially the device is a vortex unit as shown in Fig.10. Turndown ratios in excess of 12 are reported and a range of applications from a self-operating protection circuit in a flow control process to flash-back protection on flarestack burners are described.

Design of Digital Devices and Circuits.

The use of regression methods(15) for optimising the design of fluidic elements was argued in the opening paper of this session. It is shown that useful information can be obtained from simple methods using linear relationships with only eight trials.

A powerful paper dealing with some of the problems of implementing threshold logic with existing fluidic devices(16) formed the second paper in the session covering design techniques. It is argued that, although the implementation of threshold logic is more involved than is the realisation of OR/NOR logic, the complications involved are overshadowed by the versatility of the element and the complexity of the logic functions realised.

A first class and fundamental paper in the session(17) was concerned with the effect of contamination on flueric system reliability. Results are presented from a wealth of experimental results describing the degrading effects of supply gas contamination on approximately 400 circuits. Dust contaminants of different types and hardness with particles graded from 150 to 5 micron maximum size are presented and a simple equation is developed involving such independent variables as contaminant size, rate and hardness, supply pressure, nozzle area and element size. Two failure modes are postulated, erosion and clogging and the relative reliabilities of the two are determined for various conditions.

During a second session on the design of digital devices and circuits, a series of four papers on techniques were read. The first of these considered fluidic single- and two-variable pulse-width-modulated systems(18) and argues that the effects of experimental distortion of the carrier waveform can be minimised provided the time content of the resistance-capacitance network is correctly chosen. The paper speculates on the design of a hybrid, amplitude-modulated, pulse-width modulated, system to give an output product signal such as torque x speed to monitor power. A second paper considered stochastic and other time-summation fluidic digital-to-analogue converters(19) and gives details of a new family of pure fluidic, digital to analog converters which use binary pulse trains as digital weights, thus allowing the construction of simple digital-to-analog converters. The system is illustrated in Fig.11.

The third paper presented considered a method for design and classification of two-output memories applied to sequential circuit synthesis(20). The method of calculation of memory circuits with two outputs of cross-coupled type is described and the design of asynchronous sequential circuits is demonstrated. A final paper in this session(21) was concerned with the design of a pulse-width-modulated controller which includes both a wall-attachment and a beam deflection amplifier as active elements.

Design of Analogue Devices and Circuits.

This session was largely concerned with vortex units and contained a number of interesting and novel ideas. In a paper(22) describing a vortex valve and ejector combination, a design is described in which the addition of an ejector increases the turn-down ratio from 8 to 35.

The principle is illustrated in Fig.12 and underlines the fact that, if one has energy to spare, it can be put to good use - in this case some of the outgoing flow is fed back via the ejector to form the control flow.

A novel type of vortex control(23) for use in oceanology was presented and is outlined in Fig.13. Here, the Lorentz effect is used to impart spin to the conducting fluid - in this case sea water. The permanent magnet gives an axial magnetic field, and the current flow is in the radial direction, thus giving a tangential body force to the fluid. Various relationships of flowrate, electric current and salt concentration are included and the side effect due to electrolysis is noted.

A proportional fluid amplifier using a free liquid jet(24) was described in the third paper of this session. By placing the control nozzles so that they intercept the emitter jet, a coherent, constant diameter jet is achieved downstream of the deflection region. The prototype gave a blocked load pressure gain of 22.8 and a flow gain of 6.9, with a block load pressure recovery of 89% and an open load flow recovery of 97%.

General design methods applied to circuits associated with regenerative systems(25) were described in generalised terms of an ideal Eulerian 3-terminal device. The paper is particularly apt for applications involving pumping of toxic or abrasive liquids, or for directing furnace gases through heat exchangers.

Process Control and Materials Handling Applications.

This session contained four papers, the first of which described a fluidic weight checking apparatus(26) - although pneumatic would be a more accurate description. Essentially, a hemispherical ball on a seating forms a flapper valve and the moving parts are supported in air bearings. Good linearity between pressure and supported weight is reported from the experimental set-up and the discussion centred on the stability and fluid mechanics of the flow through the poppet-type valve.

Sorting by fluidics(27) was the topic of the second paper of the session. Here a Coanda unit with a supersonic jet outlet ($M = 1.6$) is triggered to an accept or reject mode by an impulse originating from a photo-cell via an electronic amplifier and air valve. Experimentally, objects of hazel nut size could be sorted between those deliberately coloured black, and the standard brown variety with about 92% reliability at about double the rate of systems using moving part pneumatic units. The paper concludes that there seems to be no clear advantage in extending the system by miniaturising the fluidic valves to sort objects of the size of rice grains.

The general theme of automation was continued in the session with a highly sophisticated and elegant paper on fluidic read-out of a scale and N C of weighing processes(28). Here two scales have been equipped

with fluidic analog to digital converters in which the code is etched into a thin aluminium sheet and is sensed by air jets. Fluidic signals are transduced into a polyadic code and converted to electric signals at a power signal low enough to ensure safety in explosion danger areas. The case is made that fluidics has proved to be the optimum solution for the high degree of automation in batch-processing technology when resolution, absolute encoding, contactless sensing, speed of response, mechanical input and output, safety, and insensitivity to the environment are considered.

The final paper of this session described the system analysis of a fluidically controlled plant(29) and, again, fluidics here includes diaphragm operated air valves. The system concerns an aircraft cabin where the pressure is to be controlled during rapid changes of altitude and theoretical calculations predict an entirely satisfactory performance.

Specialised Devices and Applications.

The first paper in the series described a fluidic application in the bio-engineering field. The paper dealt with the development of a valve block for air massaging applications(30) and concerns the performance of a valve block with oscillators, and piston repeater valves and inverter valves. Air pockets in the belt which is strapped to a patient's limb, serve as charging capacitors then undergo continual cycles of inflation and deflation.

Fluidic applications for the artificial heart(31) form the topic of another paper in the session. Here the circuits of two, low frequency, square-wave, generators using a fluidic Schmitt trigger are described, in which the output wave duty-cycle applied to the sac-type artificial heart pump can be controlled by means of a control pressure signal.

A fluidic clock(32) was the title of the third paper in the session. In this very interesting paper, three types of fluid clocks are studied - an R C fluidic oscillator; a balance-wheel with air bearings entrained by the output of a bistable unit (Fig. 14); and a balance wheel with sapphire bearings and fluidic entrainment. The timer is designed to withstand severe environmental conditions. In the sapphire bearing design, the clock has a frequency close to 23 Hz with a stability under laboratory conditions better than 5×10^{-5} . Excellent temperature insensitivity is reported with a shift within $\pm 10^{-4}$ for a temperature change within 5 to 55°C and the clock will function under an acceleration of 70 "g".

An unusual paper which stimulated a great deal of interest concerned a fluidic explosive initiator(33). This unit comprises a convergent nozzle which gives a compressible jet cell structure in which is placed axially a resonance tube - preferably stepped down in diameter towards the closed end. The very high and rapid temperature rise, Fig. 15, at the closed end is useful as an explosion initiator. The discussion brought out the similarities to the Hilsch vortex tube and posed rather more thermodynamic questions than answers.

A three-stage cascade amplifier consisting of three wall attachment devices switched by a secondary fluid, either gas or liquid(34), was described and tests were conducted on a pneumatically controlled unit of a 10 ton rocket engine. It is argued that the same ideas can be applied

to cascade amplifiers in any industrial situation in which the absence of vents is important.

The penultimate paper read at the Conference concerned a fluidic surge prevention unit for jet engines(35). The circuit diagram is reproduced in Fig. 16 and it may be readily argued that, when the rate of change of supply pressure is positive, the flow into the pneumatic capacitance does not affect the flow pattern in the vortex chamber as the tangential control duct is radially opposite the inlet duct. When the rate of change of input pressure is negative however, the retained higher pressure in the capacitance produces an input swirl in the vortex chamber and consequently, an amplified difference between reference and output pressures. The rapid reduction in compressor delivery pressure consequent on compressor surge is therefore detected and the unit has been successfully subjected to bench and engine tests.

The final paper presented at the conference concerned a fluidic systems power source study(36). An analysis is made of possible sources of gas power for fluidic systems in munition and weapon applications. In generalised form, hydrazine, liquid ammonia, solid propellants such as ammonium nitrate and subliming solids are described, and the conclusions indicate that cold gas is desirable for short-time running, when volume is available. Again, where space is at a premium, the use of hot gas shows promise over using stored gas at super pressures.

Three additional papers which were not presented completed the list of conference papers. In the first of these is described a level sensing fluidic amplifier for very loose materials(37) such as wood particles, using a back-pressure sensor which could also be developed for sensing very low velocities in fluidic anemometry.

Impedance matching of rectangular and circular pneumatic transmission lines(38) was the subject of a theoretical paper in which methods for optimal matching design of harmonic signal transmission and arbitrary shape signal transmission with spectral-response characteristic $|S(j\omega)|$ are presented and discussed.

Finally, a pure fluidic circuit applied for a fluid division ratio control in a distiller column(39) was the subject of a paper in which fluidic diverting valves are used as actuators for use in a pharmaceutical factory.

Conclusions.

Overall the conference was a great success. It may be that there is little interest in whether words such as fluidic and flueric should continue to flourish, but there is no doubt at all that the momentum created by fluidics in providing solutions to real problems is in a very flourishing state.

Underlying the applications of fluidics or pseudo-fluidics across the wide spectrum from logic to "heavy current" fluidic applications; from low-flow measurement and anemometry to thrust vector control; from very low-noise amplifiers to explosion initiation; taking on board such diverse subjects as artificial hearts, fluidic clocks, surge prevention of jet engines, and sorting by fluidics; is the constant economic driving force which ultimately distinguishes and isolates the viable applications of fluid control systems.

References.

1. "An on-line sensor for fluid flow rate or viscosity measurement." W.F.Hayes, J.W.Tanney and H.G.Tucker, National Research Council of Canada.
2. "A fluidic pneumotachograph for neonates." H.El-Gammal, Hatfield Polytechnic, U.K. and J.Bushman, Royal College of Surgeons, U.K.
3. "Edge-tone oscillator as a flow meter." M.Yonemochi and T.Nakamura, Kobe University, Japan.
4. "Investigation of a vortex flow meter." C.W.Kwok and D.Nastou, Sir George Williams University, Canada.
5. "An investigation of pneumatic neutron flux measurement device." R.G.McCutcheon, Imperial Oil Ltd., Canada, and J.N.Wilson, University of Saskatchewan, Canada.
6. "Statistical studies on the accuracy of fluidic comparators." H.Hanafusa and K.Miyata, Kyoto University, Japan.
7. "An investigation of the dynamic response of an acoustically controlled turbulence amplifier." G.W.Rankin and K.Sridhar, University of Windsor, Canada.
8. "Response time of fluid elements." H.H.Glättli, Pneumotech AG, Switzerland.
9. "Further studies of the co-flowing jet fluidic anemometer." R.K.Duggins, University of Nottingham, U.K.
10. "Laminar proportional amplifier." G.Mor, Harry Diamond Laboratories, U.S.A.
11. "Flow control by use of digital and analogue switched vortex amplifiers." H.Brcmbach, University of Stuttgart, German Federal Republic.
12. "A supersonic fluidic amplifier for operation in a vacuum environment." M.Carbonaro, Von Karman Institute of Fluid Dynamics, Belgium.
13. "Propellered fluidic nozzles for thrust vector propulsion and steering of submersible vehicles." G.Schoenau, B.Fellows and C.Taft, University of New Hampshire, U.S.A.
14. "A high gain active diode - the reverse flow vortex amplifier." N.Syred and J.Tippetts, University of Sheffield, U.K.
15. "A methodological approach to the design optimisation of fluidic elements." J.Watton, Huddersfield Polytechnic, U.K.
16. "Threshold logic and existing fluidic devices." C.A.Martin, General Motors Corporation, U.S.A.
17. "Effect of contamination on fluidic circuit performance." W.J.Westerman, McDonnell-Douglas Astronautics Ltd., U.S.A.
18. "Practical considerations for fluidic single-and two-variable pulse-width-modulated systems." F.A.Parker, University of Surrey, U.K.
19. "Stochastic and other time-summation fluidic digital-to-analogue converters." R.Massen, T.H.Aachen, German Federal Republic.
20. "A method for design and classification of two-output memories applied to sequential circuit synthesis." W.Hübl, Ruhr Universität Bochum, German Federal Republic.
21. "Fluidic pulse width modulation controller for non-electrical control unified systems." A.M.Stanescu, Polytechnical Institute of Bucharest, Romania.
22. "A vortex valve and ejector combination for improved turn down ratios." P.W.Fitt, University of Bristol, U.K.

23. "Static characteristics of an electromagnetically-controlled vortex type liquid amplifier." K.Shimada, Chuo University, Japan.
24. "Proportional fluid amplification using a free liquid jet." J.D.Malcolm, Memorial University of Newfoundland, Canada, and S.A.Alpay, University of Waterloo, Canada.
25. "General design methods applied to circuits associated with regenerative systems." J.R.Tippetts, University of Sheffield, U.K.
26. "Fluidic weight checking apparatus." P.Wiedmann and E.Illig, University of Stuttgart, German Federal Republic.
27. "Sorting by Fluidics." Y.S.Chadda, University of Singapore, R.S.Neve and P.H.G.Penny, The City University, U.K.
28. "Fluidic readout of a scale and NC weighing processes." H.H.Glättli, Pneumotech AG, Switzerland.
29. "System analysis of a fluidically controlled plant." G.Belfore, A.Romiti and G.Jacazio, Politecnico di Torino, Italy.
30. "Development of a valve block for air massaging applications." R.M.H.Cheng and C.K.Kwok, Sir George Williams University, Canada.
31. "A low frequency pneumatic square-wave generator with variable duty-cycle for artificial heart pump applications." S.Liu, J.C.Callaghan and N.Suresh, Sir George Williams University, Canada.
32. "A fluidic clock." P.Facon, C.Pavlin, Bertin & Cie, France, and C.Pascal, C.E.A., France.
33. "Fluidic explosive initiator." E.L.Rakowsky, V.P.Marchese, EMX Engineering Inc., U.S.A. and A.P.Corrado, Dept. of the Army, Picatinny Arsenal, U.S.A.
34. "A pneumatic or electrically controlled fluidic amplifier for liquid secondary injection." W.Kranz and H.Tilman, Messerschmitt-Bolkow-Blohm, German Federal Republic.
35. "Fluidic surge prevention unit for jet engines." R.Rimmer, Dowty Fuel Systems Limited, U.K.
36. "Fluidic systems power source study." A.E.Schmidlin and A.P.Corrado, Dept. of the Army, Picatinny Arsenal, U.S.A.
37. "Level sensing fluidic amplifier for very light loose materials." L.Lencz, Wood State Research Institute, C.S.S.R.
38. "Impedance matching of rectangular and circular pneumatic transmission lines." V.Chudy, Slovak Institute of Technology, C.S.S.R.
39. "Pure fluidic circuit applied for a fluid division ratio control in a distiller column." U.Pietka and Z.Wanski, Polish Academy of Sciences, Poland.

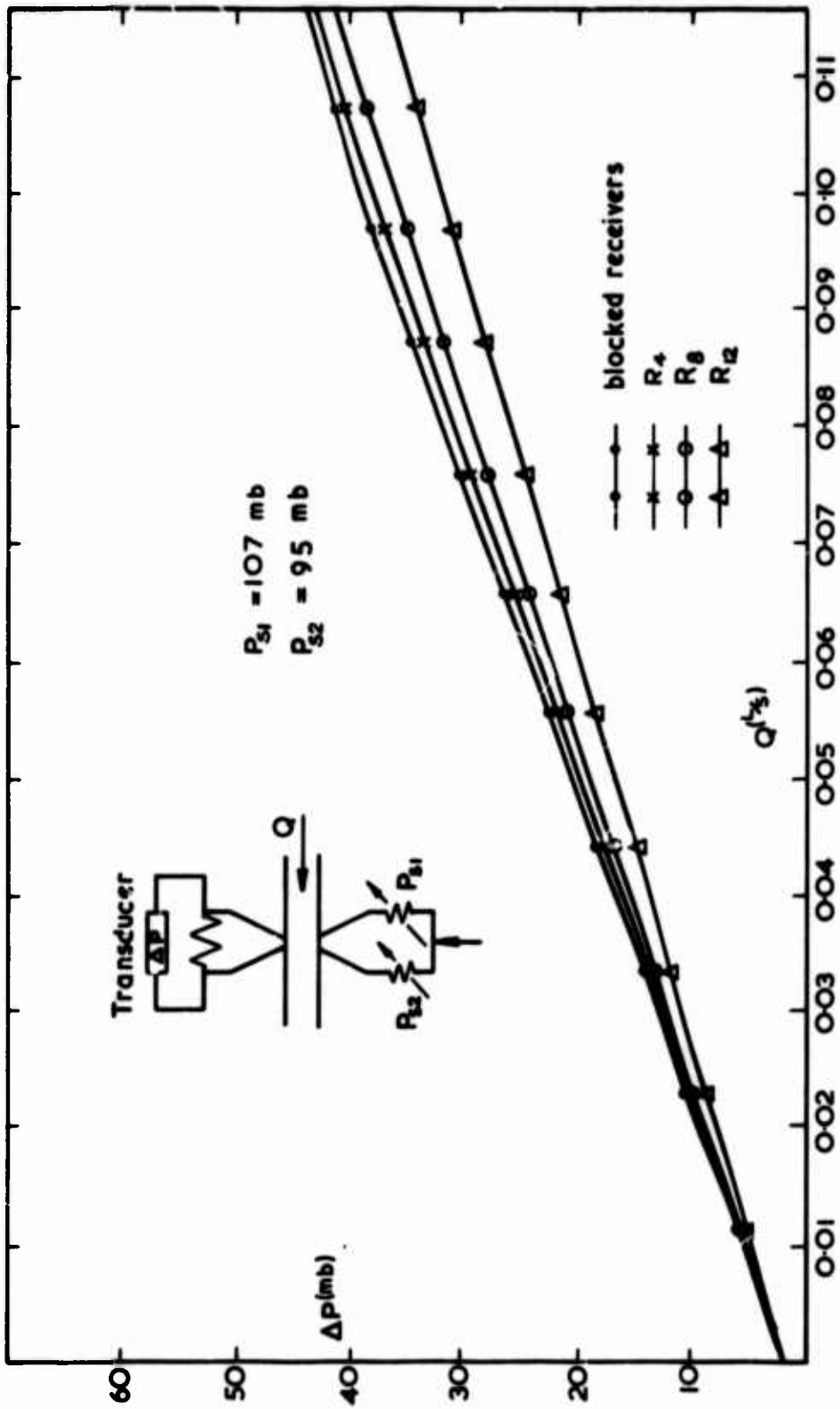


Fig. 1 Impinging jet flowmeter

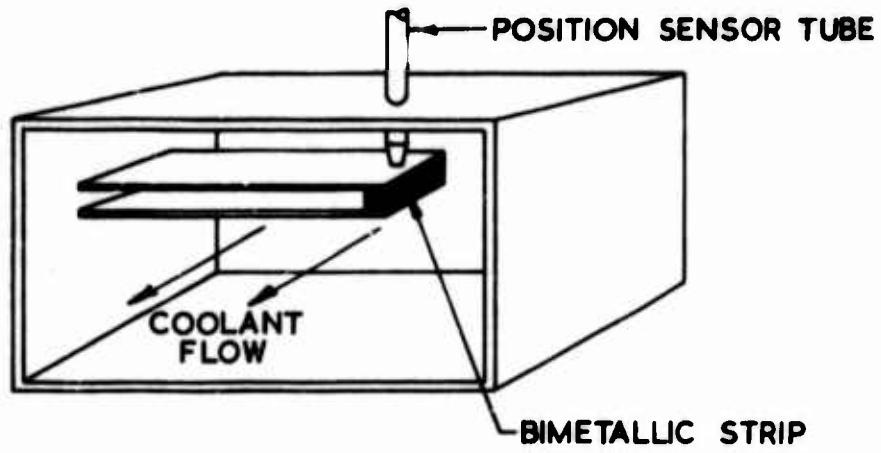


Fig.2 The Bimetallic Strip Neutron Sensor

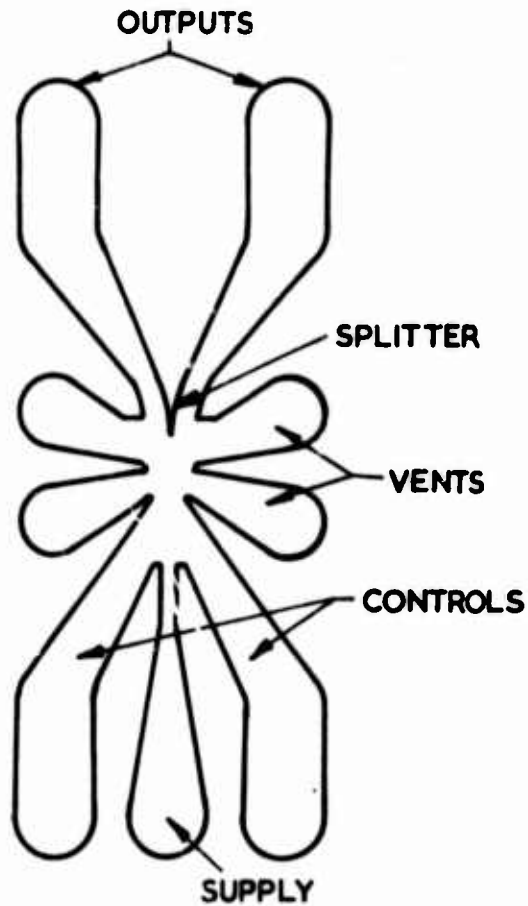


Fig.3 Present design of laminar proportional amplifier

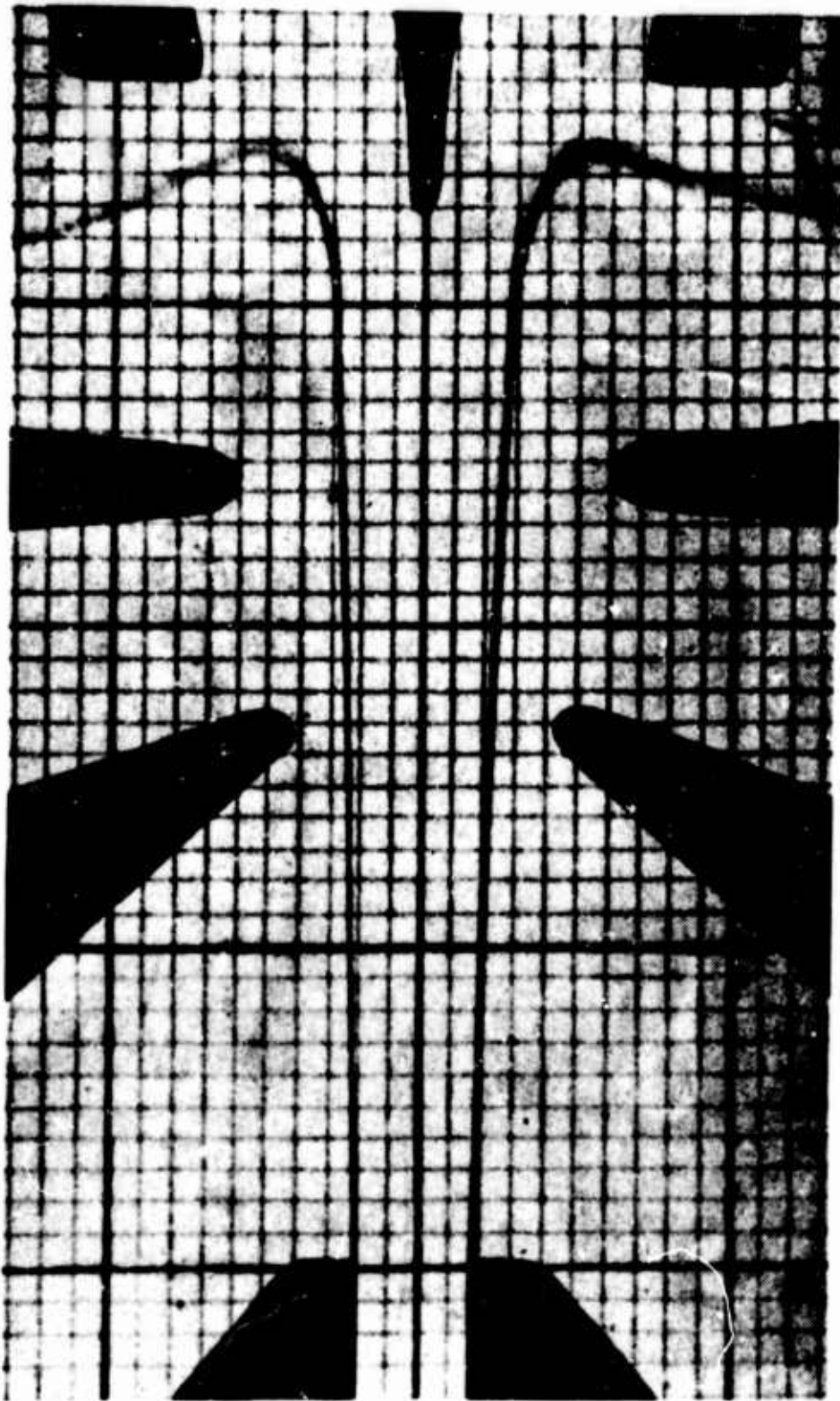


Fig.4 Flow field at proper Reynolds number ($N_{Rh} = 925$)

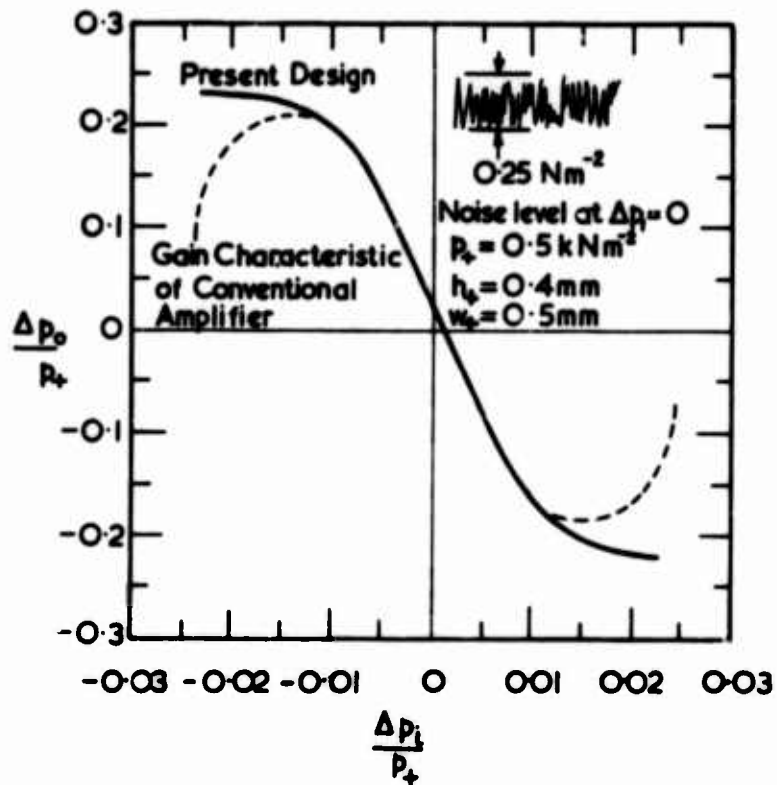


Fig.5 Single stage gain and noise level

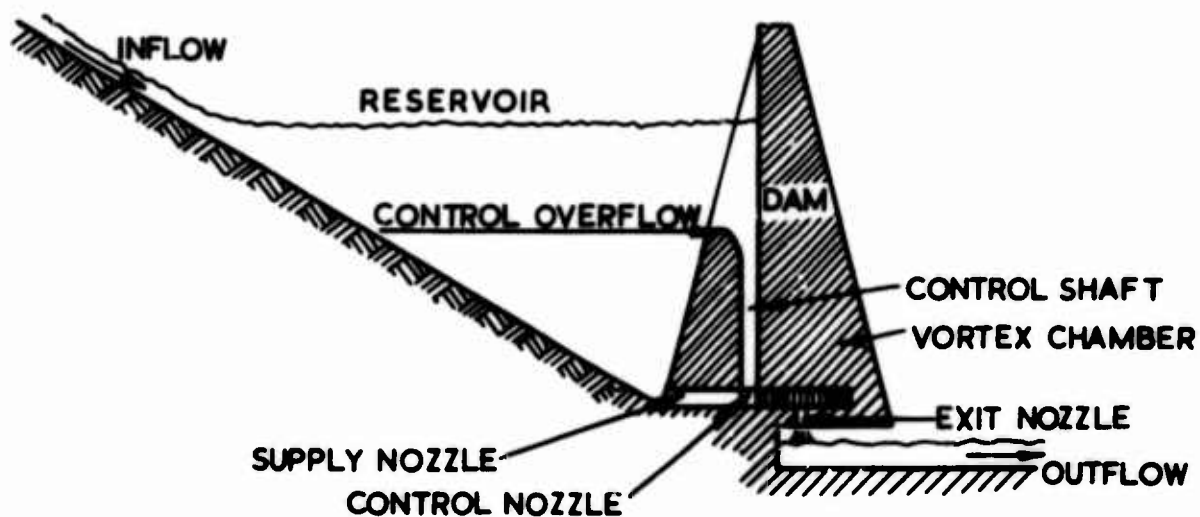


Fig.6 Arrangement of a vortex valve for flow control(simplified longitudinal section)

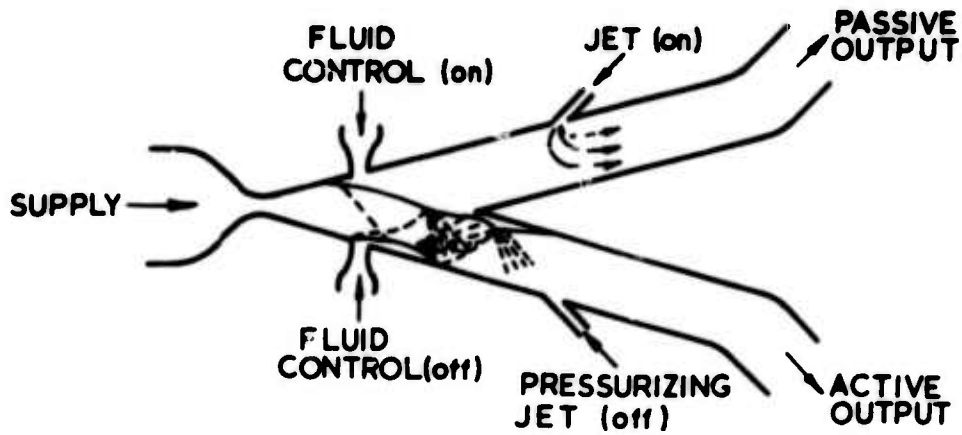


Fig.7 Use of curtain jets in the output ducts for pressurizing the interaction zone

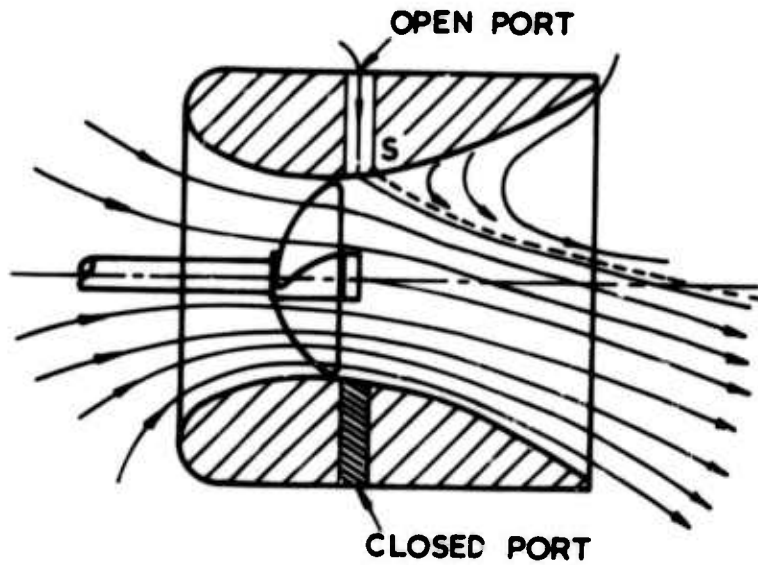


Fig.8 Cross-sectional view of wake steering nozzle (W.S.N.) with port open

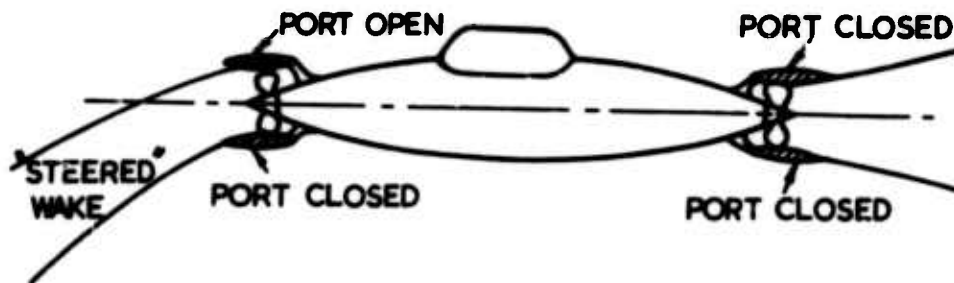


Fig.9 Proposed concept of W.S.N. mounted on a submersible vessel

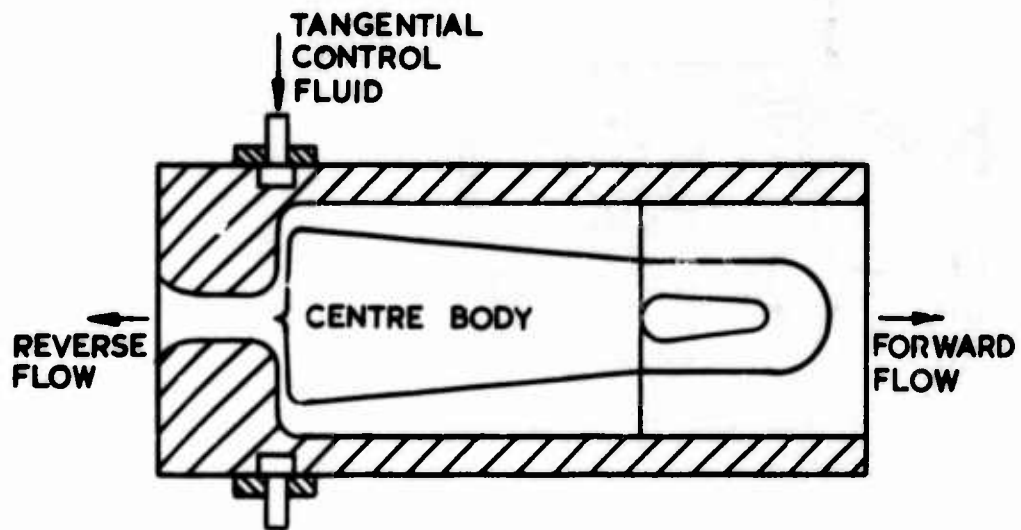


Fig.10 Details of R.F.V.A.2.

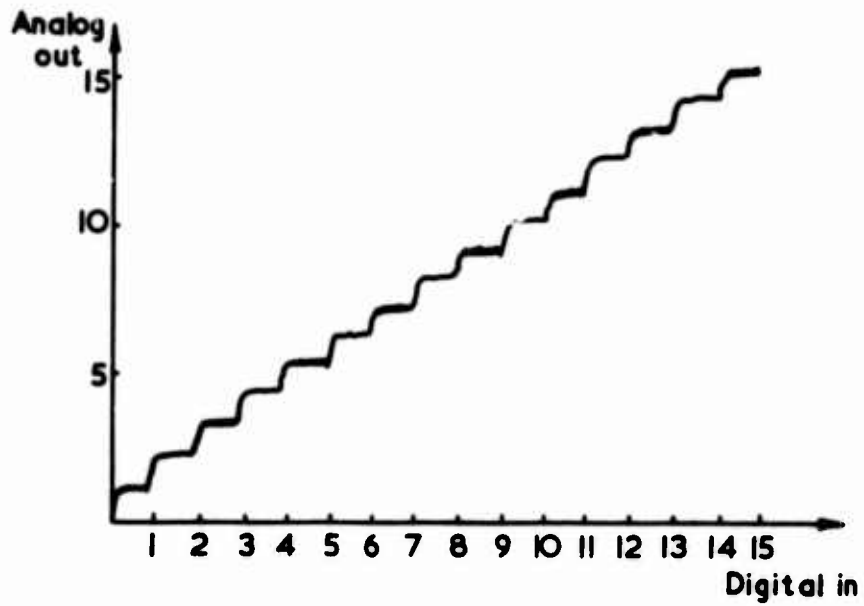


Fig.11 Pneumatic time-summation DAC with code disc

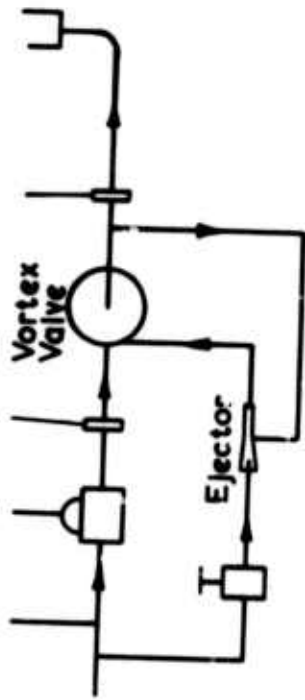


Fig. 12 Revised circuit to include ejector.

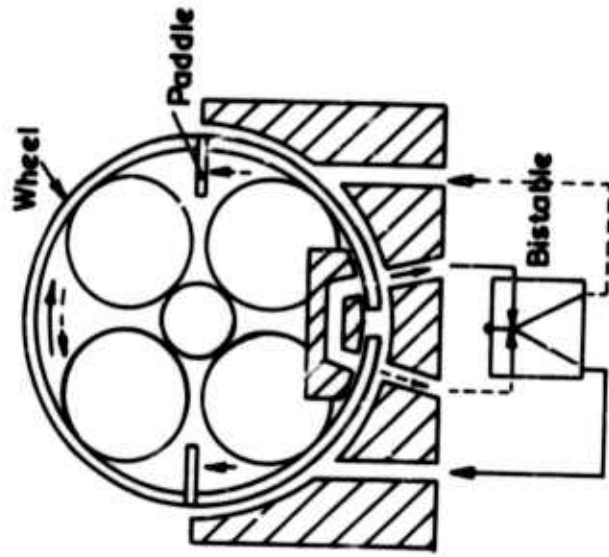


Fig. 14 Scheme of the oscillator with a balance wheel

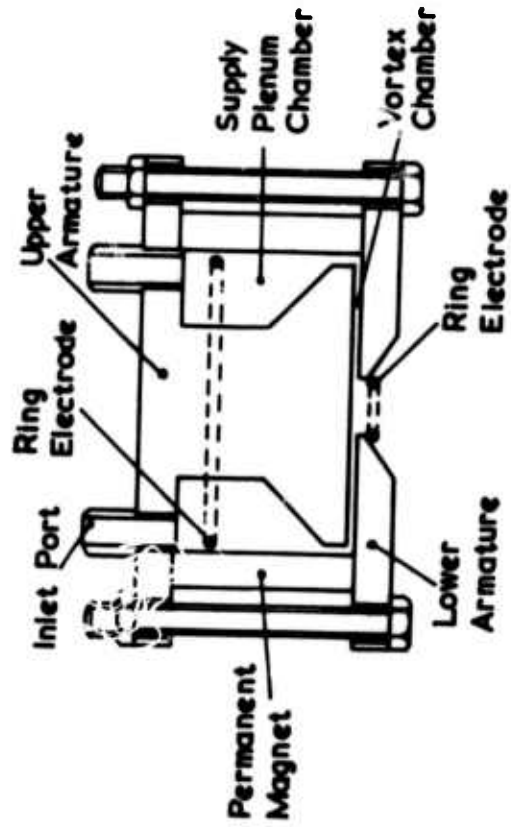


Fig. 13 Structure of vortex type liquid amplifier

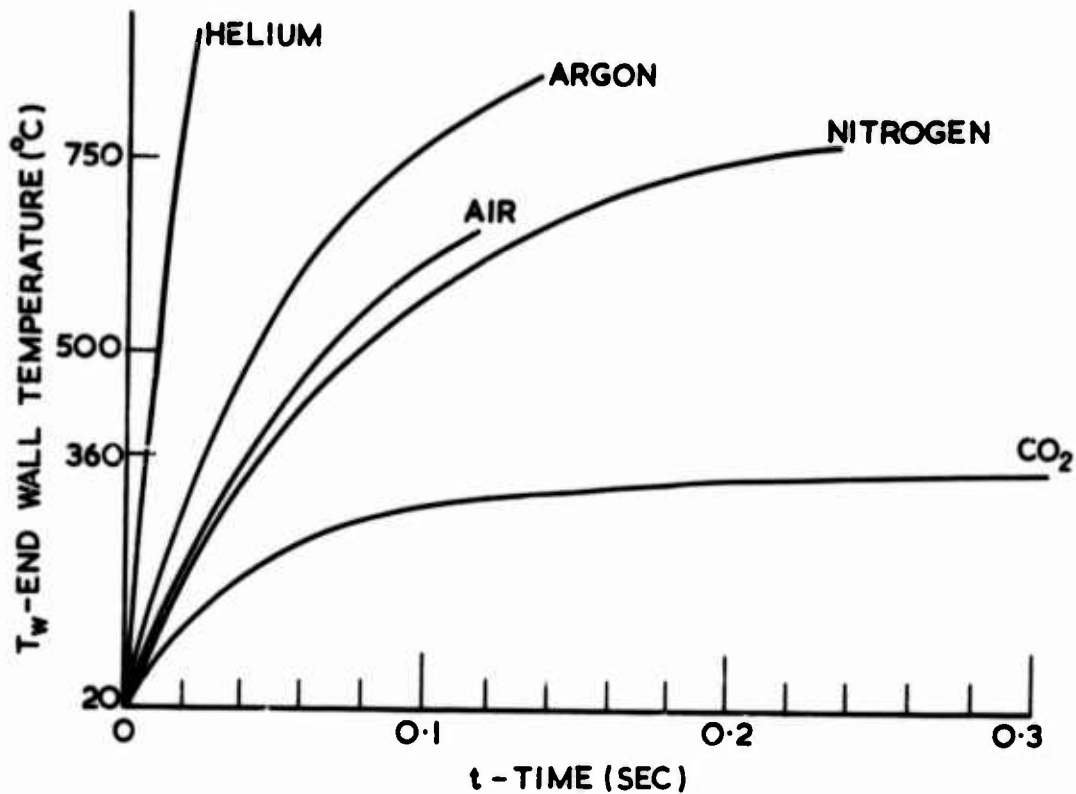
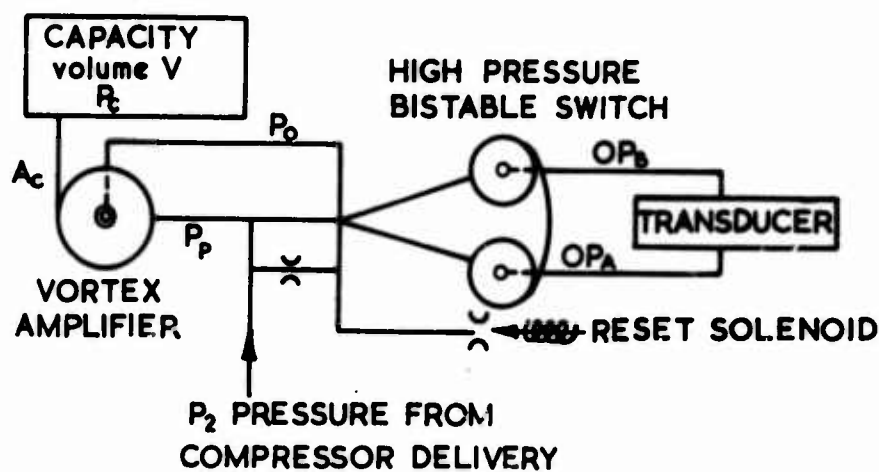


Fig. 15 Performance characteristics of various gases



AT SURGE- \dot{P}_2 EXCEEDS A PRE SET VALUE AND UNIT OUTPUT SWITCHES FROM OP_A TO OP_B

Fig. 16 Surge sensor circuit diagram

FLUIDIC STANDARDIZATION EFFORTS

By

P. Trask

Harry Diamond Laboratories
Washington, D. C.

Preceding page blank

ABSTRACT

This paper discusses fluidic standards with respect to their development, their subject material, their use within the fluidic technology, and to some extent, their relationship to other technologies. The many groups that are active in developing standards and the standard documents they issue are described. Among the most active groups are the Government Fluidics Coordination Group (GFCG) and the National Fluid Power Association (NFPA). Two military standards on fluidic terminology, symbology, and test methods, were developed and recently revised by the GFCG. Two additional standards on moving part fluid logic symbols and data presentation were developed by the NFPA. These four documents form the framework of the current fluidic standards used in the United States.

1. INTRODUCTION

The fluidic standards currently used in America have been developed by various groups and associations from both industry and government. The more active groups are the Government Fluidics Coordination Group, the National Fluid Power Association, and the Society of Automotive Engineers. However, the Instrument Society of America, the American National Standards Institute, and the International Organization for Standardization have also contributed to fluidic standardization. Each group has its own particular interest, and of course the standards and documents developed by each group reflect its own interest.

Generally, fluidic standards have been carefully compared and edited so that the different standards developed by the different organizations agree with each other when they pertain to the same subject matter. This is especially true of the initial standards that dealt with the more basic aspects of fluidics; namely, terminology and symbology. Now efforts continue to insure that this mutual acceptance is attained as old standards are revised, new documents are developed, and international standards are generated.

This paper reviews the development, contents, and use of these standards in America. Short discussions of the groups responsible for the development of each standard are included to help show the relationships among the various documents. To some extent, this paper also discusses the importance to fluidics of standards in related areas of the fluid power technology. The relationship between American and international standards and the possibilities for future fluidic standards are briefly discussed.

2. RELEVANT ORGANIZATIONS AND DOCUMENTS

2.1 The Government Fluidics Coordination Group

The Government Fluidics Coordination Group (GFCG) is an informal group of people from various government agencies. The common bond among the group members is their interest in fluidics. The membership changes as fluidic activities change in the different government agencies.

The purpose of the group is to pool information and resources; catalog what each member is doing, can do, and/or wants to do; and establish functioning lines of communication. In this way, the various agencies are able to help simplify each other's efforts and eliminate duplication.

Since one aim of the GFCG is to disseminate fluidic information, such documents as key word lists for retrieval of fluidic information,

element data specification formats, and military standards on fluidics have been developed by the GFCG. In fact, development and revisions of fluidic military standards are processed very efficiently by the GFCG relative to other military standards since the procedure for acceptance of manuscripts as fluidic military standards can be handled within the GFCG, eliminating the usual mail ballot delays encountered with other standards. The time it takes for a manuscript to become a standard can be cut in half by this GFCC activity.

In addition, the GFCG maintains files on suggested revisions and additions to its standards. Such a file is one on suggested symbols for new commercial devices. When these files contain enough material on a given subject to warrant a revision to a standard or to warrant a new standard, then a revision or new manuscript is processed.

Five areas within the fluidic technology that are covered by fluidic military standards and documents are:

- 1) Terminology,
- 2) Symbology,
- 3) Test Methods,
- 4) Instrumentation, and
- 5) Data Presentation.

The documents covering these areas are:

- 1) MIL-STD-1306A (8 Dec 72) "FLUERICs: TERMINOLOGY AND SYMBOLS,"
- 2) MIL-STD-1361A (28 Dec 73) "FLUIDICS: TEST METHODS AND INSTRUMENTATION," and
- 3) Fluidic Element Fact Sheet.

The material in MIL-STD-1306A is covered in several similar industry standards. However, this version has been revised recently and is more comprehensive and more consistent with SI than the industrial standards, although the differences are not great.

The material in MIL-STD-1361A is also covered in similar industrial standards. However, as with the first standard mentioned above, this second standard has also been revised more recently than its industrial counterparts.

The fact sheet specifies a standard, easily readable format in which basic element performance data may be presented.

2.2 The National Fluid Power Association

The National Fluid Power Association (NFPA) consists of about 150 manufacturers and users of fluid power products. The services that the NFPA performs for the fluid power industry range from marketing to educational services and include standardization activities. The scope of NFPA interests cover the entire fluid power industry including the fluidic technology.

It is natural for the NFPA to develop fluidic standards because of its extensive standardization activity in the fluid power industry, and because of its sensitivity to the needs of both fluid power consumers and manufacturers. This position helps to insure that their fluidic standards are widely accepted and consistent with other standards throughout the fluid power technology.

Specifically, the NFPA has standards in the following areas:

- 1) Terminology,
- 2) Symbolology, and
- 3) Physical Data and Performance Data Presentation.

These areas are covered in the following four documents:

- 1) T3.7.1-1968 "Glossary of Terms for Fluidic Devices and Circuits,"
- 2) T3.7.2-1968 "Graphic Symbols for Fluidic Devices and Circuits,"
- 3) T3.7.3-1960 "Method of Rating Performance of Fluidic Devices,"
- 4) T3.28.9-1973 "Method of Diagramming for Moving Parts Fluid Controls."

The first two documents cover essentially the same material as in the corresponding military standard. The third document is a good comprehensive document on its subject. The material covered in it is not covered in any other document (except an American National Standards Institutes, section 2.6, publication of nearly the same material) making this document of singular importance. This is also the only American fluidic document presently being edited for international use by the International Organization for Standardization (section 2.4). The fourth document above is the only document published on diagramming for moving part controls and is helpful in indicating the interdependence between fluid logic and the broader area of fluid power. One might think of this document as also describing the interface components into and out of the logic circuit because symbols for such items as switches, and indicators are also presented. In addition, this document describes the various ways that logic circuits are presented, such as attached and detached

diagrams, and the various equivalent ways of presenting the same logic functions.

The NFPA also publishes a compilation of fluid power standards called Fluid Power Standards (third edition). This is a very good overall volume. The strictly fluidic documents in this publication, however, are few compared with the number of other fluid power standards.

2.3 The Society of Automotive Engineers

The title, Society of Automotive Engineers (SAE), is in some ways a misnomer because the interests of this society are very broad. The SAE is organized into groups or councils according to specific interests. One of these councils is the Aerospace Council. The fluidics panel is part of the Aerospace Council's A-6 Committee on Aerospace Fluid Power and Control Technologies.

The Aerospace Council publishes three kinds of documents; 1) Aerospace Information Reports (AIR's), 2) the Aerospace Recommended Practices (ARP's), and 3) recommended Aerospace Standards (AS's). Usually, general information is presented in the AIR's. When general information is or can be refined and reduced to specific well accepted practices, this then becomes the subject of an ARP. Finally, the AS presents the society's recommended action for standard practices in the aerospace industry.

With specific relevance to fluidics the Aerospace Council has published or is processing documents in the following seven areas:

- 1) Terminology,
- 2) Symbolology,
- 3) Test Methods,
- 4) Instrumentation,
- 5) Power Supplies,
- 6) Element Specification Presentation, and
- 7) Interface Devices.

These seven areas are covered in the following four documents:

- 1) ARP 993A "Fluidic Technology" (revised 2-15-69)
- 2) ARP 1254 "Fluidic Test Methods and Instrumentation"
- 3) AIR XXX "Fluidic Power Supplies"
- 4) AIR XXX "Interface Devices"

The first two documents cover essentially the same material as the military standards, but they are out dated by the military standards. The third and fourth documents are currently proposed documents, but the information in them is not contained in any other industry or

government document, so they will be significant documents. Unfortunately, the time required for publication of these documents, if typical, may be considerable. Note that none of these is a recommended Aerospace Standard.

2.4 The International Organization for Standardization

The International Organization for Standardization (ISO) is the single, most influential standards organization in the world. Its standards reach into all areas of industry and commerce. Its efforts in the fluidic technology have only been underway for less than two years, but the number of fluidic documents that the ISO is working on is considerable. The areas covered by these documents include: logic diagramming, circuit diagramming, terminology, performance rating, and others. A large number of documents is under consideration because member countries submit their national documents, and the delegates from the other countries edit and rewrite these documents for international purposes.

Generally speaking, the European countries present a unified position and therefore manage to greatly influence, if not control, ISO's fluidics activity. In contrast to this, the American input to the ISO's fluidic effort has been fragmented and disorganized. Therefore, the American influence is weak.

Other than strictly fluidic activity, the ISO publishes several standards that influence the fluidic activity; the most important is ISO/R 1000 "Rules for the Use of Units of the International System of Units and a Selection of the Decimal Multiples and Sub-Multiples of the SI Units." Of the many ISO fluid power standards, the most important is R1219, "Graphical Symbols for Hydraulic and Pneumatic Equipment and Accessories for Fluid Power Transmission," which is very similar to ANSI/Y32.10-1967 "Graphic Symbols for Fluid Power Diagrams" (section 2.6).

2.5 The Instrument Society of America

Because the Instrument Society of America (ISA) works in the area of control technology, and pneumatics is used in this technology, some ISA work is related to fluidics. Specifically, there are two documents:

1) ISA Tentative Recommended Practice, "Dynamic Response Testing of Process Control Instrumentation," RP 26. 1-1957-Part I-General Recommendations.

2) ISA Tentative Recommended Practice, "Dynamic Response Testing of Process Control Instrumentation," RP 26. 2-1960-Part 2-Devices with Pneumatic Output Signals.

2.6 The American National Standards Institute

The American National Standards Institute (ANSI) does not develop standards as the previously mentioned groups do. However, ANSI does publish a large number of standards that are important to the fluidic technology. Some of these are as follows:

- 1) ANSI/B93.2-1971 - "Glossary of Terms of Fluid Power."
- 2) ANSI/B93.14-1971 - "Methods of Presenting Basic Performance Data for Fluidic Devices."
- 3) ANSI/Y14.17-1966 - "Drafting Practices for Fluid Power Diagrams."
- 4) ANSI/Y32.10-1967 - "Graphic Symbols for Fluid Power Diagrams."

The most important of these, the second one, has been discussed previously in section 2.2 regarding the NFPA.

3. CONTENTS OF FLUIDIC STANDARDS

3.1 Terminology

The military standard covering fluidic terminology, MIL-STD-1306A (terminology and symbology), is available as a symposium handout, so little need be said about it. As discussed previously, this standard is similar to the industrial standards on the subject, but it has been more recently revised.

One important distinction that the government makes in its standards that industry does not is in the use of the term "fluidic" to refer to the entire technology and the term "flueric" to refer to that part of the technology involving no moving parts. When references to fluidic logic having moving parts are made, it is referred to as moving part logic or MPL and is distinct from flueric logic.

It should be pointed out that the majority of the fluidic terminology standards refer specifically to the flueric terminology. The moving part terminology, which includes the moving part logic, is mostly drawn directly from the long established and more closely related fluid power terminology.

3.2 Symbology

Symbology, even the nonmilitary rendition of it, is covered by MIL-STD-1306A (terminology and symbology) and need not be discussed at length. The symbols for a considerable number of fluidic components, especially sensors, are not covered by any fluidic symbology standard, and this area needs attention.

An NFPA standard T3.21.2-1973 has been published regarding the symbology of MPL. This document bridges the material of conventional hydraulics/pneumatic and fluierics, and, as such, it is a very good document. There is additional discussion of the contents of this document in section 2.2.

3.3 Test Methods

The military standard that covers test methods is MIL-STD-1361A, which is available with this paper. Parts of this document, especially those dealing with the quasi-static tests of digital elements, have been revised recently so that it now differs in format from the SAE standard on the subject. The old test procedures were vaguely categorized, but the test procedures in the revised MIL-STD are more clearly categorized with respect to such details as loading conditions and pressures to be used. The individual initiating the test is still free to use whatever test procedures he would have used previously. However, whatever he does can be easily described by referring to a test category or test type in the standard. This material, including these detailed categories, is not covered in any other document.

3.4 Instrumentation

Test instrumentation is covered in MIL-STD-1361A and in SAE ARP 1254 (revised). A small amount of additional material regarding hot wire anemometry is in SAE's ARP993A. In all of these, the subject matter is limited since there is no intent to impose any specific instrumentation requirements or specify types of instrumentation.

3.5 Presentation of Element Characteristics

The presentation of element characteristics is covered in several ways in various documents and forms. The most extensive is NFPA T3.7.3-1970 (ANSI/B93.14-1971). This document specifies the presentation of descriptive information including function, type, configuration, materials, external connections, operating limits, and steady-state and time-dependent performance characteristics. Particular formats are defined including 12 different kinds of quasi-static impedance curves for various classes of elements and one standard format for the time response data taken from a dynamic test set up. Similar material is also covered, but less extensively, in the ARP993A. To the extent that data presentation requires standard terminology and test methods, this subject is also in MIL-STD-1306A and MIL-STD-1361A, respectively.

Two short-form formats have been specifically developed for the concise presentation of fluidic element performance data. One format used by the military is called a fluidic element fact sheet. One sheet may display specific data from an element operating with open ports, and another sheet may display data from the same element tested with blocked ports. The distinction will be clearly indicated by referencing the

specific test method used, as classified in MIL-STD-1361A. Two of these fluidic component fact sheets are included as appendices. The component described on each of these sheets is the same, but it has been tested under two different sets of conditions as indicated on the separate fact sheets.

The second short format is defined in SAE's ARP993A; it asks for the same information as the military's fluidic element fact sheet but does not require specific statements on testing conditions or specific definitions of parameters such as power gain or power amplification as does the military fact sheet.

3.6 Power Supplies and Interface Devices

The SAE is presently drafting an AIR to classify power supplies as to source and use and another to classify devices, such as pilot valves that interface with fluidic systems. These AIR's could eventually be the basis of more extensive documents or even as standards on power supplies and interface characteristics. In the meantime, they will be valuable in their own right as Information Reports when they are published.

4. NEW STANDARDIZATION EFFORTS

Very much of the overall current American standardization effort is directed toward international standards, and so any direction that our fluidic standards take in the future is likely to be imparted as a result of ISO activity.

The ISO activity is a result of the interest of its working members. The subjects of most pressing interest seem to be logic and circuit diagrams, terminology, and performance rating with emphasis on MPL. This area of MPL is an area where current American standards are few; therefore, the ISO effort will surely benefit the American technology. However, it should be emphasized that the American input to this fluidic activity has been ineffective, and so the standards that result may reflect very little of the interests of American industry or military. If American interests are to be felt, there must be a steady, continued, coordinated effort put forth to keep up with the work and to attend the American, European, and Japanese ISO working group meetings. Interested U. S. organizations and individuals should contribute; otherwise, the United States will have little effect on international fluidic standards no matter how good or how widely used our own differing standards may be.

Along with the international influence, advances in technology will continue to influence the future standards effort. For example, some recent work has been done to define the effects of power supply contamination on fluidic reliability. As this type of knowledge

accumulates, it is reasonable to expect that it will influence design parameters for the system power supplies, possibly including the operating pressures. The final outcome might be parts interchangeability, both operationally and physically. However, as desirable as this might be for the user, it does not appear possible until much more technical ground work is done.

5. USE OF FLUIDIC STANDARDS

Whether a document is good because it is used, or used because it is good, is difficult to answer. But some documents seem to enjoy greater acceptance than others. The terminology and symbology which is used within the fluidic technology is fairly uniform and consistent with the standards. (There are notable exceptions: one major manufacturer of fluidic components uses the electronic pin notation for the port designations of its flueric elements in conflict with all the relevant standards and in conflict with the general practice, and another uses complete electronic logic symbology for its circuit diagrams.)

When different standards call for opposing practices, then no particular practice will prevail. The matter of units is an example. The SAE standards call for the US Customary units, and the military standards call for SI units. The prevailing practice is a mixture. This author prefers the SI because of its relative logic, simplicity, and life expectancy. However, even among users of the SI units, exact details sometimes result in differences. For example, the basic unit of pressure in SI is "N/m²." Various multiples of this unit have been named "bars" and "pascals." Both are allowed in SI. The military chooses to use "pascals," and the fluid power industry chooses "bars" as working units. In this case, this author has a personal preference for the basic units; that is, "N/m²" at least until the difference in use is worked out.

It seems to this author that the most important fluidic standards are the two military standards, the data presentation standard, and the MPL symbols standard of the NFPA. For a person wanting to cover the entire field, the NFPA publication Fluid Power Standards and the two military standards as well as the two yet to be released SAE AIR's on power supplies and interfaces should form a very adequate library.

6. CONCLUSIONS

The American fluidic technology has been guided by several standards that have been developed and accepted by our industry and military services. These deal with terminology, symbology, data collection, and presentation. An adequate library of the current standards would consist of the MIL-STD-1306A Flueric Terminology and Symbology,

MIL-STD-1361A Fluidic Test Methods and Instrumentation, and the NFPA publication Fluid Power Standards (third edition). As the technology develops, so does its standards, and future work might be expected in the MPL area, parts interchangeability, power supply classifications and, of course, in the area of the SI.

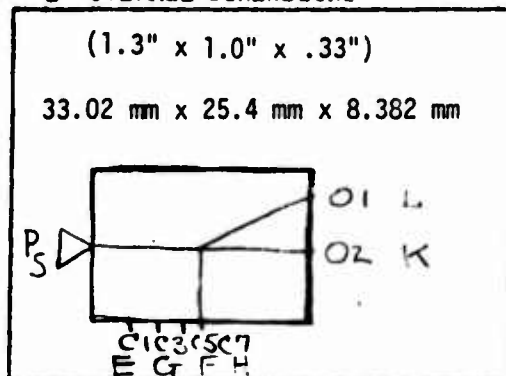
DIGITAL FLUIDIC COMPONENT FACT SHEET

1.) ELEMENT NUMBER

A - B - C - D (see code)
O/N-A-1-SECR 014 s/n1

3.) ORIGINATORS DESIGNATION FOR ELEMENT
OR/NOR GATE - 191453 (Corning)

2.) SCHEMATIC & PORT MARKINGS
& OVERALL DIMENSIONS



4.) ELEMENT FEATURES INCLUDING (1) function
(2) type (3) nozzle width
(4) aspect ratio
(5) type of port connections (manifold, tube size, etc.)

1. OR/NOR
2. wall attachment
3. 0.254 mm
4. 2.0
5. Brass fitting on manifold for: 1.905mm I.D. tube on control 4.318mm I.D. on supply, accessories available from Corning

5.) OTHER PERTINENT INFORMATION INCLUDING (1) any references (2) fabrication techniques (3) special precautions in usage (4) material (5) fluid used

1. Supplier's catalog
2. Photo processed ceramic laminates fused together.
3. Requires a manifold and other tubing hardware supplied by Corning.
4. Ceramic - Fotoceram
5. Air

6.) ORIGINATORS - ADDRESS

Corning Glass Works Corning, New York

7.) DISTRIBUTION: LIST ANY RESTRICTIONS TO DISSEMINATION OF DATA (imposed by originator)

- NONE
- FOREIGN ANNOUNCEMENT AND DISSEMINATION IS NOT AUTHORIZED
- ONLY U. S. GOVERNMENT AGENCIES ARE AUTHORIZED
- ONLY U. S. MILITARY AGENCIES ARE AUTHORIZED
- ALL DISTRIBUTION OF THIS INFORMATION IS TO BE CONTROLLED BY ORIGINATOR
- (CLASSIFIED) ALL DISTRIBUTION OF THIS INFORMATION IS TO BE ON A "NEED TO KNOW" BASIS

DATE:

ELEMENT NUMBER CODE

A	B	C (FLUID USED TO OPERATE ELEMENT)	D
FF = FLIP FLOP O/N = OR/NOR A/N = AND/ NAND S.T. = SCHMITT TRIGGER C.S. = ONE SHOT OT = OTHER	A = ACTIVE P = PASSIVE	1 = gas 2 = low viscosity liquid 3 = high viscosity liquid 4 = special	Designation assigned by Secretary

8.) PARAMETERS (IN ACCORDANCE WITH MIL-STD-1306)

- 1. Nozzle width..... 0.254 mm
- 2. Aspect ratio..... 2.0
- 3. (a) Supply Pressure (RANGE)..... 20.0 - 70.0kpa
- (b) Supply Pressure (TYPICAL).... 45.0kpa
- (c) Fluid type..... Air

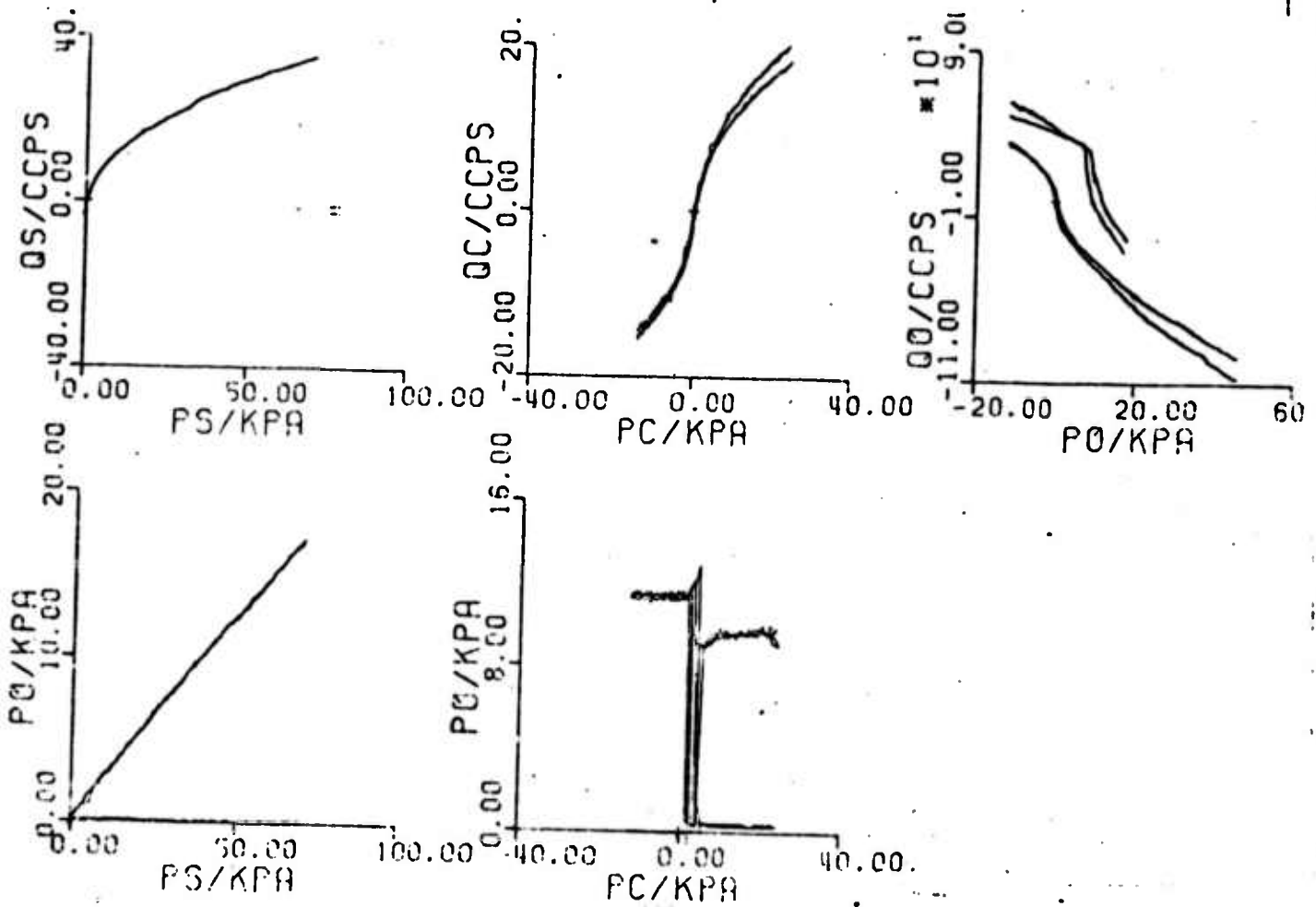
NOTE: Following data taken at typical supply pressure as per MIL-STD-1361A test type

Test methods 1001 through 1005

and under the following environmental conditions
7000 ft. altitude

- 4. Power consumption..... .883 watts
- 5. Fanout..... 4.0
- 6. Flow recovery..... 1.513
- 7. Pressure recovery..... .226
- 8. Flow gain..... 3.754
- 9. Power gain..... 6.653
- 10. Pressure gain..... 2.282
- 11. Hysteresis..... 3.825
- 12. Frequency response.....
- 13. Signal to noise ratio.....
- 14. Load sensitivity as per MIL-STD 1361A.....

USE THE FOLLOWING SPACE FOR POWER JET IMPEDANCE CURVES, CONTROL IMPEDANCE CURVES, OUTPUT IMPEDANCE CURVES, PERCENTAGE OF RECOVERY CURVES, TRANSFER FUNCTIONS AND FREQUENCY RESPONSE DATA.



DIGITAL FLUIDIC COMPONENT FACT SHEET

1.) ELEMENT NUMBER

A - B - C - D (see code)
 O/N - A - 1 - SECR 014

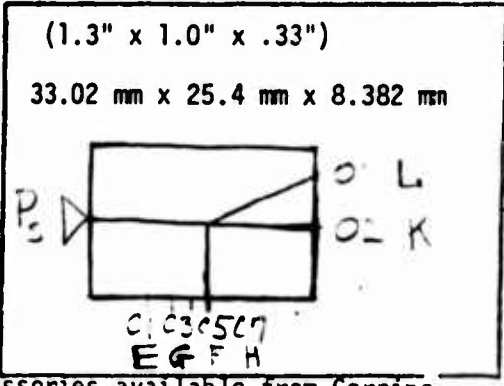
3.) ORIGINATORS DESIGNATION FOR ELEMENT

OR/NOR GATE - 191453 (Corning)

4.) ELEMENT FEATURES INCLUDING (1) function

- (2) type (3) nozzle width
- (4) aspect ratio
- (5) type of port connections (manifold, tube size, etc.)
 1. OR/NOR
 2. wall attachment
 3. 0.254 mm
 4. 2.0
 5. Brass fitting on manifold for 1.905 mm I.D. tube on control 4.318 mm, I.D. on supply, accessories available from Corning.

2.) SCHEMATIC & PORT MARKINGS & OVERALL DIMENSIONS



5.) OTHER PERTINENT INFORMATION INCLUDING (1) any references (2) fabrication techniques (3) special precautions in usage (4) material

- (5) fluid used
 1. Supplier's catalog.
 2. Photo processed ceramic laminates fused together.
 3. Requires a manifold and other tubing hardware supplied by Corning.
 4. Ceramic - Fotoceram.
 5. Air.

6.) ORIGINATORS - ADDRESS

Corning Glass Works Corning, New York

7.) DISTRIBUTION: LIST ANY RESTRICTIONS TO DISSEMINATION OF DATA (imposed by originator)

- NONE
- FOREIGN ANNOUNCEMENT AND DISSEMINATION IS NOT AUTHORIZED
- ONLY U. S. GOVERNMENT AGENCIES ARE AUTHORIZED
- ONLY U. S. MILITARY AGENCIES ARE AUTHORIZED
- ALL DISTRIBUTION OF THIS INFORMATION IS TO BE CONTROLLED BY ORIGINATOR
- (CLASSIFIED) ALL DISTRIBUTION OF THIS INFORMATION IS TO BE ON A "NEED TO KNOW" BASIS

DATE:

ELEMENT NUMBER CODE

A	B	C FLUID USED TO OPERATE ELEMENT	D
FF = FLIP FLOP O/N = OR/NOR A/N = AND/NAND S.T. = SCHMITT TRIGGER C.S. = CAP SHOT OT = OTHER	A = ACTIVE P = PASSIVE	1 = gas 2 = low viscosity liquid 3 = high viscosity liquid 4 = special	Designation assigned by Secretariat

B.) PARAMETERS (IN ACCORDANCE WITH MIL-STD-1306)

- 1. Nozzle width..... .254 mm
- 2. Aspect ratio..... 2.0
- 3. (a) Supply Pressure (RANGE)..... 20.0 - 70.0kpa
- (b) Supply Pressure (TYPICAL).... 45.0kpa
- (c) Fluid type..... Air

NOTE: Following data taken at typical supply pressure as per MIL-STD-1361A

Best type

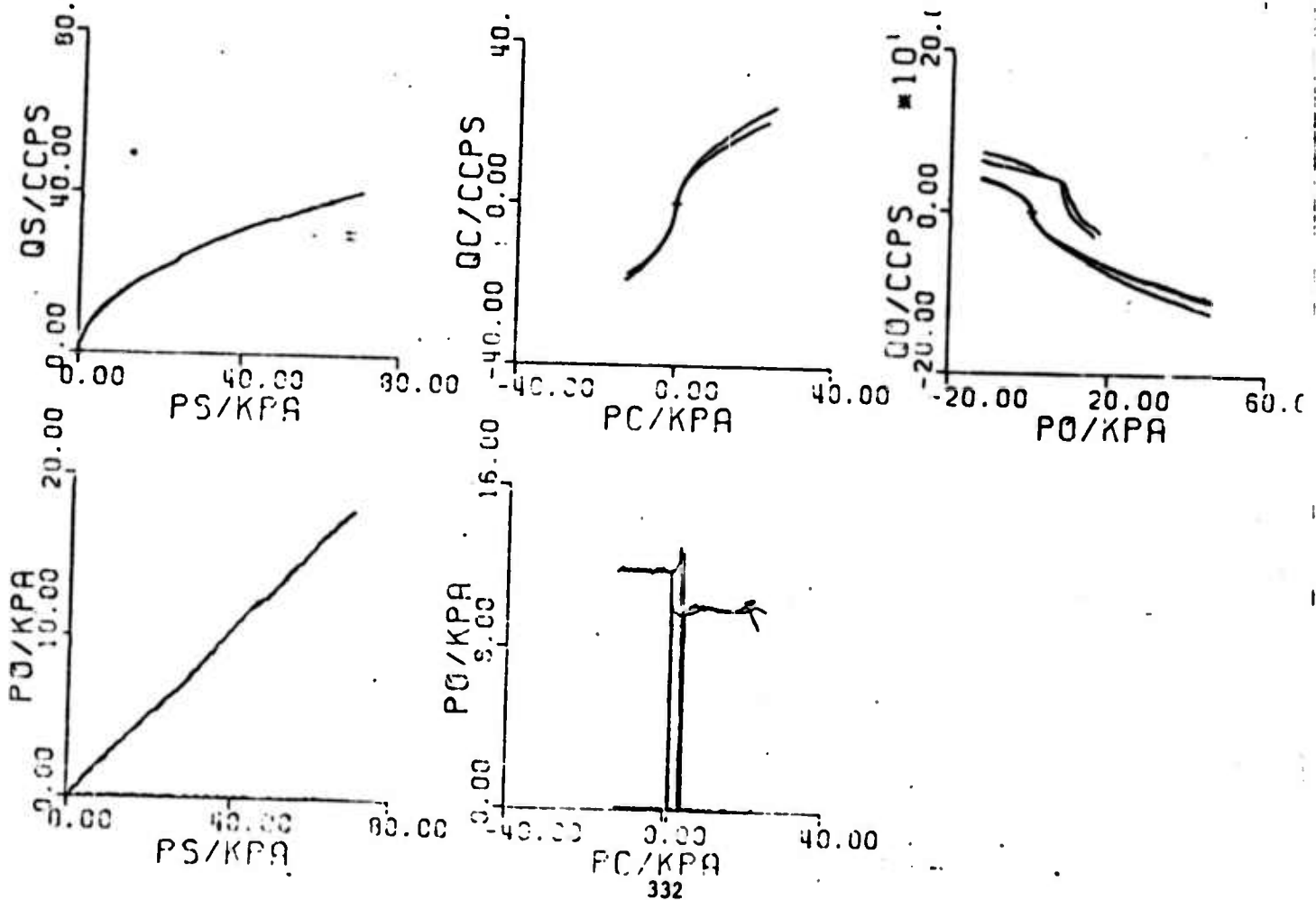
Test methods 1001 through 1005

- 4. Power consumption..... 1.03 watts
- 5. Fanout..... 4.0
- 6. Flow recovery..... 1.573
- 7. Pressure recovery..... .238
- 8. Flow gain..... 4.377
- 9. Power gain..... 7.169
- 10. Pressure gain..... 2.415
- 11. Hysteresis..... 3.622
- 12. Frequency response.....
- 13. Signal to noise ratio.....
- 14. Load sensitivity as per MIL-STD 1361A.....

and under the following environmental conditions

Room Ambient

USE THE FOLLOWING SPACE FOR POWER JET IMPEDANCE CURVES, CONTROL IMPEDANCE CURVES, OUTPUT IMPEDANCE CURVES, PERCENTAGE OF RECOVERY CURVES, TRANSFER FUNCTIONS AND FREQUENCY RESPONSE DATA.



FLUIDICS STANDARDS AND PRACTICES - THE USE OF MILITARY DOCUMENTATION IN
THE DEVELOPMENT OF FLUIDIC SYSTEMS AND EQUIPMENT

by
Harold Ott of the Naval Air Engineering Center

INTRODUCTION

The Defense Standardization Program requires the achievement of the highest practicable degree in the standardization of items and practices, applicable thereto, used throughout the Department of Defense (DoD). In order to provide adequate documentation to control the procurement and application of fluidic devices, the Military Services, under the Defense Standardization Program, are developing a series of coordinated standards, handbooks, and specifications. Inclusion of a general specification and detail specifications will provide uniform design criteria and visibility for those fluidic devices experiencing broad acceptance. The services will encourage system or equipment design optimization without constraining system designers. They will seek achievement of maximum potential benefits offered by the use of fluidics and encourage its application in military systems and equipment. The intent of this paper is to define the DoD Standardization Program and its effort to provide the military with a means for procurement and application of standardized fluidics devices and systems. It is requested that the reader refer to the appendices for further details on the procedures for obtaining documents referred to in this paper.

DISCUSSION

The Defense Standardization Program (Sec. 2451-2456), Title 10, United States Code, superseding Public law 436, 82nd Congress, requires the achievement of the highest practicable degree of standardization of items and practices applicable thereto as used throughout the Department of Defense. This program is implemented by DoD Directive 4120.3, by other DoD directives and Instructions, and Defense Standardization Manual 4120.3-M.

4120.3-M was developed and is maintained in cooperation with the Departments of the Army, Navy, Air Force, and the Defense Supply Agency, in accordance with DoD Directive 4120.3. It is mandatory for use by all defense activities.

The Assistant Secretary of Defense for Installations and Logistics OASD (I&L) is responsible for standardization policy guidance and administration. This responsibility includes establishment of policies, procedures, program guidance and reporting, and surveillance techniques for control and evaluation of program accomplishments. The program is decentralized, as necessary, with assignment of responsibilities to the Military Services with authority to further delegate portions of the operations to military activities.

In order to illustrate the development of the fluidics standardization program, the DoD policy governing microelectronics (a similar and relatively new technology) will be utilized in this paper to measure current progress in fluidics.

Early memoranda relating to the application of microelectronics, dated 8 Apr 1963 and 28 Jun 1965, were updated by an Office of the Secretary of Defense policy memorandum dated 14 Apr 1967. This memorandum specifically related microelectronics to design applications, specifications and standardization, procurement, maintenance and logistics support. If the reader will substitute "fluidics" for "microelectronics" in the following quotes from this memorandum, the objectives of the fluidics standardization program can be visualized.

"An ultimate objective in the area of military electronics is to provide equipment which satisfactorily fulfills the military need with a high probability of no failure for the entire lifetime of the equipment or system. The higher the equipment reliability, the higher becomes this probability and the simpler becomes the logistic support problem. The considerable improvement in reliability offered by microelectronics, the savings in space and weight and potential cost reduction make it most desirable to promote the widest possible appropriate use of microelectronics in military systems. Further, the reliability of microelectronics circuits is sufficiently high to warrant packaging of several, or even many, such circuits into modules for which repair is neither practical nor effective. Such design modules, to be discarded upon failure, would reduce logistic support costs and further improve reliability."

To maximize the potential benefits offered by microelectronics, DoD policy was outlined for the following areas:

1. Application of Microelectronics to Military Systems and Equipment
2. Use of Unitized or Modular Construction
3. Maintenance and Logistic Support
4. Inter-System Standardization
5. Intra-System Standardization
6. Documentation

After a review of this policy, on 23 September 1969, documentation in Section 6 was expanded to permit the issuance of a general specification and detail specifications as follows:

6. Documentation

"Standardization documentation of microelectronics will be restricted at this time to the areas of: (a) definition of terms; (b) parameters to be controlled for circuit characterization; (c) test levels including test methods and procedures; (d) general application guidance, design criteria; (e) preservation and packaging guidance; and (f) a general specification and detail specifications. Standardization, via the publication of Military Standards (MIL-STD), or equivalent lists, depicting devices as standard for new design is prohibited.

"The expansion of the standardization documentation to include a microelectronics general specification is intended to provide a set of basic design and test criteria (excluding physical characteristics) from which device specifications can be prepared. If it is necessary for DoD components to specify, prior to design, performance or physical characteristics of microelectronic circuits or modules for specific systems or equipment, such requirements will be included in the system or equipment specification, and not as a device specification prepared by the DoD component. Contractor-prepared device specifications reflecting these requirements and tailored to the specific system or equipment will utilize to the extent applicable the general specification and, to the degree practicable, be prepared in military format to facilitate logistics support and competitive procurement. Military detail specifications for microelectronic devices will be prepared as ancillary documents to the general specification so as to provide visibility to those devices having achieved broad acceptance."

Implementing the policy of the DoD memorandum, a Secretary of the Navy Instruction established Navy policy governing the use of military documentation in the development of microelectronic systems and equipment. Similarly, a Naval Air Instruction was proposed to establish Naval Air Systems Command policy.

Suppose that a hypothetical Naval Air Systems Command Instruction on policy governing the use of military documentation in the development of fluidic systems and equipment were written. The main portion would probably read something like this:

"1. Background. SECNAVINST XXXX contains current Navy policy on fluidics. It requires that all projects being initiated in various Research and Development categories be reviewed to ensure appropriate consideration of the use of fluidics. The policy is not intended arbitrarily to require the use of fluidics; rather, it directs an objective appraisal of all factors concerning the system/equipment design relative to current fluidics technology with the view of maximizing reliability and minimizing total cost of ownership, weight and space within the envelope of the other performance parameters of the design.

a. Based upon the considerable improvement in reliability offered by fluidics, SECNAVINST XXXX also requires the design of modular assemblies that can be economically discarded upon failure and, ultimately, the design of equipment capable of logistic self-support.

b. Experience over the past several years has shown that, while fluidic devices are inherently reliable, the standard commercial product lines offered by device vendors may not normally meet military reliability requirements. The manufacture of fluidic devices requires more rigorous control than that required for most other hydraulic or pneumatic parts. These controls include:

- (1) Extremely close tolerances in device design.
- (2) Control of complex processing steps.
- (3) Use of precision test equipment .
- (4) Rigid contamination control & workmanship standards.

c. In addition, the fluidic state-of-the-art changes rapidly. It is not uncommon that the cost, size and performance advantages of newly-developed fluidic devices are sufficient to motivate the choice of these devices even when comprehensive control documentation is not available, and cannot be readily developed. This tends to introduce a variety of more complex and relatively unproven devices into developmental hardware. Potentially, these devices may exhibit failure modes and mechanisms which are not yet fully controlled by the manufacturer.

d. Failure modes in fluidic devices may tend to be "catastrophic," as opposed to "degrading," and, in addition, the failures tend to appear early in the operation of the devices. Hence, it has been found that screening and other test programs, including visual examination and environmental stress, and run-in, can effectively identify the major catastrophic failures related to bonding and sealing, and to various processing and workmanship errors. Thus, early-life failures may be removed from the lot under test.

e. In an effort to provide adequate documentation to control the procurement and application of fluidic devices, the Military Services, under the Defense Standardization Program, have developed a series of coordinated specifications, standards and handbooks.

2. Policy. It is the policy of NAVAIR that the following documents shall be invoked when initiating system/equipment projects where fluidic devices will be used in the subsequent development efforts.

a. MIL-F-XXXX Fluidic Circuits, General Specification For. This specification establishes the general requirements, and the quality and reliability assurance requirements which must be met in the procurement of fluidic circuits. Options for various levels of product assurance and control are established in the specification. The specification provides for individual item requirements for fluidic circuits to be documented in detail specifications, and establishes a qualified products list and a manufacturer's product assurance program. The specification references and specifies the use of MIL-STD-1361, Fluidics Test Methods and Instrumentation; MIL-STD-1306, Fluidics Terminology and Symbols; MIL-STD-XXXX; Parameters to be Controlled for the Specification of Fluidic Circuits; and MIL-F-XXXX, Fluidic Circuits; Packaging of.

b. MIL-HDBK-XXX Fluidics and Fluidic Integrated Circuits. This document provides general information on fluidic devices and their applications. It contains valuable guidance to personnel concerned with the design, development, and production of equipment and systems employing fluidic circuits.

c. AR-XXX, Fluidic Devices Used in Military Equipment, Procedures for Selection and Approval of: This specification establishes requirements for the selection, approval and demonstration of the interchangeability of two or more fluidic devices.

3. Related Information. The Naval Material Command has issued a Navy System Design Guidelines Manual for Fluidic Packaging. "Packaging" in this sense refers to the fluidic organization and mechanical construction of fluidic equipment, ranging from circuit boards and modular assemblies, through large enclosures. The manual contains a selection of fluidic packaging approaches developed under the direction of Navy facilities, reflecting the results of extensive development efforts conditioned by experience gained in solving packaging problems for complex Navy systems. The module and circuit board configurations contained in the manual are suitable for the assembly and interconnection of fluidic circuits. To reduce proliferation of a large variety of packaging concepts, it is recommended that the packaging approaches contained in this manual be used whenever appropriate, with the ultimate decision as to suitability resting with the organization responsible for the equipment development."

SPECIFICATIONS

At the time of this writing, only MIL-STD-1306, "Fluidics Terminology and Symbols" and MIL-STD-1361, "Fluidics Test Methods and Instrumentation," have been issued and a MIL Handbook is being written. The general specification will probably be the next item of documentation to be considered.

Fluidic circuit designers should appreciate that the Department of Defense (DoD) fluidic specifications are primarily procurement specifications and are not design specifications for application and system design. Moreover, as stated in MIL-STD-143, it is the designer's responsibility to see that equipment sold to the Government operates properly and reliably. Furthermore, the use of Military Standards (MS) or specification parts is no guarantee of Government acceptance. Although the use of Government QPL'd fluidic devices is highly desirable to the Government for logistics purposes, including replacements, their use is also desirable and encouraged because the QPL'd items provide a means for contractors to obtain uniform parts from one or more manufacturers regardless of the size of the contractor. With the Government administering the QPL, contractors, regardless of their economic impact, are spared the necessity of testing each and every lot of devices for environmental and other expensive tests. However, the devices must be technically suitable for each application and circuit, no matter how attractive it might be to standardize on a limited few devices throughout the equipment.

To illustrate how a fully coordinated (FC) specification is generated and controlled, refer to Figure 1 together with, for example, MIL-F-XXXX, because no specification has been issued. OASD (I&L) is shown at the top of the organization chart of the DoD standardization program. The Federal Supply Classification (FSC) of fluidics is 1650. Standardization Directory SD-1 lists ESSD as Assignee Activity of FSC 1650. ESSD is the Engineering Specifications and Standards Department of the Naval Air Systems Command. The Assignee Activity's function, Paragraph 1-307 of 4120.3-M, is essentially, to assign project numbers for new documents, revisions, or amendments, to determine that there is no duplication of effort, and finally to check on a standardization project's progress from inception to completion.

In Figure 1, note the agency labeled "Preparing Activity." The agency responsible for preparing and maintaining a document is labeled the preparing activity (PA). For example, the PA for MIL-F-XXXX is Naval Air Systems Command. The address of the PA is pre-addressed on DD Form 1426, "Standardization Document Improvement Proposal." DD Form 1426 is attached as the last page of every Military Specification and is for the convenience of anyone who has an interest in the Standardization Document to submit his comments on any problems with the document at any time. The PA's function is to analyze each problem for its validity, and to take steps to amend or revise the document as applicable. On a fully coordinated specification it is required that proposed revisions or amendments be circulated to all interested Military and Industry activities for concurrence or comments. In the case of fluidics such as MIL-F-XXXX, circulation is as shown on the organization chart Figure 1. Generally speaking, it is difficult to obtain full concurrence on any proposal. Usually the final document is a result of give-and-take consistent with the needs of DoD. All of the activities play their individual role in the DoD standardization effort. A partial listing of addressees and functions is shown in the Appendix to this paper, and a complete listing is shown in SD-1.

Another type of specification in the system is called a limited coordinated (LC) specification. For example, a specification on a specialized fluidic device or system may be of interest only to the Naval Air Systems Command (AS). The organization chart for a hypothetical MIL-F-XXXX (AS) is shown on Figure 2. An LC document has the advantage that coordination can be effected more quickly, but has the obvious disadvantage that its usage is limited in scope. Both LC and fully coordinated documents are necessary in the DoD standardization effort.

Specifications are procurement documents and are not meant to be used for design purposes. A specification is a general document and is usually supplemented by detail sheets. These detail sheets take two forms in the military system. One type is called specification "Slash Sheets" and take the same number as the general specification followed by a slash number, for example, MIL-F-XXXX/X. Another type, called military standard sheets, have been used in the past. They are usually referred to as MS sheets. An example would be MSXXXX. By order of OASD, MS sheets are to be phased out and replaced by slash sheets whenever possible.

In addition to specifications, slash sheets, and MS sheets, DoD standardization departments also prepare book-form standards (MIL-STDs), handbooks, publications and other documents. These aforementioned documents supplement Military Specifications.

A complete list of Military and Federal documents can be found in DoD Index of Specifications and Standards (DODISS). The appendix goes into more detail on how to order publications such as DODISS, and outlines "A guide to private industry" which we hope will prove helpful in untangling some of the problems Industry faces with the DoD standardization effort.

BEWARE OF "SPECMANSHIP"

In spite of the aforementioned document standardization system the military has been confronted in the past by widescale misuse of specifications in certain areas which may result for example, in the misapplication of devices. A continuing effort is being expended via the DoD standardization effort to alert users to avoid misapplications.

The potential buyer of fluidic devices should beware of the manufacturer who implies capabilities the device does not possess under actual service conditions. Following are some typical phrases from catalog sheets and other promotional material for other devices. In parentheses are the pitfalls to watch for when reading such promotional material.

1. Promotional material claims "Military Specification Device" without having a single type on the Government's Qualified Products List (QPL). (This claim plays on the erroneous assumption that "military specification" devices have supernatural capabilities).

2. Promotional material claims "Meets MIL-X-XXXX" (Without QPL Status).
- 2A. Promotional material claims "Meets all MIL-X-XXXX requirements."
(No substantiating data are offered.)
3. Promotional material claims "Meets all applicable portions of MIL-E-XXXX" (MIL-E-XXXX is not a device specification but is an environmental specification and the so-called applicable portions are not listed. In other words, sounds good but says nothing.)
4. Promotional material assumes that the user knows fluidic devices and will apply them correctly. (e.g., Use jargon of industry without indicating to potential user where he may obtain additional information such as a military standard on application and selection.)
5. Potential supplier responds to a customer's new device specification immediately with price and delivery data. (You know the customer is going to get what you are producing so never mind taking exceptions to any unusual requirements the customer may have included.)

NON-STANDARD PARTS

It is incumbent on the equipment designer to obtain approval of all nonstandard parts by the procuring agency. Naturally, if a military standard part is technically suitable and is used rather than a non-standard part, a lot of time and money can be saved.

CONCLUSION

It is hoped that this paper, supplemented by the appendix, yields some insight on how the DoD Standardization effort serves the military and industry, and what military specifications and standards can do for you, and what they can't.

APPENDIX I
EXCERPTS FROM 4ND-NPFC-4120/3.

These excerpts are for the convenience of the readers of this paper, and explain in more detail some of the abbreviations and terms used in the body of the paper.

The pamphlet, in its entirety, is available from Naval Publications and Forms Center, 5801 Tabor Avenue, Philadelphia, Pa. 19120.

The title of the pamphlet is "DEPARTMENT OF DEFENSE SINGLE STOCK POINT (DOD-SSP) FOR SPECIFICATIONS AND STANDARDS. A GUIDE FOR PRIVATE INDUSTRY"

Types of Documents Stocked and
Distributed

Military Specifications
Military Specification Sheets
Military Standards (MS's) Sheets
Military Standards (MIL-STD's) Book Format
Qualified Products Lists (QPL's)
Industry Documents adopted for use by DoD
Military Handbooks
Air Force - Navy Aeronautical Standards
Air Force - Navy Aeronautical Design Standards

DODISS

The Department of Defense Index of Specifications and Standards (DODISS) is prepared at NPFC and is published in three parts annually with bi-monthly supplements.

The three parts are the alphabetic listing (Part I), the numeric listing (Part II), and the Federal Supply Classification (FSC) listings of the following unclassified documents

Military Specifications
Federal Specifications
Qualified Products List (QPL's)
Military Handbooks
Air Force & Navy Aeronautical Design Standards
U. S. Air Force Specifications
Air Force & Navy Aeronautical Bulletins
Military Standards (MS's) Sheets
Military Standards (MIL-STD's) Book Format
Industry Documents
Air Force & Navy Aeronautical Specifications
Other Departmental Documents
U. S. Air Force Specification Bulletins
Cancellation Lists

Parts I and II of the DODISS are available to private industry on request from the Superintendent of Documents, Government Printing Office, Washington, DC 20402, at a subscription rate of \$36.00 per year (\$9.00 additional for foreign mailing). The Federal Supply Classification Listing is available from the Superintendent of Documents at a subscription rate of \$18.00 per year (\$4.50 additional for foreign mailing). Both subscriptions include the basic index and the cumulative bi-monthly supplements for each part as they are published.

The triennial cancelled documents appendix for Part II, numerical listing is available as a single sales item at \$2.00 per copy (63 cents additional for foreign mailing).

To submit a complaint or to make an inquiry by correspondence, write to:

Commanding Officer (Code 512)
Naval Publications and Forms Center
5801 Tabor Avenue
Philadelphia, Pa. 19120

To submit a complaint or to make an inquiry by telephone call
AREA CODE 215, 697-2179.

APPENDIX II

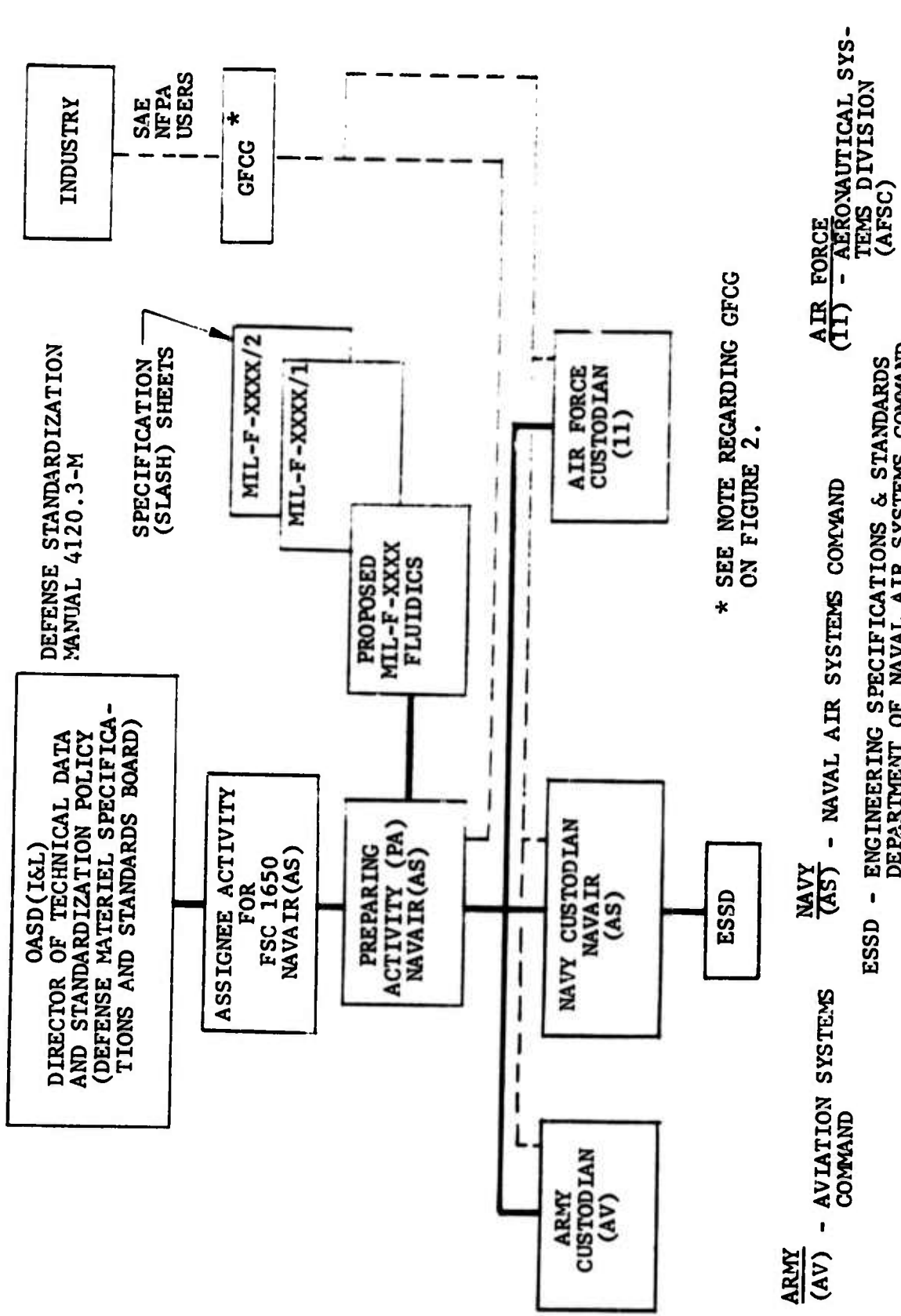
4120.3M Defense Standardization Manual (4120.3M DSM) is a compilation of Defense Standardization Policies, Procedures, and Instructions. It is a relatively lengthy and involved publication and is probably of value only to those directly involved in the Standardization line of work. However for those of you who may be interested, DOD 4120.3M DSM is available from

Superintendent of Documents
US Government Printing Office
Washington, DC 20402
Price - \$2.50

The following terms which were used in the text are gleaned directly from DSM 4120.3M

- 1-101 ACTIVITY. One of the organizational elements of the Army, Navy, Air Force, Defense Supply Agency, US Marine Corps, Coast Guard and other activities of the Department of Defense.
- 1-106 ACTIVITY, Preparing. The military activity or the activity in a Federal civil agency (for Federal documents only) responsible for document and study projects and for maintenance of the resultant standardization documents.
- 1-107 ACTIVITY, Review. An activity having Departmental, Service, Agency responsibility for the design, configuration or application of an item (s), material(s) or process(es) and which, for these reasons, has an essential technical interest in the covering document that is not susceptible to waiver, thus requiring a review of all proposed actions affecting the document. Defense Supply Centers may declare review interest in standardization documents covering items for which they have procurement, inspection and supply responsibilities and in those instances wherein advance knowledge and review of documents is necessary to assure procurability (including such factors as industrial capability, economics, and inspection), of the described items to the specified requirements. Essential comments submitted in this capacity will be limited to the functional areas for which Defense Supply Agency (DSA) has mission responsibility in management of the items. The decision to be, or not to be, a review activity will be made by the Defense Supply Center concerned.
- 1-108 ACTIVITY, User. An activity having Departmental, Service, or Agency responsibility for using a standardization document to acquire the item(s), material(s) or process(es) covered thereby, but whose interest is not sufficient to require active participation in the coordination of the document.

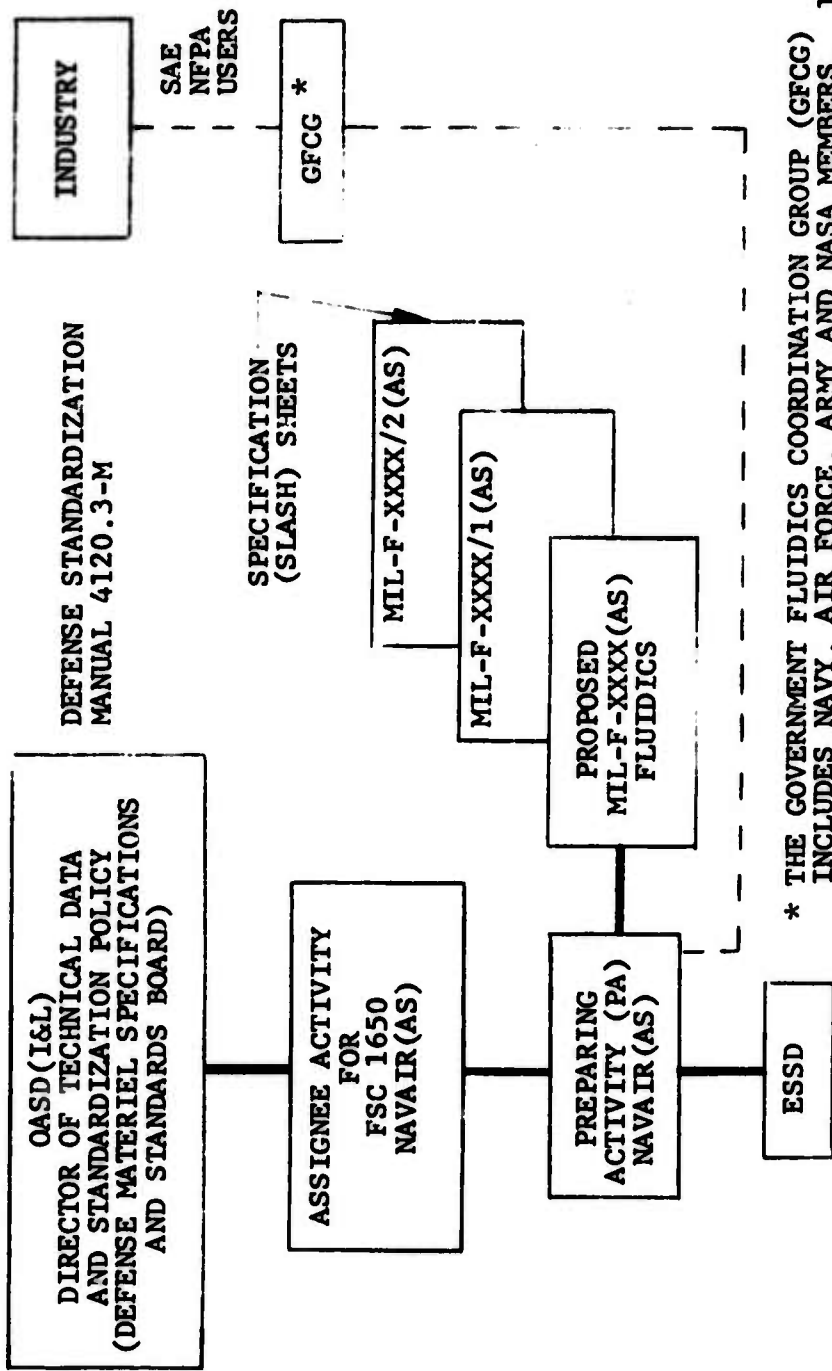
- 1-111 AGENT. An activity which acts for, and by authority of the Preparing Activity (the Preparing Activity, however does not relinquish approval responsibility for the work accomplished). Examples of agent actions are: Preparation of standardization documents; performance of study projects; and administration of Qualified Products Lists (QPL's).
- 1-121 CUSTODIAN. The activity responsible for effecting coordination and other related functions for its own department in the DoD.
- 1-147. QUALIFIED PRODUCTS LIST. A list of products qualified under the requirements stated in the applicable specification, including appropriate product identification and test reference with the name and plant address of the manufacturer and distributor, as applicable.



* SEE NOTE REGARDING GFCG ON FIGURE 2.

ARMY (AV) - AVIATION SYSTEMS COMMAND
 NAVY (AS) - NAVAL AIR SYSTEMS COMMAND
 AIR FORCE (11) - AERONAUTICAL SYSTEMS DIVISION (AFSC)
 ESSD - ENGINEERING SPECIFICATIONS & STANDARDS DEPARTMENT OF NAVAL AIR SYSTEMS COMMAND

FIGURE 1. ORGANIZATION CHART FOR PROPOSED MIL-F-XXXX FLUIDICS FULLY COORDINATED (FC) SPECIFICATION



* THE GOVERNMENT FLUIDICS COORDINATION GROUP (GFCC) INCLUDES NAVY, AIR FORCE, ARMY AND NASA MEMBERS. IT HAS A STANDARDIZATION COMMITTEE. THE GFCC COORDINATES EXCHANGE OF FLUIDICS TECHNOLOGY AND MANAGEMENT INFORMATION IN GOVERNMENT AND INDUSTRY.

FIGURE 2. ORGANIZATION CHART FOR PROPOSED MIL-F-XXXX(AS) FLUIDICS LIMITED COORDINATED (LC) SPECIFICATION

CONTAMINATION EFFECTS IN A
LAMINAR PROPORTIONAL
AMPLIFIER

R. A. Comparin
Newark College of Engineering
Newark, New Jersey

H. L. Moses
Virginia Polytechnic Institute and State University
Blacksburg, Virginia

E. E. Rowell, III
Dow Badische Co.
Williamsburg, Virginia

INTRODUCTION

Contamination effects in fluidic devices have been of concern for some time, however until recently little effort has been devoted to a detailed evaluation of such effects. (1)* Although significant contamination effects can be minimized in many circuits by proper filtration and design of enclosures (2), a thorough investigation is necessary before the long term reliability of fluidic systems can be adequately specified. The initiation of an extensive investigation of contamination effects on system reliability has been reported by Westerman (3).

A purpose of this investigation is to determine the manner in which contamination deposits accumulate in a particular device and to relate the nature and location of the deposits to degradation in performance. The primary purpose is to determine the geometric changes necessary to minimize contaminant buildup in sensitive regions of the amplifier.

EXPERIMENTAL PROCEDURE

The device which was chosen for this investigation was a laminar proportional amplifier of the type described by Manion and Mon (4). Figure 1 shows the geometry of the amplifier that was used. The normal size devices have a nozzle width of 0.5 mm and aspect ratios from 1/4 to 1. The model used for this investigation was four times normal size with a nozzle width of 2.0 mm. An experimental system was developed to supply contaminated air to the power nozzle of the test model. Figure 2 is a schematic of the system used.

The most difficult problems encountered in the development of the apparatus was the need to introduce the contaminants at a known rate. Oil and solid particles were used to contaminate the air supply so two supply techniques were required.

The oil was introduced as a vapor by simply passing a portion of the supply air through a flask in which oil was kept hot by an electric heater. Only about one-third of the total air supplied passed through the oil flask. The length of the lines and the size of the mixing chamber were such that no significant temperature rise was encountered and the air supply entering the model could be kept at room temperature. The rate of oil introduction was determined by measuring the change in weight of the flask.

The introduction of the particles was accomplished by using an S.S. White Industrial Airbrasive Unit. This device uses a high-velocity jet containing abrasive particles to perform cutting operations. The unit contains a system for mixing air and small particles in an adjustable ratio. A typical nozzle supplied with the unit was modified to produce

* Numbers in parentheses refer to items listed in the reference section.

a low velocity jet and the particle regulator was calibrated so that the flow rate of particles could be set at a desired rate. The flow from the Airbrasive Unit was mixed with the oil laden air in the mixing chamber which supplied the test model.

The effects of contamination were determined by monitoring the pressure gain of the amplifier. The input and output pressures were measured with transducers and the outputs of the instrumentation were used to drive an x-y plotter. The input was driven from only one side while applying both positive and negative pressures to cover the entire dynamic range of the amplifier. Although this procedure causes some nonlinearity in the gain curve due to the changing level it was considered satisfactory since we were concerned primarily with changes in performance.

The tests were all conducted with a constant pressure which resulted in a Reynolds number of 975 in the clean amplifier. The Reynolds number is based upon the average power nozzle velocity and the distance between the top and bottom cover plates of the amplifier. The particles used were 50 micron aluminum oxide particles and they were supplied at a rate of 3.9 gm/m³ of supply air. The oil used was SAE 30 non-detergent motor oil and it was supplied at a rate of 5.4 gm/m³ of supply air. The total contaminant rate was 9.3 gm/m³ of supply air and was held constant for the entire series of tests.

Each test was run for approximately three to four hours with the outputs open to the atmosphere. Gain curves were taken initially and at approximately one hour intervals with blocked and loaded outputs. The model was assembled with clear plastic cover plates so that photographs of the contaminant deposits could be made.

No attempt was made to define a failure criterion and the tests were run until considerable degradation of performance resulted.

CONTAMINATION EFFECTS

The original model tested had a right-angle entry and the supply flow entered the upstream section of the power nozzle through a round tube perpendicular to the nozzle. Figure 3 is a photograph of the contaminant deposits in the inlet to the amplifier. Figure 4 shows the changes in the amplifier characteristics due to the contamination. The effects of inlet blockage are apparent in the reduction of the output level of the amplifier. Very little contaminant deposits were obtained in the downstream section of the amplifier.

When the inlet was modified by machining a recess in the cover plate opposite the entry the time required for significant inlet blockage was increased.

To study the effects of contamination in the downstream portion of the amplifier the model inlet was modified to obtain a straight-through supply flow. The effect of this modification was to significantly

reduce the time required for contaminant buildup in the output region of the amplifier.

The effects of contamination in the entire amplifier are illustrated in the following figures. Figure 5 shows the deposits in the nozzle and in the downstream portion of the amplifier. Figure 6 shows the effects of the contamination on the performance characteristics with blocked outputs. Curve C illustrates the effects of contamination in the output region. (The data for Curve C were obtained after removing the contaminant deposits from the nozzle area.) In this case there was a considerable null shift which can be traced to asymmetric deposits on the splitter (see Figure 5). Similar tests show no null shift when the deposits on the splitter were symmetrical.

Figure 7 shows the effect of contamination on gain for the case illustrated in Figures 5 and 6. Curves 2 and 3 for arbitrary output loading.

SUMMARY

The results presented in this paper can be summarized as:

A. Inlet Blockage.

Inlet blockage is the first effect that will result when the device tested is subjected to a contaminated air supply. With constant supply pressure operation, contamination will cause a decrease in gain and a decrease in maximum output level.

Changes in inlet design such as recessing the cover plate opposite a right-angle entry or providing a straight-through inlet will extend the time required for significant inlet blockage.

B. Outlet Blockage.

Outlet blockage can include a buildup of deposits on the splitter which effectively change the splitter geometry. Two effects were noted; enlargement of the splitter with a corresponding decrease in gain and an asymmetric deposition on to the splitter with a corresponding null shift.

It must be emphasized that what has been presented here is the beginning of a project to identify specific effects of contamination. These results were obtained with a particular geometry and very limited operating conditions. Although the results do seem to have a wider applicability than is presumed, much more information will be required before a complete evaluation of the contamination effects in fluidic devices will be possible.

REFERENCES

1. Gottron, R. N., "Introduction to Reliability Panel Session", Fluidics Quarterly, Vol. 5, No. 1, January, 1973, pp. 69-70.
2. Holman, R. A., "Reliability of Fluidic Systems in Industrial Environments", Ibid, pp. 79-84.
3. Westerman, W. J., Jr., "Effect of Contamination on Fluoric System Reliability", Ibid, pp. 85-95.
4. Manion, F. M. and Mon, G., "Fluorics: 33. Design and Staging of Laminar Proportional Amplifiers", HDL-TR-1608, September, 1972.

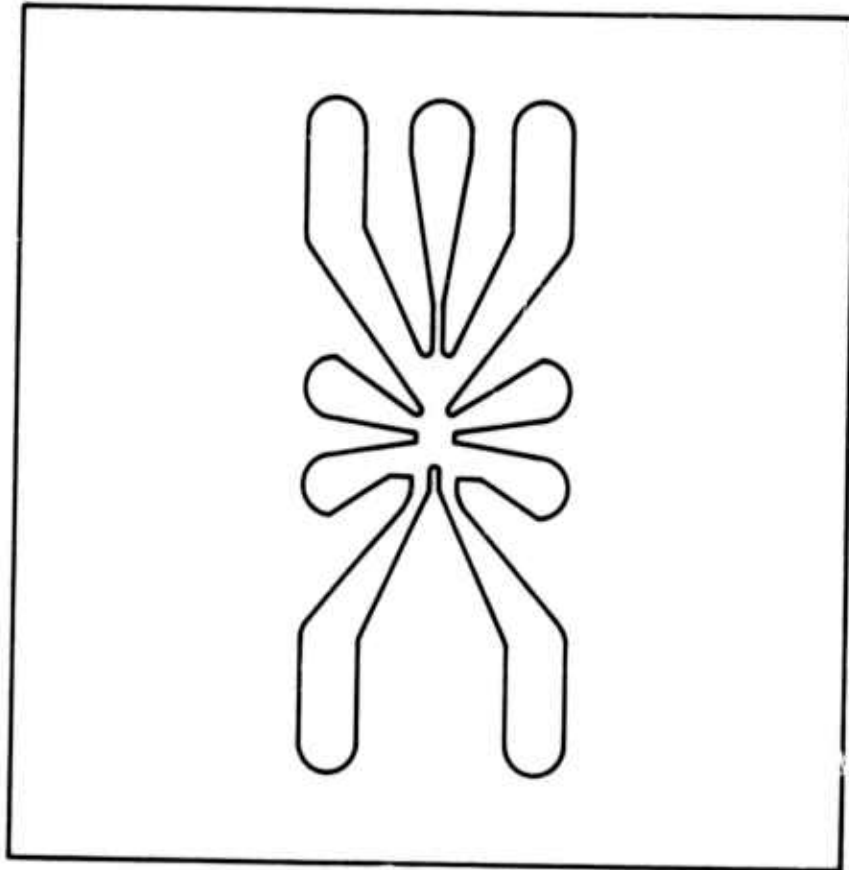


FIG. 1 AMPLIFIER GEOMETRY

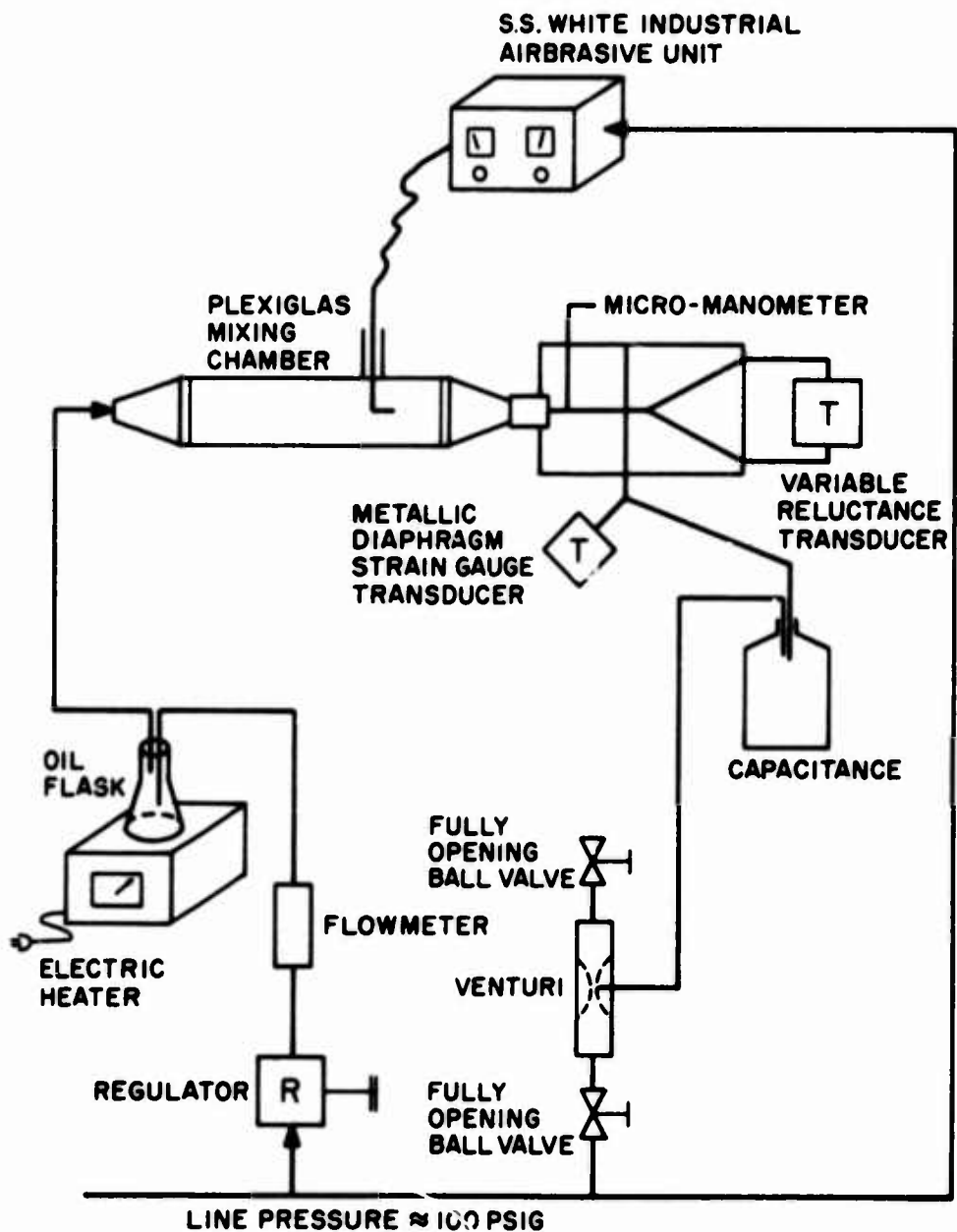


FIG. 2 EXPERIMENTAL SYSTEM

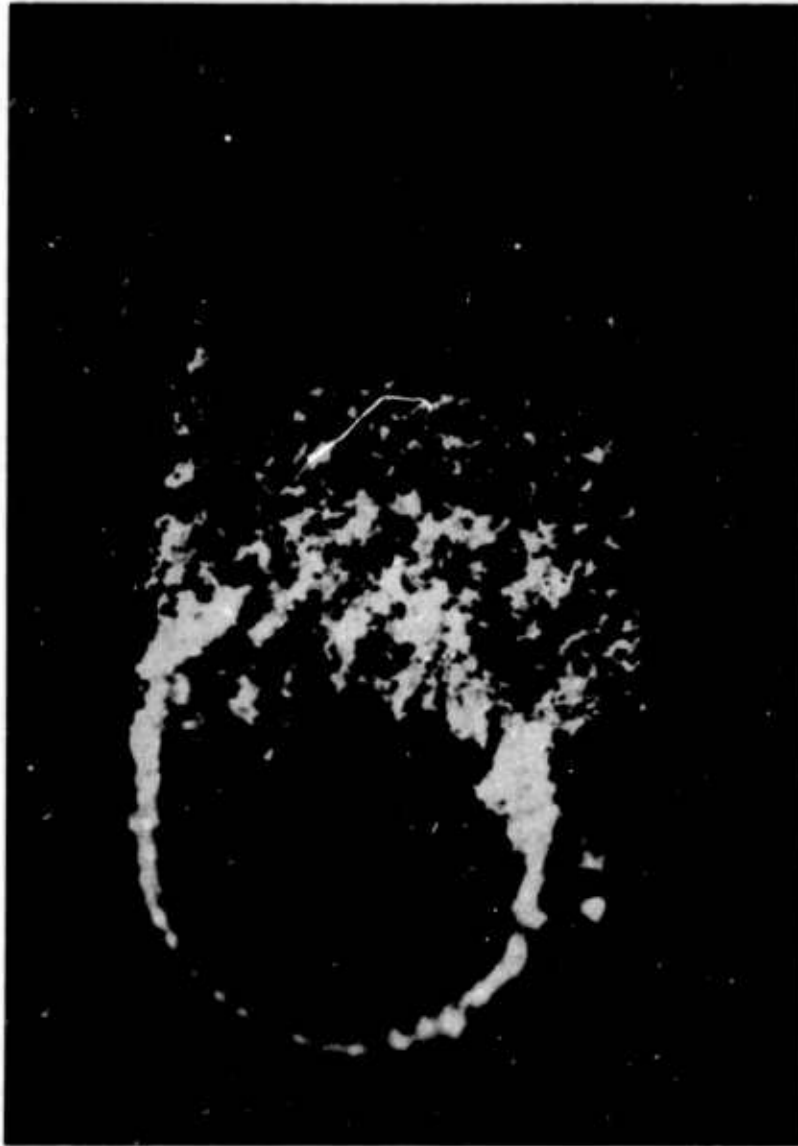


Fig. 3. Contaminant Deposits in the Inlet for a Right-Angle Entry

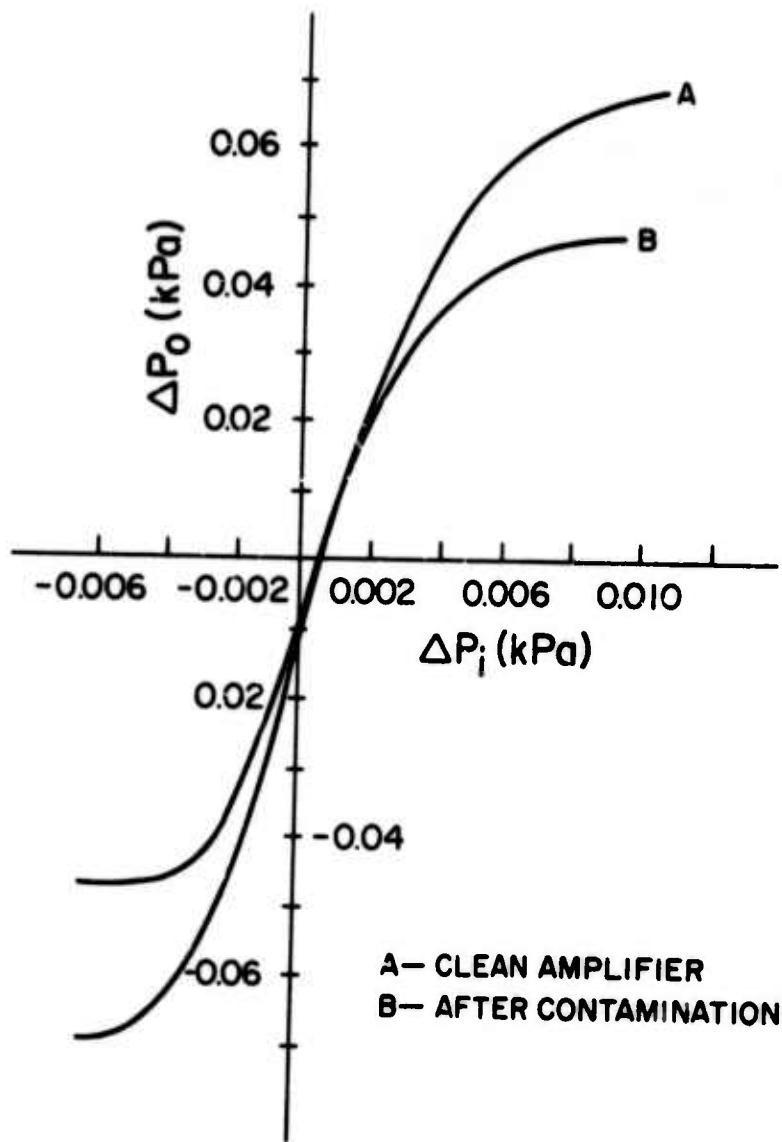
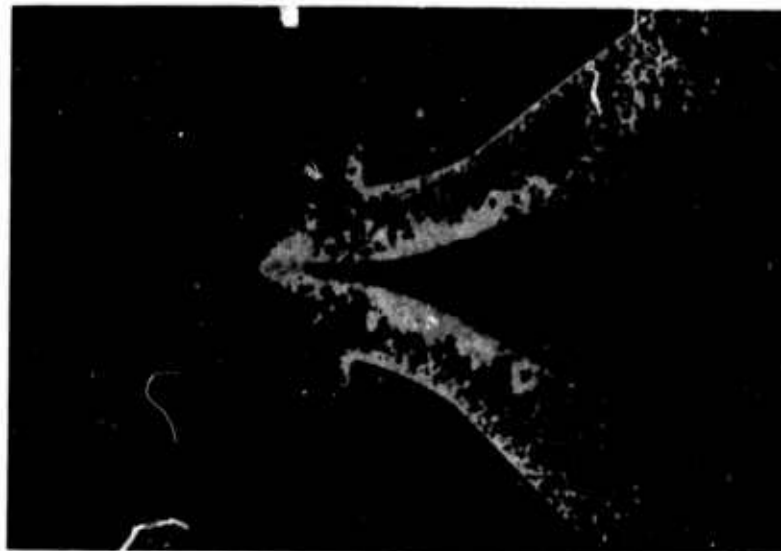


FIG. 4 CHANGE IN AMPLIFIER CHARACTERISTICS DUE TO CONTAMINANT DEPOSITS IN THE INLET: RIGHT-ANGLE ENTRY



(a) power nozzle



(b) downstream section

Fig. 5. Contamination Deposits in a Model with a Straight-Through Inlet.

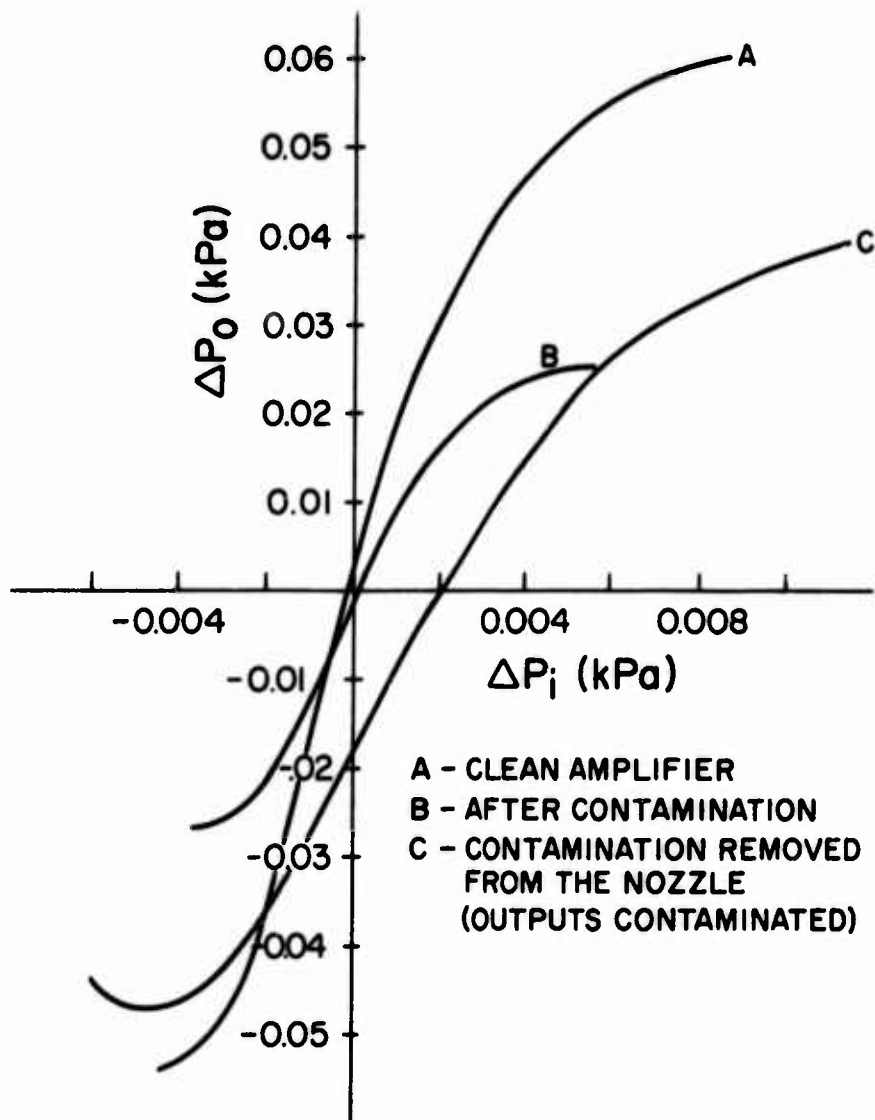


FIG. 6 CHANGE IN AMPLIFIER CHARACTERISTICS DUE TO CONTAMINATION: STRAIGHT INLET

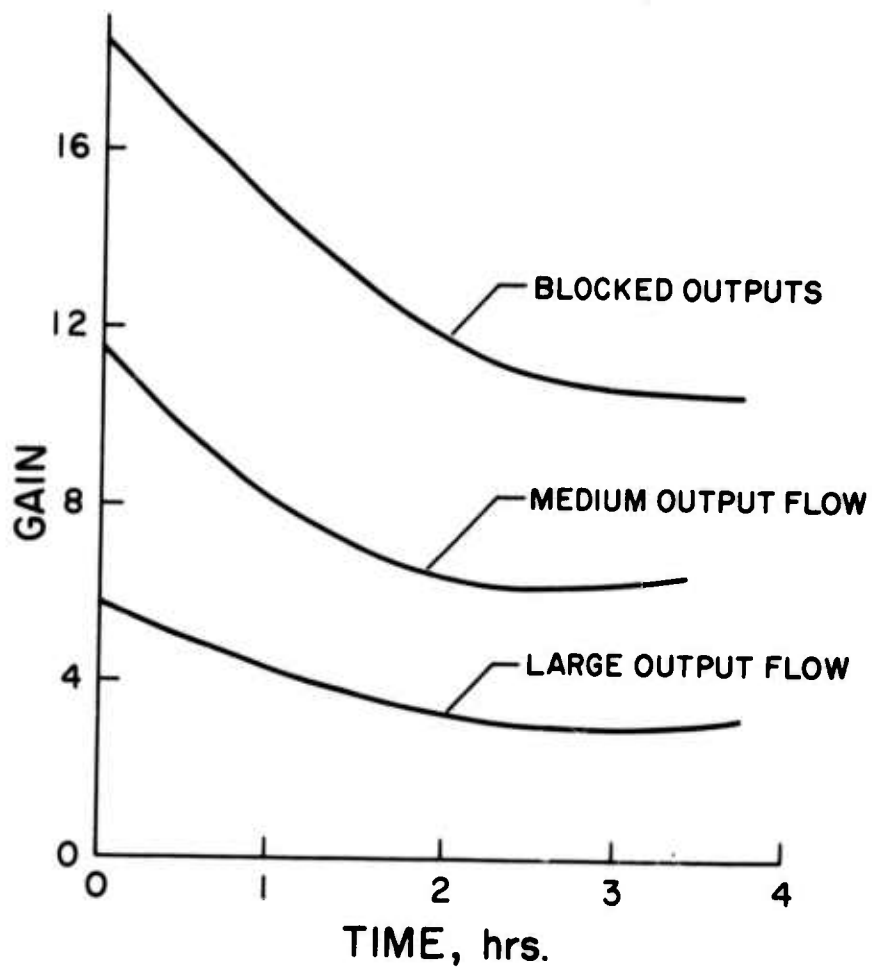


FIG. 7 CHANGE IN AMPLIFIER PRESSURE GAIN DUE TO CONTAMINATION

EFFECT OF CONTAMINATION ON FLUERIC SYSTEM RELIABILITY

W. J. Westerman, Jr., D.Sc.

McDonnell Douglas Astronautics Company, Titusville, Florida

Summary

Many claims have been made, some extravagantly, regarding fluidic system reliability. For the most part these claims have been substantiated qualitatively in many applications. However, quantitative methods have not been available to either predict reliability or to design accelerated failure experiments. This paper describes work performed over a three year period with the purpose of developing an accelerated testing method and a method of predicting system life.

Experiments have been conducted to determine the degrading effects of supply gas contamination on fluidic system performance. Artificial contaminants have been introduced into clean air supplies and the degradation of the attached fluidic circuits has been measured regularly until circuit failure. Approximately 400 circuits have been tested in this manner.

Solid dust contaminants that have been used included spectra having 150, 44, 15, and 5 micron maximum size particles; silica, attapulgite clay and aluminum oxide have been used to determine the effects of contaminant hardness. Solids combined with oil and water aerosols have also been used. The rate of contaminant introduction (grams/cubic meter air) has been varied over five orders of magnitude. Four element geometries, four nozzle areas, three supply pressures and two materials (stainless steel and copper) have been investigated. The circuits consisted of single element feedback oscillators and three element pulsewidth modulators. Performance parameters that were monitored were noise, frequency, amplitude, and gain.

Standard deviations of the data from the experiments were compared to similar controlled experiments where electronic circuits were overstressed by temperature; the standard deviations were found to be essentially the same.

BACKGROUND

The lack of reliability data on simple fluidic components limits the ability to evaluate or predict the reliability of fluidic systems. Although the reliability of fluidic devices is believed to be high, very little quantitative data presently exists. This paper describes the progress under two programs titled "Fluidic Reliability Investigations" - (Contract No. DAAG-39-72-C-0001) and "Classification of Military Fluidic Power Supplies" (Contract No. DAAG-39-73-R-9176) conducted by McDonnell Douglas Astronautics Company under contract to U. S. Army, Harry Diamond Laboratories (Contract No. DAAG-39-72-C-0001).

INTRODUCTION

The first step toward evaluating fluidic system reliability is to establish reliability of fluidic components just as electronic system reliability is dependent on the known reliabilities of its resistors, transistors and capacitors. The reliability of a major portion of the hardware (valves, "O" rings, etc.) in any fluidic system is presently known explicitly or can be established by similarity from their use in pneumatic and hydraulic systems. However, the reliability of the fluidic devices themselves is not known. Several mechanisms exist which can degrade a fluidic circuit until it no longer operates within specifications and should be considered to have "failed". The four primary degradation mechanisms are corrosion, wear, contamination by build-up or clogging, and stress induced failures including thermal and mechanical stresses. Although complex interactions exist between these failure mechanisms, contamination is generally recognized as the most probable failure mode of fluidic components. Furthermore, the effect of environmental extremes, other than contamination, is generally minimal especially in industrial control. Therefore, a study of contamination effects on fluidic system reliability was given first priority.

When considering a fluidic component separate from the system, reliability data are only useful if they express a probability that the device will perform to a specific tolerance for a specified period under stated conditions. Therefore,

continuous data are required of performance degradation as a function of contamination and operating time so that the results will be sufficiently general to be applicable to future systems.

SCOPE OF THE PROGRAM

This program had two major goals: (1) to establish confidence in a method of accelerated testing of fluidic systems to determine degradation and (2) to provide a means of predicting the reliability of future fluidic systems. With such broad goals, the challenge of designing the program was one of scaling the problem down to manageable size from which useful and accurate data would result without restricting the variables to the extent that generality would be lost. A partial listing of the variables affecting the reliability of fluidic systems is shown in Fig. 1; the ranges of those variables which have been addressed in this program are shown in the clear field of the figure. The amount of data that could be taken to record the performance of the selected circuits could, likewise, be unmanageable. Fig. 2 shows, in the clear field, those data items which were monitored. The selected data items were considered to be indicative of degradation due to contamination based upon the following reasoning:

- ° Signal Amplitude - signal amplitude is indicative of partial clogging or erosion of the supply nozzle, the output channels or an incomplete switching.
- ° Frequency or Period - a change in the frequency of the basic oscillator would indicate a change in the switching pressure/flow point, a partial clogging of the control ports and feedback paths or contamination in the interaction area of the element (as well as vents).
- ° Noise - the noise on the output signal is indicative of build-up of contaminant in the interaction area and/or the element vents, erosion of passages, etc.

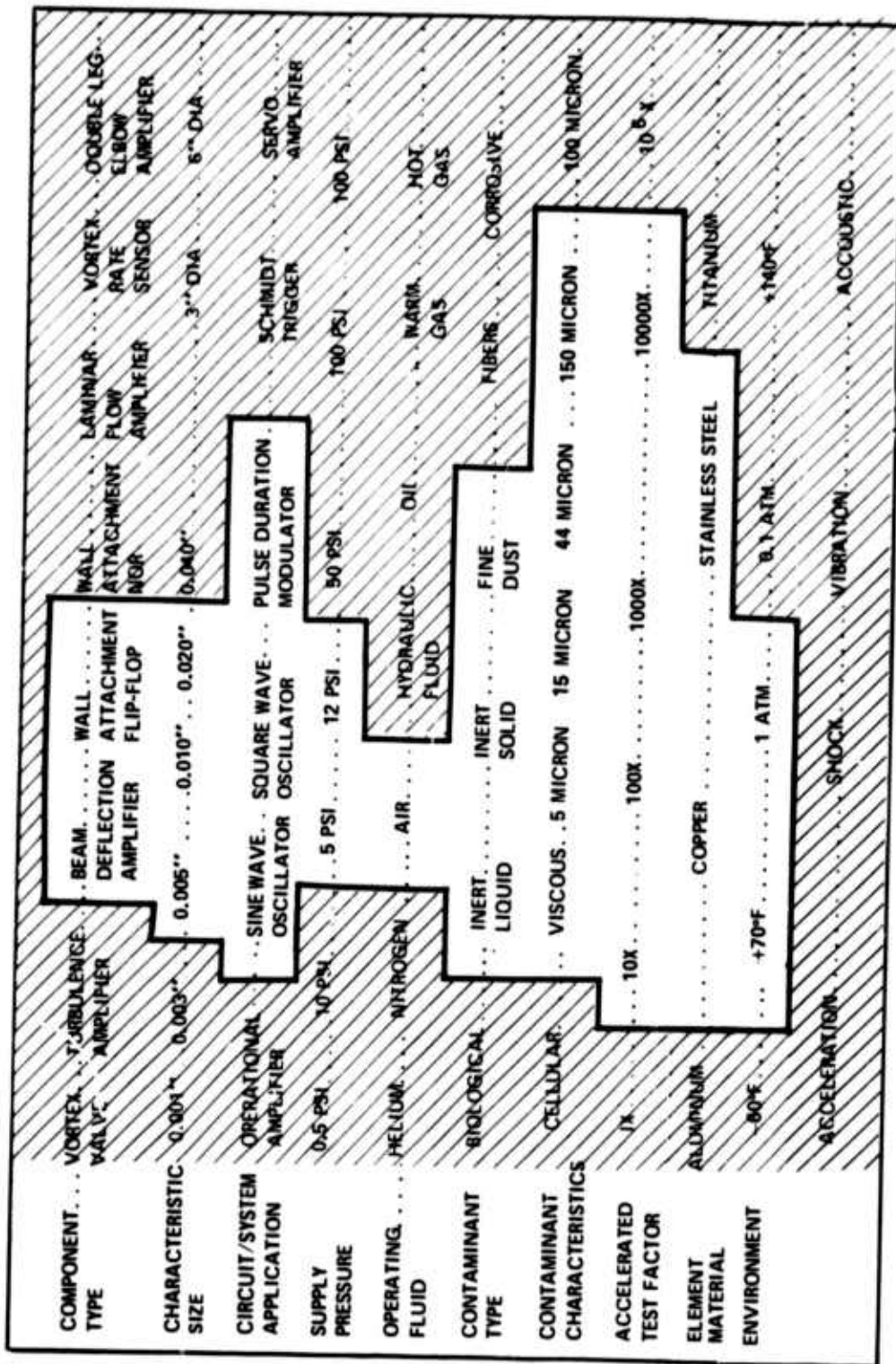


FIGURE 1 VARIABLES AFFECTING RELIABILITY

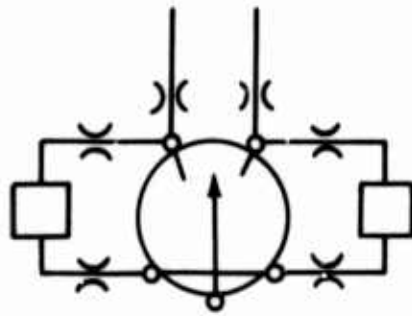
	PROPORTIONAL AMPLIFIER	BISTABLE AMPLIFIER	PULSE WIDTH MODULATOR
DATA APPLICABLE TO ELEMENT/SYSTEM	INPUT IMPEDANCE CURVES	INPUT IMPEDANCE CURVES	INPUT IMPEDANCE CURVES
	OUTPUT IMPEDANCE CURVES	OUTPUT IMPEDANCE CURVES	OUTPUT IMPEDANCE CURVES
	PRESSURE GAIN VERSUS CONTROL QUIESCENT	SWITCH PRESSURE VERSUS OUTPUT FLOW	% MODULATION BEFORE SATURATION
	PRESSURE GAIN VERSUS OUTPUT FLOW	SUPPLY IMPEDANCE CURVE	CYCLE TO CYCLE INSTABILITY
	MAXIMUM OUTPUT PRESSURE VS. SUPPLY	OFF LEG FLOW VERSUS ON LEG FLOW	GAIN / MODULATION \pm INPUT PRESSURE
	OUTPUT QUIESCENT VS. SUPPLY PRESSURE	SWITCHING TIME	FREQUENCY/PERIOD
	FREQUENCY RESPONSE (BODE CHART)	FREQUENCY/PERIOD (OSCILLATOR)	SIGNAL AMPLITUDE
	SUPPLY IMPEDANCE CURVE	SIGNAL TO NOISE RATIO	SIGNAL TO NOISE RATIO
AS AN OSCILLATOR	OUTPUT SIGNAL AMPLITUDE	SIGNAL AMPLITUDE	SYSTEM LINEARITY
	SIGNAL TO NOISE RATIO	CYCLE TO CYCLE INSTABILITY	
	FREQUENCY/PERIOD		
	FEEDBACK SIGNAL AMPLITUDE		
	GAIN		

FIGURE 2 PERFORMANCE CHARACTERISTICS

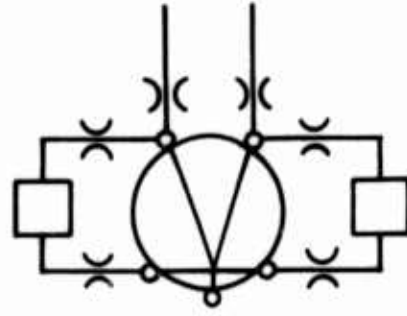
These data were taken quickly and accurately with one pressure transducer. The transducer output was fed to a counter to determine period; it was fed to an ac voltmeter to obtain signal amplitude; and it was fed through a high pass filter to a second ac voltmeter to obtain noise. In this manner the data requirements are reasonable; data can be gathered remotely without disturbing the devices or interrupting the tests; and the method lends itself to automatic data logging and computer handling which could become particularly important for future efforts where considerably more circuits would be tested.

DESIGN OF EXPERIMENTAL HARDWARE

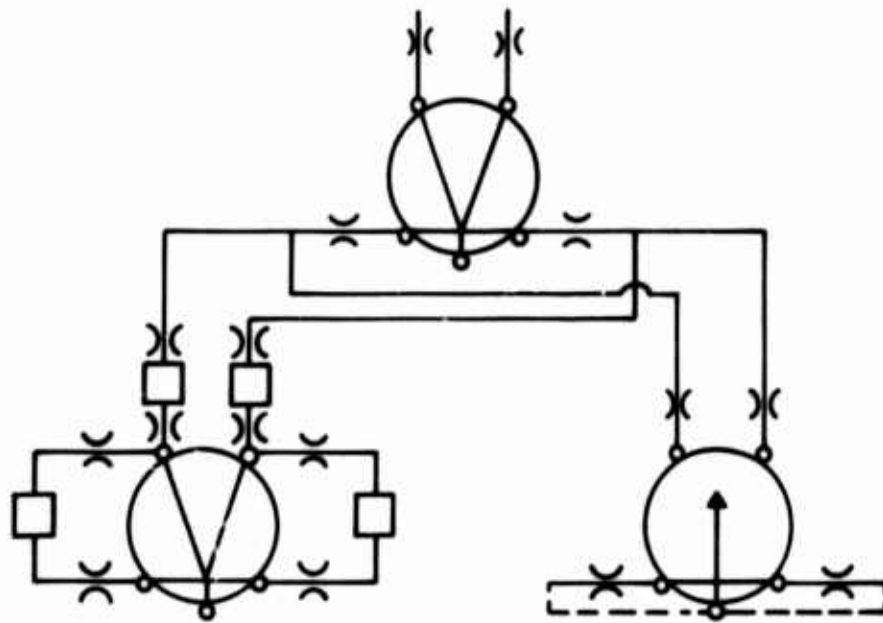
The fluoric elements that were used in this program were selected as being representative of the most common types in general use. The proportional elements were of the stream deflection type with a center vent. The bistable elements were of the wall attachment type having a cusp on the splitter. The circuits are shown in Fig. 3. Based upon an analysis of the effect of sample size on both experimental accuracy and cost, a decision was made to use eight identical circuits in each separate experiment. The eight circuits were arranged around an octagon as shown in Fig. 4. Several different experiments were run simultaneously during the course of the program as shown in Fig. 5. Contaminant was introduced into clean, dry supply air through a dispenser containing graded dust. The contaminated air then traveled an essentially vertical path downward to a constant velocity flow divider and then to each circuit. Close attention was given to the contaminant dispensers to assure regular, uniform introduction of the dust into the air stream. All exhaust gasses from the circuits were collected and run through a water trap. An arrangement was provided so that one transducer can be connected to the octagon by means of a quick disconnect and could then be selectively valved to each test point on the octagon. Each circuit was built up of etched laminates with the active element on the outside. Visibility was provided by use of a glass cover plate held against the element by bolts passing through a plastic pressure plate.



(A) PROPORTIONAL OSCILLATOR



(B) BISTABLE OSCILLATOR



(C) PULSE DURATION MODULATOR

FIGURE 3 FLUIDIC CIRCUITS



FIGURE 4 OCTAGON OF CIRCUITS

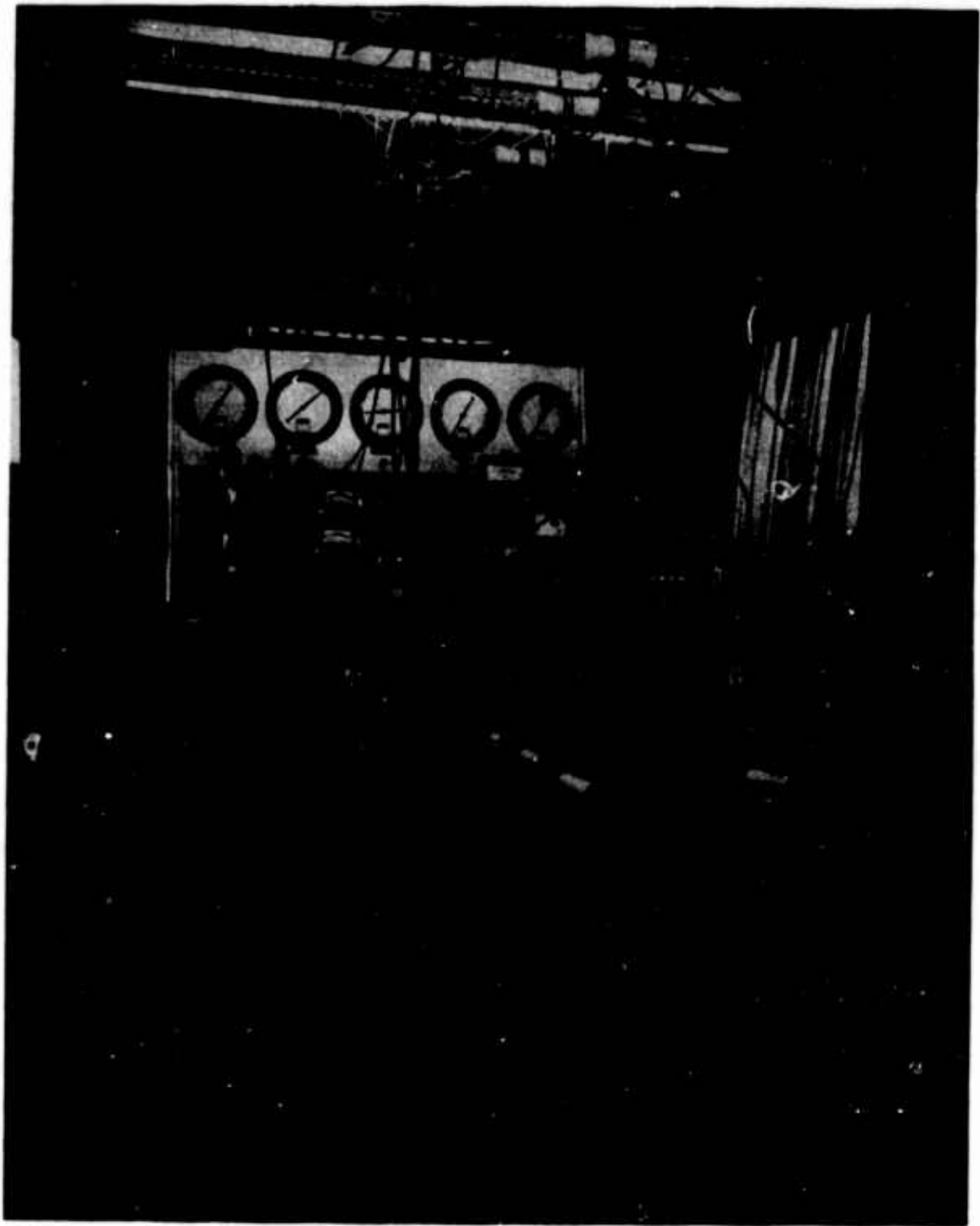


FIGURE 5 EXPERIMENTAL SET-UP

EXPERIMENTAL DATA

At this time 408 circuits have been tested in 51 separate experiments. The range of variables and the corresponding number of circuits tested is shown in Fig. 6.

The experiments were run at various levels of contamination. The level of contamination, or the "dirtiness" of the supply air, was expressed in gravimetric terms as grams of contaminant per cubic meter of air. This rate of contaminant introduction was varied over four orders of magnitude from a high of 35 gr m^{-3} . Data was taken on each circuit of an experiment at intervals that were increased geometrically throughout the life of the test; a test was concluded when the circuits ceased oscillating. All of the experiments started with the circuits running at a base frequency of $100 \text{ Hz} \pm 5 \text{ Hz}$. The values for output signal amplitude and noise amplitude were found to be essentially the same for identical circuits and no formal tolerance was placed on their initial values.

Certain of the experiments exhibited abnormally large standard deviations. Typical values for the standard deviation of a group of eight circuits, expressed as a percentage of mean life, was found to be approximately 45%; the lowest value was 17%. Several possibilities were postulated as being responsible for the large data spread.

- (a) The experiments were simply of a poor design and the data were worthless.
- (b) Several failure modes were intermixed each having relatively equal probability of occurrence.
- (c) The spread is typical of reliability type data.

The experimental set up was carefully monitored especially with regard to contaminant dispensing. Monitors were placed in every location where a disturbance or variation could reasonably be expected. These efforts yielded no explanation for the data spread. Histograms were plotted and examined for evidence of multi-failure modes. This approach did not prove or disprove the multi-failure mode explanation. However, it is obvious that clogging and erosion are two possible modes of failure, each of which can occur at several critical locations in the circuit.

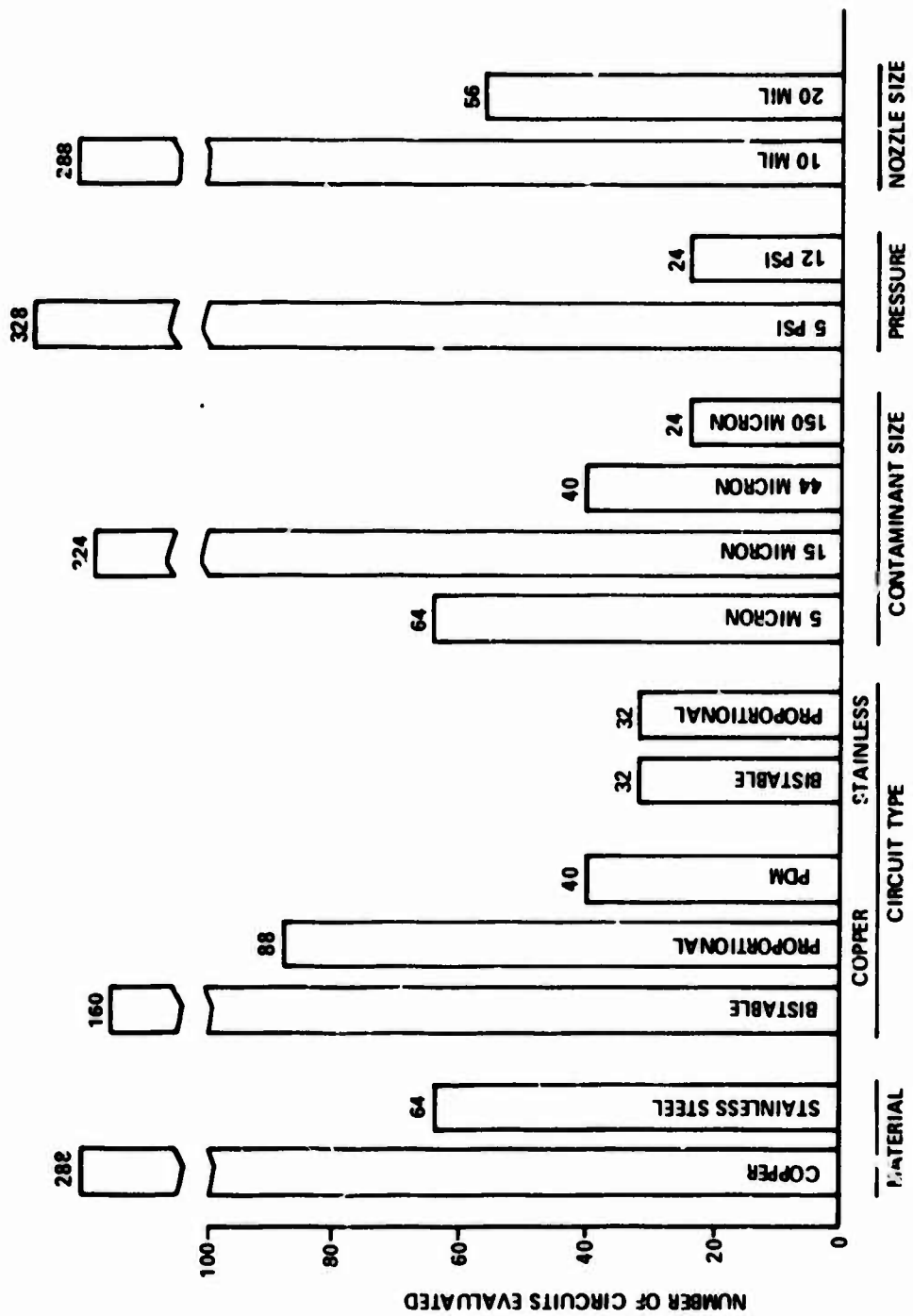


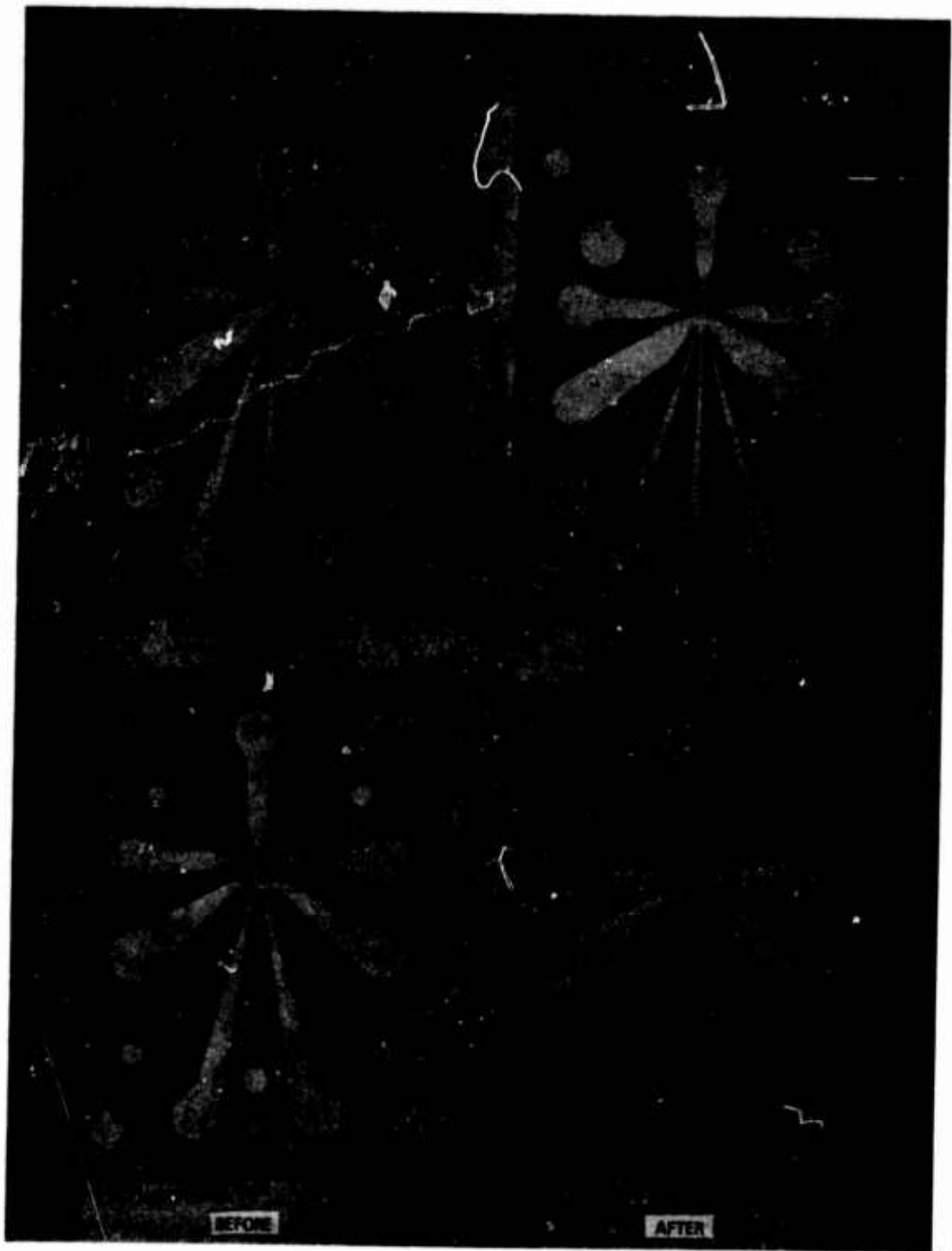
FIGURE 6 RANGE OF EXPERIMENTS

It was determined that another laboratory within the same corporate structure had been performing accelerated reliability investigations on integrated electronic circuits by subjecting the circuits, while operating, to artificially high temperatures. A well accepted theory attributed failure of solid state devices to a migration of N and P type impurities across the junction until a sufficient homogenization occurred to obliterate the junction. Elevated temperatures accelerated this migration at theoretically predictable rates. Raw data from these experiments were obtained, and when analyzed on the basis of a sample size of eight, it was found that the standard deviations, in every case, were exactly comparable to those experienced in this program. Further consultations and additional data confirmed the fact that the data spread was quite reasonable.

RESULTS OF THE EXPERIMENTS

Evidence of both clogging and erosion were observed after the circuits were carefully disassembled and examined. A method was developed to clean the tested circuits by alternately flushing with solvent and air without disassembly. The circuits could then be supplied with clean air. If the circuit then operated, although at some degraded level, clogging was assumed to be the predominant failure mode; if the circuit did not oscillate after cleaning, erosion was assumed to be the failure mode. In general, it was found that erosion was the primary failure mode especially at lower levels of contaminant introduction. Fig. 7 illustrates some typical elements before and after testing. The effects of the erosion is quite apparent and was essentially the same in all cases examined.

As the early experiments were concluded, the data were plotted and an attempt at correlation was made. As the program progressed, the data became unmanageable due to the sheer volume. All data were therefore computerized and plots were generated of the data, normalized to initial values, thereby providing graphs of degradation versus



life. Fig. 8 illustrates the form and general appearance of the data after normalization. These figures are generally typical of the data recorded throughout the program, especially at the lower contaminant levels. The data were also analyzed on the basis of average octagon life (100% degradation) and plotted on log-log paper against contamination rate. These plots yielded some rather striking results. Fig. 9 is a plot of all oscillators having .254 mm nozzles as an example. The straight line with a slope of approximately minus one was observed for every situation which was analyzed. The computer was used to perform a least squares fit of a straight line through the log-log data. Twenty eight groupings of the data were made based upon contaminant size, nozzle width, circuit type, supply pressure, etc. Two of those groupings, one showing 83 KNM⁻² oscillators versus 34.5 KNM⁻² oscillators and the other showing stainless circuits versus copper circuits, are given as Fig. 10 and 11. These experiments, which were compared in order to draw contrasts, include other variables in addition to the two in question; for example, the copper versus stainless includes a mixture of contaminant sizes. This is, of course, undesirable but was necessary because of the limited number of experiments. However, certain conclusions have been drawn pending further verification.

Over a wide range of contaminant rate, the mean time between failures of a fluidic circuit can be expressed as:

$$L = C_1 (r)^{-C_2} \quad (1)$$

- Where: L = mean life of a set of circuits (minutes)
 r = contaminant rate (grams per cubic meter of fluid)
 C₁ = experimentally determined constant
 C₂ = constant (approximately 1.0)

The values of the constant C₂ for a range of experiments are given in Table I. The values are very close to unity, especially when considering the accuracy of the experiments. Thus, a fluidic circuit will fail when it has ingested a specific weight of contaminant, regardless of how long it might take.

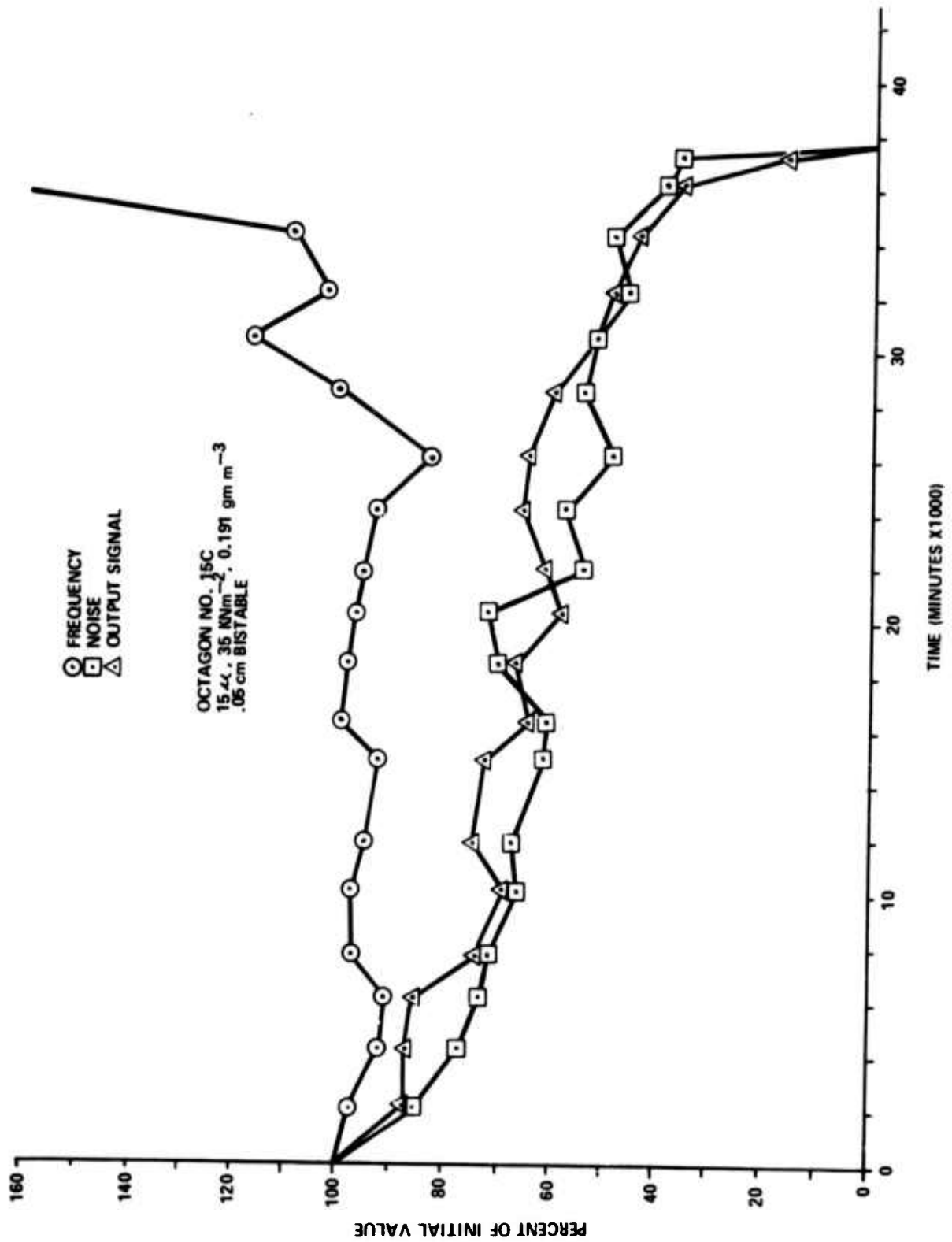


FIGURE 8(a) AVERAGE OCTAGON PARAMETERS

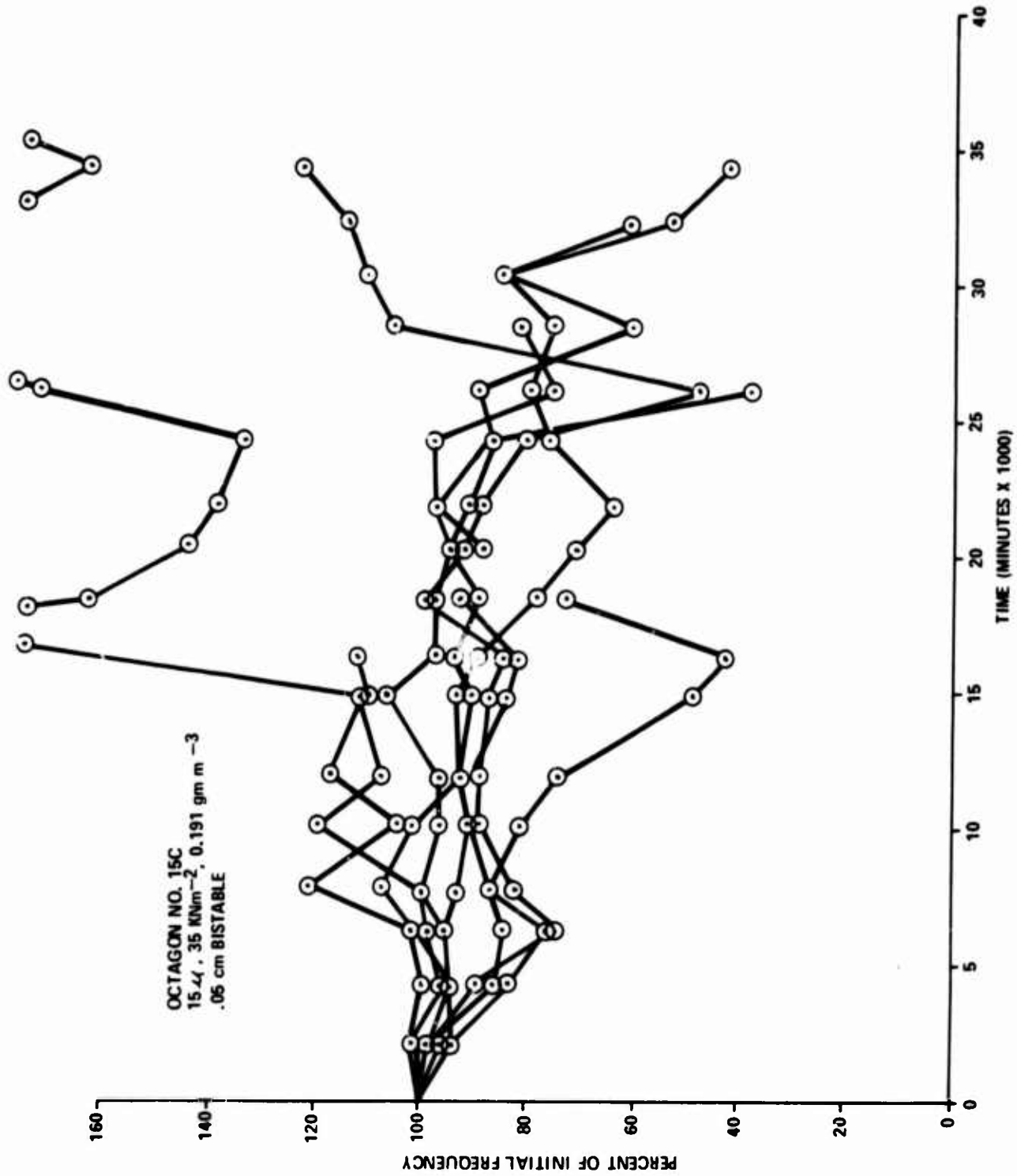


FIGURE 8 (b) INDIVIDUAL CIRCUIT FREQUENCY

OCTAGON NO. 15C
15.47 .35 MNm⁻², 0.191gm m⁻³
.05 cm BISTABLE

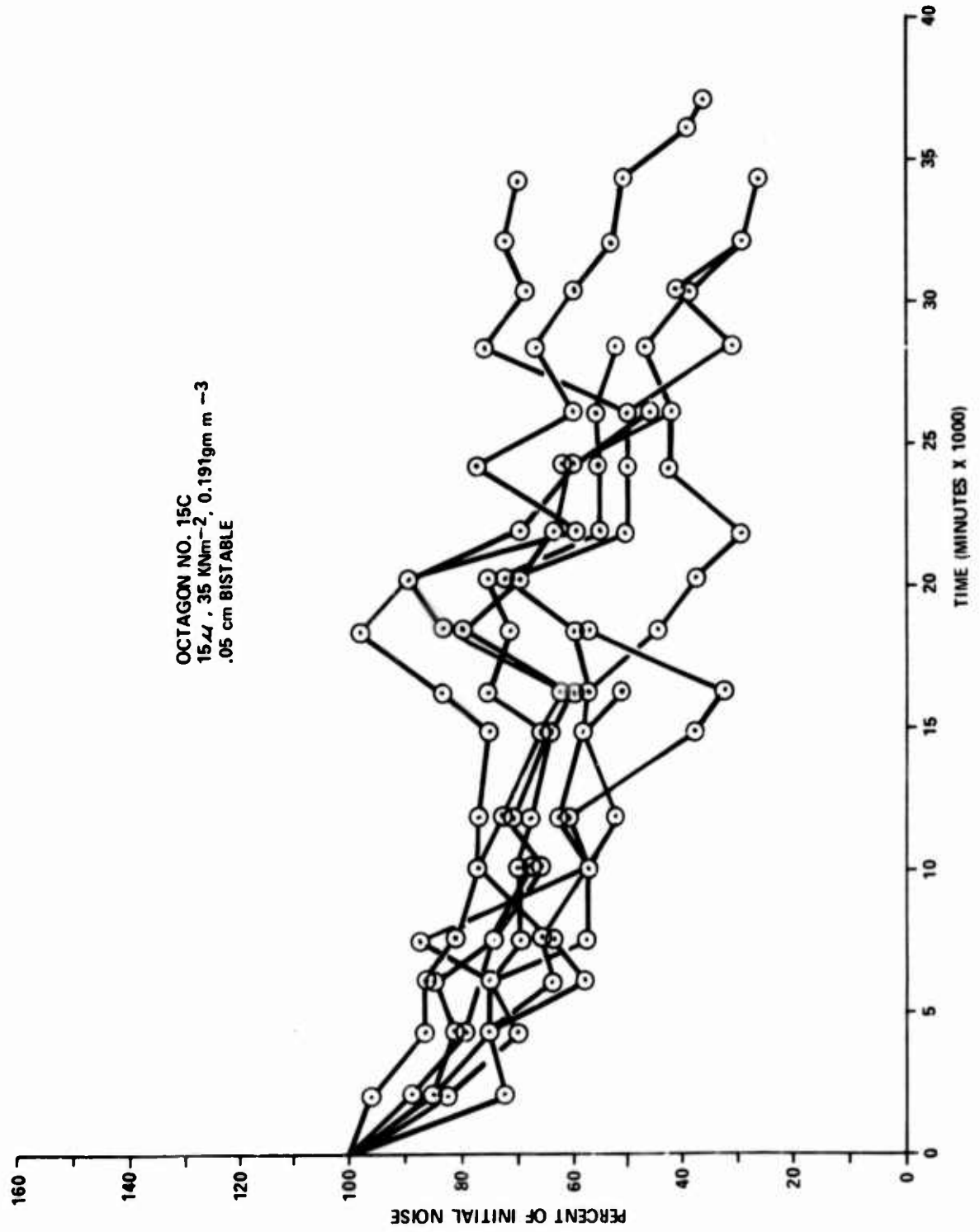


FIGURE 8 (c) INDIVIDUAL CIRCUIT NOISE

OCTAGON NO. 15C
15.44 .35 M^2 m⁻², 0.191 gm m⁻³
.05 cm BISTABLE

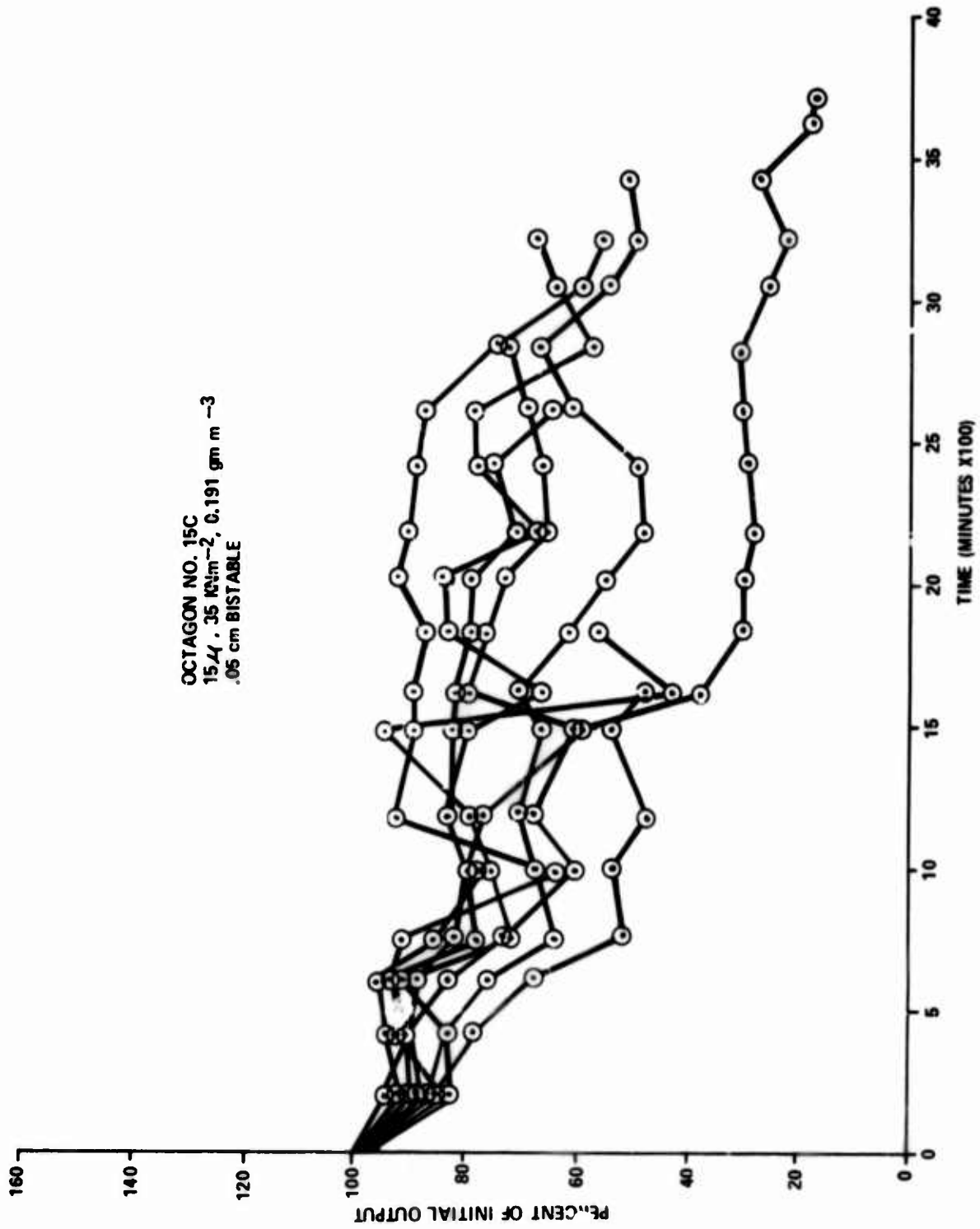


FIGURE 8 (d) INDIVIDUAL CIRCUIT OUTPUT

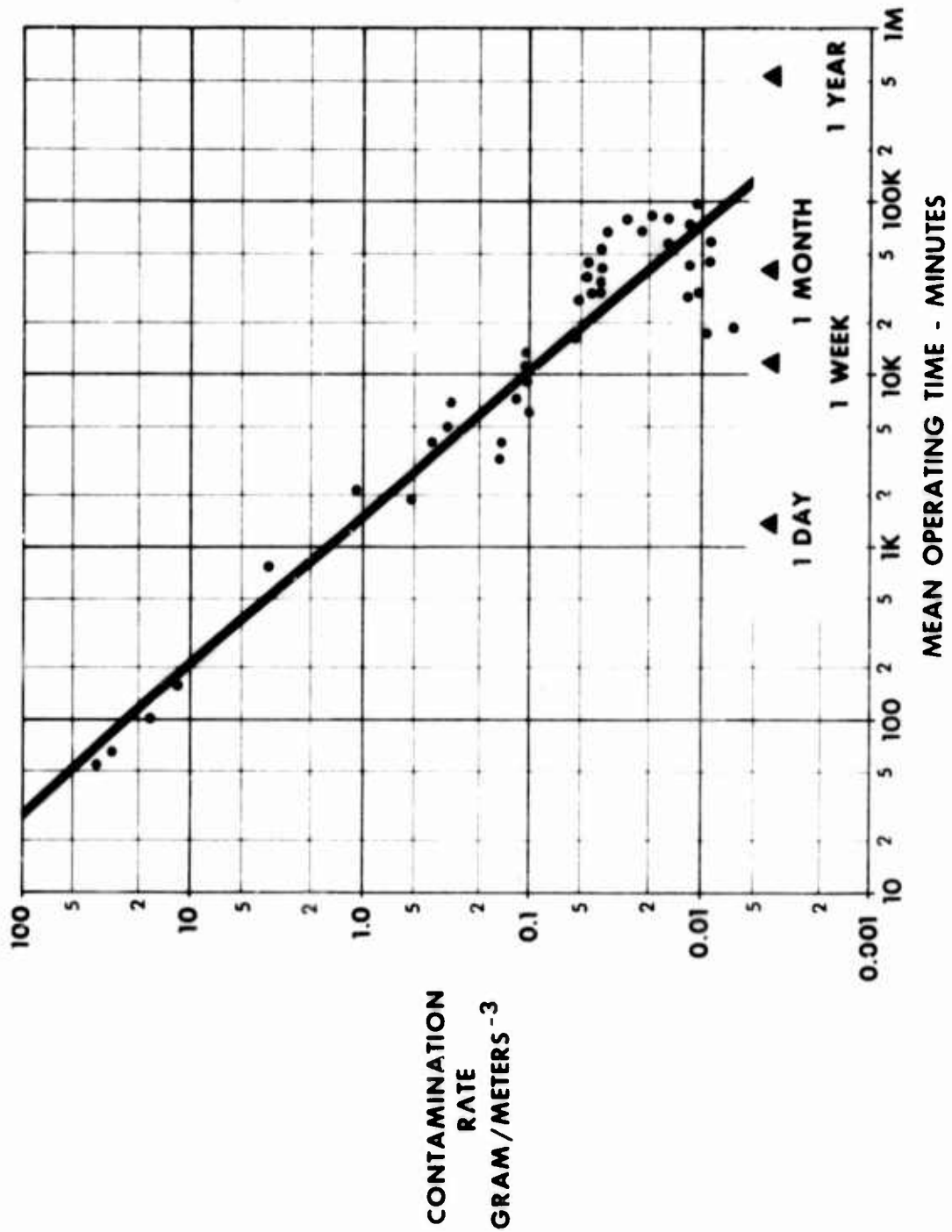


FIGURE 9 ALL .254 MM NOZZLE CIRCUITS

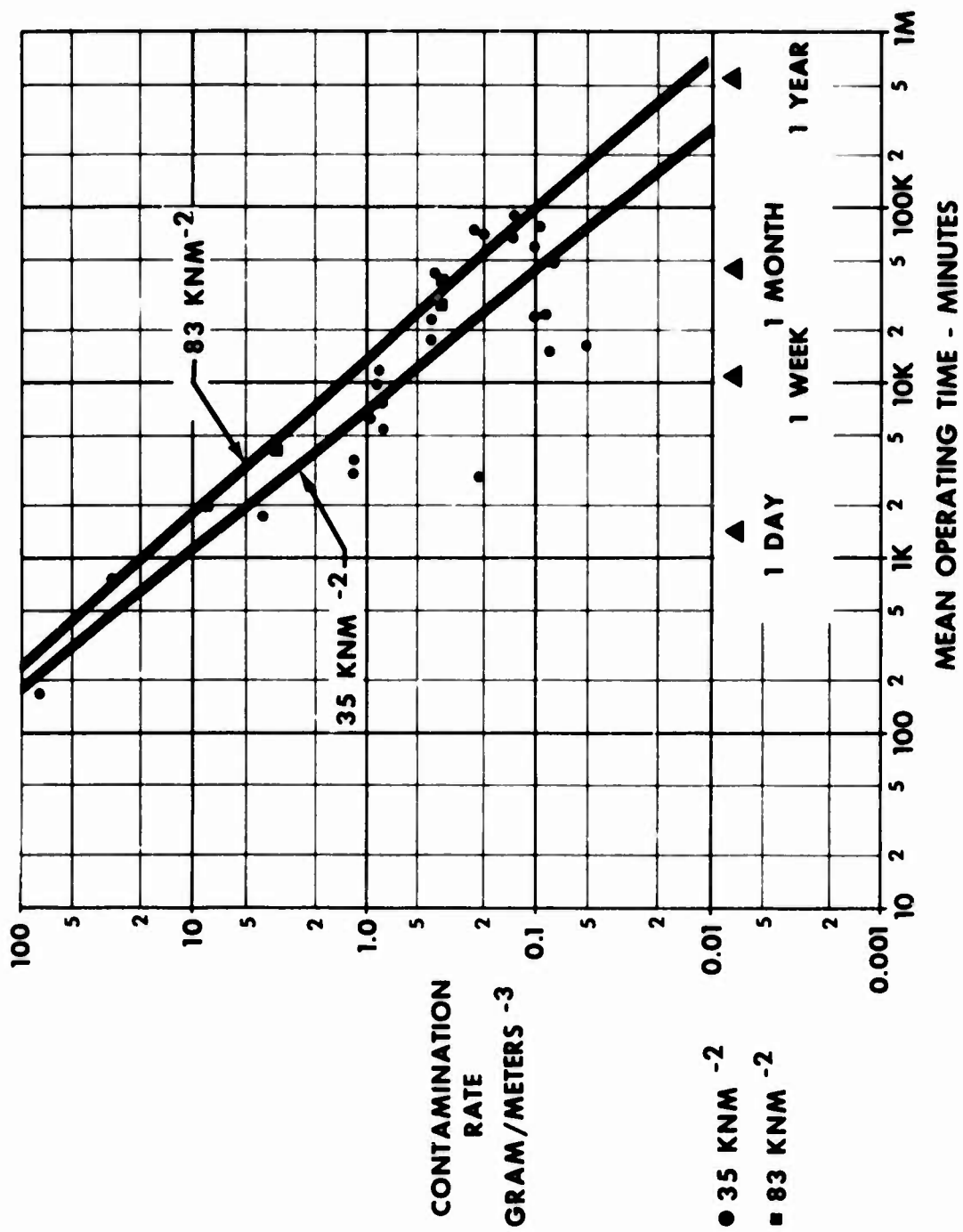


FIGURE 10 SUPPLY PRESSURE EFFECTS

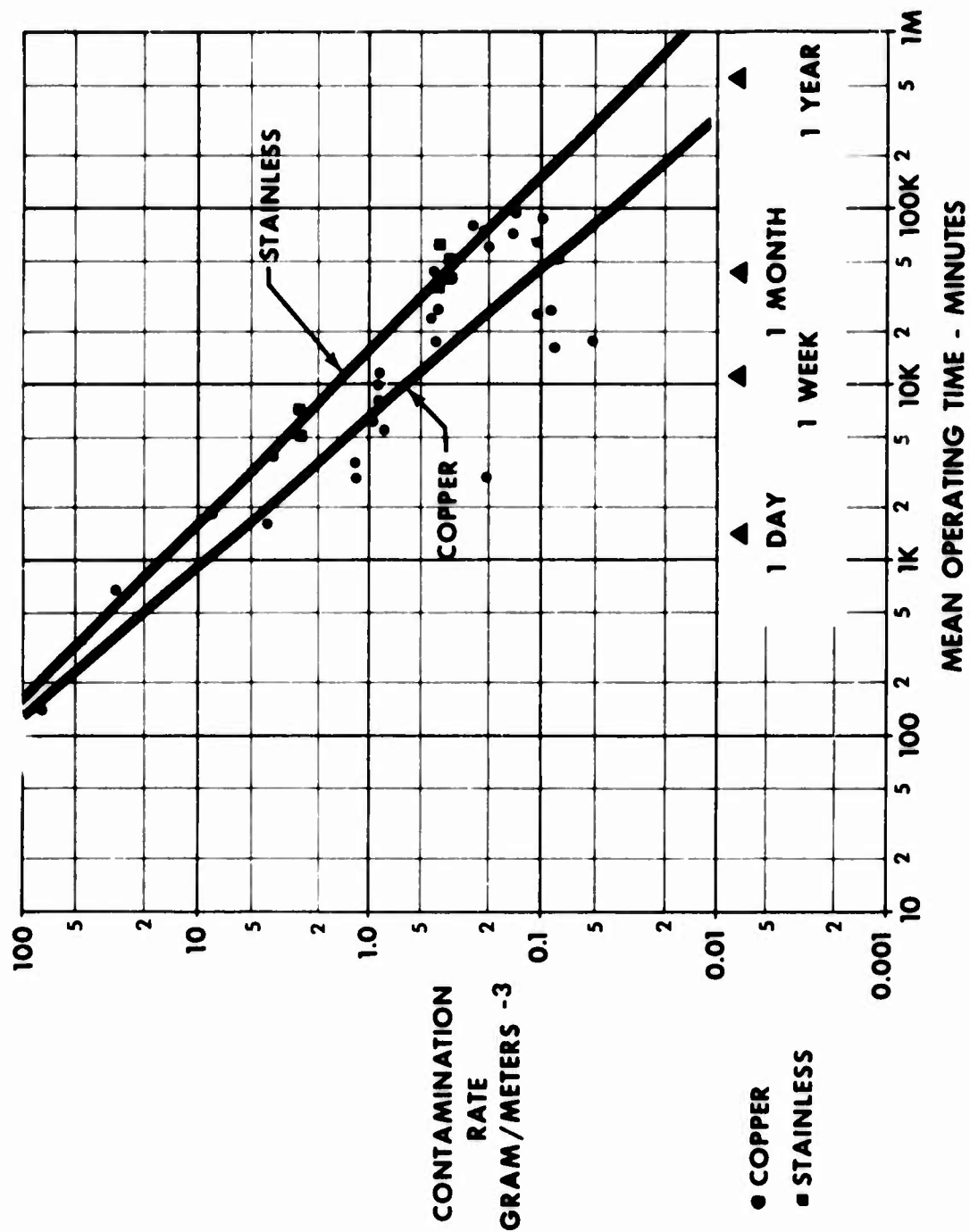


FIGURE 11 MATERIAL EFFECTS

TABLE I

ALL CASES	= 0.8968
ALL COPPER-SILICA	= 0.8778
ALL STAINLESS STEEL-SILICA	= 1.0166
.254mm, 34.5 KNM ⁻² , 15 _μ , COPPER	= 0.7982
.254mm, 34.5 KNM ⁻² , 15 _μ , STAINLESS	= 0.9390

The values of C_f that have been observed in the twenty eight cases analyzed ranged from 25.1 to 1585. Several conclusions regarding the effect of the experimental variables on C_f are:

- ° C_f is proportional to element throat area
- ° C_f is proportional to supply pressure
- ° C_f for proportional amplifiers is 70% of that for bistable element
- ° C_f is proportional to element material hardness

The effect of contaminant size is somewhat unusual. In general, life increased as the contaminant became smaller until the 15μ level was reached; 5μ contaminant, however, resulted in failure times equivalent to that of 44μ . It should be recognized that the measure of rate is "gram meter⁻³" and not "number of particles".

One set of eight circuits was run using oil and dry contaminants. The oil and dry contaminant were mixed on an equal gravimetric basis. This experiment exhibited a life only 3% of the corresponding dry contaminant experiment.

CONTAMINATION IN TYPICAL FLUIDIC POWER SUPPLIES

With the results of the contamination experiments indicating that accelerated testing was valid, an attempt was made to correlate the experiments to field conditions thereby predicting failure. Several attempts were made to obtain information on expected contamination levels in various types of pneumatic power supplies. One of these attempts involved a mail survey, as part of a Society of Automotive Engineers project, of over one hundred military and industrial contacts asking for any information available on contamination in pneumatic supplies. The net result of all of these efforts was absolutely nothing. However, a certain amount of data had been collected on hydraulic systems and several efforts had been made to organize these data. Table II gives a partial listing of references to these efforts.

TABLE II

REFERENCE DOCUMENTS FOR HYDRAULIC SYSTEMS CONTAMINATION LEVELS

1. Aerospace Recommended Practice ARP 598
"Procedure for the determination of particulate contamination of hydraulic fluids by the Particle Count Method" dated 3-1-60.
2. Aerospace Recommended Practice ARP 785
"Procedure for the determination of particulate contamination in hydraulic fluids by the control filter gravimetric procedure" dated 2-1-63.
3. Aerospace Industries Association ATC Report No. ARTC-28
"Specification for contamination control of hydraulic fluid" dated 1-15-61.
4. Proposed AIR 1101
Proposed Aerospace Information Report - A comparison of Particulate Contamination Limit Tables dated 10-10-68.
5. National Aerospace Standard NAS 1638
Cleanliness Requirements of Parts Used in Hydraulic Systems.

An effort was initiated (referenced earlier as "Classification of Fluidic Power Supplies") in order to obtain the required information on typical field supplies and to present that information in a useful manner.

Previous work on hydraulic systems had utilized two approaches to measuring contamination. One was a gravimetric method in which contamination was expressed in grams of contaminant per liter of hydraulic fluid (or similar units) and the other method involved the counting of particles in specific size ranges so as to identify the size spectra as well as the amounts associated with the contaminants.

Both methods were used in this program. The results from five representative power supplies are shown in Figure 12. It is interesting to note that only one sample contained any significant amount of oil and that the amounts of water encountered were also low.

Some earlier work on hydraulic contamination indicated that the typical spectra of solid contaminants would result in a straight line when plotted on Log-Log² paper. Figure 13 and Figure 14 illustrate the results for pneumatic systems (for compressor type supplies and stored gas supplies respectively) when handled in the same manner. The deviations of the curves from a straight line and the direction of the curvature is indicative of an impending mechanical failure (excessive large particles) or of an advanced state of wear (excessive small particles).

A system of classification has been developed as a result of this program and is presented as Table III. There are eleven classes based on the gravimetric approach each differing one order of magnitude from the previous class. Some representative supplies in each class are also cited in the table.

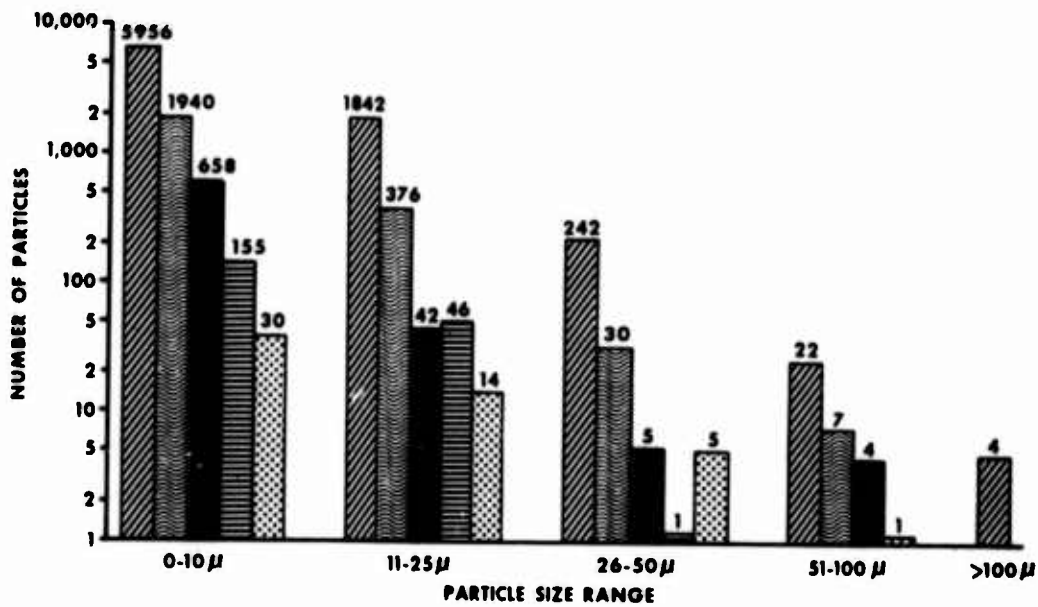
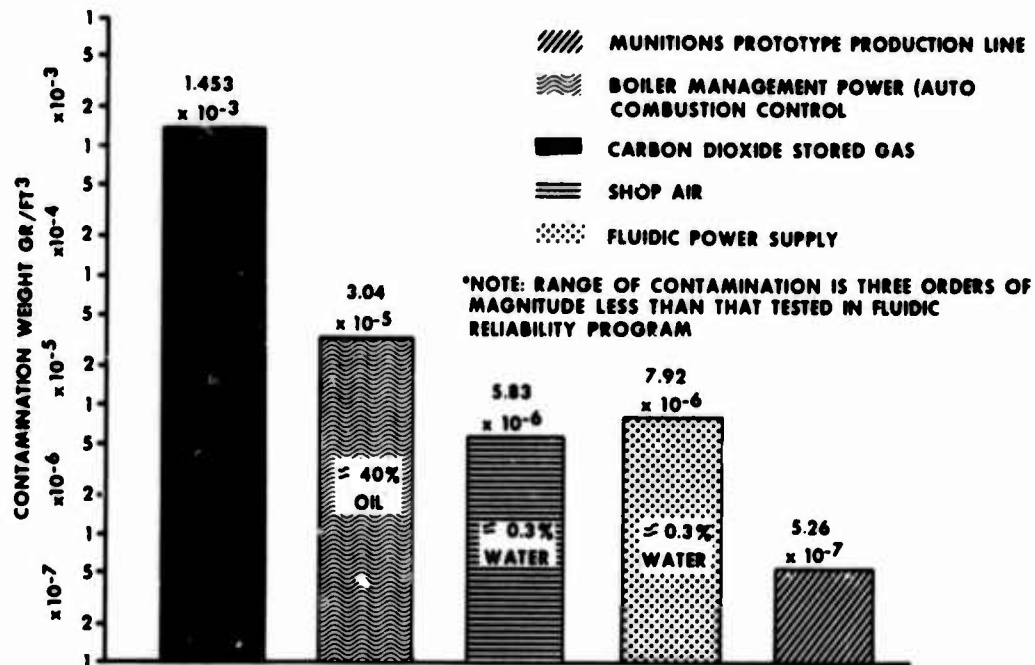


FIGURE 12 RESULTS OF CONTAMINATION SAMPLES

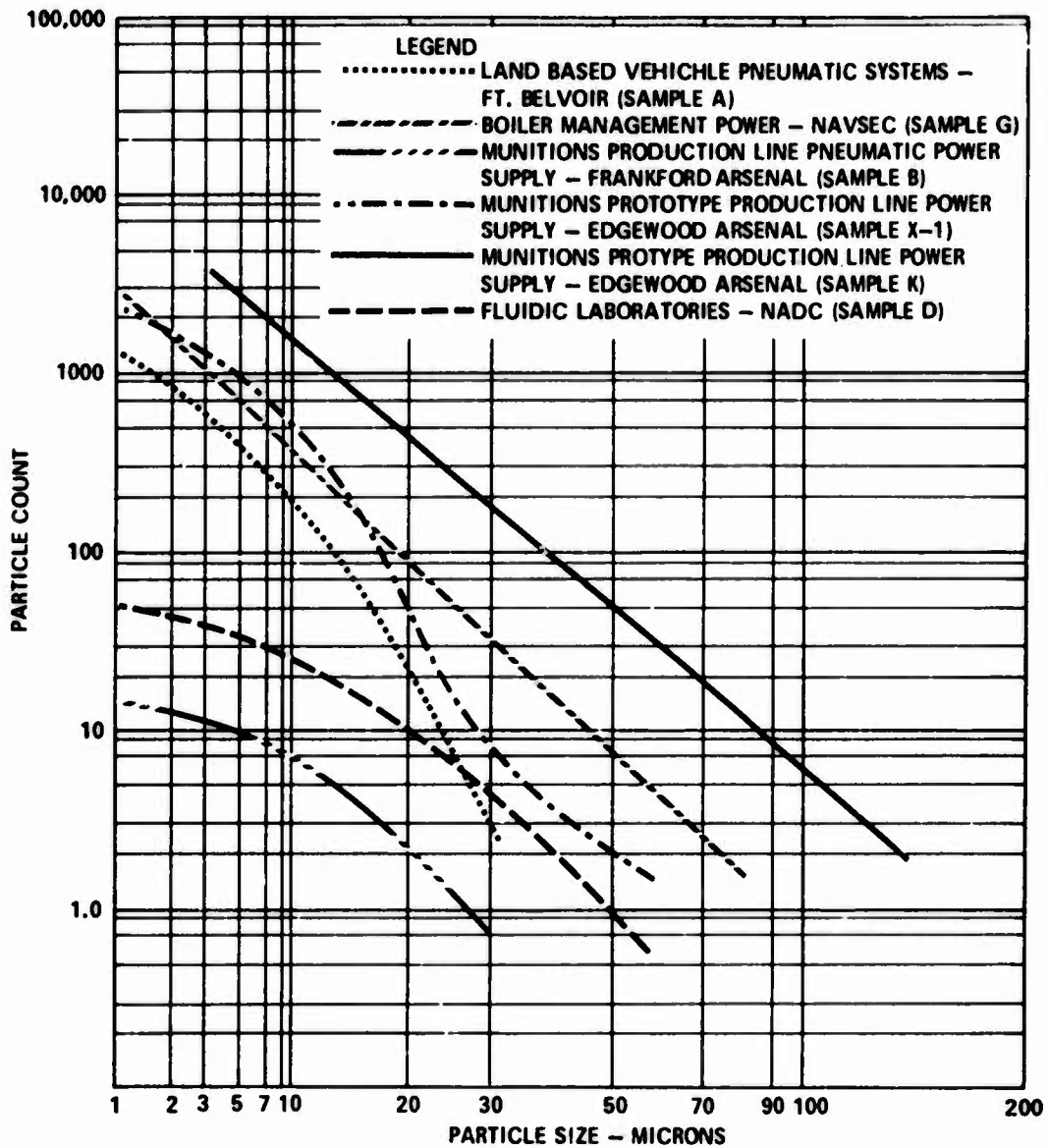


FIGURE 13 COLD GAS PARTICULATE DATA PLOTS - COMPRESSOR TYPE SUPPLIES

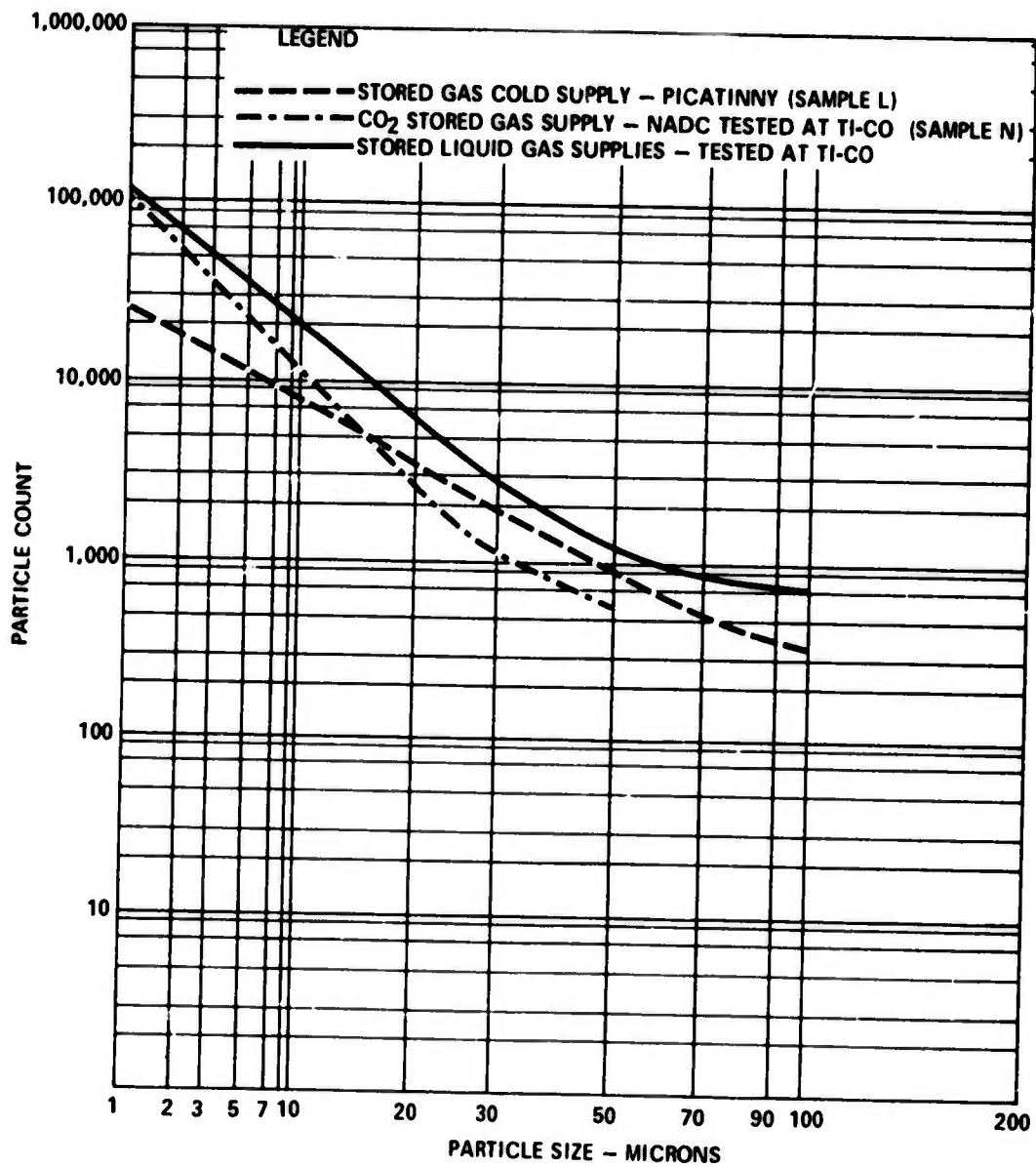


FIGURE 14 COLD GAS PARTICULATE DATA PLOTS - STORED GAS SUPPLIES

TABLE III
CLASSIFICATION OF POWER SUPPLIES

CLASSES	GRAVIMETRIC CONT. RATE grams/sft ³	
0	10 ⁻¹⁰ & Less	
1	10 ⁻⁸	REPRESENTATIVE OF ULTRACLEAN FLUIDS
2	10 ⁻⁷	TYPICAL OF CLOSELY CONTROLLED FILTERED & DRIED COMPRESSED AIR
3	10 ⁻⁶	TYPICAL OF LABORATORY POWER SUPPLIES
4	10 ⁻⁵	INDUSTRIAL; VEHICLE MOUNTED COMPRESSOR (FILTERED) - ENGINE ROOM POWER SUPPLY, TURBINE ENGINE BLEED GAS
5	10 ⁻⁴	STORED GAS SYSTEMS - METAL RUPTURE DISKS MEDIUM TO LARGE GAS VOLUMES
6	10 ⁻³	STORED GAS SYSTEMS - METAL RUPTURE DISKS SMALL GAS VOLUMES
7	10 ⁻²	MONOPROPELLANT GAS GENERATORS
8	10 ⁻¹	FILTERED SOLID PART OF SOLID PROPELLANT MOTORS
9	10	SOLID PROPELLANT MOTORS
10	>10	OPEN DUST STORM (MIL STD 810B SAND AND DUST)

The results of the contamination samples and the laboratory experiments have been combined and are presented as Fig. 15. The result of the experiments has been extrapolated and is shown as a dashed line. The power supplies that were sampled have been represented by bars shown at the proper contamination rate and centered over the extrapolated line; the length of the bars represents the average standard deviation of the laboratory experiments. Filtration would move the bars considerably to the right.

It is interesting to note that the typical power supplies which were sampled covered the same range as the reliability experiments, about four orders of magnitude.

RECOMMENDATIONS FOR FUTURE WORK

Many future applications of fluidics are dependent upon realistic reliability data which is needed to support the rather extravagant claims made earlier. This paper has described a method to test future systems on an overstressed basis to obtain accelerated reliability data. However, a theoretical basis is needed to explain the empirical data and conclusions presented here. A theoretical foundation is necessary to give confidence to a method of extrapolation since the alternative, tests lasting several decades, is clearly impractical. The parallel to solid state electronics and the testing of L.S.I. circuits described earlier is evident. At the same time, further experimentation along the lines suggested in this paper is needed to provide sufficient data for the separation of variables in the C_1 term of equation 1.

REFERENCES

- 1) "Fluidic Reliability Program - Final Report",
McDonnell Douglas Report No. L0242,
McDonnell Douglas Company, Titusville, Florida, 21 December 1972.
- 2) "Classification of Military Fluidic Power Supplies",
McDonnell Douglas Report No. L0244,
McDonnell Douglas Company, Titusville, Florida, 21 December 1973.

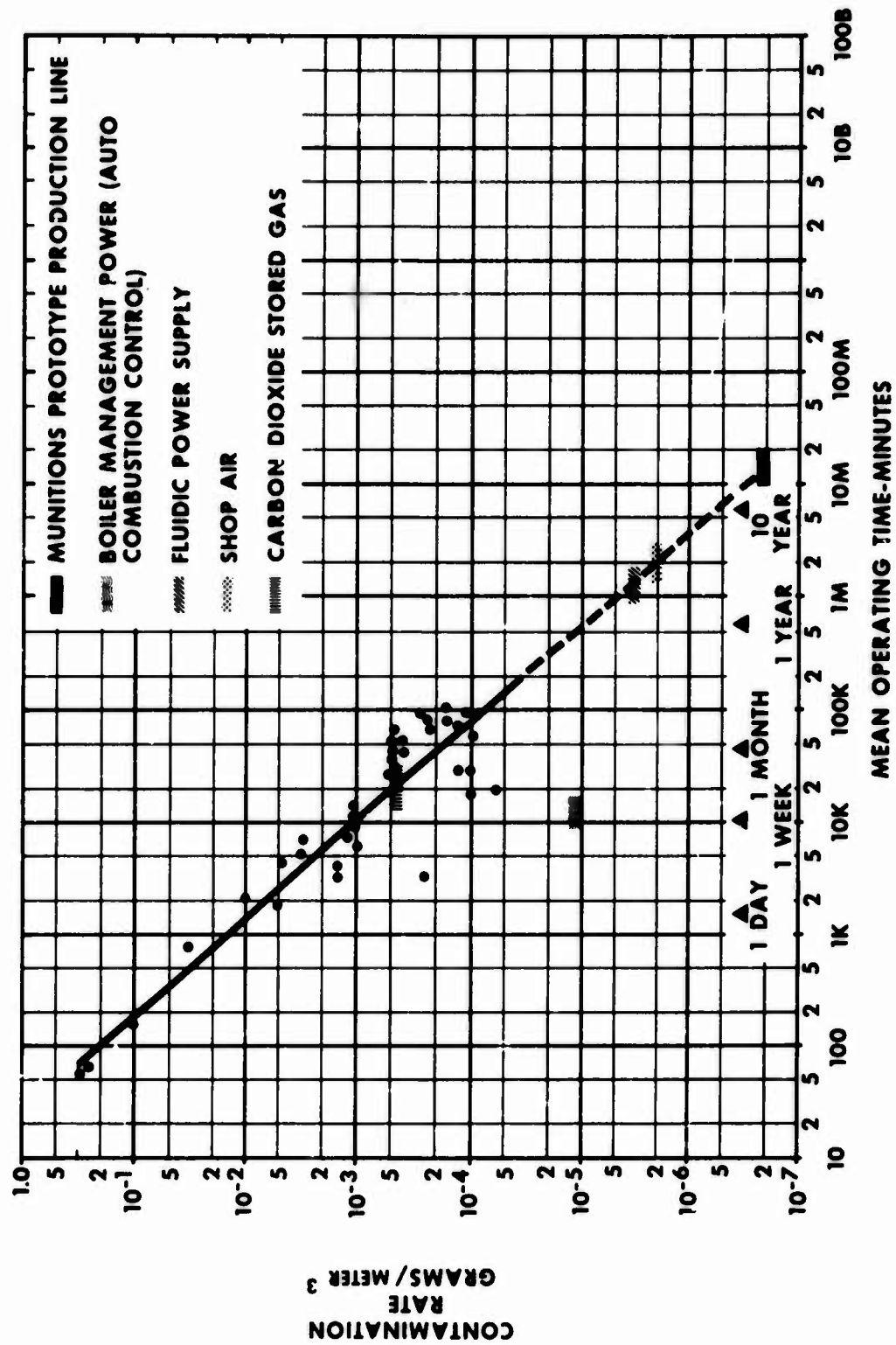


FIGURE 15 RELIABILITY PROJECTIONS